Andrew N. Makanya *Editor*

# The Vertebrate Blood-Gas Barrier in Health and Disease

## Structure, Development and Remodeling

Springer

# The Vertebrate Blood-Gas Barrier in Health and Disease

Andrew N. Makanya
Editor

# The Vertebrate Blood-Gas Barrier in Health and Disease

## Structure, Development and Remodeling

Springer

*Editor*
Andrew N. Makanya
Department of Veterinary
Anatomy and Physiology
University of Nairobi, Nairobi, Kenya

ISBN 978-3-319-18391-6 ISBN 978-3-319-18392-3 (eBook)
DOI 10.1007/978-3-319-18392-3

Library of Congress Control Number: 2015943074

Springer Cham Heidelberg New York Dordrecht London


Printed on acid-free paper

Springer International Publishing AG Switzerland is part of Springer Science+Business Media (www.springer.com)

# Preface

The blood–gas barrier (BGB) in vertebrates is the tissue interface separating the ambient oxygen from red blood cells within the capillaries of the gas-exchanging organs. The BGB allows acquisition of $O_2$ from the ambience in exchange for $CO_2$ from respiring tissues. To accomplish this, the BGB has a unique tripartite structure which can be remodelled to accomplish specific diffusion needs. Although the scope of vertebrates is very diverse in terms of zoogeography and even physiology, the structure of the BGB has been well preserved through evolution. This book broadly covers the entire BGB in 10 chapters; from aspects of diffusion, structure, embryological development, injury and remodelling, to preservation during tissue transportation. The book would therefore be interesting to students, teachers, researchers and even clinicians dealing with respiratory biology.

Passage of gases via the BGB occurs through simple diffusion because diffusion is an 'economical process'. Diffusion is an almost unavoidable phenomenon built in the energy of the universe. At temperatures above the absolute zero, all particles have some thermal energy responsible for various forms of interactions, which allows atoms to disperse spontaneously within a crystal of their own species (Piiper et al. 1971). The thermodynamic activity is responsible for intermolecular reactions and the solubility of gas molecules into liquids. Most importantly, thermodynamic activity is the source of the pressure responsible for *diffusion*, that is, the passive displacement of particles from regions of high activity to regions of low activity; no additional energy is required other than the original thermodynamic activity. This activity enables diffusion of gases across the BGB. The first chapter (Jacopo Mortola) comprehensively captures principles of gas diffusion where gas laws are adequately elucidated.

The pulmonary BGB is exceptional by its remarkable thinness and vast surface area (Weibel 1984). Its diffusing capacity of oxygen correlates directly with the surface area and inversely with the thickness. Structurally, the pulmonary BGB comprises an epithelial cell, an interstitial space and an endothelial cell. Along and across the evolutionary continuum, the thin, essentially three-ply laminated architecture of the BGB has been widely and greatly conserved in lungs of animals that remarkably differ morphologically, phylogenetically, behaviourally and ecologically. On the transition from aquatic to terrestrial life, and with it, preponderance

of air-breathing as means of acquiring oxygen ($O_2$), the 'layered' design appears to have been the only practical structural solution to supporting efficient movement of $O_2$ from air to blood by means of simple passive diffusion. The second chapter (John Maina) describes the BGB from a bioengineering perspective with details on functional capacities.

During embryological development, the vertebrate lung inaugurates as a primitive endodermal bud from the ventral aspect of the primitive foregut (Bellairs and Osmond 1998). The bud divides into primitive airways that form gas-exchanging chambers, where a thin BGB is accomplished. The development of the BGB in the compliant mammalian lung entails conversion of columnar cells of the migrating tubes to primitive type II cells and lowering of the apical intercellular tight junctions so that the gaps between the cells enlarge. The latter cells give rise to the definitive alveolar type II (AT-II) and type I (AT-I) cells. Extrusion of the lamellar bodies and thinning and stretching of the cells attains the squamous phenotype, characteristic of AT-I cells. Diminution of interstitial tissue, fusion of capillaries and apposition of capillaries to the alveolar epithelium results in formation of a thin BGB. In contrast, in the non-compliant avian lung I, attenuation proceeds through cell-cutting processes, referred to as secarecytosis (Makanya et al. 2006). Several morphoregulatory molecules including transcription factors such as Nkx2.1, GATA, HNF-3, WNT5a, signaling molecules including FGF, BMP-4, Shh and TFG-β and extracellular matrix proteins and their receptors have been implicated (Waburton et al. 2005; Makanya et al. 2013). In the postnatal period, alterations in the BGB may occur during late phases of alveolarization or as repair subsequent to lung injury. The third chapter (Andrew Makanya and Valentin Djonov) describes BGB formation in both mammals and birds, both in the prenatal and perinatal period.

The fourth chapter (David Budd, Victoria Burton and Alan Holmes) details the factors that come into play in maintenance of a healthy BGB. Besides formation of an efficient BGB, it is important that it remains healthy for optimal function. Disruption of the BGB is an early pathological event in a number of acute and chronic life-threatening pulmonary disorders. Thus, understanding the molecular processes that modulate the barrier function of the BGB is vital to aid in the development of new treatment paradigms. Airborne and blood-borne environmental challenges modulate signaling pathways that can severely compromise the ability of the BGB to maintain an effective barrier function. Successful rapid reconstitution of pulmonary epithelial and endothelial monolayers and restoration of junctional complexes following injury is essential to limit lung tissue damage, permit effective gas exchange and to preserve normal tissue architecture (Vandenbroucke et al. 2008). An inability to withstand these environmental challenges and efficiently affect endogenous reparative processes predisposes susceptible individuals to the development of lung diseases.

In Chap. 5, the authors (Panfeng Fu and Viswanathan Natarajan) discuss the signaling pathways that enhance barrier function. The endothelium and epithelium of the BGB form the size-selective barrier that controls the exchange of fluid from blood. Therefore, the integrity of vascular endothelium and epithelium is critical for lung function preservation and normal gas exchange. Movement of trans-

endothelial fluid and leukocyte flux occurs through paracellular gaps, which are formed at sites of active inflammation between vascular endothelial cells. Paracellular gap formation is regulated by the balance of competing contractile forces that generate centripetal tension and adhesive cell–cell and cell–matrix tethering forces intimately linked to the actin- and myosin-based endothelial cytoskeleton. Actin and myosin microfilaments, critically involved in endothelial barrier regulation, are physically coupled to multiple membrane-spanning target proteins found in intercellular junctions and focal adhesion complexes. Intercellular contacts along the endothelial monolayer consist primarily of adherens and tight junctions, which link to the cytoskeleton to provide both mechanical stability and transduction of extracellular signals into the cell. In addition, dynamic actin polymerization at the endothelial cell periphery produces cortical structures that are essential to barrier enhancement by barrier-enhancing agonists. Maturation of adherens and tight junctions not only forms a tight connection between cells and their surrounding environment, but also initiates signaling pathways regulating cytoskeletal remodelling. Contrarily, these junctions are targets for various intracellular signaling pathways activated by barrier-protective factors. Net movement of solute across the alveolar epithelium plays an especially important role in lung fluid homeostasis and appropriate oxygenation of the body. Apically located epithelial sodium channels, alongside the coordinated action of basolateral Na/K ATPase pumps play a critical role in generating and sustaining the osmotic gradient needed for net fluid reabsorption across lung epithelia (Eaton et al. 2009). In Chap. 6 (Charles A. Downs and My N. Helms), the dynamics of trans-barrier fluid and ion transport have been presented with an emphasis on the role of ion channel transporters, pumps that are important in maintaining alveolar fluid homeostasis and biophysical changes to the cell membrane that can occur under pathological conditions.

The lung epithelium is also uniquely exposed to an oxidizing environment, and therefore, the role of oxidants and antioxidants must be taken into careful consideration when evaluating the pathogenesis of trans-barrier dysfunction(s), which lead to lung disorders. Severe disruption to the barrier properties of the alveolar capillary membrane occurs in acute respiratory distress syndrome, whereas dysfunction in ion channels and transporters are the root cause of cystic fibrosis and chronic obstructive pulmonary disease.

Over and above disruption by disease, the BGB can undergo stress failure since it must be exceedingly thin to allow adequate transfer of gases across it by diffusion (Maina and West 2005; West et al. 1991). In Chap. 7 (John B. West), the causes and consequences of stress failure of the BGB have been documented. Under some physiological conditions, humans develop arterial hypoxemia because the diffusion rate of oxygen through the barrier is insufficient. Next, the barrier must be immensely strong to prevent bleeding into the alveoli. However, again this occurs in humans under some physiological conditions, and it is particularly striking in animals such as thoroughbred racehorses that are capable of very high aerobic activity. Mechanical failure of the barrier can occur when it is exposed to high stresses. Failure is seen if the capillary transmural pressure is greatly increased, the lung is inflated to very high volumes or the type IV collagen that is responsible for strength

becomes abnormal in disease. Remodelling of the barrier is seen if the stresses increase over a period of time.

In addition to its physiological function, the BGB also provides a barrier to protect against inhaled particles and pathogens. Chapter 8 (Holger C. Müller-Redetzky, Jasmin Lienau and Martin Witzenrath) describes the events and effects that characterize the endothelial component of the BGB. Following infectious or sterile inflammatory conditions, strictly controlled endothelial leakiness is required for leukocyte transmigration. However, increased permeability caused by host-dependent inflammatory mechanisms or pathogen-induced endothelial injury may lead to uncontrolled protein-rich fluid extravasation, lung edema and finally, acute respiratory distress syndrome (ARDS) (Bhattacharya and Matthay 2013), which still carries an unacceptably high mortality rate. A detailed overview of the major mechanisms underlying pulmonary endothelial barrier regulation and disruption, focusing on the role of specific cell populations, complement and coagulation systems and mediators including angiopoietins, sphingolipids, adrenomedullin as well as reactive oxygen and nitrogen species in the regulation of pulmonary vascular permeability is also provided in Chapter 8.

Preservation of the structural and functional status of the BGB is pivotal in successful lung transplantation. The BGB is subjected to a variety of stressors during all phases of lung transplantation. These result in ischemia-reperfusion (IR) injury and can manifest clinically as primary graft dysfunction (PGD). IR injury affects the epithelium, interstitium and endothelium of the alveolar septa as well as the pulmonary surfactant system. It leads to functional and morphological damage and death of pulmonary cells largely due to an inflammatory response by activated resident cells as well as inflammatory cell infiltration, which is governed by a large number of mediators (Yeung and Keshavjee 2014). Since PGD is the major cause of early morbidity and mortality after lung transplantation, much effort is undertaken from organ procurement, to preservation and implantation to prevent or ameliorate IR injury including surgical management procedures and pharmacological additives to perfusion solutions or ventilation gas. Particularly to increase the rate of transplantable donor organs, very promising results are achieved by the new technique of ex vivo lung perfusion (EVLP). Beyond the immediate transplantation period, the BGB is jeopardized in certain forms of acute rejection and chronic lung allograft dysfunction. Chapter 9 (Anke Schannaper and Matthias Ochs) in this book explores this subject in good detail.

Gas exchange during fetal/embryological development occurs through specialized structures, namely, the chorioallantoic membranes in oviparous vertebrates and the placenta in eutherians. The avian egg and mammalian placenta are transient structures, which are discarded after hatching or parturition but, during their lifespan, must adapt to the changing needs of the growing embryo/fetus. The embryo/fetus exerts demands on its environment whether it be the impersonal one in which an egg is laid, or the nurturing one within the body of the mother. In the case of the avian egg, nutrients are obtained internally but respiratory oxygen ($O_2$) must be obtained from the environment (Bissonnette and Metcalfe 1978). In eutherian

mammals, nutrients and $O_2$ are obtained from the mother via the placenta. The capacity of the egg and placenta to transfer $O_2$ to the embryo/fetus is expressed as a diffusive conductance ($DO_2$ in the units $cm^3O_2.min^{-1}.kPa^{-1}$). For these and other gas exchangers, a morphometric estimate of $DO_2$ can be obtained by combining stereological estimates of relevant microstructural quantities (vascular volumes, exchange surface areas and harmonic mean diffusion distances) with physiological data ($O_2$-haemoglobin reaction rates and Krogh's permeability coefficients). In Chap. 10, the avian egg and human placenta are taken as models for gas exchangers and their structures and functional capacities are compared. Particular focus is accorded to the human haemochorial placenta and its ability to serve the growing needs of the fetus is illustrated using results from normal and compromised pregnancies.

## References

Bellairs R, Osmond M. The atlas of chick development. New York: Academic Press; 1998.

Bhattacharya J, Matthay MA. Regulation and repair of the alveolar-capillary barrier in acute lung injury. Annu Rev Physiol. 2013;75:593–615.

Bissonnette JM, Metcalfe J. Gas exchange of the fertile hen's egg: components of resistance. Respir Physiol. 1978;1:209–18.

Bos JL, de Rooij J, Reedquist KA. Rap1 signalling: adhering to new models. Nat Rev Mol Cell Biol. 2001;2:369–77.

Eaton DC, Helms MN, Koval M, Bao HF, Jain L. The contribution of epithelial sodium channels to alveolar function in health and disease. Annu Rev Physiol. 2009;71:403–23.

Maina JN, West JB. Thin and strong! The bioengineering dilemma in the structural and functional design of the blood–gas barrier. Physiol Rev. 2005;85:811–44.

Makanya AN, Hlushchuk R, Duncker HR, Draeger A, Djonov V. Epithelial transformations in the establishment of the blood–gas barrier in the developing chick embryo lung. Dev Dyn. 2006;235:68–81.

Makanya A, Anagnostopoulou A, Djonov V. Development and remodeling of the vertebrate blood-gas barrier. Biomed Res Int. 2013;2013:101597.

Piiper J, Dejours P, Haab P, Rahn H. Concepts and basic quantities in gas exchange physiology. Respir Physiol. 1971;13:292–304.

Vandenbroucke E, Mehta D, Minshall R, Malik AB. Regulation of endothelial junctional permeability. Ann NY Acad Sci. 2008;1123:134–45.

Warburton D, Bellusci S, De Langhe S, Del Moral PM, Fleury V, Mailleux A, Tefft D, Unbekandt M, Wang K, Shi W. Molecular mechanisms of early lung specification and branching morphogenesis. Pediatr Res. 2005;57:26R-37R.

Weibel ER. The pathway for oxygen: structure and function in the mammalian respiratory system. Cambridge: Harvard University Press; 1984.

West JB, Tsukimoto K, Mathieu-Costello O, Prediletto R. Stress failure in pulmonary capillaries. J Appl Physiol. 1991;70:1731–42.

Yeung JC, Keshavjee S. Overview of clinical lung transplantation. Cold Spring Harb Perspect Med. 2014;4:a015628.

# Contents

# Contributors

**David C. Budd** GlaxoSmithKline, Fibrosis Discovery Performance Unit, Respiratory TAU, Medicines Research Centre, Hertfordshire, UK

**Victoria J. Burton** Therapeutics Review Team, MRC Technology, London, UK

**Valentin Djonov** Institute of Anatomy, University of Bern, Bern 9, Switzerland

**Charles A. Downs** Nell Hodgson Woodruff School of Nursing and Department of Physiology, Emory University, Atlanta, GA, USA

**Panfeng Fu** Department of Pharmacology, University of Illinois at Chicago COMRB, Chicago, IL, USA

**My N. Helms** Department of Pediatrics, School of Medicine, Emory University, Atlanta, GA, USA

Department of Pediatrics and Center for Cystic Fibrosis and Airways Disease Research at Children's Healthcare of Atlanta Hospital, Emory Children's Center, Atlanta, GA, USA

**Alan M. Holmes** Centre for Rheumatology and Connective Tissue Diseases, Department of Inflammation, UCL—Royal Free Campus, London, UK

**Jasmin Lienau** Department of Infectious Diseases and Pulmonary Medicine, Charity University of Medicine Berlin, Berlin, Germany

**John N. Maina** Department of Zoology, University of Johannesburg, Johannesburg, South Africa

**Andrew Makanya** Department of Veterinary Anatomy & Physiology, University of Nairobi, Nairobi, Kenya

**Terry M. Mayhew** School of Life Sciences, Queen's Medical Centre, University of Nottingham, Nottingham, UK

**Jacopo P. Mortola** Department of Physiology, McGill University, Quebec, Canada

**Holger C. Müller-Redetzky** Department of Infectious Diseases and Pulmonary Medicine, Charity University of Medicine Berlin, Berlin, Germany

**Viswanathan Natarajan** Department of Pharmacology, University of Illinois at Chicago COMRB, Chicago, IL, USA

**Matthias Ochs** Institute of Functional and Applied Anatomy, Hannover Medical School, Hannover, Germany

**Anke Schnapper** Institute of Functional and Applied Anatomy, Hannover Medical School, Hannover, Germany

**John B. West** Department of Medicine, University of California San Diego, La Jolla, CA, USA

**Martin Witzenrath** Department of Infectious Diseases and Pulmonary Medicine, Charity University of Medicine Berlin, Berlin, Germany

# Chapter 1
# Generalities of Gas Diffusion Applied to the Vertebrate Blood–Gas Barrier

**Jacopo P. Mortola**

## 1.1 Introduction

This chapter intends to be an introductory overview of the physical aspects of gas diffusion as they apply to the vertebrates' blood–gas barrier (BGB). Specialised cases of diffusion, like the transfer of water molecules through biological membranes (osmosis) or the protein-mediated facilitated diffusion are not pertinent to the BGB and will not be considered. The reader interested in the thermodynamic basis and mathematical derivations of the laws of diffusion should consult specific reviews (e.g., Chang 1987; Macey and Moura 2011). The current ongoing series *Comprehensive Physiology* has republished several major analyses of the interaction between diffusion and gas convective mechanisms, formerly printed in various sections of the *Handbook of Physiology* (e.g., Piiper and Scheid 1987; Forster 1987; Loring and Butler 1987; Scheid and Piiper 2011).

The first two sections of this chapter recall the most fundamental principles of diffusion of gases in air and liquids. In the remaining portions, some specific cases are presented to illustrate and expand on the concepts touched in the preceding sections. Table 1.1 recapitulates the abbreviations and units most commonly adopted, on line with what originally proposed by Piiper et al. (1971) for gas exchange physiology. I limited the references to the essential minimum and almost entirely to review articles, which can be used as a starting point for further readings.

J. P. Mortola (✉)
Department of Physiology, McGill University, McIntyre Basic Sciences Building, Promenade Sir William Osler, Montreal, H3G 1Y6, 3655 Quebec, Canada
e-mail: jacopo.mortola@mcgill.ca



A. N. Makanya (ed.), *The Vertebrate Blood-Gas Barrier in Health and Disease,*
DOI 10.1007/978-3-319-18392-3_1

**Table 1.1** Abbreviations and common units

| | Common symbols | MLT dimensions | Common units in respiratory gas exchange |
|---|---|---|---|
| Mass | M | M | g |
| Length (thickness) | θ | L | μm |
| Time | t | T | sec |
| Volume | V | $L^3$ | ml (STPD)[a] |
| Flow | $\dot{V}$ | $L^3\ T^{-1}$ | ml/sec |
| Force | N | $M\ L\ T^{-2}$ | kg m $sec^{-2}$ |
| Pressure | P | $M\ L^{-1}\ T^{-2}$ | cm $H_2O$ (or mmHg = 1.36 cm $H_2O$) |
| Diffusion rate | Q/t | $L^3\ T^{-1}$ | ml(gas) STPD/sec (or moles/sec) |
| Concentration gradient | ΔC/θ | $L^{-1}$ | (moles $cm^{-3}$)/cm |
| Diffusion coefficient | D | $L^2\ T^{-1}$ | $cm^2\ sec^{-1}$ |
| Solubility coefficient | α | $L\ T^2\ M^{-1}$ | ml(gas) STPD ml $(liquid)^{-1}$ $torr^{-1}$ |
| Permeation coefficient | K | $L^3\ T\ M^{-1}$ | ml(gas) STPD $cm^{-1}$ $sec^{-1}$ $torr^{-1}$ |
| Capacitance coefficient | β | $L\ T^2\ M^{-1}$ | ml(gas) STPD ml $(liquid)^{-1}$ $torr^{-1}$ |
| Conductance | G | $L^4\ T\ M^{-1}$ | ml(gas) $min^{-1}$ mm $Hg^{-1}$ |

*STPD* standard temperature, pressure and dry conditions

[a] Volumes of gases can be expressed in moles or in volumes (ml) at STPD (1 ml ≈ 0.0446 mMol)

## 1.2 Why Diffusion?

The answer to why diffusion is universally at the core of respiratory gas exchange (defined as the passage of respiratory gases through membranes) could be 'because diffusion is an economical process'. The economy originates from the fact that diffusion is an almost unavoidable phenomenon built in the energy of the universe. Above the absolute zero, all particles have some thermal energy responsible for various forms of interactions. Atoms disperse spontaneously within a crystal of their own species. Particles suspended in a fluid continuously collide with the molecules of the fluid itself in seemingly random (Brownian) patterns. The thermodynamic activity is responsible for intermolecular reactions and the solubility of gas molecules into liquids. Most importantly, thermodynamic activity is the source of the pressure responsible for *diffusion*, that is, the passive displacement of particles from regions of high activity to regions of low activity; no additional energy is required other than the original thermodynamic activity.

In the context of respiratory gas exchange, diffusion indicates the passive movement of oxygen ($O_2$) from the environment directly into the cells or, more commonly, into the blood and from the blood into the cells; the opposite path applies to carbon dioxide ($CO_2$). The word 'passive' is worth stressing because until the beginning of the twentieth century, a great controversy raged with eminent physiologists of the calibre of Bohr and Haldane believing that $O_2$ was actively secreted into the blood (Milledge 1985). This view, partially correct for some special cases like the fish swim-bladder (Berenbrink 2007), was given support by erroneous

measurements of arterial $O_2$ pressure, which appeared higher than the corresponding alveolar value.

For any molecule, the time required for diffusion increases with the square of the diffusion distance, as it is indicated below. Therefore, diffusion is an effective form of gas transport over very short distances; by itself, it can fulfil the metabolic needs only of protozoa and small multicellular aggregates, where the body surface area: volume ratio can be of the order of $10^5$ (Fig. 1.1a). For almost the totality of multicellular organisms, the time required by diffusion would be incompatible with the survival of organs and tissues other than the cells most superficially located. Hence, various means, cumulatively known as *mechanisms of gas convection*, have evolved to enhance the transport of $O_2$ and $CO_2$ between the environment and the metabolically active tissues and cells. They consist of a gas-carrying medium (water, blood or air) made to circulate through a network of pipes in an effort to optimise diffusion. Differently from diffusion, the molecular transport by convection requires some energy expenditure to maintain the circulation of the medium and to overcome the frictional losses within the pipes.

Blood is a particularly convenient convective medium from the view point of respiratory gas exchange chiefly because its pigments, haemoglobin or similar molecules, raise the $O_2$-carrying capacity to extraordinary high levels. The evolutionary introduction of blood circulation as a mechanism of gas transport necessitated a new diffusion barrier between environment and blood. The arrangement of diffusion (into the blood)-convection (via the blood)-diffusion (to the cells) is very efficient and represents the most common method of gas transport during the embryonic and fetal life of vertebrates (Fig. 1.1b). In mammals, the embryonic blood exchanges gases with the maternal blood via the placenta; in egg-laying vertebrates the embryonic blood exchanges gases through the chorioallantoic membrane (see Chap. 10). Postnatally, the simple coupling of cardiovascular convection and diffusion as means of $O_2$ transport is infrequent in vertebrates and extraordinarily rare in birds and mammals[1]. In almost all vertebrates, an additional convection mechanism, the respiratory system, has evolved to maximise gas exchange between environment and blood. Hence, postnatally the in-series organization of the physical mechanisms for gas transport consists of convection - diffusion - convection - diffusion (Fig. 1.1c). The medium of the first convection system is either water or air and the first diffusion barrier is the BGB that represents the focus of the present volume. There are two main differences between diffusion and convection as mechanisms of $O_2$ transport in vertebrates. First, as mentioned above, diffusion does not require active energy expenditure because it results from the gradient in thermodynamic activity across the diffusive barrier. On the contrary, transport by convection always necessitates some energy expenditure usually in the form of a pumping mechanism. Second, the thermodynamic activity of a gas is not lost through the convection path, as long as the gas composition of the medium remains unchanged. For example,

[1] The only exceptions that I am aware of for birds and mammals are some of the smallest newborn marsupials, which can satisfy their $O_2$ requirements by gas exchange through the skin for days after birth.

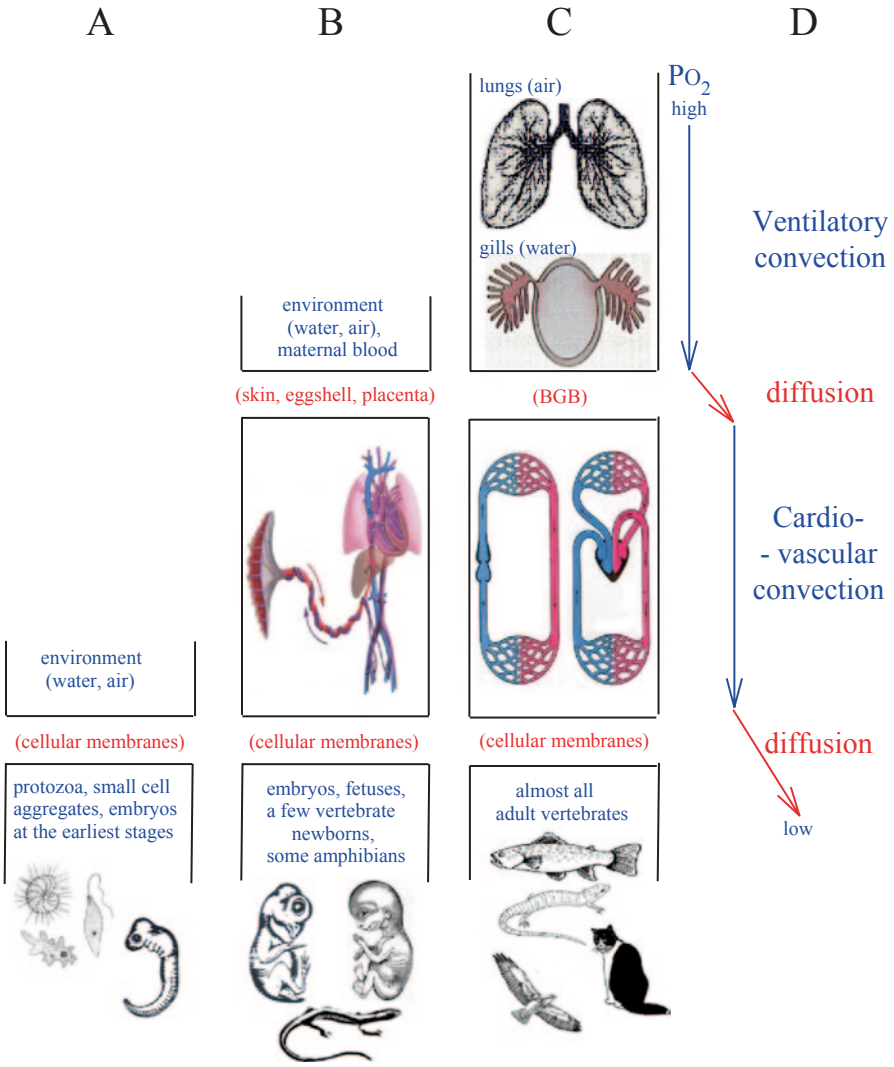


**Fig. 1.1** Schematic arrangements of the physical mechanisms of gas transport. **a** Diffusion through cell membranes is sufficient to accommodate the metabolic requirements of unicellular organism or very early embryos. **b** Diffusion is coupled to cardiovascular convection, which implies an additional diffusive barrier between blood and environment. This barrier can be the organism's skin itself, as in the lungless salamander or some newborn marsupials. In embryos and fetuses, the blood exchanges with the environment through the placenta (in which case the environment is represented by the maternal blood) or the chorioallantoic membrane. **c** The addition of another convection system, ventilation, permits further enhancement of gas transport capabilities because of the enormous increase in the blood–gas-barrier *(BGB)*. This is the arrangement for most adult vertebrates. **d** Gases transported by convection do not lose any activity (*blue vertical lines* in the cascade of the partial pressure of oxygen, $PO_2$) while diffusion always causes some loss in partial pressure *(red oblique lines)*

the partial pressure of $O_2$ ($PO_2$) remains unaltered throughout the whole arterial system irrespective of its distance from the lungs. Equally, $PO_2$ remains constant through the conductive airways of a unidirectional ventilatory system[2], like in fish or birds. Differently, diffusion always involves some loss of activity, does not matter how small the diffusive resistance may be. Hence, $PO_2$ drops whenever a diffusive step is encountered throughout the oxygen cascade between environment and cells (Fig. 1.1d).

## 1.3 Gas Diffusion

Gas molecules at higher concentration move towards the region of lower concentration until a dynamic equilibrium is reached. Nonuniform gases tend towards uniformity because the motion of a particle has less chance to be disturbed when it is heading towards a region with fewer particles. At equilibrium, the probabilities of movement are the same for all the gas particles so that there is no net displacement in any direction. Other factors being constant, the time required to reach equilibrium depends on the diffusion coefficient D of the gas. In ideal conditions, D is inversely proportional to the square root of the molecular weight w (Graham's Law). Hence, $O_2$ with $w = 32$ has a higher D than $CO_2$ with $w = 44$. In real conditions, an additional factor for D is the weak electrical intermolecular repulsive and attraction forces (van der Waals' forces). For $CO_2$, the attractive forces are more important than they are for $O_2$, which further exacerbates the differences in D between the two gases. In fact, D of $O_2$ ($\sim 0.2$ cm$^2$/sec) is 1.3 times that of $CO_2$ ($\sim 0.15$ cm$^2$/sec), a difference larger than expected simply from their respective w ($\sqrt{44}/\sqrt{32} = 1.17$). D is inversely proportional to the barometric pressure Pb and, in the temperature range 30–40 °C, increases ~0.8 % for every °C.

### *1.3.1 Fick's Laws of Diffusion*

A gas x with different concentrations separated by a surface A of thickness θ will diffuse from the region with higher to that with lower concentration. The quantity Q[3] of the gas x diffusing per unit time, or diffusion rate Qx/t, at any point through the barrier depends on the diffusion coefficient of the gas Dx and its concentration gradient $\delta Cx/\delta\theta$. If we assume for simplicity that the gradient is linear, $\delta Cx/\delta\theta$ can be expressed by the difference in concentration over the barrier $\Delta Cx/\theta$, and

[2] Differently, $PO_2$ cannot remain constant in a respiratory system with tidal ventilation like that of mammals. In the mammalian respiratory system, the $PO_2$ in the alveoli is lower than the inspired $PO_2$ because the inspired air, during its progression from the large airways to the gas exchange region, accumulates water vapour and carbon dioxide.

[3] Volumes of gases are at standard temperature, pressure and dry conditions (STPD). 1 mol contains the Avogadro's number of particles. 1 mMol $O_2 = 22.4$ ml $O_2$ and 1 ml $O_2 = 0.0446$ mMol $O_2$.

$$Qx/t = \Delta Cx \times (A/\theta) \times Dx, \tag{1.1}$$

known as the Fick's first law of diffusion after the enunciation in the middle of the nineteenth century by the German physician and physiologist Adolf Fick (who, incidentally, developed the methodology to measure cardiac output that bears his name). In essence, Eq. 1.1 states that the net movement of a quantity Q of substance x over time equals the product of the area A through which x is diffusing, the diffusion coefficient D and the concentration gradient $\Delta C/\theta$.

The dimensions for Qx/t and $\Delta C/\theta$ are, respectively, moles/min and (moles $cm^{-3}$)/cm, from which D has the dimensions of $cm^2$/min (Table 1.1).

From Dalton's law, each gas x has a partial pressure Px proportional to the product of its concentration Cx and barometric pressure Pb

$$Px = Cx \cdot Pb. \tag{1.2}$$

Therefore, Eq. 1.1 can be written as

$$Qx/t = \Delta(Px / Pb) \cdot (A/\theta) \cdot Dx. \tag{1.3}$$

Fick had likened the flux of a gas under a concentration gradient to the proportionality between a flux of heat and the temperature gradient, a relationship discovered by Joseph Fourier some years earlier. These relationships follow the general pattern 'flux = pressure/resistance', equivalent to the familiar Ohm's law of current = voltage/resistance (I = V/r); resistance is the reciprocal of 'conductance' and in the case of molecules or small particles, conductance refers to 'diffusivity'.

Because of the proportionality between Cx and Px (Eq. 1.2), usually no distinction is made between $\Delta Cx$ and $\Delta Px$, that is, between Eqs. 1.1 and 1.3. However, it is important to be aware that the latter, not the former, is responsible for diffusive transport *(1.3.2)*. At high altitude, even though the $O_2$ concentration remains the same as at sea level, $O_2$ diffusion decreases because of the lower Pb and lower partial pressure of $O_2$.

Equation 1.1 applies to a steady condition with time stability in $\delta C/\delta\theta$, that is, when the rate of change in C does not vary over time ($\delta C/\delta t = 0$). However, precisely because of diffusion, often the concentration gradient decreases over time ($\delta C/\delta t \neq 0$). Fick's second law addresses this issue and indicates that the rate of Q does not depend on the gradient $\delta C/\delta\theta$ itself but on the *rate of change* of the gradient. One advantage of introducing the element of time in the analysis of the diffusion process is that it permits to compute the time t that a particle needs in order to diffuse a given distance L, simplified as

$$t = L^2/(2D), \tag{1.4}$$

where D stands for the diffusion coefficient ($cm^2$/sec) and 2 is a numerical constant that depends on the dimensionality of the diffusion process. The main point of Eq. 1.4 is that, differently from the familiar concept of motion at constant speed

where t is proportional to the travelled distance L, in diffusive motion t is proportional to square of L. The reason for it is in the essence of the diffusion process itself, with particles continuously changing directions as the result of random collisions. On statistical grounds, the actual distance travelled by a particle with diffusive motion in steady conditions is nil, because a step in one direction gets offset by another in the opposite direction. However, as the number of random steps increases with time, the dispersion (or variance) of the distance travelled at each step increases, whatever its direction may be. Diffusion time is proportional to the variance, or mean square displacement ($L^2$), rather than to the average displacement. This means that the distance travelled by a particle with diffusive motion increases ever more slowly the greater the displacement. Hence, a particle that requires a time t to diffuse a distance d needs 4t to diffuse distance 2d and 100t to diffuse 10d. Diffusion is therefore extremely efficient for a molecule to travel very short distance, but becomes an inefficient way to move for long distances.

### *1.3.2 Gas Diffusion in Liquids*

The passage of gases through the BGB of the vertebrate respiratory system invariably involves diffusion of gases into liquids according to their partial pressure gradient. Equilibrium is reached when the net movement of particles leaving the liquid toward the gaseous phase is the same as that in the opposite direction, meaning that the gas partial pressure is the same at both sides of the BGB. Hence, in condition of equilibrium, when many gases are dissolved into the same liquid, the sum of their individual partial pressures is equal to the total pressure of the gaseous phase. For example, the total pressure of the gases in the arterial blood is the same as that of the pulmonary alveoli because in normal conditions blood and alveoli reach equilibrium.

Although liquids are fluids just like gases, their intermolecular cohesive forces are stronger, which explains why gases can be compressed while liquids practically cannot. In a liquid, the interactive forces confine the freedom of movement of the molecules, and diffusion coefficients D are several fold lower ($\sim 10^{-4}$) than in gases (Table 1.2). For example, by application of Eq. 1.4, a molecule of $O_2$ to diffuse 0.1 mm into water ($D = 2.5 \cdot 10^{-5}$ $cm^2/sec$) will take about 2 s and to diffuse 1 mm will take more than 3 min.

The volume of gas x dissolved in a liquid depends on the product between its solubility coefficient α ($mlx \cdot ml^{-1} \cdot Px^{-1}$)[4] and its partial pressure Px; therefore, the rate of diffusion of a gas x in a liquid differs from what expressed by Eq. 1.3 and becomes

$$Qx/t = (\Delta Px \cdot \alpha) \cdot (A/\theta) \cdot Dx. \quad (1.5)$$

[4] The solubility α of gases in liquids depends on temperature and concentration of solutes.

**Table 1.2** Representative physicochemical properties of respiratory gases in air and water

| | In air (~20 °C, 1 atm) | | | In water (20 °C, 1 atm) | | |
|---|---|---|---|---|---|---|
| | $O_2$ | $CO_2$ | $CO_2/O_2$ | $O_2$ | $CO_2$ | $CO_2/O_2$ |
| Diffusion (D) ($cm^2$/sec) | 0.198 | 0.155 | 0.8 | $2.5 \cdot 10^{-5}$ | $1.8 \cdot 10^{-5}$ | 0.7 |
| Capacity (β) (nMol $ml^{-1}$ $torr^{-1}$) | 54.7 | 54.7 | 1 | 1.8 | 51.4 | 28 |
| Permeation (K = D β) (nMol $cm^{-1}$ $sec^{-1}$ $torr^{-1}$) | 10.9 | 8.5 | 0.8 | $4.5 \cdot 10^{-5}$ | $9.3 \cdot 10^{-4}$ | 21 |

These values are approximate figures for temperatures around 20 °C, 1 atm. Differences among values reported in the literature can be substantial (e.g. MacDougall and Mccabe 1967). In air, the permeation coefficient K equals D·β or D·α, because β and α are the same. In water, β and α are the same for $O_2$, while for $CO_2$ β and α usually differ greatly, unless the water is carbonate free

Often, the terms D and α are lumped together into a 'permeation coefficient' (or Krogh's constant) K = D·α, with dimensions mlx $cm^{-1}$ $sec^{-1}$·mm $Hg^{-1}$ (Piiper et al. 1971), so that Eq. 1.5 simplifies into

$$Qx/t = (\Delta Px \cdot (A/\theta) \cdot Kx. \tag{1.6}$$

The permeation coefficient of $CO_2$ ($KCO_2 = 9.3 \cdot 10^{-4}$) is some 20 times higher than that of $O_2$ ($KO_2 = 4.5 \cdot 10^{-5}$) because, despite the slightly lower D, α for $CO_2$ is about 28 times higher than for $O_2$ (Table 1.2).

In essence, Eq. 1.6 states that the quantity of a gas x that diffuses per unit time is the product between the pressure gradient that drives diffusion and the gas diffusive conductance

$$Qx/t = \Delta Px \cdot Gx, \tag{1.7}$$

where Gx, with the units of mlx $min^{-1}$ mm $Hg^{-1}$, represents the product between geometric factors (A/θ) and the gas physical characteristics (K = D·α). Hence, the conductance (G) of the BGB for a gas x can be computed physiologically, by measuring ΔP and Q/t (Eq. 1.7), or can be computed from Eq. 1.5 with the knowledge of the morphological features of the BGB (A/θ) and the gas physicochemical properties (α·D). However, it should be noted that Eq. 1.7 is valid in conditions of steady state for the two media from which the gas is diffusing through. This is often not the case. For example, the alveolar-capillary $PO_2$ and $PCO_2$ gradients continuously change; hence, equilibrium may be reached only towards the end of the transit time, when the partial pressure values at the capillary and alveolar sides coincide. These dynamic events complicate the accurate computation of the diffusive G.

An increase in temperature influences the permeation coefficient K (Eq. 1.6) on two grounds; it raises D and slightly decreases the solubility α. The net effect of a rise in temperature on gas diffusion in liquids is ~1 % increase for every °C.

### *1.3.3 Gas Capacitance*

It is important to recognise that the partial pressure P of a gas in a liquid is solely determined by the gas physically dissolved; the chemically bound gas (like $O_2$ bound to haemoglobin or $CO_2$ as bicarbonate) does not contribute to P. Hence, in respiratory gas exchange, it is common to consider the total capacitance βof a liquid for a gas. This parameter, which has the same units as the solubility α (moles $ml^{-1}$ mm $Hg^{-1}$), includes both the chemically bound and the physically dissolved forms.

In air, from the general gas law,

$$P \cdot V = M \cdot R \cdot T, \tag{1.8}$$

it is apparent that the capacity β of a gas (moles M·volume $V^{-1}$·pressure $P^{-1}$) equals 1/(R·T), or

$$\beta = (M/V)/P = 1/(R \cdot T), \tag{1.9}$$

where R is the gas constant and T the temperature in Kelvin; hence, in air the capacitance β is the same for all gases. In water, $O_2$ is present only in the dissolved form; hence, $\beta o_2 = \alpha o_2$, while in the arterialised blood, the presence of haemoglobin raises $\beta o_2$ as much as 70 times. For $CO_2$, in distilled and carbonate-free water $\beta co_2 = \alpha co_2$. However, in most waters and in blood $CO_2$ is found both physically dissolved and bound to bicarbonates and other buffers, according to the pH of the water (Dejours 1988). Hence, usually in water and blood $\beta co_2$ largely exceeds $\alpha co_2$ (Table 1.2), with implications on the partial pressures that result from the $O_2$–$CO_2$ exchange *(1.4.3)*.

## 1.4 Some Considerations

Despite the simplicity and often intuitive nature of the laws governing diffusion, it may be useful to emphasise some aspects with respect to gas exchange through the BGB.

### *1.4.1 Thickness (θ) and Area (A) of the BGB*

The flux of a gas through the BGB is favoured by a short diffusive distance θ and a large surface A (Eqs. 1.1 and 1.3). Indeed, large exchange surfaces and very short diffusive distances are the most obvious characteristics of all structures involved in gas exchange, from gills and placentas to alveolar-capillary or chorioallantoic membranes. The risk of membrane fragility imposes a lower limit on how thin the

gas-exchange barrier can be. In mammals, where the lungs are organs with a high degree of volume change and subjected to the distortion and conformational changes of the chest wall, the minimum θ of the BGB is of the order 0.2–1 μm. In birds, where the lungs are rather rigid structures with air capillaries protected by a scaffold of surrounding vascular capillaries, the barrier is thinner than in mammals, possibly down to 0.1 μm. Values below these limits would jeopardise the integrity of the barrier, which seems to have reached its optimal limits with no room for further improvement. Indeed, species of different body sizes and metabolic requirements present large differences in BGB surface area but only minute differences in BGB thickness (Maina 2005). Furthermore, within each individual the possibility exists for the gas exchange area to increase further, as in the case of gills in conditions of hypoxia (Sollid and Nilsson 2006).

The physiological role of the gas exchange area needs to be considered not in absolute terms but in relation to the metabolic needs of the organism. For this reason, gas exchange through the body surface may be adequate even in organisms with small surface-to-mass ratio,[5] as long as $O_2$ needs are low such as many invertebrates and a few vertebrates, like the lungless salamander. In the majority of vertebrates, the tegument as the sole means of gas exchange is insufficient because of the large body size and the high metabolic demands. Hence, specialised organs have evolved to provide gas exchange areas much larger than body surface, both during prenatal development (the chorioallantoic membrane and the placenta) and postnatally (gills and lungs). In adult humans, the lung surface area is estimated at about 10 $cm^2$ per gram of body weight, which exceeds by 50–100 times the body surface area. In small-size species, especially those with high metabolic scope, the lung surface area can be much larger, like the ~100 $cm^2\ g^{-1}$ of the flying bats. Among birds and mammals, only some of the smallest newborn marsupials can use the skin as BGB. The newborn Julia Creek dunnart survives for weeks almost entirely by skin gas exchange because, in addition to the small body mass (~17 mg) and the extremely thin tegument, it has very low weight-specific needs for $O_2$ (Mortola et al. 1999). In the high humidity of the maternal pouch, these newborns do not risk dehydration which is a serious challenge to any terrestrial organism that uses the tegument as BGB.

At the microscopic level, biological membranes are structurally irregular. From the view point of gas diffusion, they could be compared to a mesh where regions with high G are spaced by others with low G. Extreme examples of such unevenness are the pores of the avian eggshell or the stomata of a plant leaf, which are the sole pathways out of the whole structure permitting diffusion. Indeed, any BGB, owing to unavoidable structural requirements, must be characterised by regions of low and high diffusive G. What matters for diffusive G (Eq. 1.7) is the cumulative A of the diffusive paths, irrespective of the number, distribution and size of the paths. In other words, whether a diffusive A of 1 $cm^2$ originates from the cumulative sum of 100 passages of 1 $mm^2$ each or from a single one of 1 $cm^2$ has hardly any

[5] Based on simple geometric considerations, as the size of an organism increases, its body surface-mass ratio rapidly decreases, because surfaces increase with the square of the linear dimension while volumes increase with the cube of the linear dimension ('Surface Law').

consequence on *diffusive* G. This is very different form the concept of G applied to convective transport, where a G of 100 1 $mm^2$ pores would be much lower than the G of one single 1 $cm^2$ passage. As an example, let us consider the diffusive G of an egg, which is usually measured from the daily weight loss caused by water evaporation[6]. The water vapour conductance (*diffusive* G) of chicken eggs is in the range 10–20 $\mu l\ day^{-1}\ mm\ Hg^{-1}$. This value originates from the diffusive paths of some $10^4$ eggshell pores, which all combined provide a diffusive A of 2.2 $mm^2$. On the other hand, if one had to measure the *convective* conductance of the eggshell by forcing gas through a piece of eggshell, the value would be ~1700–3900 $\mu l\ day^{-1}\ mm\ Hg^{-1}$, or some 200 times higher (Paganelli 1980).

The application of Fick's law (Eq. 1.3) becomes less valid when the pathways of diffusion through a structure are very crowded together or the thickness of the barrier θ is very short in relation to its cross section (Rahn et al. 1987). Either condition creates interference between the diffusive flows because of a boundary layer that lowers the conductance G. Under these circumstances Stefan's law applies, where diffusion is more closely proportional to the diameter, rather than the area, of the diffusive path. An additional factor that can functionally complicate the application of Fick's laws to the BGB is the formation of unstirred boundary layers. These are unlikely to alter the diffusive G in air breathers, but can offer a substantial diffusive resistance in water breathers. It was estimated that up to 90% of the total diffusive resistance at the level of the fish gill secondary lamella was produced by the unstirred film of water (Hills and Hughes 1970). Various mechanisms are in place to lower the boundary diffusive resistance, for example, locomotion as in the case of ram ventilation, or the waving movements of the gills or cilia movements. From these examples, it is apparent that G can have quite different values when obtained by a physiological approach (Eq. 1.7) or by a computation based on the morphological features (A/θ) of the BGB (Eq. 1.5).

### *1.4.2 Diffusion (D) and Permeation (K) Coefficients*

Diffusion of gases, whether within gases or liquids, depends on the partial pressure difference ΔP, not on the concentration difference ΔC. As mentioned above, the distinction has no practical importance for diffusion in air because of the direct proportionality between concentrations and partial pressures (Eq. 1.2), but it becomes relevant for gas diffusion in liquids. Because the solubility α of a gas can vary greatly among liquids, it is not unconceivable that ΔC and ΔP may have opposite sign, in which case the gas diffuses along ΔP and against ΔC.

The fact that the values of D for gases in liquids are very low (by comparison to the values in gaseous solutions) implies that equilibrium between air and liquid can take long, or very long, time to reach. For example, some waters can differ greatly

[6] The egg daily weight loss due to water evaporation permits to compute the conductance of water vapour, $G_{H_2O}$, from which $G_{O_2}$ is calculated from the molecular weight of $H_2O$ and $O_2$.

in $O_2$ partial pressure ($PO_2$) from the air they are in contact with. The $PO_2$ of a pond can oscillate daily between 30 and >400 mmHg (Truchot and Duhamel-Jouve 1980) depending on the prevalence of photosynthesis over animal respiration, and during the sunniest hours the waters may be hyperoxic even at high altitude! With respect to $CO_2$, similar differences between aquatic and aerial partial pressures are unlikely to occur because of the large capacitance β for $CO_2$ *(1.3.3)*. On a similar note, body compartments such as tissues and blood can present important differences in $PO_2$ because they never have sufficient time to reach diffusion equilibrium, while differences in partial pressure of $CO_2$ ($PCO_2$) are small. In mammals, the $P_{CO_2}$ has similar values in the alveolar regions, in the pulmonary capillaries, systemic capillaries and in tissues.

The diffusion coefficient D increases with a drop in barometric pressure Pb. To a minor extent, this improves the $O_2$ availability for those organisms relying on gas diffusion at high altitude, where ΔP is low (Eq. 1.3). Of course, the effect of Pb on D applies to all gases, meaning that at high altitude the advantage of higher D for $O_2$ diffusion has to be weighed against the risks of losing water in the form of water vapour. Avian eggs laid above sea level have eggshells with reduced G (Eq. 1.7) and small pore areas (A of Eq. 1.3), which limit water loss. Above ~3000 m, though, the needs for $O_2$ become imperative and the eggshell G rises above the sea level value by an increase in pore areas (Mortola 2009). Incidentally, this is another example of the plasticity of the BGB, where greater diffusion needs are accommodated by changes in A with no alterations in θ *(1.4.1)*.

### *1.4.3 The Environmental Side of the BGB*

Whether the environmental side of the BGB is air or liquid (Fig. 1.1), it makes a big difference on the ventilatory work and on the partial pressure of the expired gases and arterialised blood. The low $\beta_{O_2}$, coupled to the high density and viscosity of water[7], implies that animals ventilating water must perform greater respiratory work than animals ventilating air. In some fish, water pumping may take up to 50% of metabolic rate, compared to 10% or less for air ventilation in air-breathing vertebrates. In hypoxia, the cost of the hyperventilation for a fish may be so high as to increase its metabolic rate, in contrast to the hypometabolic response to hypoxia commonly observed in many air breathers.

Because all molecules of gases occupy approximately the same volume (22.4 L at standard temperature, pressure and dry (STPD) conditions), in air the values of α and β coincide and are the same for $O_2$ and $CO_2$ (Table 1.2). This means that in air breathers, as the result of $O_2$–$CO_2$ exchange, the drop in $PO_2$ will correspond to the increase in $P_{CO_2}$, the only difference being due to respiratory exchange ratios (RER) different from one. For example, with RER = 0.8, the 50 mmHg drop in $P_{O_2}$ (from 150 mmHg inspired to 100 mmHg alveolar) corresponds to a 50·0.8 = 40 mmHg

[7] At 20 °C water is about 1000 times denser and about 100 times more viscous than air.

increase in $P_{CO_2}$. Indeed, these are the $P_{O_2}$ and $P_{CO_2}$ values in the mammalian lungs and in the air cell of avian eggs towards the end of incubation. In water, $O_2$ is carried only in its dissolved form; hence $\beta_{O_2}$ is the same as $\alpha_{O_2}$ and both values are much lower than in air because of the lower $O_2$ solubility (Table 1.2). Differently, $\beta_{CO_2}$ is ~30 times larger than $\beta_{O_2}$ *(1.3.3)*. The consequence of $\beta_{CO_2} > \beta_{O_2}$ is that, differently from air-breathing, in water-breathing the $O_2$–$CO_2$ exchange causes only minor increases in $P_{CO_2}$ for the same decrease in $P_{O_2}$. On theoretical grounds, even if a water-breather were successful in extracting all the $O_2$, its expired $P_{CO_2}$ would be only 5 mmHg[8]. The difference between $\beta_{CO_2}$ and $\beta_{O_2}$ in water, not present in air, explains why arterial $P_{CO_2}$ in mammals is about 40 mmHg, while in many fish is just a few mmHg (Scheid and Piiper 2011).

In air, changes in temperature have only modest effects on gas capacitance, because the changes in temperature within the biologically significant range have little impact on absolute temperature (Eq. 1.9). Differently, in water the increase in temperature reduces β. This can pose a serious challenge to fish and other water-breathing ectotherms, the metabolic rate of which depends on ambient temperature. In fact, a rise in water temperature increases the animal's metabolic activity and $O_2$ requirements while at the same time reduces the water $O_2$ capacitance $\beta_{O_2}$.

## References

Berenbrink M. Historical reconstructions of evolving physiological complexity; $O_2$ secretion in the eye and swimbladder of fishes. J Exp Biol. 2007;209:1641–52.

Chang HK. Diffusion of Gases. Handbook of Physiology, Sect. 3: The Respiratory System. vol. IV, Gas Exchange, Farhi LE, Tenney SM, editors, Am Physiol Soc Bethesda MD ch 3: 33–50, 1987.

Dejours P. Respiration is water and air. Amsterdam: Elsevier; 1988. p. 179. [ISBN 0-444-80926-0].

Forster RE. Diffusion of gases across the alveolar membrane. Gas exchange in body cavities. Am Physiol Soc Bethesda MD ch. 1987;5:71–88. ("Handbook of Physiology, Sect. 3: The Respiratory System, vol. IV, Gas Exchange", Farhi LE, Tenney SM, editors.)

Hills BA, Hughes GM. A dimensional analysis of oxygen transfer in fish gill. Respir Physiol. 1970;9:126–40.

Loring SH, Butler JP. Gas exchange in body cavities. Am Physiol Soc Bethesda MD ch. 1987;15:283–95. (In "Handbook of Physiology, Sect. 3: The Respiratory System, vol. IV, Gas Exchange", Farhi LE, Tenney SM, editors.)

MacDougall JDB, Mccabe M. Diffusion coefficient of oxygen through tissues. Nature. 1967;215:1173–4.

Macey RI, Moura TF. Basic principles of transport. Comprehensive Physiol. 2011;1(30):181–259 (formerly Handbook of Physiology, Cell Physiology, 1997, ch. 6).

Maina JN. The Lung-air Sac system of birds. Development, structure, and function. Berlin: Springer; 2005. p. 210. [ISBN 3-540-25595-8].

Milledge JS. The great oxygen secretion controversy. The Lancet. 1985;326:1408–11.

Mortola JP. Gas exchange in avian embryos and hatchlings. Comp Biochem Physiol. A 2009;153:359–77.

[8] With water $\beta(CO_2)/\beta(O_2) \approx 30$, a drop in $PO_2$ of 150 mmHg raises $PCO_2$ by only 150/30 = 5 mmHg.

Mortola JP, Frappell PB, Wooley PA. Breathing through skin in a newborn mammal. Nature. 1999;397:660.

Paganelli CV. The physics of gas exchange across avian eggshell. Amer Zool. 1980;20:329–38.

Piiper J, Scheid P. Diffusion and convection in intrapulmonary gas mixing. Am Physiol Soc Bethesda MD ch. 4:51–88, 1987 ( Handbook of Physiology, Sect. 3: The Respiratory System, vol. IV, Gas Exchange, Farhi LE, Tenney SM, editors).

Piiper J, Dejours P, Haab P, Rahn H. Concepts and basic quantities in gas exchange physiology. Respir Physiol. 1971;13:292–304.

Rahn H, Paganelli CV, Ar A. Pores and gas exchange of avian eggs: a review. J Exp Zool. 1987;1:165–72.

Scheid P, Piiper KJ. Vertebrate respiratory gas exchange. Comprehensive Physiol. 2011;1(30):309–56.(formerly Handbook of Physiology, Comparative Physiology, 1997, ch. 5).

Sollid J, Nilsson GE. Plasticity of respiratory structures—Adaptive remodeling of fish gills induced by ambient oxygen and temperature. Respir Physiol Neurobiol. 2006;154:241–51.

Truchot JP, Duhamel-Jouve A. Oxygen and carbon dioxide in the marine intertidal environment: diurnal and tidal changes in rockpools. Respir Physiol. 1980;39:241–54.

# Chapter 2
# Morphological and Morphometric Properties of the Blood-Gas Barrier: Comparative Perspectives

**John N. Maina**

**Abbreviations**

| | |
|---|---|
| BGB | Blood-gas barrier |
| CL | Capillary loading |
| $DLO_2$ | Total morphometric diffusing capacity of the lung |
| $DtO_2$ | Morphometric diffusing capacity of the tissue barrier (BGB) of the lung |
| FM | Surface (free) macrophage |
| OLB | Osmiophilic lamellated body |
| PCBV | Pulmonary capillary blood volume |
| RSA | Respiratory surface area |
| St | Surface area of the blood-gas barrier |
| PCBV | Pulmonary capillary blood volume |
| $\tau ht$ | Harmonic mean thickness of the blood-gas barrier |
| $\tau ht_{min}$ | Minimum harmonic mean thickness of the blood-gas barrier |
| $\tau t$ | Arithmetic mean thickness of the blood-gas barrier |

## 2.1 Introduction

> Efficient gas exchange in the lung depends, as we have said repeatedly, on designing a very thin barrier of very large surface area between air and blood. (Weibel 1984)

Energy is pivotal to maintaining the intricate cellular processes such as ion pumping and enzymatic activities which drive life. Oxidative phosphorylation involves breaking down of organic molecules such as sugars in the presence of oxygen ($O_2$),

J. N. Maina (✉)
Department of Zoology, University of Johannesburg, Auckland Park 2006, Post Box 524, Johannesburg, South Africa
e-mail: jmaina@uj.ac.za



A. N. Makanya (ed.), *The Vertebrate Blood-Gas Barrier in Health and Disease,*
DOI 10.1007/978-3-319-18392-3_2

generating adenosine triphosphate (ATP), the molecular factor which cells utilize to operate physiological processess. The means of acquiring $O_2$ by simple physical diffusion began early in the evolution of aerobic life and was forthwith conserved. In some cases, occasioning catastrophic demises, shifts in the levels of $O_2$ in the biosphere, for example, as occurred in the Paleozoic's Permian–Triassic eras (Graham et al. 1995), have been important drivers in the progress and the diversification of life. Change in structural complexity, that is, from simple (unicellular) to complex (multicellular) forms, transition from aquatic life to terrestrial one and with it switch from water to air breathing, and realization of highly energetically costly lifestyles such as flight are some of the most decisive events which were directly impelled by the presence and concentrations of $O_2$ in the environment. Paradoxically, while $O_2$ is vital to life, it is also an environmental toxin and a mutagen (Auten and Davis 2009; Cabelli 2010). Brand (2007) stated that "if oxygen were invented today, it would be banned by the FDA (Federal Drug Agency)," and, respectively, Canfield (2014), Lane (2002), and Kleiber (1961) termed $O_2$ "the signature feature of Earth," "the molecule that made the world," and "the fire of life."

Possibly only exceeded by the gastrointestinal system, among the various organs of the body, the lung presents the largest surface area to the external environment which continuously and intimately interacts with air. For example, over a 24-h period, the human lung is ventilated ~25,000 times with ~20,000 L of air (Burri 1985a; Brain 1996). By weight, daily, more than 20 kg of air enters and leaves the human body, a load that considerably exceeds that of food and water consumed over the same period (Brain 1996). Gas exchange occurs by passive diffusion across a very thin tissue partition, the blood-gas barrier (BGB). Although inherently passive, the lung is a mechanically dynamic organ. The mammalian lung is, for example, ventilated with air from contractions of the diaphragm and the intercostal muscles, which attach to the ribs and perfused with blood by the contractions of the heart muscle. Regarding its construction, the BGB presents structural attributes that are at variance with each other. While a critical mass of cellular and connective tissue components is necessary to confer strength, the parts must be arranged to form the thinnest possible partitions which produce greatest conductance of $O_2$. This is brought about by a proximal–distal progressive reduction of the bulk of structural components which separate the airway and vascular systems. The epithelium lining the airways changes from a complex pseudostratified ciliated one with mucus cells in the upper airways (trachea and bronchi) to columnar and cuboidal ones in the lower parts of the airway system (the terminal bronchi and the bronchioles) to a simple squamous one on the respiratory surface (Fig. 2.1). Corresponding structural changes occur on the vascular side of the gas exchanger, where the thickness of the walls of the blood vessels become smaller, terminating in blood capillaries which are lined by endothelial cells only.

The structural properties of the BGB (thin and vast) present great challenges for efficient ventilation and perfusion of the lung (Weibel 2013). In the human lung, the thickness of the BGB (harmonic mean thickness, $\tau ht$) is 0.62 μm, which is a fraction of the thickness of a foolscap paper, and the surface area is 140 $m^2$, which is approximately that of the surface of a tennis court (Gehr et al. 1978).

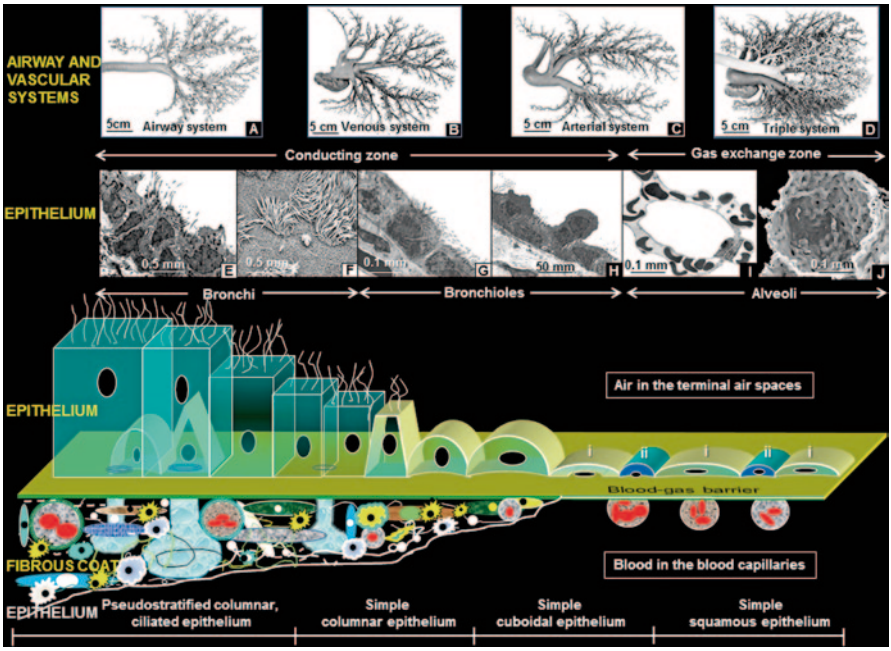


**Fig. 2.1** Proximal–distal diminution of the quantity of the tissue components separating the pulmonary airway and vascular systems. At the gas exchange level, the partition (the blood-gas barrier) is very thin. *Inserts:* **a**–**d** Casts of the airway (**a**) and vascular systems (**b**, **c**) of the lung of the pig, *Sus scrofa,* showing how the systems bifurcate and terminate in very small respiratory units and how closely the systems mirror (relate to) each other (**d**). **e**–**j** Transmission and scanning electron micrographs showing changes in the epithelial complexities in a mammalian lung at various parts of the airway system. **e** The complex pseudostratified ciliated epithelium with mucus cells (upper airways—trachea and bronchi). **f** ciliated and non-ciliated cells of the epithelium of the upper airways. **g**, **h** Columnar and cuboidal epithelial cells of the lower parts (terminal bronchi and bronchioles) of the airway system. **i**, **j** Epithelial cells lining the gas exchange (alveolar) surface. *i* type-1 cell, *ii* type-2 cell. Concept from Weibel (1984)

### *2.1.1 Cellular Organisation of the Lung Parenchyma*

At the gas exchange level, the lung parenchyma comprises motley of cellular and connective tissue components. The number, size, and location of these constituents are important for optimal functions of the organ which are gas exchange and metabolic activity. More than 40 different kinds of cells have been reported in the lung, with ~20 of them found on the respiratory surface (Breeze and Wheeldon 1977; Andrews 1981; Burri 1985b; Weibel 1985). The gas exchange surface is formed mainly by the type-1 and type-2 cells (pneumocytes; Fig. 2.2a) while endothelial cells delimit the blood capillaries (Fig. 2.2b). The type-2 cells are a highly specialized group of cells (Fig. 2.3a–e). By the process of exocytosis, they secrete surfactant (Pattle 1976; Daniels et al. 1994; Bastacky et al. 1995), a complex surface-active phospholipid substance which stabilizes the alveoli by lowering surface

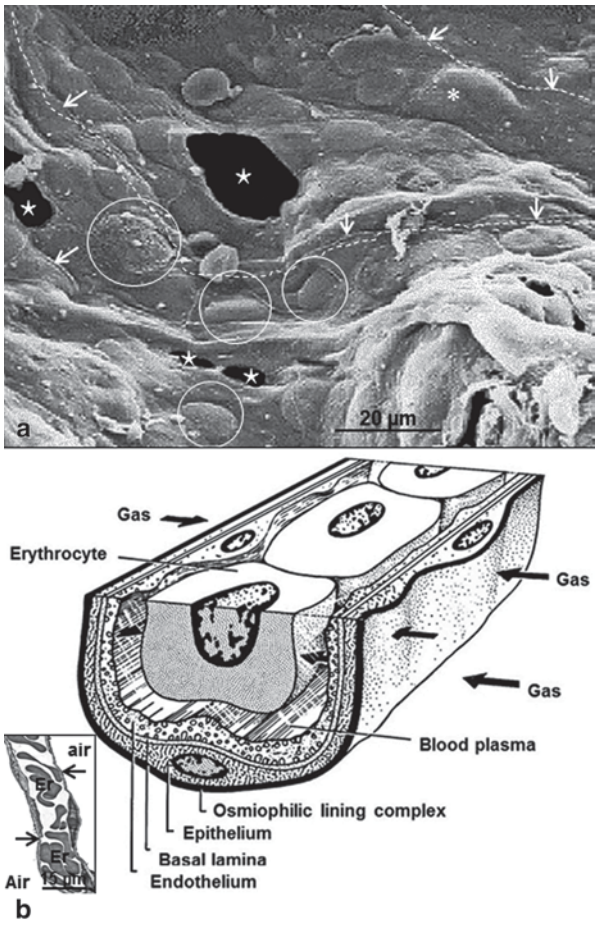


**Fig. 2.2** **a** Alveolar surface showing boundaries of a squamous type-I cell *(dashed line)* with the intercellular junctions marked with arrows. The type-II cells are *encircled*. *Stars:* interalveolar pores (formerly the Pores of Kohn), *asterisk:* likely cell body (perikaryon) of the type-I cell. **b** A schematic diagram of a blood capillary showing the various structural components. *Arrows:* gas (oxygen) diffusing across the blood-gas barrier and the plasma layer. *Insert:* Longitudinal section of a blood capillary showing erythrocytes *(Er)* which are separated from air by a blood-gas barrier *(arrows)*

tension on the respiratory surface. The surfactant is removed from the respiratory surface mainly by the type-II cells themselves and recycled and by the surface macrophages, which break it down (Rooney et al. 1994; Clements 1997; Veldhuizen et al. 1998; Veldhuizen and Haagsman 2000; Fehrenbach 2001): The macrophages account for ~10–20 % of the removal of the surfactant.

Although the surfactant occurs in different forms and quantities on the respiratory surface of the vertebrate lungs (Daniels et al. 1994; Bernhard et al. 2001a, b; Maina 1998, 2011), differences in the degrees of differentiation and location of the pneumocytes occur in different taxa. For example, in the lungs of the lungfishes, Dipnoi (Fig. 2.3a, b), amphibians (Fig. 2.3c), and the less-derived reptilian species, the cells are not morphologically different. They combine features of the fully differentiated type-1 and type-2 cells in being cuboidal in shape, having microvilli on their free surface, and containing various organelles of which the characteristic ones are the intracellular inclusions called osmiophilic lamellated bodies (OLBs; Fig. 2.3a–e; Rooney et al. 1994; Vanhecke et al. 2010). The precursors of the

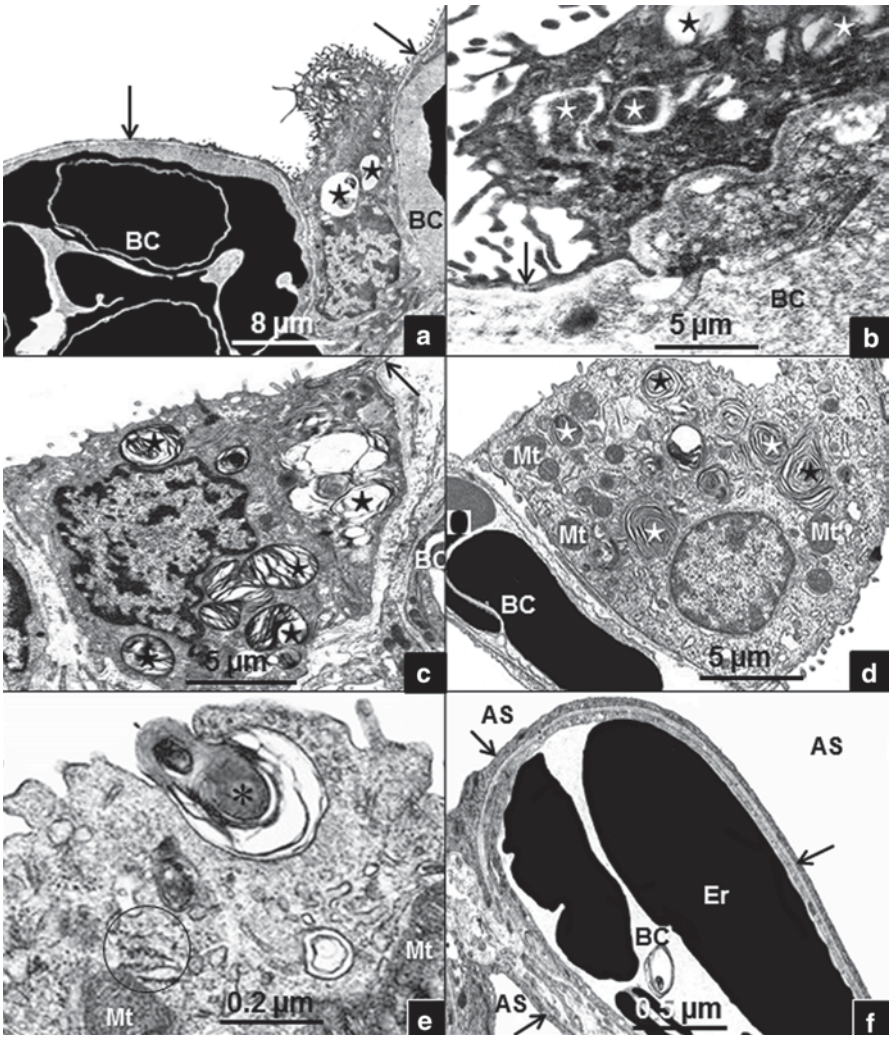


**Fig. 2.3 a, b** Type-II cells of the lung of the lungfish, *Protopterus aethiopicus,* containing osmiophilic lamellated bodies *(stars)*. Cuboidal/columnar in shape, the cells also have thin cytoplasmic extensions *(arrows)*. **c** Type-II cell of the reptilian lung showing osmiophilic lamellated bodies *(stars)*. *Arrow:* cytoplasmic extension. **d** A type-II cell of a mammalian lung showing osmiophilic lamellated bodies *(stars)* and mitochondria *(Mt)*. **e** Close-up of a type-II cell of a mammalian lung shown secreting surfactant by exocytosis *(asterisk)*. *Circled:* rough endoplasmic reticulum. **f** A pulmonary blood capillary showing the extremely thin type-I cells *(arrows)* fronting an air space *(AS)*. *BC* blood capillary, *Er* erythrocytes

surfactant (the OLBs) consist of large tightly packed concentric layers. In the lungs of the more-derived reptilian species (e.g., crocodiles), birds, and mammals, the pneumocytes are morphologically and ultrastructurally different: The type-1 cells have very thin and long cytoplasmic extensions which lack organelles (Fig. 2.3f),

and the type-2 ones are cuboidal in shape and, in addition to having OLBs, contain intracytoplasmic organelles such as mitochondria, rough endoplasmic reticulum, and Golgi complexes (Fig. 2.3d, e). Indicating its importance in lung function, the surfactant has been conserved for ~300 million years (Orgeig and Daniels 1995; Sullivan et al. 1998; Power et al. 1999).

In the human lung, the type-1 cells have an average volume of ~1,500 $\mu m^3$, cover a mean surface area of ~5,000 $\mu m^2$ (Crapo et al. 1982, 1983), and the cytoplasmic extensions extend to a distance of ~50 μm from the cell body (perikaryon). The type-2 cells (Fig. 2.2a) are small (~550 $\mu m^3$ in volume), form ~12% of the total cell population, and cover only ~4% of the alveolar surface (Haies et al. 1981; Crapo et al. 1982). Morphological specializations and strategic location of the pneumocytes and the connective tissue and other cellular components contribute to formation of thin BGB. The more metabolically active cuboidal and better-organelles-endowed cells and hence thicker type-2 cells cover much less of the respiratory surface while the type-1 cells which are metabolically inert and extremely thin (Figs. 2.2a, 2.3f) line most of it. While comprising ~10% of the total number of cells in the mammalian lung, the type-1 cells cover as much as 96% of the alveolar surface (Haies et al. 1981; Crapo et al. 1982, 1983). The location of the epithelial cell bodies (perikarya) away from the respiratory surface (Fig. 2.4a) and placing of connective tissue elements such as collagen (Fig. 2.4b, c), elastic tissue, and even nerve axons (Fig. 2.4d) in non-gas exchanging areas of the parenchyma contribute to thinning of the BGB. In the avian lung, the type-2 cells do not exist on the air capillaries (the respiratory units of the lung): Practically all the perikarya of the type-1 ones are confined to the atria and the infundibulae, non-respiratory parts of the parabronchial mantle (Fig. 2.5a, b). The location of the perikarya of the cells, normally the thickest part of the cell, away from the air capillaries contributes to thinner BGB than would otherwise be the case. In the mammalian lung, the interalveolar septum

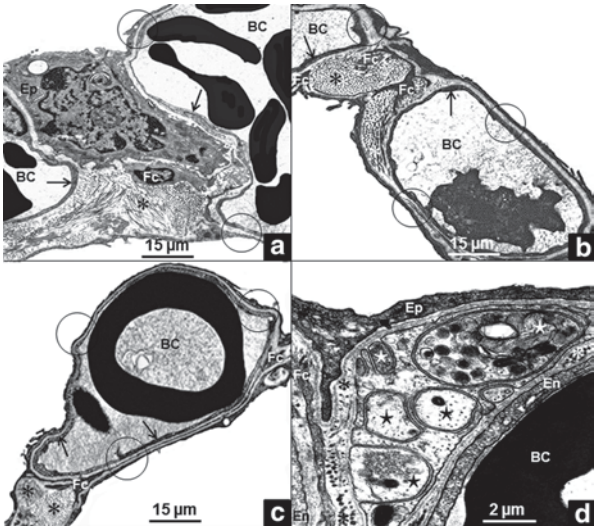


**Fig. 2.4 a–c** Placement of a type-II epithelial cell (*Ep,* **a**), collagen fibers (*asterisks,* **a**–**c**), and fibrocytes (*Fc,* **a**–**c**) away from the thinnest parts of the blood-gas barrier *(circles)*. *Arrows:* endothelial cells. **d** Lung of the black mamba, *Dendroaspis polylepis,* showing axonal profiles *(stars)* offset from a blood capillary *(BC)*. *Asterisk:* collagen fibres, *En* endothelial cell

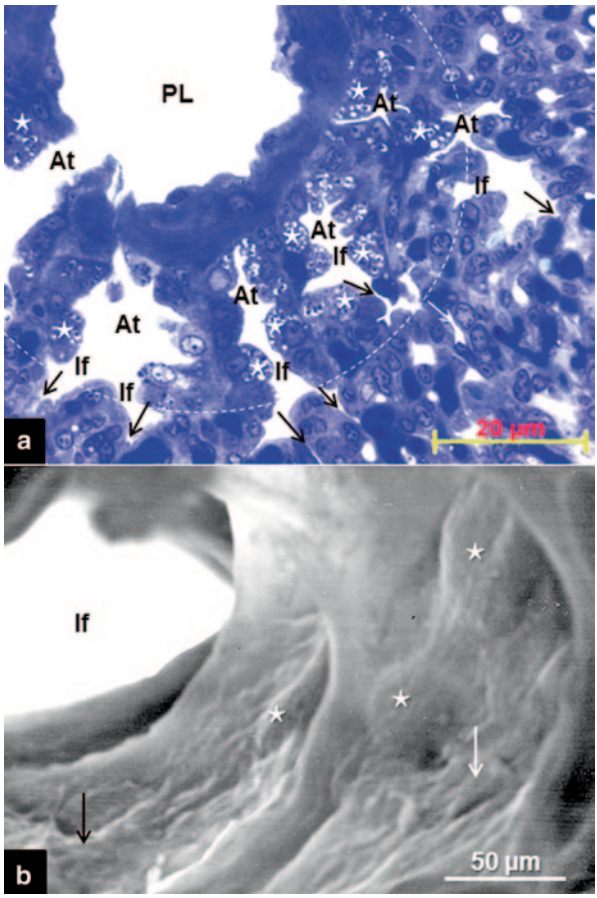


**Fig. 2.5** **a** Location of type-II cells *(stars)* in the atria *(At)* and infundibulae *(If)*. The air capillaries, the respiratory units, are shown by *arrows*. *PL* parabronchial lumen. *Dashed line:* approximate limit of the distribution of the type-II cells in the exchange tissue. **b** Close-up of an infundibulum *(If)* showing type-II cells *(stars)* and macrophages *(arrows)* on the surface

displays distinctively thick (supporting) and thin (respiratory) sites (Fig. 2.6a): Connective tissue elements such as collagen, elastic tissue, and cells such as fibrocytes and interstitial macrophages are found on the supporting side while the respiratory area comprises an epithelial cell, an interstitium, and an endothelial cell (Weibel and Bachofen 1997; Weibel 1984). Such functionally distinct sites are lacking in the avian lung (Fig. 2.6b).

The endothelial cells which line the pulmonary blood capillaries connect through intercellular junctions (Fig. 2.7a, b). Their thin cytoplasmic extensions contain numerous micropinocytotic vesicles. Compared to the epithelial cells, the endothelial cells are less permeable to solutes and are more selective to some ions (Effros et al. 1986). The endothelial cells constitute ~41 % of the entire population of lung cells (Crapo et al. 1983) and are considerably involved in the metabolic functions of the lung (Bakhle 1975; Bakhle and Vane 1977; Becker 1984). The type-3 cells, the so-called brush cells, have only rarely been described in the lung (Dormans 1985; Goniakowska-Witalinska and Leuweryns 1991; Meyrick and Reid 1968; Gomi 1982).

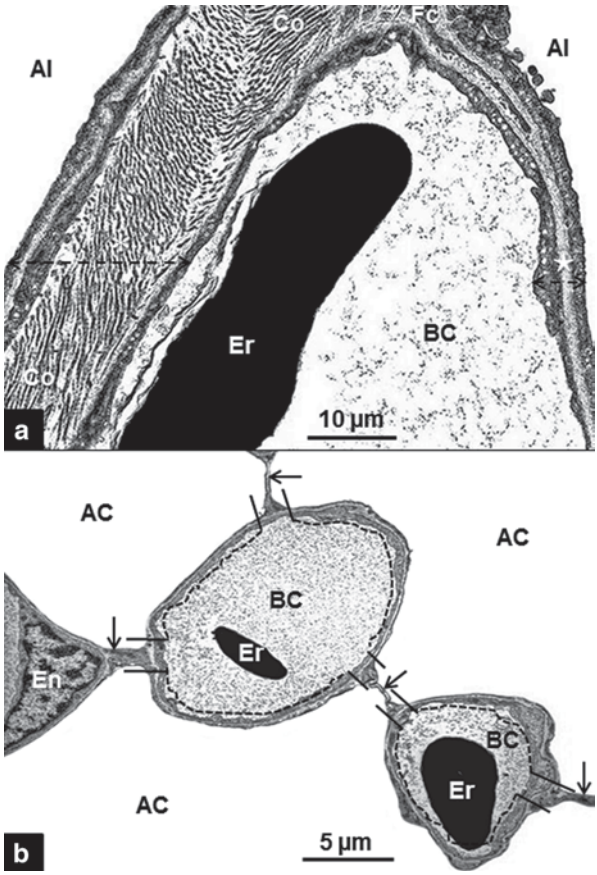


**Fig. 2.6** **a** Interalveolar septum in a mammalian lung showing a thick (supporting) side *(asterisk and dashed arrow)* and a thin (gas exchange) side *(star* and *dashed arrow)*. The thick side contains a large amount of collagen *(Co), alveolus (Al)*. **b** Exchange tissue of the avian lung showing air capillaries *(AC)* and blood capillaries *(BC):* thick and thin sides of the blood-gas barrier do not exist. Practically all the blood-gas barrier *(dashed line)* is involved in gas exchange while only a small part, the areas where blood capillaries interconnect *(areas between the lines),* is not involved in gas exchange. *Arrows:* epithelial–epithelial cell connections, *En* endothelial cell, *Er* erythrocyte, *Fc* fibrocyte

They are characteristically pyramidal in shape; their free surface has large blunted microvilli, numerous intracytoplasmic glycogen granules, and plentiful microfilaments which constitute a cytoskeletal system. The type-3 cells have been associated with chemoreceptive, absorptive, and secretory roles (Dormans 1985). A rare "mitochondria-rich cell" was identified in the lung of the turtle *Pseudemys scripta* by Bartels and Welsch (1984), and neuroepithelial cells have been described in lungs of several amphibian species (Rogers and Cutz 1978; Goniakowska-Witalinska et al. 1990; Cutz and Jackson 1999).

The motile surface (free) macrophages (FMs) protect the respiratory surface by ingesting and destroying or sequestering pathogenic microorganisms and injurious particulates (Fig. 2.8a–f; Nguyen et al. 1982; Brain and Hyg 1988; Nganpiep and Maina 2002). By keeping the respiratory surface "clean," the FMs ensure that the surface of the BGB remains uncluttered and therefore thin. The cells are rare in healthy amphibian and reptilian lungs, abundant in the mammalian lungs, and scarce in those of birds (Nganpiep and Maina 2002; Kiama et al. 2008; Maina 2005). The efficiency of the FMs and other phagocytic cells and immune-competent cells in

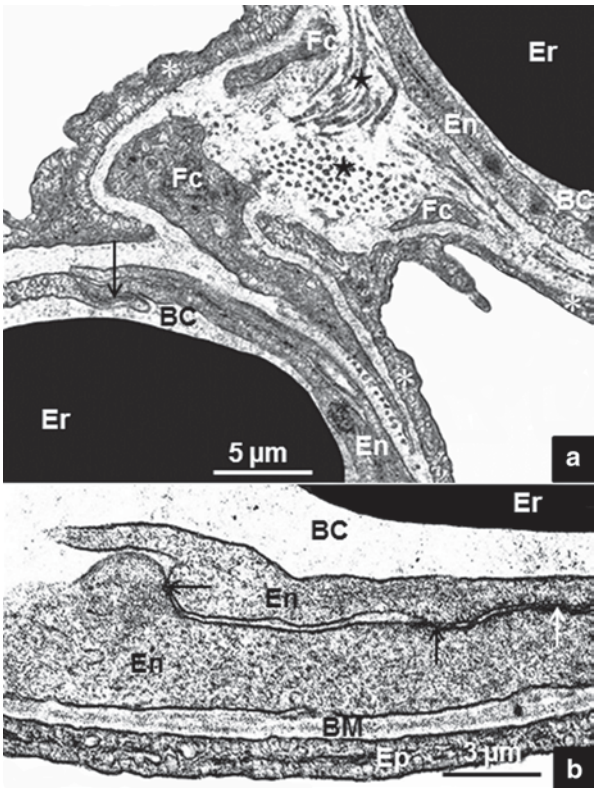


**Fig. 2.7** **a** Interconnection of endothelial *(En)* cells of the pulmonary blood capillaries *(arrow)* and location of connective tissue elements between adjacent blood capillaries *(BC)*. *Stars:* collagen, *asterisks:* epithelial cells. **b** Close-up of a blood-gas barrier *(BC)* showing an endothelial cell junction *(arrows)*. *Ep* epithelial cell, *BM* basement membrane, *Er* erythrocyte, *Fc* fibrocyte

the lung is so high that in, for example, healthy human beings, below the larynx, the respiratory surface is reportedly sterile (Skerret 1994). The surface macrophages of the lung derive from the bone marrow. They circulate in blood as monocytes before ultimately settling on the surface of the lung after passing through the blood capillary endothelium by the process of diapedesis.

### *2.1.2 Structure of the Blood-Gas Barrier*

Basically, the BGB comprises an epithelial cell which fronts air, an interstitial space which contains various cellular and connective tissue elements, including extracellular matrix, and an endothelial cell which lines the blood capillaries (Fig. 2.9a, b; Weibel 1973; Meban 1980; Maina and King 1982; Maina and West 2005). In the lungs of the air-breathing vertebrates, the "tripartite, laminated" structural design of the BGB has been greatly conserved (Maina and West 2005). Among other roles which include regulation of movement of molecular factors, maintenance of normal cellular cytoarchitecture, prevention of passage of noninflammatory cells, and control of morphogenesis, proliferation, and differentiation of cells, the basement

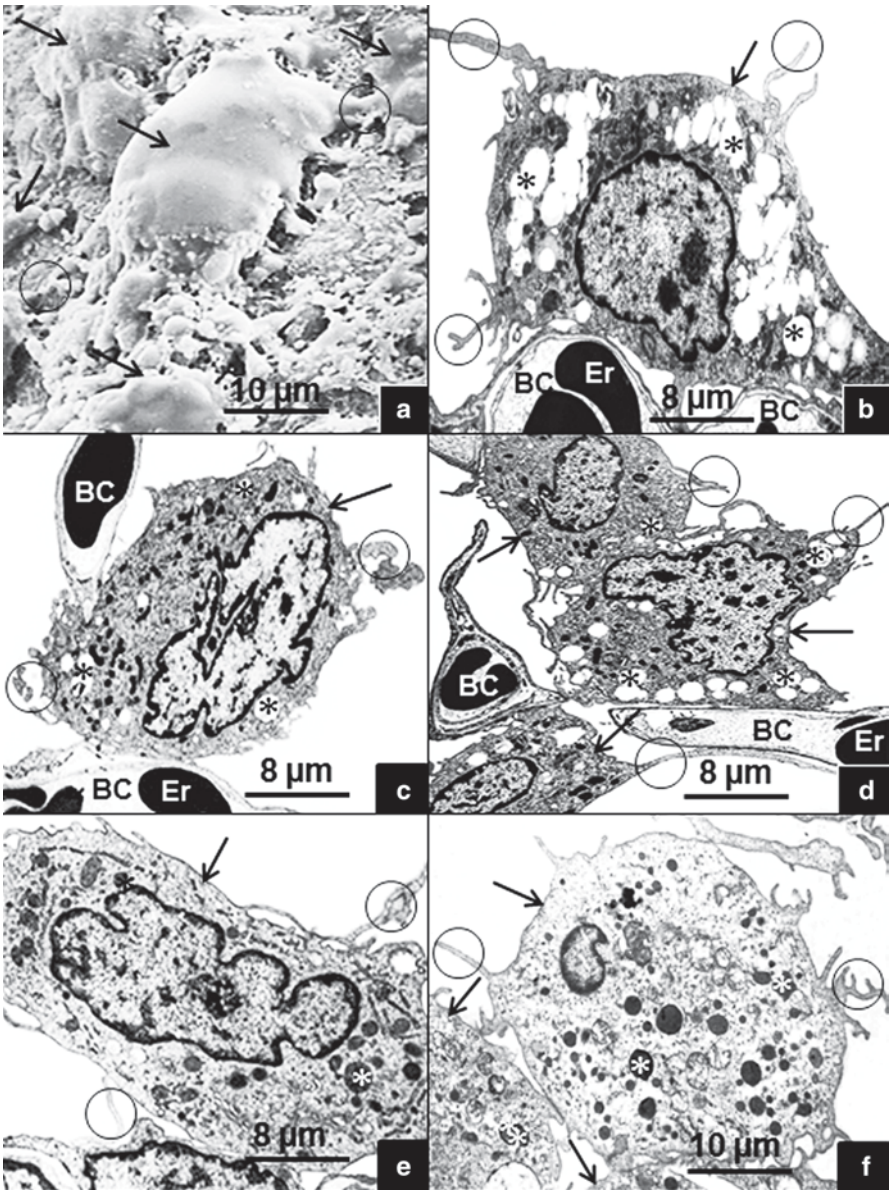


**Fig. 2.8** Free (surface) macrophages *(arrows)* of lungs of various air-breathing vertebrates. **a** Amphibian lung—tree frog, *Chiromantis petersi*. **b**–**e** Mammalian lungs. **f** Avian lung, domestic fowl, *Gallus gallus* variant *domesticus*. The cells are large and move using cytoplasmic extensions, filopodia *(circles)*. *Asterisks:* vesicular bodies, *BC* blood capillary, *Er* erythrocytes

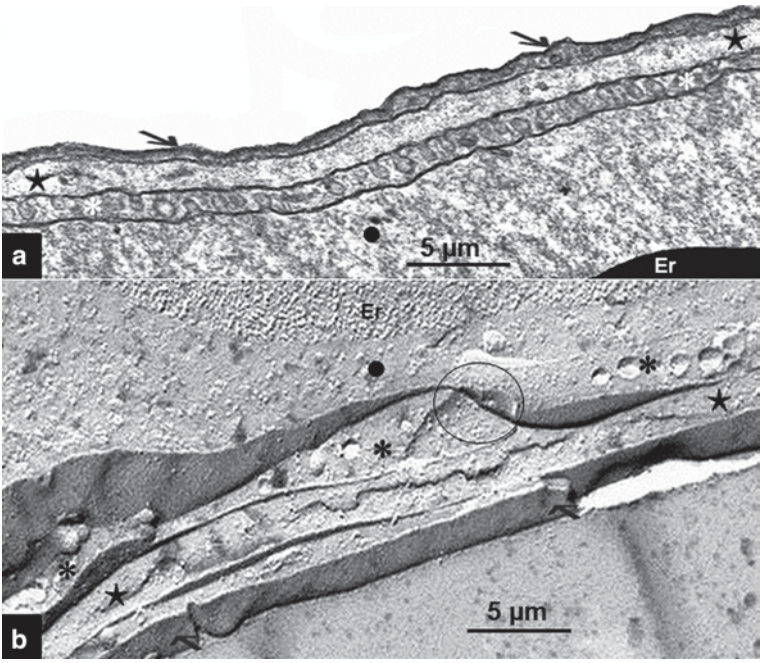


**Fig. 2.9** A transmission electron micrograph (**a**) and a freeze fracture preparation (**b**) showing the structure of the blood-gas barrier. The blood-gas barrier comprises an epithelial cell *(arrow),* a basement membrane *(star),* and an endothelial cell *(asterisk)*. *Dot:* blood plasma, *circle:* intercellular junction, *Er* erythrocyte

membrane is a continuous sheet of specialized extracellular matrix (Crouch et al. 1997; Leblond and Inoue 1989; Schuger et al. 1991). From the border of the epithelial cell, it comprises a lamina rara externa, a lamina densa, and a lamina rara interna. The lamina densa contains type-IV collagen which strengthens the BGB (West and Mathieu-Costello 1992, 1999; West 2003). In the avian lung, type-IV collagen was immunocytochemically localized in the basement membrane of the BGB of the lung of the domestic fowl, *Gallus gallus* variant *domesticus,* by Jimoh and Maina (2013).

### *2.1.3 Sporadic Attenuation of the Blood-Gas Barrier*

In the avian lung in particular, the BGB displays conspicuous structural unevenness (Fig. 2.10a–c; Maina and King 1982). Sporadic corrugation of the BGB, that is, presence of very thin parts between relatively thicker ones, may be a compromise (trade-off) design by which gas exchange is optimized and the strength to the BGB conserved (Weibel and Knight 1964). According to Weibel (1989), if the same

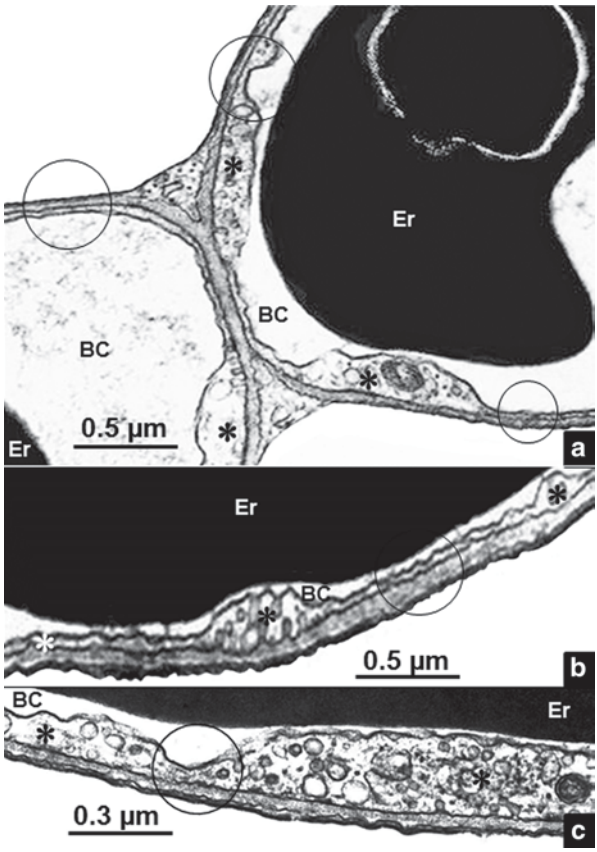


**Fig. 2.10 a–c** The sporadic attenuation of the blood-gas barrier in the avian lung where thin *(circles)* and relatively thicker *(asterisks)* parts coexist *(asterisks)*. *BC* blood capillary, *Er* erythrocyte

quantity of structural material is used to form a BGB, periodic attenuation forms a barrier which has a harmonic mean thickness *(τht)* that is three times thinner than if the barrier was of uniform thickness. Thinning of the BGB greatly increases gas exchange efficiency. Irregularity of the BGB gives a diffusing capacity of $O_2$ which is 25 % more than that granted by a uniform one (Weibel 2000). The importance of irregularity of the BGB in gas exchange is shown by the fact that the feature occurs more conspicuously in the lungs of endothermic vertebrates (mammals and birds; Weibel and Knight 1964; Maina and King 1982), the groups of animals with the highest demands for $O_2$. In the avian lung, the unevenness of the BGB of the endothelial cell is more pronounced compared to that of the epithelial one (Fig. 2.6b, 2.10a–c), and in the mammalian lung, the endothelial cell attenuations are more pronounced on the thinner (gas exchange) side of the interalveolar septum compared to the thicker (supporting) one (Fig. 2.6a; DeFouw 1984).

The corrugation of the BGB is mathematically expressed as the ratio of the arithmetic mean thickness of the BGB *(τt)* to its harmonic mean thickness (*τht;*

Weibel and Knight 1964). The volume density of the cellular and connective tissue elements which form the BGB are conveyed in the $\tau t$ while $\tau ht$ emphasizes the lengths of the thinnest parts of the BGB: reciprocals of the intercept lengths of the BGB thickness are used in calculating the $\tau ht$ (Weibel and Knight 1964; Weibel 1970/1971). Compared to $\tau t$, $\tau ht$ is therefore the more appropriate factor for determining the morphometric diffusing capacity of the BGB for $O_2$ ($Dto_2$). The ratios of $\tau t$ to $\tau ht$ vary in the vertebrate lungs (Maina and King 1982). In the avian lung, the highest value (10.8) was reported in the house sparrow, *Passer domesticus,* and the lowest one (1.2) in the ostrich (Maina and King 1982; Maina 1989a; Maina and Nathaniel 2001); in the mammalian lung, a ratio of 1.11 exists in the dog, *Canis familiaris* (Gehr et al. 1981), 4.49 in the naked mole rat, *Heterocephalus glaber,* 3.34 in the ground mole rat, *Tachyoryctes splendens* (Maina et al. 1992), and 6.04 in bats (Maina et al. 1991); in the reptilian lung, the highest ratio of 2.3 occurs in the lungs of the blind slow worm, *Anguis fragilis,* and the smooth snake, *Coronella austriaca,* while the lowest one occurs in the grass snake, *Natrix natrix,* the European tortoise, *Testudo graeca,* and the red-eared turtle, *Pseudemys scripta* (Meban 1980); in the amphibian lung, the highest ratios are 1.44 in the fire-bellied newt, *Paramesotriton hongkongensis,* and the Nigerian clawed toad, *Xenopus tropicalis,* and the lowest in the common toad, *Bufo bufo,* and the common newt, *Triturus vulgaris* (Meban 1980).

The minimum harmonic mean thickness ($\tau ht_{min}$) indicates the extent to which the BGB thins out. For the avian lung where data are available (Maina and King 1982; Maina 1989a), in the graylag goose, *Anser anser*, and the Muscovy duck, *Cairina moschata,* $\tau ht_{min}$ is 0.05 μm. Using the ostrich as an example, a scheme of some of the most important morphometric parameters which determine the total morphometric diffusing capacity of the lung for $O_2$ ($DLo_2$) are shown in Fig. 2.11 (Maina and Nathaniel 2001): A pulmonary capillary blood volume of 250 $cm^3$ is literally spread over a respiratory surface area (RSA) of 120 $m^2$ and is separated from air across a BGB which is 0.560 μm thick *(τht)*.

### *2.1.4 Exposure of Pulmonary Capillary Blood to Air*

The manner in which the pulmonary capillary blood is exposed to air across the BGB differs among the lungs of the various air-breathing vertebrates. This arises from the positioning of the blood capillaries on the surface of the lung or on the septa, the partitions which compartmentalize the more complex lungs into small air spaces. The extent of the bulging of the blood capillaries determines how much of the blood capillary endothelium participates in gas exchange, that is, forms part of the BGB. In the lungs of the basal (less-derived ("primitive") air breathers such as the pneumonate gastropod, *Trichotoxon copleyi* (Fig. 2.12a, b; Maina 1989b), the accessory respiratory organs (suprabranchial membrane and labyrinthine organs) of air-breathing fish such as the African catfish, *Clarias mossambicus* (Fig. 2.12c, d;

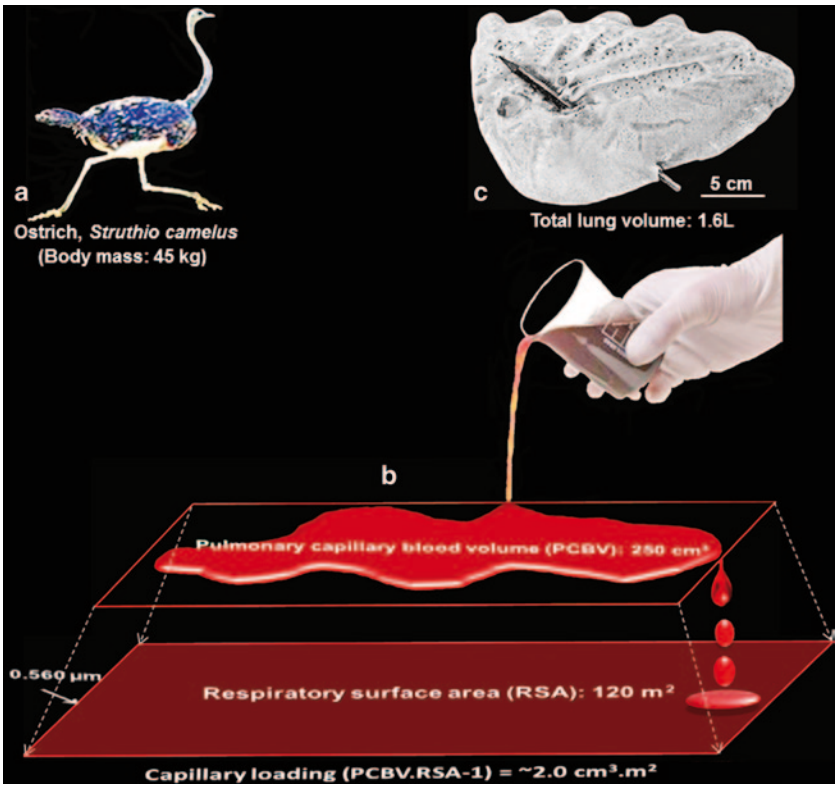


**Fig. 2.11** Some morphometric properties of the lung of the ostrich, *Struthio camelus* (**a**). In a 45 kg (young) bird with a total lung volume of 1.6 L, a pulmonary capillary blood volume of 250 $cm^3$ is literally spread over a surface area of 120 $m^2$, and the blood and air are separated by a tissue barrier of a harmonic mean thickness of 0.560 µm (**b**). A pencil has been inserted through the intrapulmonary primary bronchus of the lung (**c**)

Maina and Maloiy 1986), the air bladder of fish (Fig. 2.12e, f) and in the skin, for example, of amphibians (Fig. 2.12e—insert), the blood capillaries bulge from the surface of the gas exchanger forming a "frontage" capillary system. In the lungfish, *Protopterus aethiopicus,* and the amphibian and the reptilian lungs, a "double" capillary system exists: The blood capillaries are located on opposite sides of the septa (Fig. 2.13a–f; Maina 1989c, 1990). In the mammalian lung, a "single" capillary system occurs: The blood capillaries are supported by a relatively thinner septum, and blood is exposed to air more efficiently on the thinner part of the interalveolar septum (Fig. 2.14a–f). In the avian lung, a "diffuse" pulmonary blood capillary arrangement exists: Capillary blood is exposed to air practically all over the blood capillary wall (Figs. 2.6b, 2.15a–f).

Noteworthy departure from the "single" capillary exposure design which occurs in the adult mammalian lung exists in the lungs of the placid herbivorous adult

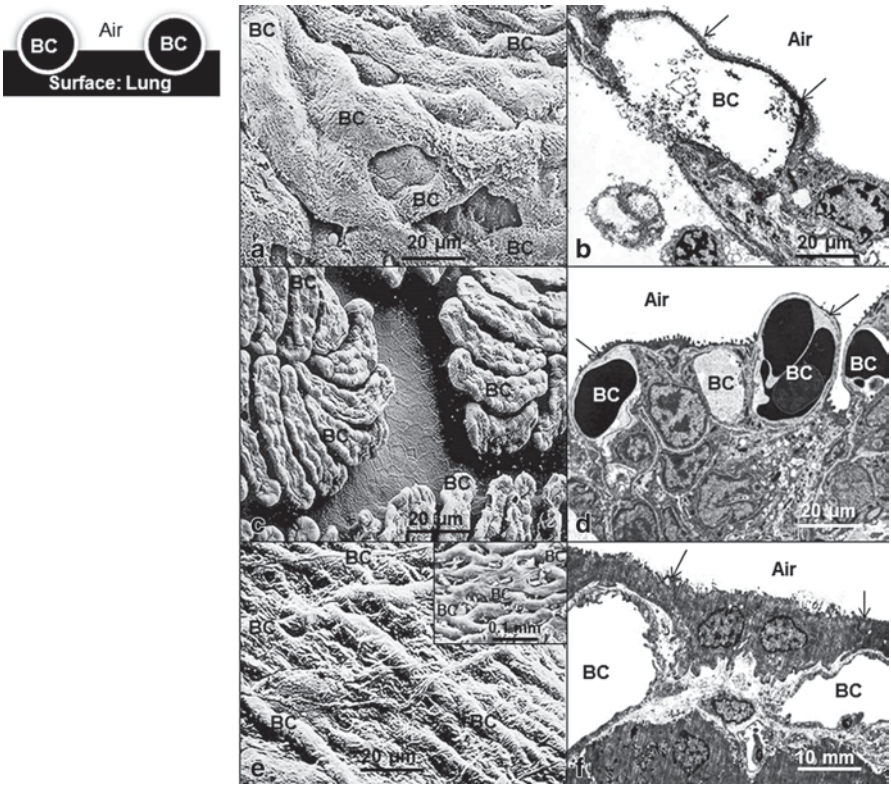


**Fig. 2.12 a–f** Exposure of pulmonary capillary blood to air in lungs. A "frontage" pulmonary blood capillary exposure occurs in the lung of the slug, *Trichotoxon copleyi* (**a**, **b**), in the labyrinthine organ of the catfish, *Clarias mossambicus* (**c**, **d**), and surface of the air bladder of the tilapiine fish, *Alcolapia graham* (**e**, **f**). In these cases, blood capillaries protrude from the surface of the gas exchanger. *Arrows,* blood-gas barrier. **e** (insert)—protrusion of the blood capillaries *(BC)* of the skin of a frog

marine mammals, for example, the manatees and the dugongs (Belanger 1940; Wislocki and Belanger 1940; Henk and Haldiman 1990) where a "double" capillary arrangement similar to that in the embryonic mammalian lung and that in the lungs of lungfishes, amphibians, and reptiles instead exists. In diving animals, the thick interalveolar septa which occur in the lungs may provide support to the blood capillaries when they are subjected to high pressures during deep dives (Welsch and Aschauer 1986). Neotenic (paedomorphic) features were observed in the lungs of the mature naked mole rat, *Heteroccephalus glaber,* by Maina et al. (1992); a double capillary arrangement exists. Compared to the more superior constructions such as the "single" capillary and the "diffuse" capillary systems, the "frontage" and the "double capillary" systems are functionally less efficient since the potentially available respiratory surface is reduced by as much as one half.

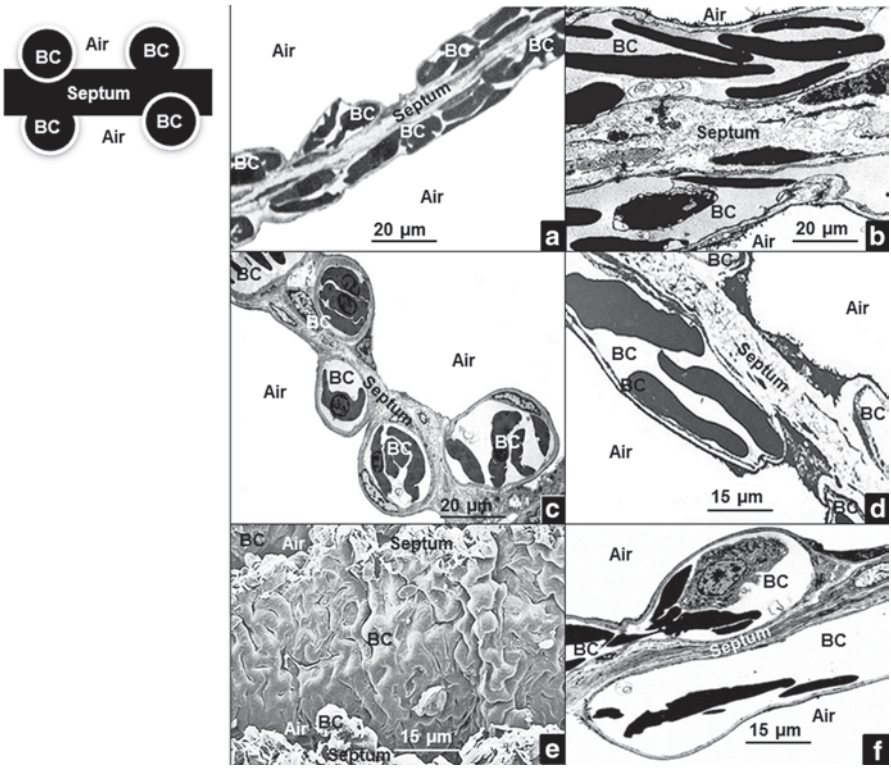


**Fig. 2.13** Exposure of pulmonary capillary blood to air in the amphibian (**a**, **b**) and the reptilian (**b**–**f**) lungs. In the "double" capillary arrangement, the blood capillaries protrude into the air space on one side of the septum. *BC* blood capillary

Capillary loading (CL) is the ratio between the pulmonary capillary blood volume (PCBV) and the respiratory surface area (St), that is, the surface area of the BGB. It is an appropriate indicator of how the PCBV is exposed to air. A low value indicates more optimal exposure of the PCBV to air and consequently more efficient gas exchange. In the avian lungs, CL ranges from 0.7 $cm^3\ m^{-2}$ in the small, extremely energetic African rock martin, *Hirundo fuligula,* to 4 $cm^3\ m^{-2}$ in the non-volant Humboldt penguin, *Spheniscus humboldti* (Maina and King 1987). In the lung of the turtle, *Pseudemys scripta elegans* (Perry 1978), and the lungfish, *Lepidosiren paradoxa* (Hughes and Weibel 1976), CL is 13 $cm^3\ m^{-2}$ and 16 $cm^3\ m^{-2}$, respectively. In the ostrich, *Struthio camelus* (body mass of 45 kg and total lung volume of 1.6 L, a PCBV of 240 $cm^3$ spreads over a surface area of 120 $m^2$; the tissue partitioning (the BGB) is 0.560 µm (*τht;* Fig. 2.11; Maina and Nathaniel 2001).

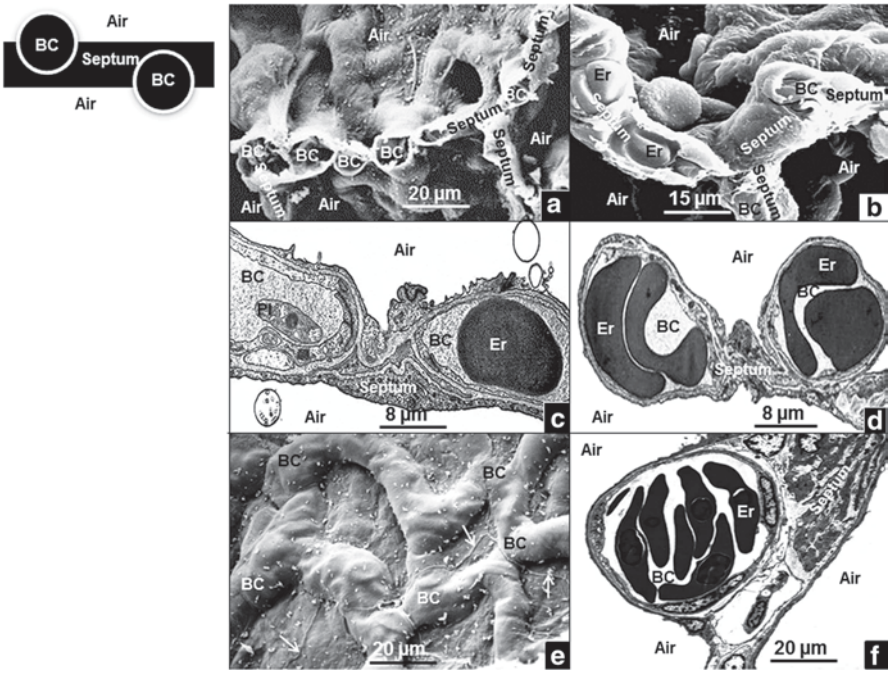


**Fig. 2.14 a–f** Exposure of pulmonary capillary blood to air in the mammalian lung. In the "single" blood capillary arrangement, the blood capillaries distend above the respiratory surface. Blood is better exposed to air on a thinner (respiratory) compared to a thicker (supporting) side of the inter-alveolar septum (**f**). *BC* blood capillary, *Er* erythrocyte, *Pl* blood platelet, arrows (**e**) intercellular functions of the type-I cells

### *2.1.5 Morphometry of the Blood-Gas Barrier*

In the human lung, the epithelial and endothelial cells constitute 25% each, the interstitial cells form 35%, and the interstitial space connective tissue components contribute no more than 15% of the barrier (Weibel 1984). For the domestic fowl, the epithelium forms 12%, the basement membrane 21%, and the endothelium 67% of the BGB (Maina and King 1982). Welsch and Aschauer (1986) attributed the particularly thick BGB and the abundance of connective tissue components in the interstitial space in the penguin lung to its capacity of tolerating high pressures during dives.

Existing data show that among the air-breathing vertebrates, the thickness of the BGB correlates with the metabolic capacities of animal taxa. The BGB becomes thinner from the lungs of amphibians, reptiles, mammals, to birds (Geelhaar and Weibel 1971; Meban 1980; Dubach 1981; Gehr et al. 1981; Maina 1984, 1989a, 2005; Maina and King 1987; Maina et al. 1989; Maina and Nathaniel 2001; Maina and West 2005): In amphibian lungs, the thinnest BGB *(τht)* occurs in the South African crawed toad, *Xenopus laevis* (1.21 µm), while the thickest one is found in

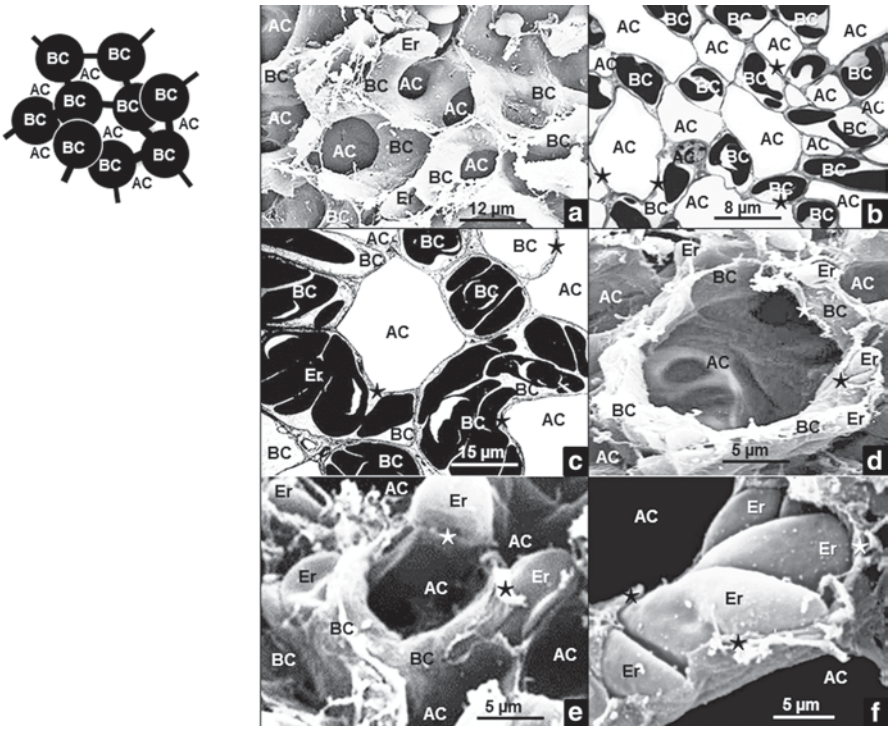


**Fig. 2.15 a–f** Exposure of pulmonary capillary blood to air in bird lungs. In the "diffuse" blood capillary arrangement, blood is exposed to air practically all around the capillary wall. *Stars:* blood-gas barrier, *arrows:* intercellular junctions of the type-1 cells, *BC* blood capillaries, *AC* air capillaries, *Er* erythrocytes

the common newt, *Triturus vulgaris* (2.34 µm); in the reptilian lungs, the thinnest BGB exists in the monitor lizard, *Vanus exanthematicus,* and the Teju, *Tupinambis nigropunctus* (0.46 µm), while the thickest one is found in the Nile crocodile, *Crocodylus niloticus,* and the American alligator, *Alligator mississippiensis* (1.4 µm); in the mammalian lungs, the thinnest BGBs have been reported in the pathologically hyperactive Japanese waltzing mouse, *Mus Wagneri* (0.256 µm), and the very small (1.7 g) shrew, *Suncus minutus* (0.26 µm), while the thickest ones occur in the camel, *Camelus dromedarus,* the giraffe, *Giraffa camelopardalis* (0.6 µm), and the pig, *Sus scrofa* (0.72 µm); in birds, the thinnest BGBs have been reported in the violet-eared hummingbird, *Colibri coruscans* (7.3 g), and the African rock martin, *Hirundo fuligula* (13.7 g; 0.090 µm), while the thickest ones occur in the Humboldt penguin, *Spheniscus humboldti* (0.53 µm), and the ostrich (0.56 µm). In the avian lung, the BGB is 56–67% thinner compared to that in the lungs of the nonflying mammals (Maina et al. 1989). The very small slopes (scaling factors, b) of the allometric equations in birds, bats, and nonflying mammals (Fig. 2.16) show that at least in these taxa, the thicknesses of the BGB are about optimized: The thickness of the BGB increases marginally with increasing body mass. For example, the thickness

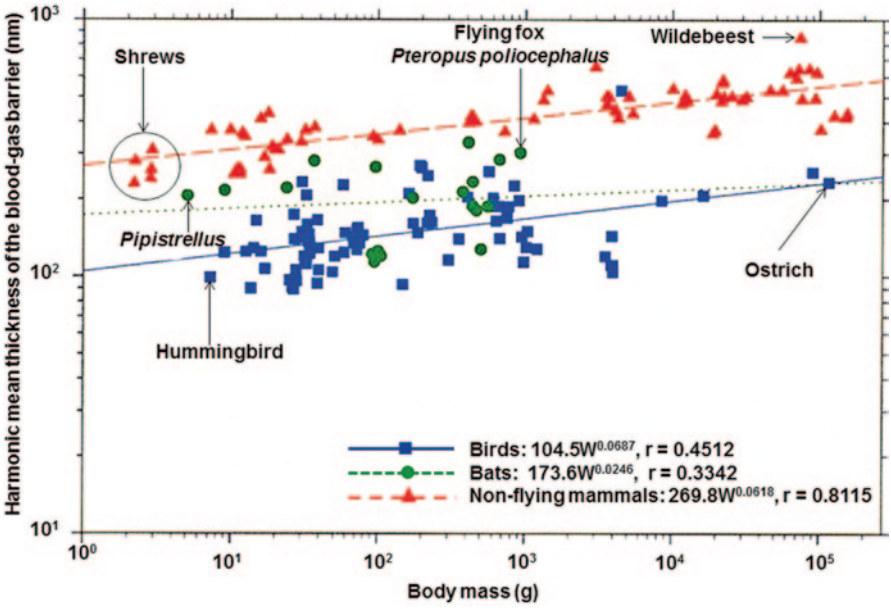


**Fig. 2.16** Allometric comparison of the harmonic mean thicknesses of the blood-gas barrier in birds, bats, and nonflying mammals. Birds have the thinnest blood-gas barriers followed by bats and nonflying mammals. The very small slopes of the regression lines show that the thickness of the blood-gas barrier is greatly optimized. Data for birds are summarized in Maina (2005), those on nonflying mammals in Gehr et al. (1981), and the bat data are found in Maina and King (1984) and Maina et al. (1991)

of the BGB in the minute shrew, *Neomys fodiens* (~2 g), is 0.29 μm (Gehr et al. 1980) compared to that of the lung of the bow-head whale, *Balaena mysticetus* (the colossal body mass was not given by the investigators), which is 0.35 μm (Henk and Haldiman 1990), a factorial difference between the thicknesses of the BGB of only 1.2 while that of body mass is massive; in bats, the thickness of the BGB in the small *Pipistrellus pipistrellus* (5 g) is 0.206 μm (Maina and King 1984) while that of the flying fox, *Pteropus poliocephalus,* weighing 900 g (one of the heaviest species of bats), is 0.303 μm (Maina et al. 1991): The factorial difference between the thicknesses of the BGB of only 1.5 while that for the body masses is ~200; in birds, the thickness of the BGB in a violet-eared hummingbird of a body mass of 7.3 g is 0.09 μm (Dubach 1981) while that in the lung of a young ostrich (45 kg) is 0.560 μm (Maina and Nathaniel 2001): The factorial difference of the thickness of the BGB is ~6 while that of the body mass is ~$6.10^3$.

Comparison of the RSA of the BGB in birds, bats, and nonflying mammals shows that bats have the largest RSA (Fig. 2.17). In smaller birds, the RSA is greater compared to that in smaller mammals while the relationship is reversed in the larger birds and nonflying mammals (Fig. 2.17; Maina 2002, 2006, 2008). The diffusing

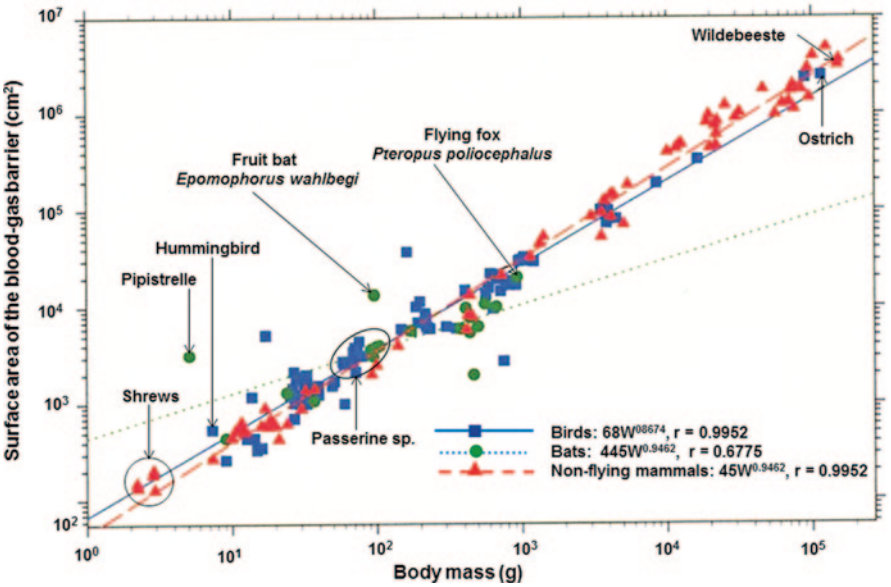


**Fig. 2.17** Allometric comparison of the respiratory surface area of the blood-gas barrier in birds, bats, and nonflying mammals. Small birds have greater respiratory surface area compared to nonflying mammals, and bats have much higher values compared to birds and nonflying mammals. For birds and nonflying mammals, at the higher body mass range, birds have relatively lower respiratory surface areas compared to nonflying mammals. Data for birds are summarized in Maina (2005), those on nonflying mammals in Gehr et al. (1981), and the bat data are found in Maina and King (1984) and Maina et al. (1991)

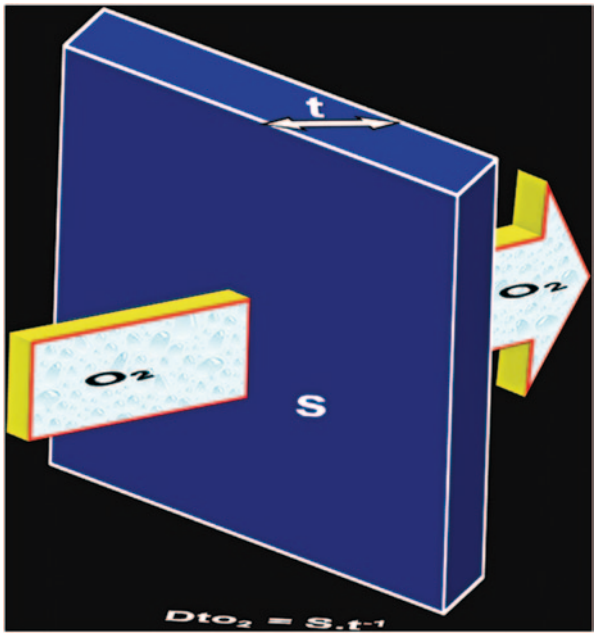


**Fig. 2.18** The diffusing capacity of the blood-gas (tissue) barrier for oxygen ($Dto_2$) correlates directly with the respiratory surface area *(S)* and inversely with the thickness of the barrier *(t)*

capacity of the BGB to oxygen ($Dto_2$) correlates directly with the RSA and inversely with the harmonic mean thickness (*τht;* Fig. 2.18).

**Acknowledgments** Financial support by the National Research Foundation (NRF) of South Africa in the preparation of this chapter is gratefully appreciated. The views expressed here are, however, those of the author and not those of the NRF.

## References

Andrews P. Characteristic surface topographies of cells lining the respiratory tract. Biomed Res. 1981;2:281–8.

Auten RL, Davis JM. Oxygen toxicity and reactive oxygen species: the devil is in the details. Pediatr Res. 2009;66:121–7.

Bakhle YS. Pharmacokinetic function of the lung. In: Junod AF, Haller R, editors. Lung metabolism. London: Academic Press; 1975. pp. 293–9.

Bakhle YS, Vane JR. Metabolic functions of the lung. New York: Marcel Dekker; 1977.

Bartels H, Welsch U. Freeze-fracture study of the turtle lung. 2. Rod shaped particles in the plasma membrane of a mitochondria-rich pneumocyte *Pseudemys (Chrysemys) scripta*. Cell Tissue Res. 1984;236:453–67.

Bastacky J, Lee CY, Goerke J, Koushafar H, Yager D, et al. Alveolar lining layer is thin and continuous: low temperature scanning electron microscopy of rat lung. J Appl Physiol. 1995;79:1615–28.

Becker KL. The endocrine lung. In: Becker KL, Gadzar AF, editors. The endocrine lung in health and disease. Philadelphia: WB Saunders; 1984. pp. 3–46.

Belanger LF. A study of the histological structure of the respiratory portion of the lungs of aquatic mammals. Am J Anat. 1940;67:663–96.

Bernhard W, Gilbert A, Vieten R, Rau G, Hollfred P, et al. Pulmonary surfactant in birds: coping with surface tension in a tubular lung. J Physiol Regul Inter Comp Physiol. 2001a;281:R327–37.

Bernhard W, Postle AD, Rau G, Freihorst J. Pulmonary and gastric surfactants. A comparison of the effect of surface requirements on function and phospholipids composition. Comp Biochem Physiol A Mol Integr Physiol. 2001b;129:173–82.

Brain JD. Environmental lung disease: exposure and mechanisms. Chest. 1996;109:74–8.

Brain JD, Hyg SD. Lung macrophages: how many kinds are there: what do they do? Am Rev Respir Dis. 1988;137:507–9.

Brand M. Mitochondrial biogenesis: processes, regulation, functions and disease. Amsterdam: Elsevier; 2007.

Breeze RG, Wheeldon EB. The cells of the pulmonary airways. Am Rev Respir Dis. 1977;116:705–77.

Burri PH. Morphology and respiratory function of the alveolar unit. Int Arch Allergy Appl Immunol. 1985a;76:2–12.

Burri PH. Development and growth of the human lung. In: Fishman AP, Fisher AB, editors. Handbook of physiology, Sect. 3: the respiratory system. Bethesda: American Physiological Society; 1985b. pp. 1–46.

Cabelli DE. Superoxide dismutases and reactive oxygen species. Brookhaven National Laboratory: Brookhaven, Report No. 2010. BNL-93775-2010-BC.2010. p. 1–32.

Canfield DE. Oxygen: a four year billion history. Princeton (NJ): Princeton University Press; 2014.

Clements JA. Lung surfactant: a personal perspective. Annu Rev Physiol. 1997;59:1–21.

Crapo JD, Barry BE, Gehr P, Bachofen M, Weibel ER. Cell number and cell characteristics of the normal human lung. Am Rev Respir Dis. 1982;126:332–37.

Crapo JD, Young SL, Fram EK, Pinkerton KE, Barry BE, Crapo RO. Morphogenetic characteristics of cells in the alveolar region of mammalian lungs. Am Rev Respir Dis. 1983;128:S42–S6.
Crouch EC, Martin GR, Jerome BS, Laurie GW. Basement membranes. In: Crystal RG, West JB, Weibel ER, Barnes PJ, editors. The lung: scientific foundations. 2nd edn. Philadelphia: Lippincott-Raven; 1997. pp. 769–91.
Cutz E, Jackson A. Neuroepithelial bodies as airway oxygen sensors. Respir Physiol. 1999;115: 201–14.
Daniels CB, Orgeig S, Wilsen J, Nicholas TE. Pulmonary type surfactants in the lungs of terrestrial and aquatic amphibians. Respir Physiol. 1994;95:24–58.
DeFouw DO. Vesicle numerical densities and cellular attenuation: comparisons between endothelium and epithelium of the alveolar septa in normal dog lungs. Anat Rec. 1984;209:77–84.
Dormans JA. The alveolar type-III cell. Lung. 1985;163:327–5.
Dubach M. Quantitative analysis of the respiratory system of the house sparrow, budgerigar, and violet-eared hummingbird. Respir Physiol. 1981;46:43–60.
Effros RM, Mason GR, Silverman P, Reid E, Hukkanen J. Movement of ions and small solutes across endothelium and epithelium of perfused rabbit lungs. J Appl Physiol. 1986;60:100–7.
Fehrenbach H. Alveolar epithelial type-II cell: defender of the alveolus revisted. Respir Res. 2001;2:33–46.
Geelhaar A, Weibel ER. Morphometric estimation of pulmonary diffusion capacity. 3. The effect of increased oxygen consumption in Japanese waltzing mice. Respir Physiol. 1971;11:354–66.
Gehr P, Bachofen M, Weibel ER. The normal human lung: ultrastructure and morphometric estimation of diffusion capacity. Respir Physiol. 1978;32:121–40.
Gehr P, Sehovic S, Burri PH, Claasen H, Weibel ER. The lung of shrews: morphometric estimation of diffusion capacity. Respir Physiol. 1980;44:61–6.
Gehr P, Mwangi DK, Amman A, Maloiy GMO, Taylor CR, Weibel ER. Design of the mammalian respiratory system. V. Scaling morphometric pulmonary diffusing capacity to body mass: wild and domestic animals. Respir Physiol. 1981;44:61–6.
Gomi T. Electron microscopic studies of the alveolar brush cell of the striped snake (*Elaphe quadrivirgata*). J Med Soc, Toho Univ. 1982;29:402–81.
Goniakowska-Witalinska L, Leuweryns JM. Brush cells in the lungs of *Bombina orientalis* (Boulenger) (Anura, Amphibia). J Submicrosc Pathol. 1991;23:123–30.
Goniakowska-Witalinska L, Lauweryns JM, van Ranst L. Neuroepithelial bodies in the lung of *Bombina orientalis*. In: Acker H et al., editor. Chemoreceptors and chemoreceptor reflexes. New York: Plenum; 1990. pp. 111–17.
Graham JB, Dudley R, Agullar NM, Gans C. Implications of the late Paleozoic oxygen pulse for physiology and evolution. Nature. 1995;375:117–20.
Haies D, Gil J, Weibel ER. Morphometric study of rat lung cells. I. Numerical and dimensional characteristics of parenchymal cell population. Am Rev Respir Dis. 1981;123:533–41.
Henk WG, Haldiman JT. Microanatomy of the lung of the bowhead whale, Balaena mysticetus. Anat Rec. 1990;226:187–97.
Hughes GM, Weibel ER. Visualization of layers lining the lung of the South Americanlungfish, *Lepidosiren paradoxa* and a comparison with the frog and the rat. Tissue Cell. 1976;10:343–53.
Jimoh SA, Maina JN. Immuno-localization of type-IV collagen in the blood-gas barrier and the epithelial-epithelial cell connections of the avian lung. Biol Lett. 2013;9(1):20120951. doi:10.1098/rsbl.2012.0951.
Kiama SK, Adekunle JS, Maina JN. Comparative *in vitro* study of interactions between particles and respiratory surface macrophages, erythrocytes and epithelial cells of the chicken and the rat. J Anat. 2008;213:452–63.
Kleiber M. The fire of life: an introduction to animal energetics. New York: Wiley; 1961.
Lane N. Oxygen: the molecule that made the World. Oxford: Oxford University Press; 2002.
Leblond CP, Inoue S. Structure, composition, and assembly of basement membrane. Am J Anat. 1989;185:367–90.
Maina JN. Morphometrics of the avian lung. 3. The structural design of the passerinelung. Respir Physiol. 1984;55:291–309.

Maina JN. The morphometry of the avian lung. In: King AS, McLelland J, editors. Form and function in birds. Vol. 4. London: Academic Press; 1989a. pp. 307–68.
Maina JN. The morphology of a tropical terrestrial slug *Trichotoxon copleyi*-Verdcourt, Mollusca: Gastropoda: Pulmonata. A scanning and transmission electron microscopic study. J Zool, Lond. 1989b;217:355–66.
Maina JN. The morphology of the lung of the East African tree frog *Chiromantis petersi* with observations on the skin and the buccal cavity as secondary gas exchange organs: a TEM and SEM study. J Anat. 1989c;165:29–43.
Maina JN. The morphology of the lung of the black mamba, *Dendroapis polylepis* (Reptilia: Ophidia: Elapidae): a scanning and transmission electron microscopic study. J Anat. 1990;167:31–46.
Maina JN. The gas exchangers: structure, function, and evolution of the respiratory processes. Heidelberg: Springer-Verlag; 1998.
Maina JN. Some recent advances on the study of the functional design of the avian lung: morphologic and morphometric perspectives. Biol Rev. 2002;77:97–152.
Maina JN. The lung-air sac system of birds: development, structure, and function. Heidelberg: Springer; 2005.
Maina JN. Development, structure and function of a novel respiratory organ, the lung-air sac system of birds: to go where no other vertebrate has gone. Biol Rev. 2006;81:545–79.
Maina JN. Functional morphology of the avian respiratory system, the lung-air sac system: efficiency built on complexity. Ostrich. 2008;79:117–32.
Maina JN. Bioengineering aspects in the design of gas exchangers: comparative evolutionary, morphological, functional, and molecular perspectives. Heidelberg: Springer; 2011.
Maina JN, King AS. The thickness of the avian blood-gas barrier: quantitative and quantitative observations. J Anat. 1982;134:553–62.
Maina JN, King AS. The structural functional correlation in the design of the bat lung. A morphometric study. J Exp Biol. 1984;111:43–63.
Maina JN, King AS. A morphometric study of the lung of a humboldt penguin (*Spheniscus humboldti*). Zentralb Vet Med Anat Histol Embryol. 1987;16:293–97.
Maina JN, Maloiy GMO. The morphology of the respiratory organs of the African air-breathing catfish (*Clarias mossambicus*) (Peters): a light- and electron microscopic study, with morphometric observations. J Zool, Lond. 1986;209A:421–45.
Maina JN, Nathaniel C. A qualitative and quantitative study of the lung of an ostrich, *Struthio camelus*. J Exp Biol. 2001;204:2313–30.
Maina JN, West JB. Thin but strong! The dilemma inherent in the structural design of the blood-water/gas barrier: comparative functional and evolutionary perspectives. Physiol Rev. 2005;85:811–44.
Maina JN, King AS, Settle JG. An allometric study of the pulmonary morphometric parameters in birds, with mammalian comparison. Philos Trans R Soc Lond B Biol Sci. 1989;326:1–57.
Maina JN, Thomas SP, Dallas DM. A morphometric study of bats of different size: correlations between structure and function of the chiropteran lung. Philos Trans R Soc Lond B Biol Sci. 1991;333:31–50.
Maina JN, Maloiy GMO, Makanya AN. Morphology and morphometry of the lungs of two East African mole rats, *Tachyoryctes splendens* and *Heterocephalus glaber* (Mammalia, Rodentia). Zoomorphology. 1992;112:167–79.
Meban C. Thicknesses of the air-blood barriers in vertebrate lungs. J Anat. 1980;131:299–307.
Meyrick BL, Reid L. The alveolar brush cell in rat lung - a third pneumocyte. J Ultrastruct Res. 1968;23:71–80.
Nganpiep L, Maina JN. Composite cellular defense stratagem in the avian respiratory system: functional morphology of the free (surface) macrophages and specialized pulmonary epithelia. J Anat. 2002;200:499–516.
Nguyen BT, Peterson PK, Verbrigh HA, Quie PG, Oídla JR. Differences in phagocytosis and killing by alveolar macrophages from humans, rabbits, rats, and hamsters. Infec Immun. 1982;36:504–9.

Orgeig S, Daniels CB. The evolutionary significance of pulmonary surfactant in lungfish(Dipnoi). Am J Respir Cell Mol Biol. 1995;13:161–6.
Pattle RE. The lung surfactant in the evolutionary tree. In: Hughes GM, editor. Respiration ofamphibious vertebrates. London: Academic Press; 1976. pp. 233–55.
Perry SF. Quantitative anatomy of the lungs of the red-eared turtle, *Pseudemys scripta elegans*. Respir Physiol. 1978;35:245–62.
Power JHT, Doyle IR, Davidson K, Nicholas TE. Ultrastructural and protein analysis of surfactant in the Australian lungfish *Neoceratodus forsteri*. J Exp Biol. 1999;202:2543–50.
Rogers RM, Cutz E. Innervation and cytochemistry of the neuroepithelial bodies in the ciliated epithelium of the toad lung, *Bufo marinus*. Cell Tiss Res. 1978;195:395–410.
Rooney SA, Young SL, Mendelson CR. Molecular and cellular processing of lung surfactant. FASEB. 1994;8:957–67.
Schuger L, Skutitz APN, O'Shea S, Chang JF, Varani J. Identification of laminin domains involved in branching morphogenesis: effects of antilaminin monoclonal antibodies on mouse embryonic lung development. Dev Biol. 1991;146:531–41.
Skerret SJ. Host defenses against respiratory infection. Med Clin North Am. 1994;78:941–66.
Sullivan LC, Daniels CB, Phillips ID, Orgeig S, Whitsett JA. Conservation of surfactant protein A: evidence for a single origin for vertebrate pulmonary surfactant. J Mol Evol. 1998;46:131–8.
Vanhecke D, Herrmann G, Graber W, Hillmann-Marti T, Mühlfeld C, Studer D, Ochs M. Lamellar body ultrastructure revisited: high-pressure freezing and cryo-electronmicroscopy of vitreous sections. Histochem Cell Biol. 2010;134:319–26.
Veldhuizen EJ, Haagsman HP. Role of pulmonary surfactant components in surface film formation and dynamics. Biochim Biophys Acta. 2000;1467:255–70.
Veldhuizen R, Nag K, Orgeig S, Possmayer F. The role of lipids in pulmonary surfactant. Biochim Biophys Acta. 1998;1408:90–108. doi:10.1016/S0925-4439(98)00061-1.
Weibel ER. Morphological basis of the alveolar-capillary gas exchange. Physiol Rev. 1973;53: 419–95.
Weibel ER. The pathway for oxygen: structure and function in the mammalian respiratory system. Cambridge (MA): Harvard University Press; 1984.
Weibel ER. Lung cell biology. In: Fishman AP, Fisher AB, editors. Handbook of Physiology;the respiratory system; circulation and non-respiratory functions: Sect. 3, Vol 1, Chap. 2. Bethesda (MD): American Physiological Society; 1985. pp. 47–91.
Weibel ER. Lung morphometry and models in respiratory physiology. In: Chang HK, Paiva M, editors. Respiratory physiology: an analytical approach. New York: Dekker; 1989. pp. 1–55.
Weibel ER. Symmorphosis: on form, and function in shaping life. Cambridge (MA): Harvard University Press; 2000.
Weibel ER. It takes more than cells to make a good lung. Am J Respir Crit Care Med. 2013;187:342–6.
Weibel ER. Morphometric estimation of pulmonary diffusion capacity. I. Model and method. Respir Physiol. 1970/71;11:54–75.
Weibel ER, Bachofen H. The fibre scaffold of lung parenchyma. In: Crystal RG, West JB, Weibel ER, Barnes PJ, editors. The lung: scientific foundations. 2nd edn. Philadelphia: Lippincott-Raven; 1997. pp. 1139–46.
Weibel ER, Knight BW. A morphometric study of the thickness of the pulmonary air-blood barrier. J Cell Biol. 1964;21:367–84.
Welsch U, Aschauer B. Ultrastructural observations on the lung of the emperor penguin (*Aptenodytes forsteri*). Cell Tissue Res. 1986;243:137–44.
West JB. Thoughts on the pulmonary blood-gas barrier. Am J Physiol Lung Cell Mol Physiol. 2003;285:L501–L13.
West JB, Mathieu-Costello O. Strength of the pulmonary blood-gas barrier. Respir Physiol. 1992;88:141–8.
West JB, Mathieu-Costello O. Structure, strength, failure, and remodelling of the pulmonary blood-gas barrier. Annu Rev Physiol. 1999;61:543–72.
Wislocki GB, Belanger LF. The lungs of the larger cetacean compared to those of smaller species. Science. 1940;78:289–97.

# Chapter 3
# Prenatal and Postnatal Development of the Vertebrate Blood–Gas Barrier

**Andrew Makanya and Valentin Djonov**

**Abbreviations**

| | |
|---|---|
| AC | Air capillaries |
| AT-I | Alveolar type I cell |
| AT-II | Alveolar type II cell |
| BC | Blood capillaries |
| bFGF | Basic fibroblast growth factor |
| BGB | Blood gas barrier |
| BMP-4 | Bone morphogenetic protein 4 |
| CCSP | Clara cell secretory protein |
| ECM | Extracellular matrix |
| EGF | Epithelial growth factor |
| EGFR | Epithelial growth factor receptor |
| ELF5 | E74-like factor 5 |
| ErbB | Epidermal growth factor receptor |
| ERK | Extracellular signal-regulated kinases |
| ETS | E26 transformation-specific family |
| FGF | Fibroblast growth factor |
| FGFRs | Fibroblast growth factor receptors |
| FosB | FBJ murine osteosarcoma viral oncogene homolog B |
| FOX | Forkhead orthologs |
| GR | Glucocorticoid receptor |
| HA | Human influenza hemagglutinin |
| HIF2α | Hypoxia inducible factor 2α |

A. Makanya (✉)
Department of Veterinary Anatomy & Physiology, University of Nairobi, Riverside Drive, Chiromo Campus, P. O. Box 30197-00100, Nairobi, Kenya
e-mail: makanya@uonbi.ac.ke

V. Djonov
Institute of Anatomy, University of Bern, Baltzerstrasse 2, 3000 Bern 9, Switzerland
e-mail: valentin.djonov@uana.unibe.ch



A. N. Makanya (ed.), *The Vertebrate Blood-Gas Barrier in Health and Disease,*
DOI 10.1007/978-3-319-18392-3_3

| | |
|---|---|
| HNF-3 | Hepatocyte nuclear factor |
| MPK-1 | Mitogen-activated protein kinase |
| mRNA | Messenger RNA |
| mutHIF2α | Mutant hypoxia inducible factor 2α |
| NICD | Notch intracellular domain |
| PDGF | Platelet derived growth factor |
| RA | Retinoic acid |
| RAR | Retinoic acid receptor |
| Sema3A | Semaphorin 3A |
| Shh | Sonic hedge hog |
| SMA | Smooth muscle actin |
| SP | Surfactant proteins |
| TFG-β | Transforming growth factor β |
| TGF-β1 | Transforming growth factor β1 |
| TTF-1 | Thyroid transcription factor 1 |
| VEGF | Vascular endothelial growth factor |
| WNT5a | Wingless type 5a |

## 3.1 Overview of Vertebrate Lung Development

In vertebrates, the lung originates from the endoderm, as do all the organs of the alimentary tract (Wells and Melton 1999). The vertebrate lung develops from the ventral aspect of the primitive gut, where the endodermal layer forms a laryngotracheal groove, which later forms the lung bud (Burri 1984). This event is species specific and occurs at about embryonic day 9(E9) in mice, E11 in rats, E26 in humans (Schittny and Burri 2008) and E3–E4 in the chick (Bellairs and Osmond 1998). Dichotomous branching of the primitive tubes of the early lung leads to formation of the gas exchange units. In birds, the initial step in dichotomous branching gives rise to the primary bronchi, which proceed to form the mesobronchi. However, development of the subsequent conducting and gas exchange conduits does not follow the dichotomous pattern since the topography of the various categories of secondary bronchi and parabronchi is specific as they arise from prescribed areas and have a specific 3D orientation (Sakiyama et al. 2003; Makanya and Djonov 2008). While a wealth of literature exists on the mammalian lung development, the picture on the avian is just beginning to emerge. In contrast, development in ectotherms appears to have been ignored by contemporary investigators.

## 3.2 Biological Design of the Blood–Gas Barrier in Vertebrates

A detailed description of the structure of the blood–gas barrier (BGB) is provided in Chapter 2. The basic components are the epithelium on the aerated side, the intermediate extracellular matrix (ECM), and the capillary endothelium on the perfused

side. The thickest of the three components in mammals is the ECM (Watson et al. 2007). In the horse and dog, the ECM takes 42 and 40% of the entire thickness, respectively, whereas the epithelium and the endothelium take almost equal proportions at about 28–30% (Watson et al. 2007). In contrast, in the avian lung, the ECM is the thinnest component of the BGB at 17%, while the endothelium is the thickest at 51% (Makanya et al. 2011, 2013). Additionally, the layers of the BGB in the chicken lung are remarkably uniform in thickness over wide regions. The chicken ECM measures about 0.135 μm (arithmetic mean thickness) and mainly comprises of fused basement membranes of the epithelium and endothelium. In ectotherms, the ECM is abundant and lies between the two capillary layers as well as within the BGB, hence they have a thicker BGB than either mammals or birds (Makanya et al. 2013).

The embryonic/prenatal BGB develops in lungs of air-breathing vertebrates, gills of water breathers, skins of percutaneous gas exchangers, and placentas of eutherians and extraembryonic membranes of oviparous vertebrates (Ferner 2011). In each of the aforementioned categories, the BGB is appropriately bioengineered to meet the requirements of oxygen supply and carbon dioxide elimination.

## 3.3 Embryonic Formation of the Blood–Gas Barrier

In vertebrates, formation of the BGB occurs well before birth. In mammals, this process starts at the canalicular stage (see below) while it starts somewhat at mid-incubation in birds. In both mammals and birds, the chronology of events leading to the formation of a functional BGB have been well documented (Makanya 2013). Little is known about the situation in amphibians and reptiles**.**

### *3.3.1 Development of the Mammalian Blood–Gas Barrier*

#### 3.3.1.1 Prenatal Formation of the Mammalian Blood–Gas Barrier

Five lung developmental stages based on the structural alterations of the lung have been recognized in mammals. Chronologically the stages include: (i) embryonic, (ii) pseudoglandular, (iii) canalicular, (iv) saccular, (v) alveolar, and (vi) microvascular maturation (Burri 1984; Makanya et al. 2001; Rackley 2012). The structures of the embryonic stage, namely the laryngotracheal groove and diverticulum as well as the lung bud are all lined with a columnar epithelium derived from the endoderm. The primitive migrating tubes of the pseudoglandular stage are also lined by tall columnar cells that are filled with glycogen (Burri 1984). Towards the end of this stage, cell heights are progressively reduced to form the squamous pneumocytes that participate in formation of the BGB. The latter step signals the onset of canalicular stage, where the first portions of thin BGB are encountered (Burri 1984; Makanya et al. 2001; Schittny and Burri 2008). The columnar epithelial cells are initially converted to primitive pneumoblasts containing numerous lamellar bodies (Makanya et al. 2007b; Fig. 3.1), later differentiating to definitive alveolar type I

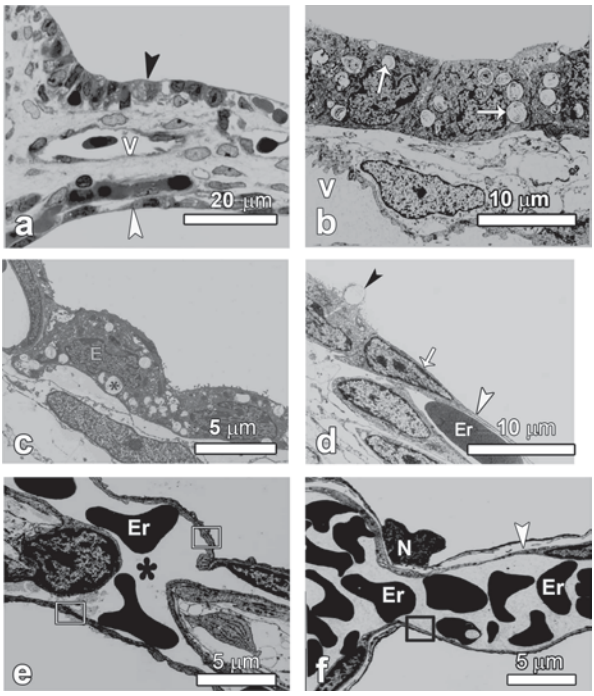


**Fig. 3.1** Micrographs showing the changing pulmonary epithelium in the developing quokka lung. **a** At the canalicular stage, both cuboidal (*dark arrowhead*) and squamous epithelium (*white arrowhead*) are present. At the center of the thick interstitium is a large blood vessel (V). **b** The cuboidal epithelium comprises of cells well-endowed with lamellar bodies (*white arrows*). These cells notably lack microvilli and may be described as pneumoblasts with a potential to form either of the two definitive alveolar pneumocytes (AT-I or AT-II). Note the large blood vessel (V) below the epithelium. **c** and **d** During the saccular stage the epithelial cells (E) possess numerous lamellar bodies (*asterisk*) and have become low cuboidal in the process of conversion to AT-I cells. AT-II cells converting to AT-I pneumocytes appear to do so by extruding entire lamellar bodies (*dark arrowhead* in **d**) and flattening out (*arrow*). Notice the already formed thin BGB (*white arrowhead*) and an erythrocyte (Er) in the conterminous capillary. **e** and **f** Immature interalveolar septa (E) are converted to mature ones through fusion of capillary layers (*asterisk* in **e** and reduction in interstitial tissue. This process starts during the alveolar stage and continues during the microvascular maturation stage. Notice the thin BGB (*square frames*) and the thick side of the BGB in adults (*white arrowhead* in **f**). Erythrocytes (Er) and a nucleus (N) belonging to an AT-I cell are also shown. **a**–**c** are from Makanya et al. 2007, **d** is from Makanya et al. 2001 while **e** and **f** were obtained from Burri et al. 2003, all with permission from the publisher

(AT-I) and alveolar type II (AT-II) cells (Makanya et al. 2001; Schittny and Burri 2003; Makanya et al. 2007b). Majority of these AT-II cells are converted to AT-I cells (Figs. 3.1 and 3.2), which form the internal (alveolar) layer of the BGB (Mercurio and Rhodin 1978; Makanya et al. 2007b).

Conversion of AT-II to AT-I cells entails several events, which include lowering of the intercellular tight junctions between adjacent epithelial cells (Fig. 3.2) such that the apical part of the cells appears to protrude into the lumen (Burri and Weibel 1977). Extrusion of lamellar bodies and subsequent spreading out of the cell

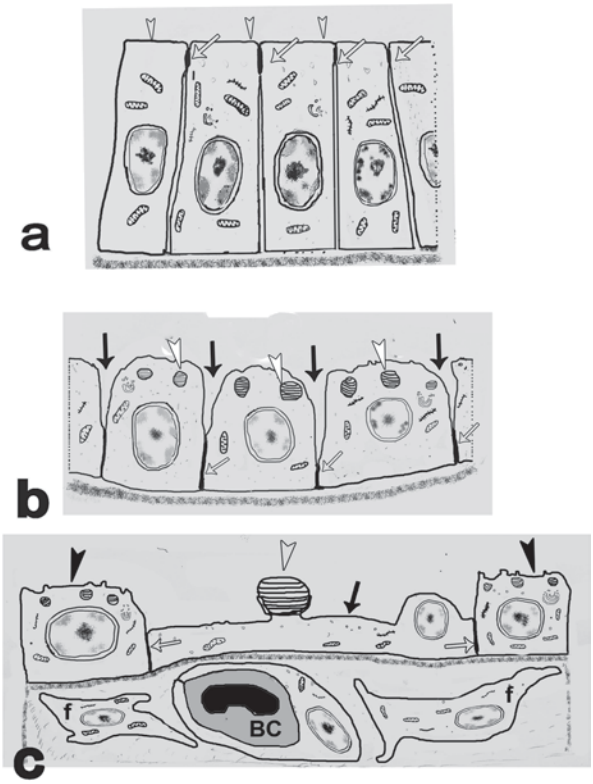


**Fig. 3.2** Schematic diagrams showing the steps in attenuation of the epithelium in the mammalian lung. **a** At the pseudoglandular stage, lung tubules are lined with high columnar homogeneous cells with the intercellular tight junctions placed high up towards the tubular lumen (*white arrows*). Notice also that the cells are devoid of microvilli (*white arrowheads*). **b** As the epithelium attenuates, cells develop lamella bodies (*white arrowheads*) and there is lowering of intercellular tight junctions as the cells become stretched and also the intercellular spaces widen (*black arrows*). The epithelial cells at this stage are no longer columnar but cuboidal and the tight junctions have been lowered to the basal part of the epithelium (*white arrows*). **c** The cells destined to become squamous pneumocytes (AT-I cells) flatten and thin out (*black arrow*), extrude their lamellar bodies (*white arrowhead*) and approximate blood capillaries (BC) so that a thin BGB is formed. Other cells differentiate to ultimate AT-II pneumocytes (*black arrowheads*) and have well-developed lamellar bodies. Notice also the depressed position of tight junctions (*white arrows*). Fibroblasts (f) are abundant in the interstitial tissue and are important in laying down collagen

cytoplasm as the airspaces expand (Figs. 3.1 and 3.2), as well as thinning of the cells and ultimate apposition of the blood capillaries (BC) accomplishes the thin BGB (Makanya et al. 2001; Schittny and Burri 2003; Makanya et al. 2007b).

Apoptosis of putative superfluous AT-II cells (Schittny et al. 1998) and their subsequent clearance by alveolar macrophages creates space for spreading incipient AT-I cells (Makanya et al. 2001). During the saccular stage, the interalveolar septa have a double capillary system, the epithelium is thick and the interstitium is abundant. Progressive diminution of the interstitium, leads to fusion of the two capillary

layers, resulting in a single capillary layer of the mature lung (Makanya et al. 2001; Schittny and Burri 2003). The structure of the BGB in mammals has been described in generous details (West and Mathieu-Costello 1999) and is well presented in Chapter 2. Notably, the BGB needs to be extremely thin while maintaining an appreciable strength to withstand stress failure and an adequate surface area for gas exchange. The basic structure of the BGB has been well conserved through evolution and comprises an epithelium, interstitium, and endothelium (Maina and West 2005).

#### 3.3.1.2 Perinatal Developmental of the Mammalian Blood–Gas Barrier

It is requisite that sufficient maturation of the BGB occurs for neonates to survive. In addition, synthesis and secretion of surfactant together with resorption of the fluid in the airspaces are essential. In rats, arithmetic mean thickness of the BGB decreases from 4.9 ± 0.39 μm at postnatal day 4 (P4) to 1.21 ± 0.13 μm at P60 (Tschanz et al. 2003). The harmonic mean thickness (Thb) of the BGB, however, does not change much decreasing from 0.53 ± 0.004 μm at P4 to 0.51 ± 0.003 at P60. For the quokka wallaby (*Setonix brachyurus*), the only animal so far known to be born with a lung at the canalicular stage (Makanya et al. 2001), Tt decreases from 9.21 ± 2.31 μm at birth to 1.29 ± 0.1 in the adults but without much change in Thb, which decreases from 1.31 ± 0.31 μm in the neonate (Burri et al. 2003) to 1.04 ± 0.11 μm in adults (Burri et al. 2003). It is noteworthy that at the microvascular maturation stage in the quokka, Tt at 2.15 ± 0.84 μm is appreciably greater than in the adults showing that even at this stage, some changes affecting the BGB occur. These changes primarily entail diminution of the interstitium (Fig. 3.1) so that the endothelial layer of the BGB is positioned much closer to epithelial layer.

### *3.3.2 Development of the Avian Blood–Gas Barrier*

Formation of the BGB in birds is somewhat dramatic compared to that in mammals. Lung growth in avians has not been divided into phases but the early stages of formation very closely resemble those in mammals. The laryngotracheal groove is formed from the chick primitive foregut at the pharynx at about 3–4 days of incubation. The laryngotracheal groove evaginates to form a laryngotrachel diverticulum, which morphs into the lung primordia, the lung buds. The proximal part of each lung bud differentiates into the extrapulmonary primary bronchus and the distal one forms the lung. The distal part of the primary bronchus (mesobronchus) grows into the surrounding mesenchyme and gives rise to the secondary bronchi (Bellairs and Osmond 1998). The endoderm forms the epithelium of the airway system while the surrounding mesenchyme gives rise to the muscles, connective tissues, and lymphatics (Bellairs and Osmond 1998). Blood vessels are formed through vasculogenesis (Anderson-Berry et al. 2005) as well as sprouting angiogenesis (Makanya et al. 2007a). Intussusceptive angiogenesis is responsible for augmentation, reorganization, and reorientation of the capillaries that participate in forming the thin BGB and

also accomplishes the architectural pattern characteristic of the parabronchial unit (Makanya and Djonov 2009).

Just like in mammals, lung development in avians follows a strict time plan. Formation of the BGB in the chick lung, for example, is recognizable at about E8 (E24 in the ostrich) when the cuboidal epithelium is converted to a columnar one and by E12 it is stratified and shows signs of losing the apical parts (Fig. 3.3). Interestingly, cells positive for α-SMA align themselves around the parabronchial tubes leaving gaps for migration of the prospective gas exchanging units. Such cells finally become the smooth muscle cells that support the interatrial septa (Fig. 3.3).

The events in the developing lung of the ostrich closely resemble those of the chick but appear to be delayed by twice the duration (incubation period at 40–42 days is twice that of the chicken). The early events in the ostrich have not been documented, but at E24, the lung resembles that of the chick embryo at embryonic day 8 (E8), with parabronchi lined with a cuboidal to tall columnar epithelium. At this stage, some cells are seen to have tapered apical portions and formation of double membranes separating the apical protrusion (aposome) from the basal part of the cell (Fig. 3.4). A detailed description of these cell attenuation processes is only available for the chicken lung (Makanya et al. 2006). A recent report on the ostrich lung indicates that these events are well conserved in the avian species (Makanya et al. 2012). For the aforementioned reason, the description here below is mainly based on the chick lung but is taken to represent the avian species, with specific reference to the ostrich where differences are encountered.

#### 3.3.2.1 Cell Decapitation by Constriction or Squeezing (Peremerecytosis)

Attenuation of epithelial cells by constriction, strangulation, or even squeezing was observed in the avian lung at around mid incubation and the process was dubbed peremerecytosis (Makanya et al. 2006). This process was seen to be either spontaneous or was mediated by neighboring cells. Growth and expansion of epithelial cells leads to competition for space so that the better endowed ones squeeze out the aposomes of their sandwiched neighbors. Presumably, membranes of squeezed out cells adhere with subsequent fusion of the lateral membranes of the squeezed cell and as such the aposome is discharged (Fig. 3.4). Spontaneous strangulation may follow aposome formation and subsequent discharge (Fig. 3.5). Lowering of the tight junctions between adjacent cells is followed by constriction of the cell just above the tight junction (Fig. 3.5). Similar epithelial cell protrusions into the parabronchial lumina were reported in the developing quail lung (Scheuermann et al. 1998) and in the developing chicken lung (Maina 2003) but the precise cellular events were not recognized then. The various morphogenetic events involved in attenuation were presented in details on the chicken lung (Makanya et al. 2006) and similar processes have recently been demonstrated in the ostrich (Makanya et al. 2012).

The mechanisms governing this cell strangulation are not well understood. Progressive thinning of the stalk of the protrusion results in severing of the aposome, a process analogous to aposecretion in exocrine glands (Gesase and Satoh 2003).

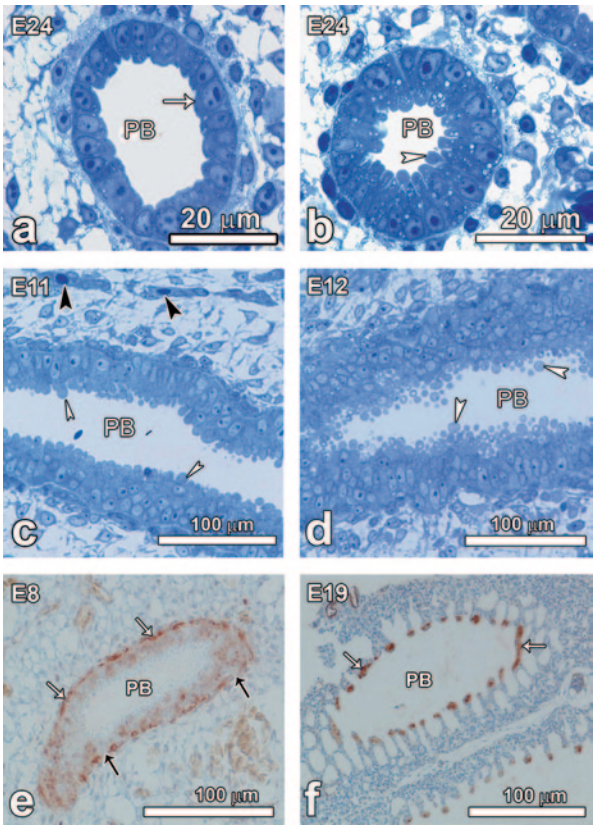


**Fig. 3.3** Micrographs from the developing parabronchial epithelium of the avian lung showing the coarse changes in semithin sections (**a**–**d**) and the pattern of α-smooth muscle actin staining in paraffin sections (**e** and **f**). **a** and **b** A close-up of individual parabronchial tubes (PB) in the ostrich at embryonic day 24 (E24), showing a cuboidal epithelium (*white arrow* in **a**) and a thickened columnar epithelium (*open arrowhead* in **b**). Note that in both cases, the nuclei remain in the basal region; the apical part of the cell becomes elongated thus reducing the parabronchial lumen (PB). **c** and **d** By E11 in the chick embryo **c**, the parabronchial epithelium is pseudostratifed and the apical parts of the cells appear club-like (*white arrowheads* in **c**). By E12, these apical parts are severed such that they appear to fall off into the parabronchial (PB) lumen (*white arrowheads* in **d**). Dark arrowheads in **c** show developing capillaries. **e** and **f** Chick lung stained for alpha-SMA at E8 and E19, respectively. The alpha-SMA positive cells (*white arrows* in **e**) surround the developing parabronchus (PB) while leaving some gaps (*dark arrowheads* in **e**) for future migration of atria. At E19, the atria are well formed and the alpha-SMA positive cells are restricted to the apical parts of the interatrial septa (*white arrows* in **f**). **a** and **b** are modified from Makanya et al. 2012 while **c**–**f** are from Makanya et al. 2011

In aposecretion, however, cell organelles are not discharged. In addition, peremerecytosis occurs in a specific developmental window, unlike aposecretion, which is a continual physiological process. In archetypical aposecretion there is bulging of the apical cytoplasm, absence of subcellular structures, and presence of membrane bound cell fragments, the so-called aposomes (Deyrup-Olsen and Luchtel 1998).

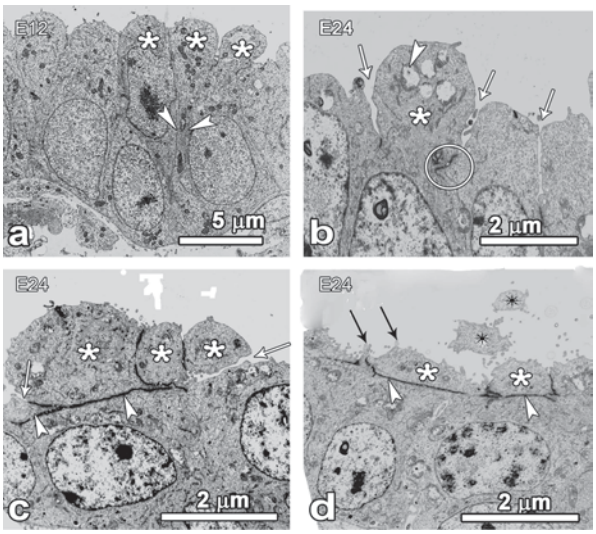


**Fig. 3.4** Transmission electron micrographs showing the various stages in attenuation of the avian air conduit epithelium. **a** At E12 in the chick embryo, apical elongation of the epithelial cells results in formation of aposomes (*stars*) and this precedes constriction of the cell at a region below the aposome (*arrowheads*), due to squeezing by adjacent better endowed cells (Makanya et al. 2006). **b** In the ostrich embryo at E24 several attenuation processes are evident contemporaneously. In addition to development of lamellar bodies (*white arrowhead*), there is lowering of tight junctions (*white arrows and circle*) so that the aposome (*star*) is clearly delineated. **c** and **d** A second method of extruding the aposomes demonstrated in the ostrich involves formation of a double membrane separating the basal part of the cell from the aposome (*arrowheads*). With subsequent unzipping of the double membrane (*white arrows* in **c**), the aposome is discharged. Notice the still attached aposomes (*stars*) and the discharged ones (*asterisks* in **d**). *Black arrows* in **d** indicate microfolds formed after rapture of vesicles. Micrograph a is from Makanya et al. 2006, **b**–**d** are from Makanya et al. 2012

#### 3.3.2.2 Cell Cutting by Cavitation or Double Membrane Unzipping (Secarecytosis)

The processes that lead to cell height reduction through cutting of the epithelial cells during attenuation have been grouped together under one name, *secarecytosis*. The latter terminology was derived from the Greek word "secare," which means "to cut" and describes all the processes that lead to severing of the cell aposome, or cell processes such as microfolds, without causing constriction. Cutting in this case proceeds through intracellular cavitation or double membrane formation (Makanya et al. 2006).

##### 3.3.2.2.1 Cell Cutting by Intracellular Space Formation

The processes involving cell attenuation by cavitation preponderate in the later stages of BGB formation in the avian lung (see reviews; Makanya et al. 2011,

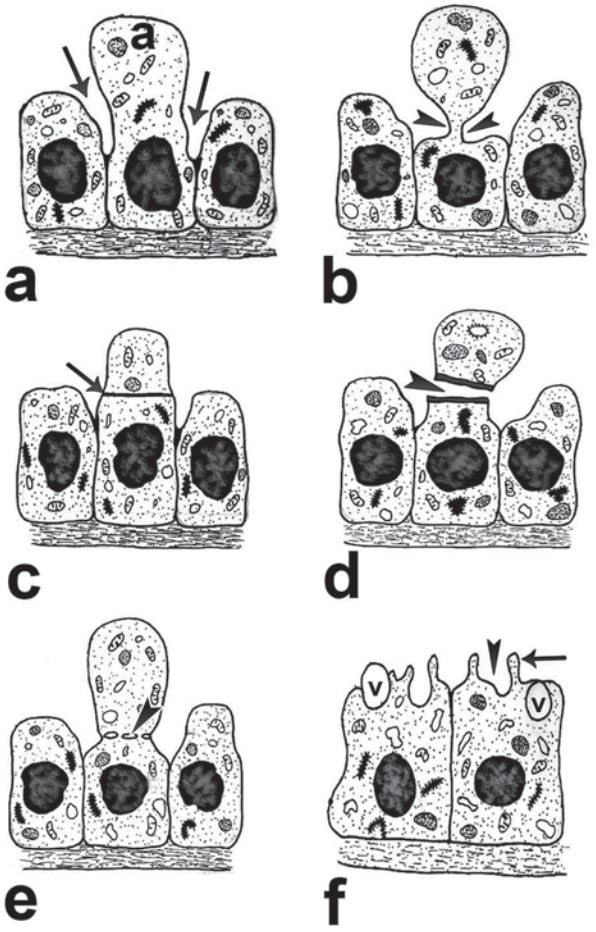


**Fig. 3.5** Schematic diagrams showing the early events that characterize the attenuating epithelia of the formative gas exchange conduits. The diagrams are not drawn to scale. In all cases, BM denotes the basement membrane. **a** and **b** Basal relocation of the intercellular tight junctions (*arrows* in **a**) coupled with apical elongation of the aposome **a** precedes constriction of the cell at a region below the aposome (*see arrowheads* in **b**). This constriction may be spontaneous or may be due to squeezing by adjacent better endowed cells (see also Fig.3.3a). **c** and **d** A second method of extruding aposomes involves formation of a double membrane separating the basal part of the cell from the aposome (*see arrow* in **c**). With subsequent unzipping of the double membrane (*arrowhead* in **b**), the aposome is discharged. Note that the discharged aposome contains major organelles such as mitochondria (*arrows* in **d**). **e** and **f** Formation of cavities, either vesicles (*see arrowhead* in **e**) or vacuoles (V in **f**) may culminate in severing of the components of the apical part of the cell. In secarecytosis by coalescing vesiculation, several such vesicles form at the separation belt, fuse with adjacent cognates and with the basolateral cell membranes thus separating the basal part of the cell from the aposome. Alternatively, such cavities may just fuse with the apical plasma membrane, discharge their contents while remaining as shallow concavities separated by microfolds (*arrowhead* and *arrow* in **f**)

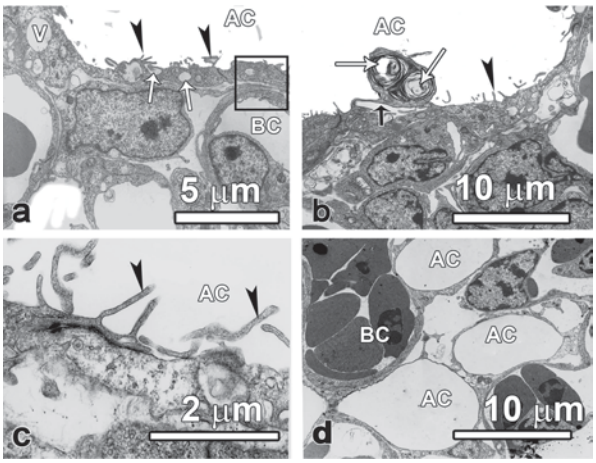


**Fig. 3.6** Transmission electron micrographs illustrating the additional mechanisms of epithelial attenuation that occur later during BGB formation process in the chicken lung. In all cases the rectangular frame delineates the BGB, BC is blood capillary and AC is air capillary. a is modified from (Makanya et al. 2009) while the rest are from (Makanya et al. 2006), with the kind permission of the publishers. **a** and **b** Formation of vacuoles (V) and vesicles (*white arrows*) and their subsequent rapture (fusion with the apical plasmalemma) results in formation of numerous microfolds that resemble microvilli (*black arrowheads*). Notice an aposome with lamellar bodies (*white arrows* in **b**) still attached to the cell apical membrane but still hanging above a vacuole (*black arrow*). **c** and **d** Microfolds formed as a result of vesicle rapture (*black arrowheads*) are severed so that by the time of hatching **d** there are virtually no microfolds. The BGB is similar to that of adults and the air capillaries (AC) were well developed

2013). The events entail either formation of vesicles (endocytic cavities smaller than 50 nm in diameter) or vacuoles (endocytic cavities greater than 50 nm in diameter) in rows beneath the cell portion to be severed (Figs. 3.5 and 3.6). Subsequently, the cavities fuse with their neighboring cognates and then with apicolateral plasma membranes and, in doing so, sever the aposomal projection from the rest of the cell, a process referred to as coalescing vesiculation. The latter processes are most common during attenuation of the low cuboidal epithelium in the formative atria and infundibulae as well as in the migrating air capillaries (AC). Plausibly, the microfolds result from the fusion of contiguous vesicular/vacuolar membranes at the interphase between the aposome and the basal part of the cell, hence discharging the aposome. The process has been referred to as coalescing vesiculation and is contrasted from rapturing vesiculation (Makanya et al. 2006) where vesicles and vacuoles move towards the apical plasma membrane, fuse with it and discharge their entire contents (Figs. 3.5, 3.6 and 3.7). The result is that the vacuole remains like a concavity bounded on either side by a microfold that resembles a microvillus on 2D section (Figs. 3.5, 3.6, and 3.7). If the participating cavities are vacuoles, large folds separating the concavities are formed while rapture of vesicles leaves tiny microfolds resembling microvilli. Whatever the circumstance, there is concomitant reduction in the cell height.

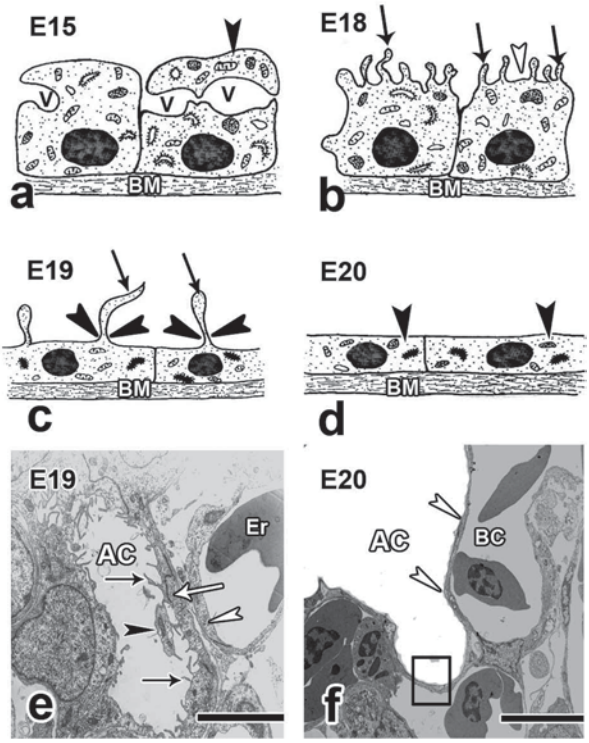


**Fig. 3.7** Schematic diagrams (**a**–**d**) and transmission electron micrographs **e** and **f** showing the terminal mechanisms involved in cell attenuation during the development of a thin blood. **a**–**d** Continued vesiculation and vacuolation, fusion, and rupture of vacuoles and vesicles (v in **a**) results in numerous cell attenuation bodies of varied sizes and shapes (*arrowhead* in **a**) within the air capillaries as well as microfolds of irregular shapes and sizes (*arrows* in **b** and **c**). Later on the microfolds are severed by constriction at the base (*arrowheads* in **c**). Ultimately, smooth surfaced squamous cells are formed (*arrowheads* in **d**) and these constitute the luminal component of the tripartite BGB) by E20. **e** and **f** At E19 much of the BGB attenuation is accomplished so that the mesenchyme is reduced, and the air capillary epithelium (*open arrow* in **e**) is closely opposed to the blood capillary endothelium (*open arrowhead* in **e**). Note that only scanty tiny aposomal bodies (*closed arrowhead* in **e**) and scattered tiny microfolds (*closed arrows* in **e**) are encountered at this stage. At E20, virtually no microfolds are encountered on the air capillary (AC) surface (*see open arrowheads* in **f**), the BGB (*rectangles* in **f**) is thin and composed of an endothelial layer and a fused basement membrane intervening between the endothelium and the epithelium. Figures **e** and **f** are from Makanya and Djonov (2009)

#### 3.3.2.2.2 Cell Cutting by Double Membrane Unzipping

Dark bands become evident across a cell usually between the protruding aposome and the basal part of the cell. The band is believed to be a double plasma membrane, probably associated with cytoskeletal proteins. The double membrane may form the site of separation, whereby the apical part is severed from the basal one (Figs. 3.4 and 3.5). In some cases, the dark band forms a boundary above which the processes of cell cutting such as rapturing vesiculation take place (Fig. 3.4).

## 3.4 Mechanisms of Epithelial Cell Attenuation

The described mechanisms of BGB formation in the mammalian lung appear rather simple. At the transition from the pseudoglandular to the canalicular stage, there is lowering of the tight junctions towards the basal part of the cell, followed by stretching of the cell as the airspaces expand. Additionally, there is summary discharge of lamellar bodies (Figs. 3.1 and 3.2) rather than discharge of the contents (Makanya et al. 2007b). Discharge of surfactant during physiological secretion by type II cells proceeds through tiny pores averaging 0.2–0.4 μm in diameter on the luminal surface of AT-II cells (Kliewer et al. 1985), hence, discharge of entire lamellar bodies during development is an entirely different process (Makanya et al. 2006). The details on how exactly the tight junctions are lowered, how the cells become stretched, or even how entire lamellar bodies are squeezed out are lacking.

The processes and mechanisms involved in attenuation of the epithelium of the avian lung are much more complicated but to a large extent resemble physiological secretory processes. Generally, they lead to progressive reduction in the cell height until the required thickness is attained. The primitive tubes in the developing chicken lung, at E8 are lined by cuboidal epithelium, which converts to high columnar, then becomes stratified columnar with the onset of the first signs of attenuation (Fig. 3.3). Subsequent events lead to dramatic epithelial height reduction and loss of morphological polarization by the processes described above. The latter processes closely resemble aposecretion, where a portion of a cell is discharged with its contents, minus the organelles. However, in this case portions of the cells together with organelles, including mitochondria are discharged. The significance of this loss of cell organelles is unknown.

Events in physiological aposecretion are thought to be mediated through proteins such as myosin and gelsolin (Aumuller et al. 1999) or even actin (Stoeckelhuber et al. 2000). Actin filaments have been demonstrated in the constricting aposome of the attenuating epithelium of the chick embryo lung, plausibly implicating it in the cell cutting process (Makanya et al. 2006). The actin filaments were localized at the level of the aposomal constriction since they are associated with the cell adhesion belt (Volberg et al. 1986) and are also indicators for distal relocation of cell junctions (Makanya et al. 2006). Ingressing embryonic cells have been shown to be capable of changing their shapes, plausibly through actinomyosin contraction (Shook and Keller 2003) with the result that organelles are displaced basally in readiness for migration. Over and above the actinomyosin activity, physiological aposecretion as occurs in the reproductive system, is also driven by hormones and muscarinic receptors (Aumuller et al. 1999).

Smooth muscle cells have been implicated in epithelial cell attenuation in the avian lung. Cells staining positively for alpha smooth muscle actin have been shown to be associated with the developing parabronchi in the chicken lung. Such cells become aligned at the basal aspects of parabronchial epithelial cells delineating gaps through which incipient atria sprout (Fig. 3.3). The α-SMA-positive cells, while playing a role in tubular patterning, may be important in epithelial attenuation. For example, during milk secretion, myoepithelial cells aligned beneath the

secretory epithelium squeeze the epithelial cells above and in so doing, facilitate release of milk into the secretory acinus (Macuhova et al. 2004). Possibly, association of α-SMA-positive cells with the attenuating air conduit epithelium during epithelial attenuation is important in facilitating such aposecretion-like cell processes.

## 3.5 Molecular Regulation of Blood–Gas Barrier Development

The three major components that come into play during formation of the BGB are the endothelium, the interstitium, and the epithelium. A detailed discussion of molecular control of BGB formation needs to consider these coarse components. On the vascular side is the capillary endothelium, the middle layer is the extracellular matrix (ECM) while the epithelium lines the airspaces. A broad-based review of the transcriptional control of lung development was previously provided (Makanya et al. 2013) with the notion that so much is still unknown. Reports by Hebert and Stainier (2011) have provided an updated review of the molecular control of the endothelial cell differentiation, with the notion that VEGF and Notch signaling are important pathways. Angiogenesis itself is a complex process, that has this far attracted intensive investigation and whose molecular control is slowly falling into shape (Carmeliet and Jain 2011). The intermediate layer of the BGB starts by being excessively abundant but is successfully diminished, and in doing so, the capillary endothelium approximates the attenuating gas exchange epithelium. Thus, the genes that come into play in production and regulation of the matrix metalloproteinases, the enzymes that lead to reduction in ECM, are important in lung development (Lee et al. 2011) and BGB formation.

Except in avian species, the lung in vertebrates is known to be compliant. Commonalities would, therefore, be expected in the inauguration and early stages of lung development among all vertebrates with lung compliance. While lung development has been well studied in mammals and to some reasonable extent in birds, not much has been done on the ectotherms. Studies on the reptilian lung (Maina 1989a; Perry 1990; Fleetwood and Munnell 1996) and frog lung (Maina 1989b) as well as fish lung (Maina 2002) indicate that the parenchymal inter-airspace septa do not mature and a double capillary system is retained in these ectotherms, but detailed developmental studies are lacking. While controlling molecules may be similar to those in mammals and birds at the inaugural stages of lung development, subtle differences would be expected when it comes to later stages of lung maturation. Indeed, many of the controlling factors have been highly conserved through evolution (Maina and West 2005; Warburton et al. 2005).

Both intrinsic and extrinsic factors are important in driving lung development. Intrinsic factors include a host of regulatory molecules while extrinsic factors include mechanical forces, the main one being extracellular lung fluid (Demayo et al. 2002). The intrinsic factors include molecules which can be grouped into three classes: transcription factors, e.g., Nkx2.1 also known as thyroid transcription

factor 1 (TTF-1), GATA, and HNF-3; signaling molecules such as FGF, BMP-4, PDGF, Shh, and TGF-β; as well as extracellular matrix proteins and their receptors (Demayo et al. 2002; Shannon and Hyatt 2004; Warburton et al. 2005).

Mechanical forces have been shown to be important for fetal alveolar epithelial cell differentiation in mammals. Such forces emanate from fetal lung movements that propel fluid through incipient air conduits (Schittny et al. 2000).

In mammals, formation of BGB involves the attenuation of the developing lung epithelium, which includes conversion of the columnar epithelium of the pseudoglandular stage to a mainly cuboidal one with lamellar bodies (Fig. 3.1). Subsequently, there is lowering of the intercellular tight junctions, spreading or stretching of the cell, and total extrusion of lamellar bodies (Fig. 3.2) leading to differentiated AT-I and AT-II epithelial cells. Much of the air space surface area is made up of AT-I cells, which constitute a thin squamous epithelium that covers over 90% of the alveolar surface area. AT-II are interspersed throughout the alveoli and are responsible for the production and secretion of pulmonary surfactant; regulation of alveolar fluid homeostasis and differentiation into AT-I cells during lung development and injury.

Genetic control of the specific steps in formation of A-TI and AT-II cell has not been completely elucidated but there are reports on the differentiation of AT-II and AT-I cells and conversion of AT-II to AT-I cells in mammals (Herriges et al. 2012). Some of the molecular signals that have been proposed to be involved in the differentiation of AT-II and AT-I cells are: (i) transcription factors such as thyroid transcription factor-1 (TTF-1) and Forkhead orthologs (FOX), GATA6, HIF2α, Notch, Glucocorticoid receptor (GR), Retinoic acid, and ETS family members; (ii) growth factors such as epithelial growth factor (EGF) and bone morphogenetic protein 4 (BMP4); (iii) other signaling molecules including connexin 43, T1alpha, and semaphorin 3 A. The roles of these molecules in epithelial cell differentiation in the distal lung are briefly described here below.

## *3.5.1 Molecular Regulation of Blood–Gas Barrier Development in Mammals*

### 3.5.1.1 Growth Factors

#### 3.5.1.1.1 ErbB Growth Factor Receptors

The mitogenic activities of growth factors are mediated through tyrosine kinase receptors. Epithelial growth factor receptor (EGFR), a member of the ErbB transmembrane tyrosine kinases and its ligand (EGF), has been shown to be involved in alveolar maturation. EGF deficiency in rats during perinatal development using EGF autoantibodies results in mild respiratory distress syndrome (RDS) and delayed alveolar maturation (Raaberg et al. 1995). Miettinen and co-workers demonstrated that inactivation of EGFR/ErbB1 by gene targeting in mice results in respiratory

failure as a result of impaired alveolarization, including presence of collapsed or thick-walled alveoli (Miettinen et al. 1997). Lungs from EGFR$^{-/-}$ mice show decreased expression of AT-II specification markers, surfactant proteins (SP)—B, C and D (Huang et al. 2012) indicating that EGFR is also important for the AT-II differentiation. Similarly, developing lungs from ErbB4$^{-/-}$ mice exhibited impaired differentiation of AT-II cells with decreased expression of SP-B and reduced surfactant phospholipid synthesis, indicating that ErbB4 plays a role in the differentiation of AT-II cells (Liu et al. 2003). ErbB4 is a member of the ErbB receptor family and has been also shown to be involved in alveolar maturation. Deletion of ErbB4 in mice results in alveolar hypoplasia during development and hyperreactive airways in adults. Recently, it has been demonstrated that EGFR and ErbB4 regulate stretch-induced differentiation of fetal type II epithelial cells via the ERK pathway (Huang et al. 2012).

#### 3.5.1.2 Transforming Growth Factor-β

During lung development, BMP4, a transforming growth factor-β (TGFβ), is highly expressed in the distal tips of the branching lung epithelium, with lower levels in the adjacent mesenchyme. Transgenic mice overexpressing BMP4 throughout the distal epithelium of the lung have significantly smaller than normal lungs, with greatly distended terminal buds at E16.5 and E18.5 and at birth contain large air-filled sacs which do not support normal lung function (Bellusci et al. 1996). In addition, whole-mount in situ hybridization analysis of BMP4 transgenic lungs using probes for the proximal airway marker, CC10 and the distal airway marker, SP-C showed normal AT-II differentiation of bronchiolar club cells but a reduction in differentiated cells, indicating that BMP4 plays an essential role in the alveolar epithelial differentiation (Bellusci et al. 1996). Expression of TGF-b1 arrested lung morphogenesis in the pseudoglandular stage of development, inhibiting synthesis of differentiation-dependent proteins, SP-B, SP-C, and CCSP, and maintaining embryonic patterns of staining for TTF-1 and hepatocyte nuclear factor-3b (HNF-3b) (Zeng 2001).

### *3.5.2 Transcription Factors and Nuclear Receptors*

#### 3.5.2.1 GATA-6 Transcription Factor

Normal expression of GATA-6, a member of the GATA family of zinc finger transcription factors occurs in respiratory epithelial cells throughout lung morphogenesis. Dominant negative GATA-6 expression in respiratory epithelial cells inhibits lung differentiation in late gestation and decreases expression of aquaporin-5, the specific marker for AT-I, and SP (Liu et al. 2003) GATA6 often acts synergistically with TTF-1 (Yang et al. 2003). GATA-6 over-expression in the epithelium was shown to inhibit alveolarization and there was lack of differentiation of AT-II and

AT-I epithelial cells as well as failure of surfactant lipid synthesis (Liu et al. 2003). In mice expressing increased levels of GATA-6 in respiratory epithelial cells, postnatal alveolarization was disrupted, resulting in airspace enlargement.

#### 3.5.2.2 Forkhead Orthologs (FOX) Transcription Factors

Members of the winged-helix/forkhead transcription family, namely Foxa1 and Foxa2, are expressed in the epithelium of the developing mouse lung and are important for epithelial branching and cell differentiation. Previously it has been demonstrated that mice null for Foxa1 do not develop AT-I cells and although the pulmonary capillaries are well developed, no thin BGB is formed (Wan et al. 2005). Foxa2 controls pulmonary maturation at birth. Neonatal mice lacking Foxa2 expression die at birth due to archetypical RDS with all of the morphological, molecular, and biochemical features found in preterm infants, including atelectasis, hyaline membranes, and the lack of pulmonary surfactant lipids and proteins (Wan et al. 2004).

#### 3.5.2.3 Thyroid Transcription Factor (TTF-1)

Lung morphogenesis and epithelial cell differentiation is also mediated through thyroid transcription factor (TTF-1) signaling. TTF1 is a member of the Nkx homeodomain gene family. It is expressed in the forebrain, thyroid gland, and lung. In the lung, TTF-1 plays an essential role in the regulation of lung development. It acts via trans-activating several lung-specific genes including the SP A, B, C, D, and CC10 (Maeda et al. 2007). Mice harboring a null mutation in the TTF-1 gene exhibit severely attenuated lung epithelial development with a dramatic decrease in airway branching. Moreover, lung epithelial cells in these mice lack expression of SP-C suggesting that TTF-1 is the major transcription factor for lung epithelial gene expression (Kimura et al. 1996). Mutations in the human TTF-1 gene have been associated with hypothyroidism and respiratory failure in human infants (Devriendt et al. 1998). TTF-1 was previously demonstrated in the lung of developing turtle (Johnston et al. 2002), showing that to some extent molecular control of differentiation is preserved through evolution.

#### 3.5.2.4 Hypoxia-Inducible Factor 2α (HIF2α)

Levels of oxygen tension are important for lung development. Mild hypoxia induces production of hypoxia inducible factors such as hypoxia-inducible factor 2α (HIF2α), an oxygen-regulated transcription factor. In the lung, HIF2α is primarily expressed in endothelial, bronchial, and AT-II cells. The role of HIF2α in AT-II cells was examined by using transgenic mice that conditionally expressed an oxygen-insensitive mutant of HIF2α (mutHIF2α) in airway epithelial cells during development (Huang et al. 2012). The result was that the mice had dilated alveolar

structures during development and newborn mice died shortly after birth due to respiratory distress. Moreover, in mutHIF2α the distal airspaces of lungs contained abnormal morphology of AT-II cells including an enlarged cytoplasmic appearance, decreased formation of lamellar bodies, and a significantly reduced number of AT-I cells with decreased expression of aquaporin-5. Thus, it was shown that HIF2α negatively regulates the differentiation of AT-II to AT-I cells. Inactivation of HIF2α in transgenic mice resulted in fatal respiratory distress in neonatal mice due to insufficient surfactant production by AT-II cells. Furthermore, lungs of HIF2α$^{-/-}$ mice exhibited disruption of the thinning of the alveolar septa and decreased numbers of AT-II cells, indicating that HIF2α regulates the differentiation of AT-II cells (Compernolle et al. 2002).

#### 3.5.2.5 Notch

In mammals, Notch signaling, is also involved in the differentiation of AT-II cells to AT-I cells. Overexpression of Notch1 in the lung epithelium of transgenic mice constitutively expressing the activation domain (NICD) of Notch 1 in the distal lung epithelium using an SP-C promoter/enhancer prevented the differentiation of the alveolar epithelium (Guseh et al. 2009). Instead of forming saccules, lungs of these mice at E18.5 had cysts. The cysts composed of cells that were devoid of alveolar markers including SP-C, keratin 5, and p63, but expressed some markers of proximal airway epithelium including E-cadherin and Foxa2. Therefore, Notch1 arrests differentiation of alveolar epithelial cells.

The Notch signaling pathway also includes Notch3. The latter factor has also been shown to play a role in alveolar epithelial differentiation. Transgenic mice that constitutively express the activated domain of Notch3 (NICD) in the distal lung epithelium using an SP-C promoter/enhancer were shown to be embryonic lethal at E18.5 and harbored altered lung morphology in which epithelial differentiation into AT-I and AT-II cells was impaired. Metaplasia of undifferentiated cuboidal cells in the terminal airways was also evident (Dang et al. 2003). Constitutive activation of Notch3, therefore, arrests differentiation of distal lung alveolar epithelial cells. Pharmacological approaches to disrupt global Notch signaling in mice lung organ cultures during early lung development resulted in the expanding of the population of the distal lung progenitors, altering morphogenetic boundaries and proximal-distal lung patterning (Tsao et al. 2008).

#### 3.5.2.6 Glucocorticoid Receptor and Retinoic Acid

Endogenous glucocorticoids are important for the maturation of the fetal lung and glucocorticoid actions are mediated via the intracellular GR, a ligand-activated transcriptional regulator. Glucocorticoids act through GR-signaling, a fact demonstrated by using GR-null mice (Cole et al. 2004). The lungs of fetal GR-null mice were found to be hypercellular with blunted septal thinning leading to a sixfold increase in the airway to capillary diffusion distance, and hence failure to develop a

functionally viable BGB (Cole et al. 2004). The phenotype of these mice had a concomitant increase in number of AT-II cells and decreased number of AT-I cells with decreased mRNA expression of AT-I specific markers T1 alpha and aquaporin-5. The conclusion in these studies was that receptor-mediated glucocorticoid signaling facilitates the differentiation of epithelial cells into AT-I cells, but has no effect on AT-II cell differentiation. Therefore, it is plausible to conclude that glucocorticoid action via GR signaling is essential in fetal lung maturation.

In the inaugural stages of lung development, retinoic acid receptor (RAR) signaling is important but its role has a temporal disposition. RAR signaling establishes an initial program that assigns distal cell fate to the prospective lung epithelium. It was demonstrated that down-regulation of RAR signaling in late prenatal period is requisite for eventual formation of mature AT-I and AT-II cells (Wongtrakool et al. 2003; Cole et al. 2004). Furthermore, RAR activation interferes with the proper temporal expression of GATA6, a gene that is critical in regulation of surfactant protein expression in branching epithelial tubules and establishment of the mature AT-II and AT-I cell phenotypes (Keijzer et al. 2001). Later during lung development, RAR signaling is essential for alveolar formation (Massaro et al. 2003).

#### 3.5.2.7 E74-Like Factor 5 (ELF5)

Among the ETS family of transcription factors, E74-like factor 5 (ELF5) is the one conspicuously expressed in the distal lung epithelium during early lung development, and then becomes restricted to proximal airways at the end of gestation. Overexpression of ELF5 specifically in the lung epithelium during early lung development by using a doxycycline inducible HA-tagged ELF5 transgene under the SP-C promoter/enhancer, resulted in disrupted branching morphogenesis and delayed epithelial cell differentiation (Metzger et al. 2008). Lungs overexpressing ELF5 exhibited reduced expression of the distal lung epithelial differentiation marker; SP-C (Metzger et al. 2008), indicating that ELF5 negatively regulates AT-II differentiation.

#### 3.5.2.8 Wnt/β-Catenin

Alveolar epithelial differentiation has also been shown to be regulated by the Wnt/β-catenin pathway. This pathway generally regulates intracellular signaling, gene transcription, and cell proliferation and/or differentiation. Transgenic mice in which β-catenin was deleted in the developing respiratory epithelium, were developed using a doxycycline-inducible conditional system to express Cre recombinase-mediated, homologous recombination strategy (Mucenski et al. 2003). The mice had deficiency of β-catenin in the respiratory epithelium with resultant pulmonary malformations consisting of multiple, enlarged, and elongated bronchiolar tubules and disruption of the formation and differentiation of distal terminal alveolar saccules, including the specification of AT-I and AT-II epithelial cells in the alveolus (Mucenski et al. 2003).

### *3.5.3 Other Molecular Signals*

#### 3.5.3.1 Semaphorin 3A

Generally, Semaphorin 3A mediates cell migration, proliferation, and apoptosis, and inhibits branching morphogenesis. Semaphorin 3A (Sema3A) is a neural guidance cue, but is also involved in maturation and/or differentiation of the distal lung epithelium during development. The latter role was deduced from studies on Sema3A null mice. Lungs from Sema3A$^{-/-}$ embryos had reduced airspace size and thickened alveolar septae with impaired epithelial cell maturation of AT-I and AT-II cells (Becker et al. 2011). Thus, it was plausible to conclude that Sema3A is important in AT-I and AT-II cell differentiation.

#### 3.5.3.2 Connexin 43

Connexins are proteins that participate in formation of gap junctions. Connexin 43, one of the connexin family members, is one of the most studied proteins in organogenesis. It is highly expressed in the distal tip endoderm of the embryonic lung at E11.5 during early lung branching morphogenesis in mice, and after birth connexin-43 is expressed between adjacent AT-I cells in rats and mice. Connexin 43 knockout mice die shortly after birth due to hypoplastic lungs (Nagata et al. 2009). Lungs from connexin 43$^{-/-}$ mice exhibit delayed formation of alveoli, narrow airspaces, and thicker interalveolar septae. In addition, such lungs have decreased mRNA expressions of AT-II specific marker SP-C gene, AT-I specific marker aquaporin-5 and α–SMA actin, and have reduced numbers of AT-I cells (Nagata et al. 2009).

#### 3.5.3.3 T1 Alpha

T1 alpha is a differentiation gene that is only expressed in AT-I cells but not AT-II cells. At the end of gestation, it is highly expressed in the lung. Evidence for participation of T1 alpha in differentiation of AT-I cells but not AT-II cells was adduced from studies on knock-out mice. Homozygous T1 alpha null mice die at birth due to respiratory failure with lungs exhibiting abnormally high expression of proliferation markers in the distal lung (Dang et al. 2003). There is normal differentiation of AT-II cells with normal expression of SP. In contrast, there is lack of differentiation of AT-I cells with decreased expression of aquaporin-5, narrower and irregular airspaces and defective formation of alveolar saccules. Comparison of microarray analyses of T1 alpha$^{-/-}$ and wild-type lungs showed that there was an altered expression of genes including up-regulation of the cell–cell interaction gene ephrinA3 and downregulation of negative regulators of the cell-cycle such as FosB, EGR1, MPK-1, and Nur11 (Millien et al. 2006).

## 3.6 Molecular Regulation of BGB Formation in Other Vertebrates

Among vertebrates, the mammalian lung is the most studied, with an appreciable amount of insights into the avian lung (Makanya et al. 2013). The avian lung differs fundamentally from that of other vertebrates in having noncompliant terminal gas exchange units. The upstream control of lung development that leads to formation of the lung bud may be close or similar among vertebrates, but later events indicate that in avians a totally different process occurs. Formation of the BGB entails migration of BC and the attenuating AC through progressively decreasing interstisium to approximate each other (Makanya et al. 2006; Makanya and Djonov 2009). Elevation of levels of basic FGF (bFGF), VEGF-A, and PDGF-B during the later phase of avian lung microvascular development (Makanya et al. 2007a), indicated that they may be important during interaction of the BC and the AC. In avians, other genes shown to be important in lung development include Wnt5a, Shh, L-CAM, and Fibronectin. In the chicken lung, pulmonary noncanonical Wnt5a uses Ror2 to control patterning of both distal airway and vascular tubulogenesis and perhaps guides the interfacing of the AC with the BC (Loscertales et al. 2008). Lungs with mis/overexpressed Wnt5a were hypoplastic with erratic expression patterns of Shh, L-CAM, fibronectin, VEGF, and Flk1. Wnt5a is important for coordinated development of pulmonary air conduits and vasculature. Wnt5a, plausibly works through fibronectin-mediated VEGF signaling through its regulation of Shh (Loscertales et al. 2008). Mesenchymal–epithelial interactions are important for proper lung differentiation. Fibroblast growth factors (FGFs) and their cognate receptors (FGFRs) are expressed in the developing chick lung and are essential for the epithelial–mesenchymal interactions. It is such interactions that determine epithelial branching (Moura et al. 2011) and may be essential for ultimate BGB establishment.

## 3.7 Conclusion

In this chapter, we have presented an overview of the events that take place during inauguration, prenatal/prehatch as well as postnatal/posthatch development of the vertebrate BGB. The events differ fundamentally between the compliant mammalian lung and the rigid avian lung, as do the events and stages of lung development. This chapter emphasizes formation of the internal (alveolar/air capillary) layer of the BGB. Specific studies on molecular control of BGB formation are lacking but investigations on the AT-II and AT-I cell differentiation in mammals and birds exist. While there is a rapidly increasing wealth of studies on molecular control of the mammalian lung development, very little has been done on the avian species. Studies on the factors guiding and controlling the newly described cell processes of secarecytosis and peremerecytosis in the avian lung are strongly recommended. Furthermore, investigations focused on epithelial attenuation and epithelial–endothelial interactions would illuminate the mechanisms preponderant during BGB formation.

## References

Anderson-Berry A, O'Brien EA, Bleyl SB, Lawson A, Gundersen N, Ryssman D, Sweeley J, Dahl MJ, Drake CJ, Schoenwolf GC, Albertine KH. Vasculogenesis drives pulmonary vascular growth in the developing chick embryo. Dev Dyn. 2005;233:145–53.

Aumuller G, Wilhelm B. Seitz J. Apocrine secretion—fact or artifact? Ann Anat. 1999;181:437–46.

Becker PM, Tran TS, Delannoy MJ, He C, Shannon JM, McGrath-Morrow S. Semaphorin 3A contributes to distal pulmonary epithelial cell differentiation and lung morphogenesis. PLoS ONE. 2011;6:e27449.

Bellairs R, Osmond M. The atlas of chick development. New York: Academic; 1998.

Bellusci S, Henderson R, Winnier G, Oikawa T, Hogan BL. Evidence from normal expression and targeted misexpression that bone morphogenetic protein (Bmp-4) plays a role in mouse embryonic lung morphogenesis. Development. 1996;122:1693–702.

Berg JT, Fu Z, Breen EC, Tran HC, Mathieu-Costello O, West JB. High lung inflation increases mRNA levels of ECM components and growth factors in lung parenchyma. J Appl Physiol. 1997;83:120–8.

Birks EK, Mathieu-Costello O, Fu Z, Tyler WS, West JB. Comparative aspects of the strength of pulmonary capillaries in rabbit, dog, and horse. Respir Physiol. 1994;97:235–46.

Birks EK, Mathieu-Costello O, Fu Z, Tyler WS, West JB. Very high pressures are required to cause stress failure of pulmonary capillaries in thoroughbred racehorses. J Appl Physiol. 1997;82:1584–92.

Burri PH. Fetal and postnatal development of the lung. Annu Rev Physiol. 1984;46:617–28.

Burri PH, Weibel ER. Ultrastructure and morphometry of the developing lung. In: Hudson WA, editor. Development of the lung. New York: Mercwel Dekker; 1977; p. 215–268.

Burri PH, Haenni B, Tschanz SA, Makanya AN. Morphometry and allometry of the postnatal marsupial lung development: an ultrastructural study. Respir Physiol Neurobiol. 2003;138(2–3):309–24.

Carmeliet P, Jain RK. Molecular mechanisms and clinical applications of angiogenesis. Nature. 2011;473:298–307.

Cole TJ, Solomon NM, Van Driel R, Monk JA, Bird D, Richardson SJ, Dilley RJ, Hooper SB. Altered epithelial cell proportions in the fetal lung of glucocorticoid receptor null mice. Am J Respir Cell Mol Biol. 2004;30:613–9.

Compernolle V, Brusselmans K, Acker T, Hoet P, Tjwa M, Beck H, Plaisance S, Dor Y, Keshet E, Lupu F, Nemery B, Dewerchin M, Van Veldhoven P, Plate K, Moons L, Collen D, Carmeliet P. Loss of HIF-2alpha and inhibition of VEGF impair fetal lung maturation, whereas treatment with VEGF prevents fatal respiratory distress in premature mice. Nat Med. 2002;8:702–10.

Dang TP, Eichenberger S, Gonzalez A, Olson S, Carbone DP. Constitutive activation of Notch3 inhibits terminal epithelial differentiation in lungs of transgenic mice. Oncogene. 2003;22:1988–97.

Demayo F, Minoo P, Plopper CG, Schuger L, Shannon J, Torday JS. Mesenchymal–epithelial interactions in lung development and repair: are modeling and remodeling the same process? Am J Physiol Lung Cell Mol Physiol. 2002;283:L510–7.

Devriendt K, Vanhole C, Matthijs G, de Zegher F. Deletion of thyroid transcription factor-1 gene in an infant with neonatal thyroid dysfunction and respiratory failure. N Engl J Med. 1998;338:1317–8.

Deyrup-Olsen I, Luchtel DL. Secretion of mucous granules and other membrane-bound structures: a look beyond exocytosis. Int Rev Cytol. 1998;183:95–141.

Fernandes MN, da Cruz AL, da Costa OT, Perry SF. Morphometric partitioning of the respiratory surface area and diffusion capacity of the gills and swim bladder in juvenile Amazonian air-breathing fish, *Arapaima gigas*. Micron. 2012;43:961–70.

Fleetwood JN, Munnell JF. Morphology of the airways and lung parenchyma in hatchlings of the loggerhead sea turtle, *Caretta caretta*. J Morphol. 1996;227:289–304.

Gehr P, Bachofen M, Weibel ER. The normal human lung: ultrastructure and morphometric estimation of diffusion capacity. Respir Physiol. 1978;32:121–40.

Gesase AP, Satoh Y. Apocrine secretory mechanism: recent findings and unresolved problems. Histol Histopathol. 2003;18:597–608.

Guseh JS, Bores SA, Stanger BZ, Zhou Q, Anderson WJ, Melton DA, Rajagopal J. Notch signaling promotes airway mucous metaplasia and inhibits alveolar development. Development. 2009;136:1751–9.

Henk WG, Haldiman JT. Microanatomy of the lung of the bowhead whale *Balaena mysticetus*. Anat Rec. 1990;226:187–97.

Herbert SP, Stainier DYR. Molecular control of endothelial cell behaviour during blood vessel morphogenesis. Nat Rev Mol Cell Biol. 2011;12:551–64.

Herriges JC, Yi L, Hines EA, Harvey JF, Xu G, Gray PA, Ma Q, Sun X. Genome-scale study of transcription factor expression in the branching mouse lung. Dev Dyn. 2012;241(9):1432–53.

Hopkins SR, Schoene RB, Henderson WR, Spragg RG, Martin TR, West JB. Intense exercise impairs the integrity of the pulmonary blood–gas barrier in elite athletes. Am J Respir Crit Care Med. 1997;155:1090–4.

Huang Z, Wang Y, Nayak PS, Dammann CE, Sanchez-Esteban J. Stretch-induced fetal type II cell differentiation is mediated via ErbB1–ErbB4 interactions. J Biol Chem. 2012a;287:18091–102.

Huang Y, Kempen MB, Munck AB, Swagemakers S, Driegen S, Mahavadi P, Meijer D, van IW, van der Spek P, Grosveld F, Gunther A, Tibboel D, Rottier RJ. Hypoxia-inducible factor 2-alpha plays a critical role in the formation of alveoli and surfactant. Am J Respir Cell Mol Biol. 2012b;46:224–32.

Johnston SD, Daniels CB, Cenzato D, Whitsett JA, Orgeig S. The pulmonary surfactant system matures upon pipping in the freshwater turtle *Chelydra serpentina*. J Exp Biol. 2002;205:415–25.

Keijzer R, van Tuyl M, Meijers C, Post M, Tibboel D, Grosveld F, Koutsourakis M. The transcription factor GATA6 is essential for branching morphogenesis and epithelial cell differentiation during fetal pulmonary development. Development. 2001;128:503–11.

Kimura S, Hara Y, Pineau T, Fernandez-Salguero P, Fox CH, Ward JM, Gonzalez FJ. The T/ebp null mouse: thyroid-specific enhancer-binding protein is essential for the organogenesis of the thyroid, lung, ventral forebrain, and pituitary. Genes Dev. 1996;10:60–9.

Kliewer M, Fram EK, Brody AR, Young SL. Secretion of surfactant by rat alveolar type II cells: morphometric analysis and three-dimensional reconstruction. Exp Lung Res. 1985;9:351–61. (1996).

Lee Y, Fryer JD, Kang H, Crespo-Barreto J, Bowman AB, Gao Y, Kahle JJ, Hong JS, Kheradmand F, Orr HT, Finegold MJ, Zoghbi HY. ATXN1 protein family and CIC regulate extracellular matrix remodeling and lung alveolarization. Dev Cell. 2011;21:746–57.

Liu C, Ikegami M, Stahlman MT, Dey CR, Whitsett JA. Inhibition of alveolarization and altered pulmonary mechanics in mice expressing GATA-6. Am J Physiol Lung Cell Mol Physiol. 2003;285:L1246–54.

Loscertales M, Mikels AJ, Hu JK, Donahoe PK, Roberts DJ. Chick pulmonary Wnt5a directs airway and vascular tubulogenesis. Development. 2008;135:1365–76.

Macuhova J, Tancin V, Bruckmaier RM. Effects of oxytocin administration on oxytocin release and milk ejection. J Dairy Sci. 2004;87:1236–44.

Maeda Y, Dave V, Whitsett JA. Transcriptional control of lung morphogenesis. Physiol Rev. 2007;87:219–44.

Maina JN. The morphology of the lung of the black mamba *Dendroaspis polylepis* (Reptilia: Ophidia: Elapidae). A scanning and transmission electron microscopic study. J Anat. 1989a;167:31–46.

Maina JN. The morphology of the lung of the East African tree frog *Chiromantis petersi* with observations on the skin and the buccal cavity as secondary gas exchange organs: a TEM and SEM study. J Anat. 1989b;165:29–43.

Maina JN. Structure, function and evolution of the gas exchangers: comparative perspectives. J Anat. 2002;201:281–304.

Maina JN. A systematic study of the development of the airway (bronchial) system of the avian lung from days 3 to 26 of embryogenesis: a transmission electron microscopic study on the domestic fowl, *Gallus gallus* variant domesticus. Tissue Cell. 2003;35:375–91.

Maina JN, King AS. A morphometric study of the lung of a Humboldt penguin (*Sphenicus humboldti*). Anat Histol Embryol. 1987;16:293–7.

Maina JN, King AS. The lung of the emu, *Dromaius novaehollandiae*: a microscopic and morphometric study. J Anat. 1989;163:67–73.

Maina JN, Nathaniel C. A qualitative and quantitative study of the lung of an ostrich, *Struthio camelus*. J Exp Biol. 2001;204:2313–30.

Maina JN, West JB. Thin and strong! The bioengineering dilemma in the structural and functional design of the blood–gas barrier. Physiol Rev. 2005;85:811–44.

Maina JN, Thomas SP, Hyde DM. A morphometric study of the lungs of different sized bats: correlations between structure and function of the chiropteran lung. Philos Trans R Soc Lond B Biol Sci. 1991;333:31–50.

Makanya AN, Djonov V. Development and spatial organization of the air conduits in the lung of the domestic fowl, *Gallus gallus* variant domesticus. Microsc Res Tech. 2008;71:689–702.

Makanya AN, Djonov V. Parabronchial angioarchitecture in developing and adult chickens. J Appl Physiol. 2009;106:1959–69.

Makanya AN, Sparrow MP, Warui CN, Mwangi DK, Burri PH. Morphological analysis of the postnatally developing marsupial lung: the quokka wallaby. Anat Rec. 2001;262:253–65.

Makanya AN, Hlushchuk R, Duncker HR, Draeger A, Djonov V. Epithelial transformations in the establishment of the blood–gas barrier in the developing chick embryo lung. Dev Dyn. 2006;235:68–81.

Makanya AN, Hlushchuk R, Baum O, Velinov N, Ochs M, Djonov V. Microvascular endowment in the developing chicken embryo lung. Am J Physiol Lung Cell Mol Physiol. 2007a;292:L1136–46.

Makanya AN, Tschanz SA, Haenni B, Burri PH. Functional respiratory morphology in the newborn quokka wallaby (*Setonix brachyurus*). J Anat. 2007b;211:26–36.

Makanya AN, Hlushchuk R, Djonov V. The pulmonary blood–gas barrier in the avian embryo: inauguration, development and refinement. Respir Physiol Neurobiol. 2011;178:30–8.

Makanya AN, Koller T, Hlushchuk R, Djonov V. Pre-hatch lung development in the ostrich. Respir Physiol Neurobiol. 2012;180:183–92.

Makanya A, Anagnostopoulou A, Djonov V. Development and remodeling of the vertebrate blood–gas barrier. Biomed Res Int. 2013;2013:101597.

Massaro GD, Massaro D, Chambon P. Retinoic acid receptor-alpha regulates pulmonary alveolus formation in mice after, but not during, perinatal period. Am J Physiol Lung Cell Mol Physiol. 2003;284:L431–L3.

Meban C. Thickness of the air–blood barriers in vertebrate lungs. J Anat. 1980;131:299–307.

Mercurio AR, Rhodin JA. An electron microscopic study on the type I pneumocyte in the cat: prenatal morphogenesis. J Morphol. 1978;156:141–55.

Metzger DE, Stahlman MT, Shannon JM. Misexpression of ELF5 disrupts lung branching and inhibits epithelial differentiation. Dev Biol. 2008;320:149–60.

Miettinen PJ, Warburton D, Bu D, Zhao JS, Berger JE, Minoo P, Koivisto T, Allen L, Dobbs L, Werb Z, Derynck R. Impaired lung branching morphogenesis in the absence of functional EGF receptor. Dev Biol. 1997;186:224–36.

Millien G, Spira A, Hinds A, Wang J, Williams MC, Ramirez MI. Alterations in gene expression in T1 alpha null lung: a model of deficient alveolar sac development. BMC Dev Biol. 2006;6:35.

Moura RS, Coutinho-Borges JP, Pacheco AP, Damota PO, Correia-Pinto J. FGF signaling pathway in the developing chick lung: expression and inhibition studies. PLoS ONE. 2011;6:e17660.

Mucenski ML, Wert SE, Nation JM, Loudy DE, Huelsken J, Birchmeier W, Morrisey EE, Whitsett JA. Beta-catenin is required for specification of proximal/distal cell fate during lung morphogenesis. J Biol Chem. 2003;278:40231–8.

Nagata K, Masumoto K, Esumi G, Teshiba R, Yoshizaki K, Fukumoto S, Nonaka K, Taguchi T. Connexin43 plays an important role in lung development. J Pediatr Surg. 2009;44:2296–301.

Parker JC, Breen EC, West JB. High vascular and airway pressures increase interstitial protein mRNA expression in isolated rat lungs. J Appl Physiol. 1997;83:1697–705.

Perry SF. Gas exchange strategy in the Nile crocodile: a morphometric study. J Comp Physiol B: Biochen Syst Eviron Physiol. 1990;159:761–9.

Raaberg L, Nexo E, Jorgensen PE, Poulsen SS, Jakab M. Fetal effects of epidermal growth factor deficiency induced in rats by autoantibodies against epidermal growth factor. Pediatr Res. 1995;37:175–81.

Ravikumar P, Bellotto DJ, Johnson RL Jr, Hsia CC. Permanent alveolar remodeling in canine lung induced by high-altitude residence during maturation. J Appl Physiol. 2009;107:1911–7.
Sakiyama J, Yamagishi A, Kuroiwa A. Tbx4-Fgf10 system controls lung bud formation during chicken embryonic development. Development. 2003;130:1225–34.
Scheuermann DW, Klika E, de Groodt-Lasseel MH, Bazantova I, Switka A. The development and differentiation of the parabronchial unit in quail (*Coturnix coturnix*). Eur J Morphol. 1998;36:201–15.
Schittny JC, Burri PH. Morphogenesis of the mammalian lung: aspects of structure and extracellular matrix. In: Massaro JD, Massaro G, Chambon P, editors. Lung development and regeneration. New York: Mercel Dekker; 2003. p. 275–317.
Schittny JC, Burri PH. Development and growth of the lung. In: Fishman AP, Elias JA, A. FJ, Grippi MA, Kaiser LR, Senior RM, editors. Fishman's pulmonary diseases and disorders. New-York: McGraw-Hill; 2008. p. 91–114.
Schittny JC, Djonov V, Fine A, Burri PH. Programmed cell death contributes to postnatal lung development. Am J Respir Cell Mol Biol. 1998;18:786–93.
Schittny JC, Miserocchi G, Sparrow MP. Spontaneous peristaltic airway contractions propel lung liquid through the bronchial tree of intact and fetal lung explants. Am J Respir Cell Mol Biol. 2000;23:11–8.
Shannon JM, Hyatt BA. Epithelial–mesenchymal interactions in the developing lung. Annu Rev Physiol. 2004;66:625–45.
Shook D, Keller R. Mechanisms, mechanics and function of epithelial–mesenchymal transitions in early development. Mech Dev. 2003;120:1351–83.
Stoeckelhuber M, Sliwa A, Welsch U. Histo-physiology of the scent-marking glands of the penile pad, anal pouch, and the forefoot in the aardwolf (*Proteles cristatus*). Anat Rec. 2000;259:312–26.
Stoeckelhuber M, Stoeckelhuber BM, Welsch U. Human glands of Moll: histochemical and ultrastructural characterization of the glands of moll in the human eyelid. J Invest Dermatol. 2003;121:28–36.
Tsao PN, Chen F, Izvolsky KI, Walker J, Kukuruzinska MA, Lu J, Cardoso WV. Gamma-secretase activation of notch signaling regulates the balance of proximal and distal fates in progenitor cells of the developing lung. J Biol Chem. 2008;283:29532–44.
Tschanz SA, Makanya AN, Haenni B, Burri PH. Effects of neonatal high-dose short-term glucocorticoid treatment on the lung: a morphologic and morphometric study in the rat. Pediatr Res. 2003;53:72–80.
Tsukimoto K, Mathieu-Costello O, Prediletto R, Elliott AR, West JB. Ultrastructural appearances of pulmonary capillaries at high transmural pressures. J Appl Physiol. 1991;71:573–82.
Volberg T, Geiger B, Kartenbeck J, Franke WW. Changes in membrane-microfilament interaction in intercellular adherens junctions upon removal of extracellular $Ca^{2+}$ ions. J Cell Biol. 1986;102:1832–42.
Wan H, Xu Y, Ikegami M, Stahlman MT, Kaestner KH, Ang SL, Whitsett JA. Foxa2 is required for transition to air breathing at birth. Proc Natl Acad Sci U S A. 2004;101:14449–54.
Wan H, Dingle S, Xu Y, Besnard V, Kaestner KH, Ang SL, Wert S, Stahlman MT, Whitsett JA. Compensatory roles of Foxa1 and Foxa2 during lung morphogenesis. J Biol Chem. 2005;280:13809–16.
Warburton D, Bellusci S, De Langhe S, Del Moral PM, Fleury V, Mailleux A, Tefft D, Unbekandt M, Wang K, Shi W. Molecular mechanisms of early lung specification and branching morphogenesis. Pediatr Res. 2005;57:26R–37R.
Watson RR, Fu Z, West JB. Morphometry of the extremely thin pulmonary blood–gas barrier in the chicken lung. Am J Physiol Lung Cell Mol Physiol. 2007;292:L769–77.
Weibel ER. The pathway for oxygen. Cambridge: Harvard University Press.
Wells JM, Melton DA. Vertebrate endoderm development. Annu Rev Cell Dev Biol. 1999;15:393–410. (1984).
West JB. Invited review: pulmonary capillary stress failure. J Appl Physiol. 2000;89:2483–9. (discussion 2497).

West JB. Comparative physiology of the pulmonary blood–gas barrier: the unique avian solution. Am J Physiol Regul Integr Comp Physiol. 2009;297:R1625–34.
West JB, Mathieu-Costello O. Pulmonary blood–gas barrier—a physiological dilemma. News Physiol Sci. 1993;8:249–53.
West JB, Mathieu-Costello O. Stress-induced injury of pulmonary capillaries. Proc Assoc Am Physicians. 1998;110:506–12.
West JB, Mathieu-Costello O. Structure, strength, failure, and remodeling of the pulmonary blood–gas barrier. Annu Rev Physiol. 1999;61:543–72.
Wongtrakool C, Malpel S, Gorenstein J, Sedita J, Ramirez MI, Underhill TM, Cardoso WV. Down-regulation of retinoic acid receptor alpha signaling is required for sacculation and type I cell formation in the developing lung. J Biol Chem. 2003;278:46911–8.
Yang L, Naltner A, Yan C. Overexpression of dominant negative retinoic acid receptor alpha causes alveolar abnormality in transgenic neonatal lungs. Endocrinology. 2003;144:3004–11.

# Chapter 4
# Molecular Mechanisms Regulating the Pulmonary Blood–Gas Barrier

**David C. Budd, Victoria J. Burton and Alan M. Holmes**

## 4.1 The Structure of Junctional Complexes Regulating Barrier Function in the Lung

Endothelial and epithelial cells of the pulmonary blood–gas barrier (BGB) regulate the movement of liquids, solutes, macromolecules, and cells from the airways and bloodstream into the lung interstitium via the process of transcellular and paracellular transport. The paracellular transport mechanism is governed by a number of proteineaceous complexes that form between adjacent cells which comprise tight junctions (TJs) and adherens junctions (AJs) that are found in both epithelial and endothelial cell monolayers (for review see, Vandenbroucke et al. (2008)) and desmosomes that are unique to the epithelium (for review see, Kowalczyk and Green (2013)).

Although TJs (also known as *Zonula Occludins*), and AJs (also known as *Zonula Addherens*) junctional complexes are present on endothelial and epithelial lung barriers, the distribution and frequency of occurrence of the junctions differ between the lung epithelium and endothelium. For instance, TJs are exclusively located at the apical-most region of the lateral plasma membranes of epithelial monolayers (Farquhar and Palade 1963), whereas their localisation in endothelial cell monolayers are

The viewpoint contained herein reflects the author's personal opinions and does not necessarily reflect the viewpoint of GlaxoSmithKline.

D. C. Budd (✉)
GlaxoSmithKline, Fibrosis Discovery Performance Unit, Respiratory TAU, Medicines Research Centre, Gunnels Wood Road Stevenage, Hertfordshire SG1 2NY, UK
e-mail: david.c.budd@gsk.com

V. J. Burton
Therapeutics Review Team, MRC Technology, 7– 12 Tavistock Square, London WC1H 9LT, UK
e-mail: victoria.burton@tech.mrc.ac.uk

A. M. Holmes
Centre for Rheumatology and Connective Tissue Diseases, Department of Inflammation, UCL—Royal Free Campus, Rowland Hill Street, London NW3 2PF, UK
e-mail: alan.holmes@ucl.ac.uk



A. N. Makanya (ed.), *The Vertebrate Blood-Gas Barrier in Health and Disease,*
DOI 10.1007/978-3-319-18392-3_4

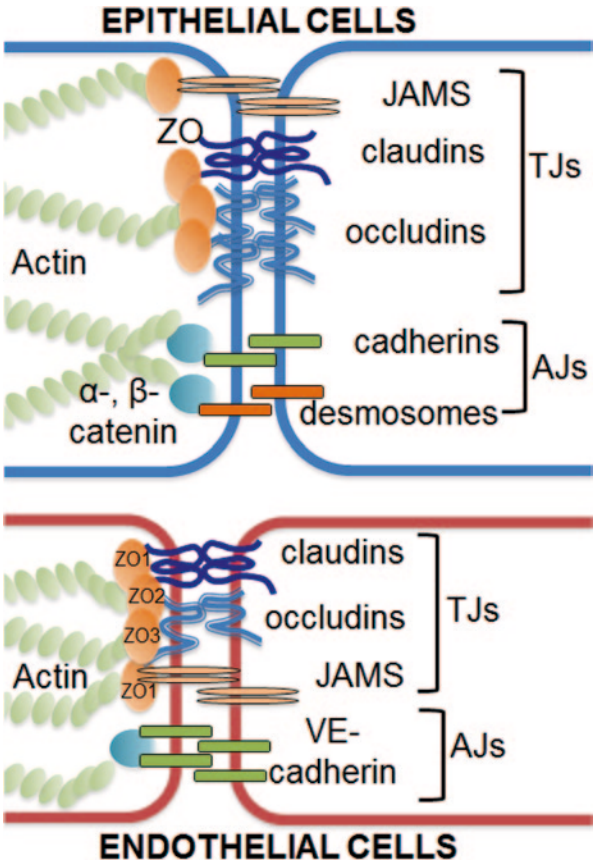


**Fig. 4.1** Schematic of tight junctions (TJs; also known as *Zonula Occludins*) and Adherens Junctions (AJs; also known as *Zonula Addherens*) on endothelial and epithelial cells of the pulmonary blood gas barrier (BGB). TJ proteins (claudin, occludin, and junctional adhesion molecule (JAM). Zona Occludin family (ZO-1-3) form a scaffold linking TJs to the actin cytoskeleton. In contrast AJs, largely composed of cadherins (e.g. E; epithelial, VE; vascular endothelial) and nectins are tethered to the actin cytoskeleton through the multi-functional catenin family (e.g. α-, β- catenin)

less restricted (Leach et al. 2000). TJs have also been suggested to represent the predominant junctional complex found in epithelial cells (Vandenbroucke et al. 2008), conversely AJs appear to form the predominant junctional complex in endothelial cells (Wojciak-Stothard et al. 2001). Despite the differences in frequency and localisation of TJs and AJs between epithelium and endothelium, the molecular composition of TJs and AJs between the two cell types follows a common theme with the extracellular domains of their specialised transmembrane proteins binding adjacent cells akin to 'molecular velcro' with the intracellular domains of these transmembrane proteins forming links to the actin cytoskeleton via actin-binding proteins (Fig. 4.1). As described later, this molecular design ensures that the barrier function of the TJs and AJs is highly dependent on the contractile status of the actin cytoskeleton.

TJs have been described to form 'gasket-like' seals (Capaldo et al. 2014) that lead to the tight regulation of paracellular transport of solutes and macromolecules, first described by Simionescu and colleagues (Simionescu et al. 1978). These seminal studies using tracers administered intravenously to the femoral artery of mice suggested that molecules with a Stokes radius of ≤3 nm could freely diffuse across open endothelial TJs in the veins of the mouse diaphragm, whereas tracers with a Stokes radius ≥3 nm were completely impermeable (Simionescu et al. 1978). Indeed, these early studies also demonstrated that the paracellular movement of substances could be facilitated through treatment of the mouse diaphragm with agents such as 5-hydroxtrypamine and histamine thus providing the first tantalising glimpses of the dynamically regulated nature of paracellular transport via TJs (Simionescu et al. 1978). TJs exhibit a latticework of proteineaceous strands that form a continuous belt that encircles the entire cell when observed under the electron microscope following freeze-fracture (Farquhar and Palade 1963). These proteineaceous strands are formed through tight homotypic and heterotypic binding interactions between the extracellular domains of the transmembrane proteins primarily composed of the claudin (Gunzel and Yu 2013), occludin (Cummins 2012), junctional adhesion molecule (JAMs) (Iden et al. 2012), marvelD3 (Steed et al. 2009), and tricellulin (Ikenouchi et al. 2005) family of proteins. The intracellular domains of the transmembrane proteins that clasp adjacent cells together in a molecular embrace are linked to the actin cytosekeleton via proteins of the zona occludins family (ZO-1-3) (Fanning and Anderson 2009; Fanning et al. 2012). ZOs are multidomain scaffolding proteins of the membrane-associated guanylate kinase (MAGUK) homologue family of proteins. The N-termini of the ZO-1 and ZO-2 proteins share three postsynaptic density protein (PSD95), *Drosophila* disc large tumour suppressor (Dlg1), and zonula occludins-1 protein (ZO-1) (PDZ) domains, a Src homology-3 (SH3) domain, a Unique motif (U5), and guanylate kinase (GUK)-like domain that collectively facilitate interactions with claudins (Fanning et al. 2007; Itoh et al. 1999), JAMs (Ebnet et al. 2000; Nomme et al. 2011), and occludins (Fanning et al. 2007). ZO-1 and ZO-2 also link TJs directly to the actin cytoskeleton through discrete actin binding regions located at the C-terminal ends of the respective proteins (Fanning et al. 2002) or indirectly through interactions with other actin binding proteins such as cortactin (Katsube et al. 1998) and cingulin (Cordenonsi et al. 1999). A recent innovative study using ZO-1-fused biotin ligase to enable biotinylation of proximal proteins followed by capture and purification on streptavidin beads and identification using mass spectroscopy has given insights into the protein complexes that comprise TJs (Van Itallie et al. 2013). In this study between 247 and 350 proteins were identified that exhibit close proximity to ZO-1 (8–9 nm). These proteins included those predicted to interact with TJs (e.g. actin, cingulin, claudin) and novel components of TJs, or to have some functional role in barrier function or TJ assembly/disassembly, (e.g. YES-associated protein 1, Lim domain only protein 7, and casein kinase 1 α (Van Itallie et al. 2013).

AJs were first observed in murine enterocytes (Farquhar and Palade 1963) and further studies using cryo-electron microscopy provided more refined structural insights regarding the composition of AJs with several major components identified including the appearance of transmembrane proteins with extracellular rod-like

structures and globular intracellular domains attaching these rods to the actomyosin cytoskeleton (Hirokawa and Heuser 1981). This structural arrangement of the AJs in epithelial monolayers also appears to be shared by endothelial monolayers (Lambert et al. 2005). The transmembrane rods in epithelial AJs have been identified as being largely composed of two integral membrane proteins namely cadherins (Indra et al. 2013; Saito et al. 2012) and nectins (Indra et al. 2013; Rikitake et al. 2012). Additional transmembrane integral proteins have been identified that are components of AJs such as vezatin (Bahloul et al. 2009; Kussel-Andermann et al. 2000). The cadherin family, which is subgrouped into classical members based on tissue location (E; epithelial, VE; vascular endothelial, N; neural, K; Kidney) and desmosomal members, mediates the intercellular adhesive properties between adjacent cells by forming $Ca^{2+}$-dependent homophilic binding interactions (Harrison et al. 2011; Nagar et al. 1996), in contrast to nectins that form homo- and heterophilic interactions (Samanta et al. 2012). The molecular zipper functions of AJ glues adjacent cells together in the monolayer through the actions of cadherins and nectins. The AJs are tethered to the actin cytoskeleton through the multifunctional catenin family (Harris and Tepass 2010). Although considerable debate has raged over the exact molecular events that allow this to happen (Weis and Nelson 2006), recent structural studies focusing on *Drosophila* suggest that α-catenin acts as a molecular bridge between cadherin and the actin cytoskeleton via the related catenin family member, β-catenin (Desai et al. 2013). Other studies have demonstrated a role for additional linker proteins such as vinculin (Huveneers et al. 2012), p120 catenin (Rajput et al. 2013), α-actinin (Ooshio et al. 2004), or epithelial protein lost in neoplasm (EPLIN) (Chervin-Petinot et al. 2012) in linking the actin cytoskeleton to AJs. The structure of the AJ is ideally designed to act not only as a sensor of cellular tension but it appears that it also exhibits a remarkable ability to adapt to differing levels of mechanical stress.

Recent studies using atomic force microscopy have shown that cadherins are capable of forming at least three distinct types of bonds with neighbouring cadherins on adjacent cells namely: (i) slip bonds which are weak bonds that are short-lived and 'slip' in response to pulling (ii) catch bonds which become longer-lived during mechanical tension, and (iii) ideal bonds which are insensitive to mechanical tension, but contribute to the adhesive properties of the AJ (Rakshit et al. 2012). These biophysical studies indicate that the binding interactions between the cadherin molecules is dynamic and interchangeable between the three types of bonds, and that the proportion of particular bonds that exist between interacting cadherins is determined by the degree of mechanical tension encountered by the cell. Thus, catch, slip, and ideal bonds allow cadherins to withstand tensile force and fine tune the barrier properties of AJs to counter the mechanical stress impacting the cellular monolayer. Similarly, other studies examining α-catenin (Yonemura et al. 2010) and vinculin (Grashoff et al. 2010) have shown that these components of the AJ also function in a tension-dependent manner underscoring the fact that the efficiency of the barrier function of the AJ is rheostatically regulated depending on the mechanical forces acting on the epithelial and endothelial monolayers. This property of the AJ was very elegantly demonstrated in studies examining the size of AJs in endothelial cells in response to different traction forces by subjecting the cells to static conditions, disturbed, or laminar flow. The size of the AJs and TJs matched closely

with intercellular forces for these flow conditions with increasing laminar stress resulting in larger AJs and TJs (Ting et al. 2012), again demonstrating that mechanical tension is sensed by the junctional complexes which then adapt their molecular composition according to the degree of mechanical stress in order to appropriately regulate barrier function. Due to the association of the AJs and TJs with the actin cytoskeleton, their adhesive and barrier function properties are tightly regulated by environmental signals that modulate signalling pathways that control cytoskeletal actin dynamics as discussed below.

## 4.2 Molecular Mechanisms that Modulate the BGB

The dynamic opening and closing of AJs and TJs to create transient gaps between endothelial and epithelial cell borders is a highly ordered phenomenon which is necessary to allow the transport of solutes, large molecules, and cells. Mediators which modulate directly or indirectly the permeability of the endothelial or epithelial cell barriers are themselves highly regulated and many molecular mechanisms have been implicated. Inappropriate modulation or dysregulation of the pathways involved in maintaining the barrier function of these cells can result in loss of BGB integrity, and is a hallmark of many pulmonary diseases such as acute lung injury (Herold et al. 2013), pulmonary fibrosis (Camelo et al. 2014), asthma (Tsicopoulos et al. 2013), cystic fibrosis (Castellani et al. 2012), and pulmonary arterial hypertension (Bartsch et al. 2001; Burton et al. 2011).

The permeability index of the BGB is dictated by contractile forces produced by the actin cytoskeleton and their subsequent effects on the AJ and TJ junctional complexes. Actin filaments are organised at the cell periphery as cortical actin rings which stabilise the AJs and TJs resulting in the maintenance of endothelial barrier function. Indeed, signalling pathways that result in the generation of cyclic adenosine monophosphate (cAMP), subsequent activation of protein kinase A (PKA), and the small guanosine triphosphatase (GTPase) of the Ras super-family; Ras-related C3 botulinum toxin substrate (Rac1) are known to enhance barrier function of AJs through stabilisation of the cortical actin cytoskeleton. A number of factors have been shown to promote this effect including sphingosine-1-phosphate (S1P) (Zhao et al. 2009), adenosine triphosphate (ATP) (Jacobson et al. 2006), oxidised phospholipids (Birukova et al. 2007), and hepatocyte growth factor (HGF) (Birukova et al. 2008a). Actin binding proteins such as cortactin are dynamically redistributed to the cell circumference in quiescient cells and by barrier enhancing pharmacological agents that activate the cAMP/PKA/Rac1 pathway leading to tyrosine phosphorylation of cortactin (Maeng et al. 2013; Maharjan et al. 2013). The translocation of cortactin to cell edges appears to be necessary for barrier enhancement (Jacobson et al. 2006) which likely occurs as a consequence of actin nucleation, polymerisation of actin filaments, and incorporation into the cortical actin structure. This occurs by direct binding of peripherally tethered, phosphorylated cortactin to actin (Yamada et al. 2013) and recruitment and activation of the neuronal Wiskott–Aldrich syndrome protein (N-WASP), and the actin-related proteins 2/3 (Arp2/3)

complex that drives the process of actin nucleation and polymerisation (Martinez-Quiles et al. 2004).

Regulation of the epithelial and endothelial barrier function mediated by Rac1 is also a feature shared by other members of the Ras superfamily of small GTPases particularly members of the Ras homolog gene family (Rho), cell division control protein 42 homolog (cdc42), Rho member A (RhoA) and Ras-associated protein 1 (Rap1) (Spindler et al. 2010). Indeed, cdc42 also appears to promote barrier stabilisation in a similar manner to Rac1. For example, cdc42 translocation to the cell membrane from the cytoplasm has been shown to be a key event in the reassembly of AJs following protease-activated receptor 1 (PAR1), receptor subtype-induced barrier disruption in human lung microvascular cells (MVEC), and the subsequent restoration of barrier function (Kouklis et al. 2004). The mechanism through which cdc42 may alter AJ barrier function has been demonstrated to be in part mediated through regulation of the binding of α-catenin with β-catenin and the resultant interaction of the VE-cadherin/catenin complex with the actin cytoskeleton (Broman et al. 2006). The pathophysiological importance of cdc42 in maintaining microvascular endothelial barrier function has also been demonstrated in vivo using murine models over-expressing a dominant active V12cdc42 mutant in an endothelial-restricted manner. In this study the V12cdc42 transgenic animals were protected from an increase in lung vascular permeability following intraperitoneal lipopolysaccharide (LPS) challenge which may be mediated through cross-talk and suppression of the barrier disrupting small GTPase, RhoA by GTP-loaded cdc42 (Ramchandran et al. 2008). A series of recent studies have also highlighted the complex interplay between the barrier disruptive small GTPase, RhoA and barrier protective small GTPases, Rac1 and cdc42 (Xing et al. 2013), and small GTPase Rap1/afadin axis (Birukova et al. 2013) in regulating lung endothelial cell permeability.

Activation of the AMP-activated protein kinase (AMPK) using the potent AMPK activator, 5-aminoimidazole-4-carboxamide-1-d-ribofuranoside (AICAR) attenuated LPS-induced endothelial hyper-permeability in cultured human pulmonary artery endothelial cells (PAECs) (Xing et al. 2013). In addition, treatment of mice with AICAR also reduced LPS-mediated lung permeability and AMPK subunit α-deficient mice exhibited similar responses (Xing et al. 2013). The mechanism through which AMPK protects the endothelial barrier function appears to be through activation of Rac/cdc42/p21 protein (Cdc42/Rac)-activated kinase 1 (PAK) pathway and inhibition of the RhoA pathway (Xing et al. 2013). In a second study investigating the interplay between the small GTPases with respect to regulation of endothelial barrier function, treatment of lung endothelial cells with thrombin resulted in the rapid plasma membrane translocation of RhoA, remodelling of the actin cytoskeleton, dissolution of AJs, and loss of barrier function (Birukova et al. 2013). This sequence of events leading to loss of endothelial barrier integrity appears to be closely followed by Src-mediated phosphorylation of the Rap1-specific guanine nucleotide exchange factor (GEF) 3CG, activation of Rap1 and suppression of RhoA activity, and as a consequence of this interplay, re-annealing of AJs which was facilitated by increased interactions between VE-cadherin and p120-catenin mediated by the Rap1 effector, afadin (Birukova et al. 2013).

As outlined above, the small GTPase RhoA represents a central player orchestrating the dissolution of AJs/TJs and reduction in the barrier function of the BGB by numerous mediators including lysophosphatidic acid (LPA) (van Nieuw Amerongen et al. 2000), thrombin (Qiao et al. 2003), histamine (Chava et al. 2012), vascular endothelial growth factor (VEGF) (Birukova et al. 2008a), transforming growth factor β (TGF β) (Clements et al. 2005), tumour necrosis factor α (TNFα) (Mong et al. 2008), and cytokines such as interleukin-8 (IL-8) (Petreaca et al. 2007) and IL-6 (Kruttgen and Rose-John 2012). Treatment of human MVECs with the barrier disruptive agent, thrombin has been demonstrated to result in a dynamic and rapid activation and membrane translocation of RhoA that precedes loss of barrier integrity, effects which could be suppressed through activation of PKA (Qiao et al. 2003). The permeability increasing effects of thrombin are predominantly mediated through the PAR1 receptor subtype since PAR1 knockout mice fail to show an increase in lung microvascular permeability in response to thrombin challenge or treatment with a selective PAR1 agonist peptide (Vogel et al. 2000). Inhibition of ARHGAP21 and ARHGAP24, two RhoA GTPase-activating proteins (GAPs) also resulted in impairment of the barrier function of human endothelial cells underscoring the importance of RhoA activation in disrupting the barrier function of the lung endothelium (Pirot et al. 2014). Conversely, limiting the activity of RhoA through acceleration of the GTPase activity of the protein is a mechanism that has been described to result in stabilisation and enhancement of the barrier function of the lung endothelium (Zebda et al. 2013). This effect could be achieved through the plasma membrane recruitment of Rho190GAP mediated through an interaction with the C-terminal portion of p120-catenin bringing the Rho190GAP protein into close juxtaposition with RhoA-GTP to facilitate GTP turnover (Zebda et al. 2013). The aforementioned mechanism appears to be utilised by oxidised phospholipids to enhance pulmonary vascular barrier function and to protect against ventilator-induced lung vascular leak in vivo (Birukova et al. 2011). Additional mechanisms also exist to dampen the activation of RhoA that are utilised by mediators that have been reported as possessing barrier stabilising properties. For example, adenosine and homocysteine appear to restore barrier function following thrombin treatment of pulmonary endothelial cell monolayers by promoting the association of Rho GDP-dissociation inhibitor (RhoGDI) with RhoA (Harrington et al. 2004). The importance of this mechanism in the contribution of maintaining endothelial barrier function in vivo has also been demonstrated in RhoGDI knockout mice which exhibit markedly elevated basal permeability of the lung endothelium (Gorovoy et al. 2007).

The upstream mechanisms that lead to disassembly of AJs/TJs are complex, and in some instances, context- and pathway-specific. However, remodelling of the cortical actin cytoskeleton into contractile actin stress fibres and concomitant microtubule (MT) disassembly appears to represent a universal mechanism utilised by many barrier disrupting pathways and agents (Dudek and Garcia 2001). Remodelling of the actin cytoskeleton into contractile actin filaments is fundamental in promoting epithelial and endothelial cell contraction and involves the enhanced phosphorylation status of myosin light chain (MLC) which is a phosphosubstrate for the calcium ($Ca^{2+}$)/calmodulin-dependent MLC kinase (MLCK) (Sheldon et al.

1993; Shen et al. 2010). The barrier disrupting small GTPase, RhoA also contributes to the phosphorylation status of MLC through activation of MLC phosphatase (MLCP) via the Rho-associated, coiled-coil containing protein kinase 1 (ROCK) (Birukova et al. 2005), further enhancing the phosphorylation of MLC. The consequence of this sequence of events that leads to the co-ordinated potentiation of MLC phosphorylation is the dynamic process of cross-bridge assembly/disassembly between the actin myosin complex that drives cellular contraction via centripedal force (Dudek and Garcia 2001; Sheldon et al. 1993). In the context of AJ composition and function, endothelial cell contraction induced by vascular disrupting agents such as platelet activating factor (PAF) results in 'un-zippering' of the homotypic binding interactions between VE-cadherins on adjacent cells leading to intercellular gaps and loss of barrier function (Yuan and He 2012).

Intracellular $Ca^{2+}$ influx also plays a fundamental role in modulating the BGB function through diverse mechanisms (Tiruppathi et al. 2002). For example, PAR1 couples promiscuously to the heterotrimeric G proteins of the $G\alpha_q$, $G\alpha_{12/13}$, $G\alpha_i$, and $G\alpha_s$ families (Macfarlane et al. 2001) leading to the induction of downstream RhoA signalling through activation of $G\alpha_q$/phospholipase C (PLC) and subsequent transient receptor potential channel subtype C6 (TRPC6)-mediated receptor store-operated calcium ($Ca^{2+}$) channels (ROC) that results in myosin MLC phosphorylation, and actin stress fiber formation as well as a concomitant reduction in endothelial barrier function (Singh et al. 2007). This increase in intracellular $Ca^{2+}$ drives endothelial cell contraction (Hicks et al. 2010; Nilius and Droogmans 2001; Tiruppathi et al. 2002) which may be mediated in part through post-translational modifications of proteins such as the myosin-binding protein, caldesmon (Borbiev et al. 2003), and loss of barrier function. Regulation of ZO-1 expression levels has also been shown to be dependent on TRP channel-mediated $Ca^{2+}$ influx and subsequent activation of calpain which leads to proteolysis of ZO-1 (Wang et al. 2012), underscoring the multitude of ways that the BGB can be modulated. In addition to TRPC6, several other TRP channels have been shown to play important roles in mediating changes in the BGB function including TRPC1 (Jho et al. 2005; Sundivakkam et al. 2012), TRPC4 (Sundivakkam et al. 2012), TRPM2 (Wang et al. 2012), and TRPV4 (Sidhaye et al. 2008) as well as L-type voltage-gated $Ca^{2+}$ channels (Sidhaye et al. 2008). Perhaps, one of the best studied TRP channels known to regulate the BGB is TRPV4 which appears to mediate changes in pulmonary epithelial and endothelial permeability through a number of mechanisms including alterations in coupling to large conductance $Ca^{2+}$ -dependent potassium ($K^+$) channel (Fernandez-Fernandez et al. 2008) as well as modulation aquaporin-5 (AQ5) expression levels through increased internalisation and degradation (Sidhaye et al. 2008). Interestingly, TRPV4 expression is spatially-restricted in the vasculature with the highest expression levels observed in the microvascular endothelium. Thus, TRPV4 may represent one of the main mechanisms that drives capillary endothelial barrier permeability (Cioffi et al. 2009).

The RhoA/ROCK axis also appears to act as a 'signalling node' to direct the activity of multiple additional downstream kinase activities that participate in the regulation of the BGB barrier function. One notable example is LIM domain kinase 1 (LIMK1) which is activated downstream of RhoA/ROCK (Maekawa et al. 1999) and appears to mediate lung edema formation, microvascular permeability,

and neutrophil infiltration in response to LPS challenge (Gorovoy et al. 2009). The molecular mechanism through which LIMK1 regulates BGB permeability is likely related to the well characterised role for cofilin, a LIMK1 phosphosubstrate, in regulating actin cytoskeletal remodelling (Slee and Lowe-Krentz 2013). However, additional mechanisms also exist including the modulation of occludin levels within TJs (Shiobara et al. 2013) and redistribution of claudin-1 and ZO-1 in TJ junctional complexes (Nagumo et al. 2008) in epithelial cells following capasacin treatment. Similarly, the intricate interplay between ROCK and the p38 mitogen-activated kinase (MAP) kinase pathways also appears to promote disruption of the lung endothelial barrier function. Following treatment of human pulmonary artery endothelial monolayers with the antitumour agent, 2-methoxyestradiol (2ME), resulted in the disruption of the monolayer integrity in a process that involves MT disassembly and phosphorylation of heat shock protein 27 (HSP27) (Bogatcheva et al. 2007), which may be related to the role of phospho-HSP27 in modulating actin filament dynamics (Guay et al. 1997). The RhoA/ROCK axis also appears to be associated with focal adhesions and focal adhesion kinase (FAK); however, the role of these components in regulating BGB properties are confusing with some reports demonstrating a barrier strengthening and restoration function through suppression of RhoA activity in the pulmonary endothelium (Holinstat et al. 2006), and in response to treatment of pulmonary endothelial cells with 2-amino-2-[2-(4-octylphenyl)ethyl]propane-1,3-diol (FTY720), a pharmaceutical analogue of the potent barrier-enhancing phospholipid S1P which also appears to require the tyrosine kinase activity of mammalian Abelson murine leukemia viral oncogene homolog 1 (c-Abl) (Wang et al. 2011a). In contrast, the involvement of FAK in mediating barrier disruption in response to treatment of pulmonary endothelial cells with combinations of cigarette smoke extract and LPS has been demonstrated (Lu et al. 2011). More recently, an elegant study by Chen and colleagues has shown that VEGF-mediated permeability is also dependent on FAK. Using an inducible FAK knock-in mouse, this group could demonstrate that genetic and pharmacological inhibition of FAK in endothelial cells could attenuate VEGF-stimulated permeability downstream of the VEGF receptor and Src kinase (Chen et al. 2012).

The involvement of multiple kinase cascades in regulating the BGB function also suggests that components of the AJs/TJs may be regulated by post-translational modifications such as phosphorylation that regulates their function. In this regard there are numerous examples of phosphorylation of VE-cadherin that occurs following stimulation of lung endothelial cells with barrier disrupting agents which leads to disruption of VE-cadherin function, internalisation, and loss of barrier function. For example, TNFα can induce loss of endothelial barrier function in human lung MVECs and PAECs by inducing the activation of Src family kinase, Fyn resulting in tyrosine phosphorylation and redistribution of VE-cadherin, γ-catenin, and p120-catenin (Angelini et al. 2006). Pharmacological inhibition of Src kinase has been shown to prevent phosphorylation of VE-cadherin and gap formation in response to TNFα suggesting that Src kinase also acts upstream of VE-cadherin to drive endothelial permeability (Nwariaku et al. 2002). This mechanism of regulation of VE-Cadherin is also shared by G protein-coupled receptor (GPCRs) which act via $G\alpha_{13}$ to stimulate Src kinase and phosphorylation of VE-cadherin at Y658, a region of the protein known to be important for p120-catenin interaction and internalisation

(Gong et al. 2014). The physiological importance of this post-translational modification was elegantly demonstrated in vivo where Y658 phosphorylation was shown to occur in venular endothelium following shear stress-induced activation of Src kinase (Orsenigo et al. 2012). Interestingly, scaffolding functions of the cytoplasmic tail of VE-cadherin are also exploited by Src kinase in order to achieve the correct spatial orientation to phosphorylate other components of the AJ. For example, phosphorylation of β-catenin Y142 following stimulation of endothelial cells with VEGF leads to the dissociation of the VE-cadherin/β-catenin complex and the loss of barrier function (Chen et al. 2012). Phosphorylation of junctional complexes may also target these proteins for ubiquitination and degradation. For example, VEGF rapidly phosphorylates occludin on position S490 in endothelial cells leading to down-regulation of this protein and loss of barrier function (Murakami et al. 2009). Phosphorylation on S879 of p120-catenin by protein kinase C α (PKCα) also appears to play a key regulatory role in the homotypic binding of VE-cadherin and subsequent internalisation in lung endothelium in response to LPS and thrombin challenge via the PAR1 receptor (Vandenbroucke St Amant et al. 2012). Numerous examples of phosphorylation of other components of the junctional complexes of the BGB such as cortactin by Src kinase (Truffi et al. 2014), cingulin by AMPK (Yano et al. 2013), claudin-1 by MAP kinases (Fujibe et al. 2004), and claudin-5 by PKA (Fujibe et al. 2004) underscores the complexity and importance of this mechanism in regulating BGB function.

## 4.3 Environmental Factors Affecting the BGB

The BGB is anatomically placed to encounter a huge plethora of air- and blood-borne environmental insults, including pollutants, hypoxia, infectious agents, shear stress, and transmural pressure gradients. These environmental insults mediate their effects through many of the signalling pathways discussed previously, leading to disruption of the BGB (Fig. 4.2). For the purpose of this chapter, we focus on how the BGB responds to the effects of stretch in regulating barrier function and the signalling mechanisms that are utilised.

Ventilator-induced lung injury (VILI) occurs when the lung parenchyma and vasculature are exposed to repetitive and excessive mechanical stress via mechanical ventilation utilised as supportive care for the acute respiratory distress syndrome (ARDS). In vitro models using devices that apply equibiaxial mechanical stretch have been developed to mimic the process of VILI and have been widely utilised to understand the molecular pathways that are engaged during this process leading to modulation of the BGB. Studies examining the molecular mechanisms associated with over-distension of pulmonary endothelium and loss of BGB function, suggest that the process of over-distension leads to production and secretion of barrier disruptive mediators such as high mobility group box 1 protein (HMGB1) (Wolfson et al. 2014), VEGF (Gurkan et al. 2011), and IL-8 (Fu et al. 2013). Additional studies have demonstrated that human PAECs subjected to high-amplitude cyclic stretch (18%) undergo rapid remodelling of the actin cytoskeleton towards a contractile

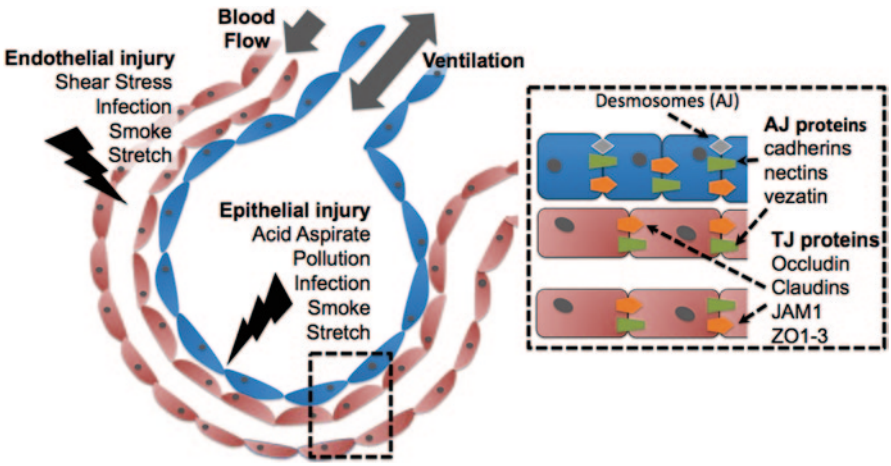


**Fig. 4.2** Endothelial and epithelial cells of the pulmonary blood gas barrier (BGB) regulate the movement of liquid, solutes, macromolecules, and cells from the airways and bloodstream into the lung interstitium via transcellular and paracellular transport. Damage to epithelial and endothelial BGB must contend with air and blood borne damage as well as biomechanical stresses (left panel). Paracellular transport is regulated by Tight Junctions (TJs) and Adherens Junctions (AJs) that are found in both epithelial and endothelial cell monolayers (right panel). Insults to the lung (pollution, bacterial infection or smoke) can lead to cellular changes in AJs or TJs and a loss of integrity of the endothelial and epitherlial barriers.

phenotype within 10 min. This process involves the activation of a number of cell signalling pathways including MLC phosphorylation, the MAP kinases, p38, and extracellular signal regulated kinase 1/2 (ERK1/2) activation (Birukov et al. 2003). Interestingly, subjecting these cells to prolonged high amplitude cyclic stretch (18%) for 48 h but not physiologic levels of stretch (5%) resulted in significantly enhanced thrombin-induced reduction in endothelial barrier function (Birukov et al. 2003; Birukova et al. 2008b). This apparently pathological response to high amplitude cyclic stretch may result from the induction of genes known to diminish barrier function such as RhoA, MLC, MLCK, zipper-interacting kinase 1 (ZIP kinase), PAR1, caldesmon, and HSP27 (Birukov et al. 2003; Birukova et al. 2008b). Sensitisation of the pulmonary endothelium to the effects of barrier disruptive agents by prior chronic application of pathologic cyclic stretch is not unique to thrombin, as similar effects have been observed for VEGF (Birukova et al. 2008a). Interestingly, further studies have shown that subjecting pulmonary endothelial cells to physiologic stretch (5%) activates the barriers restorative small GTPase, Rac. In contrast, pathological stretch (18%) led to the activation of the barrier disruptive small GTPase RhoA underscoring the remarkable plasticity that the endothelial monolayer exhibits in response to mechanical deformation (Birukova et al. 2006). Anatomical location of the endothelial cells also appears to be lead to differential sensitivities to endothelial distension on barrier function. This was elegantly demonstrated by Adkison and colleagues who established that rat lung MVECs are less sensitive to the effects of biaxial cyclical strain than PAECs as they more readily retain intact E-cadherin/β-catenin protein–protein interactions within junctional complexes (Adkison et al.

2006). Interestingly, TRPV4, a biomechanically activated TRP channel (Matthews et al. 2010), also demonstrates a spatially restricted pattern of expression within endothelial cells with the predominant expression occurring within microvascular endothelial (Alvarez et al. 2006). MVEC interactions with the extracellular matrix (ECM) are localised to discrete cellular focal adhesions that are composed of β1 integrin and the transmembrane integrin binding protein CD98 which connects the cell with the ECM (Matthews et al. 2010). Cyclic strain applied to cultured bovine capillary endothelial cells through their ECM-integrin focal adhesions activates $Ca^{2+}$ influx through TRPV4 ion channels expressed at the plasma membrane. In turn this leads to the downstream phosphatidylinositol 3-kinase (PI3 kinase)-dependent activation and binding of additional β1 integrin receptors, which in turn leads to cytoskeletal remodelling and cell reorientation (Thodeti et al. 2009). Further studies have shown that other components of the focal adhesions mediate endothelial cells responses to stretch. For example, paxillin promotes the activity of RhoA through activation of the Rho-specific GEF, GEF-H1 in a p42/44 MAP kinase-dependent manner (Gawlak et al. 2014). The location and distribution of the focal adhesions within human lung endothelial cells also appears to undergo dynamic remodelling in response to cyclic stretch. Focal adhesions are spatially redistributed to the ends of newly formed stress fibres which coincided with alterations to the phosphorylation profile of FAK with increased phosphorylation observed at positions Y397 and Y576 (Shikata et al. 2005). Interestingly, auto-phosphorylation of FAK at Y397 is a crucial step involved in the dimerisation and activity of FAK (Brami-Cherrier et al. 2014) suggesting that endothelial cell distension mediated through cyclic stretch promotes the activation of FAK which can in turn, facilitate the disruption of endothelial barrier function (Arnold et al. 2013; Chen et al. 2012; Lu et al. 2011).

The pulmonary alveolar epithelial cell barrier function is also influenced as a consequence of cellular distension involving similar mechanisms to those engaged in the pulmonary alveolar endothelial compartment. For example, activation of the RhoA pathway has been shown to occur in alveolar epithelial cells subjected to cyclic stretch (Birukova et al. 2012; DiPaolo and Margulies 2012) with the degree of pathway activation dependent on the magnitude of cellular stretching (DiPaolo and Margulies 2012). The magnitude and duration of cyclic stretch applied to alveolar epithelial cells also determines the resultant gene expression profile in the cells (Yerrapureddy et al. 2010). Application of biaxial cyclic stretch in alveolar epithelial cells also augments the loss of permeability induced by IL-6 (Birukova et al. 2012). This mirrors what has been described in endothelial cells regarding the potentiation of loss of endothelial barrier function following co-application of biaxial cyclic stretch and treatment with the barrier disrupting agents, thrombin (Birukova et al. 2006) and VEGF (Birukov et al. 2003). Taken together, the data supports the notion that common mechanism(s) contribute to alterations in the efficiency of pulmonary biological barriers.

Studies comparing the effects of varying the magnitude and applying different modes of stretch upon alveolar epithelial barrier function have also highlighted the important contribution of cellular energetics in regulating barrier function. For example, the application of biaxial cyclic stretch (15 cycles/min) or uniform stretch (37% change in alveolar epithelial cell surface area) led to a marked reduction in

the expression of TJ components. This includes the expression of peripheral and total cellular occludin and the degree of cell–cell attachment which was accompanied with a significant reduction in cellular ATP levels (Cavanaugh et al. 2001). Modulation of ATP levels in alveolar epithelial cells through the use of the glycolytic metabolic inhibitors, 2-deoxy-D-glucose and (2{R},3{S},6{S},7{R},8{R})-3-[(3-formamido-2-hydroxybenzoyl)amino]-8-hexyl-2,6-dimethyl-4,9-dioxo-1,5-dioxonan-7-yl 3-methylbutanoate (antimycin A), also leads to reductions in occludin expression levels (Cavanaugh et al. 2001), collectively suggesting a direct link between the energetic status of the cells and the regulation of TJ protein composition. The link between oxidative stress and alveolar epithelial cell permeability in response to cellular distension has also recently been strengthened. Application of biaxial cyclic stretch to alveolar epithelial cells was associated with increased generation of reactive oxygen species, superoxide, and nitric oxide (NO) with a concomitant decreases in barrier function (Davidovich et al. 2013). The permeability induced by cyclic stretch is decreased by the superoxide scavenger sodium 4,5-dihydroxybenzene-1,3-disulfonic acid (tiron) and benzyl N-[(2S)-4-methyl-1-[[(2S)-4-methyl-1-[[(2S)-4-methyl-1-oxopentan-2-yl]amino]-1-oxopentan-2-yl]amino]-1-oxopentan-2-yl]carbamate (MG132) (Davidovich et al. 2013), with the former agent demonstrating a dramatic protective effect on in vivo lung permeability under mechanical ventilation conditions (Davidovich et al. 2013).

Additional mechanisms that result in alterations in the expression of components that comprise the junctional complexes in alveolar epithelial cells in response to cellular over-distension have also been described. The loss of p120-catenin expression that occurs in a Src kinase-dependent manner is a key process driving the loss of barrier function of alveolar epithelial cells in response to cyclic stretch (Dai et al. 2013). The importance of this mechanism was shown using VILI models in Sprague Dawley (SD) rats where pre-treatment of the animals with Src kinase inhibitors protected the animals from pulmonary edema induced by the high tidal volume ventilation (Dai et al. 2013). Further analysis of the mechanisms govern the reduction of p120-catenin expression in alveolar epithelial cells after application biaxial stretch has shown the involvement of calpain-mediated degradation (Wang et al. 2011b). This suggests that restoration of the alveolar epithelial barrier function following over-distension may require new protein synthesis.

## 4.4 Conclusion

The molecular design of the thin-walled, large surface area of the pulmonary BGB that is comprised of single monolayers of juxtaposed alveolar epithelial cells and pulmonary MVECs, separated by an extremely strong basement membrane composed mainly of type IV collagen has undergone evolutionary adaptation to enable the lung to perform its primary function; blood–gas exchange (West 2006). Key to optimal blood–gas exchange is the ability of the pulmonary BGB to maintain effective barrier function and a major part of this process is the regulation of paracellular movement of solutes, small molecules, and cells that are regulated by the AJ and TJ junctional com-

plexes, which are expressed in the epithelial and endothelial monolayers. An inability to maintain effective BGB function is linked to the development and progression of many pulmonary disorders. Understanding the molecular mechanisms involved in maintaining BGB function in health and how these mechanisms become dys-regulated in disease, will be fundamental in designing novel therapeutic strategies to restore and augment barrier function for the treatment of acute and chronic lung diseases.

## References

Adkison JB, Miller GT, Weber DS, Miyahara T, Ballard ST, Frost JR, Parker JC. Differential responses of pulmonary endothelial phenotypes to cyclical stretch. Microvasc Res. 2006;71:175–84.

Alvarez DF, King JA, Weber D, Addison E, Liedtke W, Townsley MI. Transient receptor potential vanilloid 4-mediated disruption of the alveolar septal barrier: a novel mechanism of acute lung injury. Circ Res. 2006;99:988–95.

Angelini DJ, Hyun SW, Grigoryev DN, Garg P, Gong P, Singh IS, Passaniti A, Hasday JD, Goldblum SE. TNF-alpha increases tyrosine phosphorylation of vascular endothelial cadherin and opens the paracellular pathway through fyn activation in human lung endothelia. Am J Physiol Lung Cell Mol Physiol. 2006;291:L1232–L45.

Arnold KM, Goeckeler ZM, Wysolmerski RB. Loss of focal adhesion kinase enhances endothelial barrier function and increases focal adhesions. Microcirculation. 2013;20:637–49.

Bahloul A, Simmler MC, Michel V, Leibovici M, Perfettini I, Roux I, Weil D, Nouaille S, Zuo J, Zadro C, et al. Vezatin, an integral membrane protein of adherens junctions, is required for the sound resilience of cochlear hair cells. EMBO Mol Med. 2009;1:125–38.

Bartsch P, Swenson ER, Maggiorini M. Update: High altitude pulmonary edema. Adv Exp Med Biol. 2001;502:89–106.

Birukov KG, Jacobson JR, Flores AA, Ye SQ, Birukova AA, Verin AD, Garcia JG. Magnitude-dependent regulation of pulmonary endothelial cell barrier function by cyclic stretch. Am J Physiol Lung Cell Mol Physiol. 2003;285:L785–L97.

Birukova AA, Birukov KG, Adyshev D, Usatyuk P, Natarajan V, Garcia JG, Verin AD. Involvement of microtubules and Rho pathway in TGF-beta1-induced lung vascular barrier dysfunction. J Cell Physiol. 2005;204:934–47.

Birukova AA, Chatchavalvanich S, Rios A, Kawkitinarong K, Garcia JG, Birukov KG. Differential regulation of pulmonary endothelial monolayer integrity by varying degrees of cyclic stretch. Am J Pathol. 2006;168:1749–61.

Birukova AA, Malyukova I, Mikaelyan A, Fu P, Birukov KG. Tiam1 and betaPIX mediate Rac-dependent endothelial barrier protective response to oxidized phospholipids. J Cell Physiol. 2007;211:608–17.

Birukova AA, Moldobaeva N, Xing J, Birukov KG. Magnitude-dependent effects of cyclic stretch on HGF- and VEGF-induced pulmonary endothelial remodeling and barrier regulation. Am J Physiol Lung Cell Mol Physiol. 2008a;295:L612–L23.

Birukova AA, Rios A, Birukov KG. Long-term cyclic stretch controls pulmonary endothelial permeability at translational and post-translational levels. Exp Cell Res. 2008b;314:3466–77.

Birukova AA, Zebda N, Cokic I, Fu P, Wu T, Dubrovskyi O, Birukov KG. p190RhoGAP mediates protective effects of oxidized phospholipids in the models of ventilator-induced lung injury. Exp Cell Res. 2011;317:859–72.

Birukova AA, Tian Y, Meliton A, Leff A, Wu T, Birukov KG. Stimulation of Rho signaling by pathologic mechanical stretch is a “second hit” to Rho-independent lung injury induced by IL-6. Am J Physiol Lung Cell Mol Physiol. 2012;302:L965–L75.

Birukova AA, Tian X, Tian Y, Higginbotham K, Birukov KG. Rap-afadin axis in control of Rho signaling and endothelial barrier recovery. Mol Biol Cell. 2013;24:2678–88.

Bogatcheva NV, Adyshev D, Mambetsariev B, Moldobaeva N, Verin AD. Involvement of microtubules, p38, and Rho kinases pathway in 2-methoxyestradiol-induced lung vascular barrier dysfunction. Am J Physiol Lung Cell Mol Physiol. 2007;292:L487–L99.

Borbiev T, Verin AD, Birukova A, Liu F, Crow MT, Garcia JG. Role of CaM kinase II and ERK activation in thrombin-induced endothelial cell barrier dysfunction. Am J Physiol Lung Cell Mol Physiol. 2003;285:L43–L54.

Brami-Cherrier K, Gervasi N, Arsenieva D, Walkiewicz K, Boutterin MC, Ortega A, Leonard PG, Seantier B, Gasmi L, Bouceba T, et al. FAK dimerization controls its kinase-dependent functions at focal adhesions. EMBO J. 2014;33:356–70.

Broman MT, Kouklis P, Gao X, Ramchandran R, Neamu RF, Minshall RD, Malik AB. Cdc42 regulates adherens junction stability and endothelial permeability by inducing alpha-catenin interaction with the vascular endothelial cadherin complex. Circ Res. 2006;98:73–80.

Burton VJ, Ciuclan LI, Holmes AM, Rodman DM, Walker C, Budd DC. Bone morphogenetic protein receptor II regulates pulmonary artery endothelial cell barrier function. Blood. 2011;117:333–41.

Camelo A, Dunmore R, Sleeman MA, Clarke DL. The epithelium in idiopathic pulmonary fibrosis: breaking the barrier. Front Pharmacol. 2014;4:173.

Capaldo CT, Farkas AE, Nusrat A. Epithelial adhesive junctions. F1000Prime Rep. 2014;6:1.

Castellani S, Guerra L, Favia M, Di Gioia S, Casavola V, Conese M. NHERF1 and CFTR restore tight junction organisation and function in cystic fibrosis airway epithelial cells: role of ezrin and the RhoA/ROCK pathway. Lab Invest. 2012;92:1527–40.

Cavanaugh KJ Jr, Oswari J, Margulies SS. Role of stretch on tight junction structure in alveolar epithelial cells. Am J Respir Cell Mol Biol. 2001;25:584–91.

Chava KR, Tauseef M, Sharma T, Mehta D. Cyclic AMP response element-binding protein prevents endothelial permeability increase through transcriptional controlling p190RhoGAP expression. Blood. 2012;119:308–19.

Chen XL, Nam JO, Jean C, Lawson C, Walsh CT, Goka E, Lim ST, Tomar A, Tancioni I, Uryu S, et al. VEGF-induced vascular permeability is mediated by FAK. Dev Cell. 2012;22:146–57.

Chervin-Petinot A, Courcon M, Almagro S, Nicolas A, Grichine A, Grunwald D, Prandini MH, Huber P, Gulino-Debrac D. Epithelial protein lost in neoplasm (EPLIN) interacts with alpha-catenin and actin filaments in endothelial cells and stabilizes vascular capillary network in vitro. J Biol Chem. 2012;287:7556–72.

Cioffi DL, Lowe K, Alvarez DF, Barry C, Stevens T. TRPing on the lung endothelium: calcium channels that regulate barrier function. Antioxid Redox Signal. 2009;11:765–76.

Clements RT, Minnear FL, Singer HA, Keller RS, Vincent PA. RhoA and Rho-kinase dependent and independent signals mediate TGF-beta-induced pulmonary endothelial cytoskeletal reorganization and permeability. Am J Physiol Lung Cell Mol Physiol. 2005;288:L294–L306.

Cordenonsi M, D'Atri F, Hammar E, Parry DA, Kendrick-Jones J, Shore D, Citi S. Cingulin contains globular and coiled-coil domains and interacts with ZO-1, ZO-2, ZO-3, and myosin. J Cell Biol. 1999;147:1569–82.

Cummins PM. Occludin: one protein, many forms. Mol Cell Biol. 2012;32:242–50.

Dai CY, Dai GF, Sun Y, Wang YL. Loss of p120 catenin aggravates alveolar edema of ventilation induced lung injury. Chin Med J (Engl). 2013;126:2918–22.

Davidovich N, DiPaolo BC, Lawrence GG, Chhour P, Yehya N, Margulies SS. Cyclic stretch-induced oxidative stress increases pulmonary alveolar epithelial permeability. Am J Respir Cell Mol Biol. 2013;49:156–64.

Desai R, Sarpal R, Ishiyama N, Pellikka M, Ikura M, Tepass U. Monomeric alpha-catenin links cadherin to the actin cytoskeleton. Nat Cell Biol. 2013;15:261–73.

DiPaolo BC, Margulies SS. Rho kinase signaling pathways during stretch in primary alveolar epithelia. Am J Physiol Lung Cell Mol Physiol. 2012;302:L992–L1002.

Dudek SM, Garcia JG. Cytoskeletal regulation of pulmonary vascular permeability. J Appl Physiol. 2001;(1985) 91:1487–500.

Ebnet K, Schulz CU, Meyer Zu Brickwedde MK, Pendl GG, Vestweber D. Junctional adhesion molecule interacts with the PDZ domain-containing proteins AF-6 and ZO-1. J Biol Chem. 2000;275:27979–88.

Fanning AS, Anderson JM. Zonula occludens-1 and -2 are cytosolic scaffolds that regulate the assembly of cellular junctions. Ann N Y Acad Sci. 2009;1165:113–20.
Fanning AS, Ma TY, Anderson JM. Isolation and functional characterization of the actin binding region in the tight junction protein ZO-1. FASEB J. 2002;16:1835–7.
Fanning AS, Little BP, Rahner C, Utepbergenov D, Walther Z, Anderson JM. The unique-5 and -6 motifs of ZO-1 regulate tight junction strand localization and scaffolding properties. Mol Biol Cell. 2007;18:721–31.
Fanning AS, Van Itallie CM, Anderson JM. Zonula occludens-1 and -2 regulate apical cell structure and the zonula adherens cytoskeleton in polarized epithelia. Mol Biol Cell. 2012;23:L577–90.
Farquhar MG, Palade GE. Junctional complexes in various epithelia. J Cell Biol. 1963;17:375–412.
Fernandez-Fernandez JM, Andrade YN, Arniges M, Fernandes J, Plata C, Rubio-Moscardo F, Vazquez E, Valverde MA. Functional coupling of TRPV4 cationic channel and large conductance, calcium-dependent potassium channel in human bronchial epithelial cell lines. Pflugers Arch. 2008;457:149–59.
Fu W, Mao P, Zhang R, Pang XQ, Mo HY, He WQ, Liu XQ, Li YM. [Effects of cyclic stretch on expression of cytokines and intercelluar adhesion molecule-1 in human pulmonary artery endothelial cell]. Zhonghua Wei Zhong Bing Ji Jiu Yi Xue. 2013;25:484–8.
Fujibe M, Chiba H, Kojima T, Soma T, Wada T, Yamashita T, Sawada N. Thr203 of claudin-1, a putative phosphorylation site for MAP kinase, is required to promote the barrier function of tight junctions. Exp Cell Res. 2004;295:36–47.
Gawlak G, Tian Y, O'Donnell JJ, 3rd, Tian X, Birukova AA, Birukov KG. Paxillin mediates stretch-induced Rho signaling and endothelial permeability via assembly of paxillin-p42/44MAPK-GEF-H1 complex. FASEB J. 2014;28(7):3249–60.
Gong H, Gao X, Feng S, Siddiqui MR, Garcia A, Bonini MG, Komarova Y, Vogel SM, Mehta D, Malik AB. Evidence of a common mechanism of disassembly of adherens junctions through Galpha13 targeting of VE-cadherin. J Exp Med. 2014;211:579–91.
Gorovoy M, Neamu R, Niu J, Vogel S, Predescu D, Miyoshi J, Takai Y, Kini V, Mehta D, Malik AB, et al. RhoGDI-1 modulation of the activity of monomeric RhoGTPase RhoA regulates endothelial barrier function in mouse lungs. Circ Res. 2007;101:50–8.
Gorovoy M, Han J, Pan H, Welch E, Neamu R, Jia Z, Predescu D, Vogel S, Minshall RD, Ye RD, et al. LIM kinase 1 promotes endothelial barrier disruption and neutrophil infiltration in mouse lungs. Circ Res. 2009;105:549–56.
Grashoff C, Hoffman BD, Brenner MD, Zhou R, Parsons M, Yang MT, McLean MA, Sligar SG, Chen CS, Ha T, et al. Measuring mechanical tension across vinculin reveals regulation of focal adhesion dynamics. Nature. 2010;466:263–6.
Guay J, Lambert H, Gingras-Breton G, Lavoie JN, Huot J, Landry J. Regulation of actin filament dynamics by p38 map kinase-mediated phosphorylation of heat shock protein 27. J Cell Sci. 1997;110 (Pt 3):357–68.
Gunzel D, Yu AS. Claudins and the modulation of tight junction permeability. Physiol Rev. 2013;93:525–69.
Gurkan OU, He C, Zielinski R, Rabb H, King LS, Dodd-o JM, D'Alessio FR, Aggarwal N, Pearse D, Becker PM. Interleukin-6 mediates pulmonary vascular permeability in a two-hit model of ventilator-associated lung injury. Exp Lung Res. 2011;37:575–84.
Harrington EO, Newton J, Morin N, Rounds S. Barrier dysfunction and RhoA activation are blunted by homocysteine and adenosine in pulmonary endothelium. Am J Physiol Lung Cell Mol Physiol. 2004;287:L1091–L7.
Harris TJ, Tepass U. Adherens junctions: from molecules to morphogenesis. Nat Rev Mol Cell Biol. 2010;11:502–14.
Harrison OJ, Bahna F, Katsamba PS, Jin X, Brasch J, Vendome J, Ahlsen G, Carroll KJ, Price SR, Honig B, et al. Two-step adhesive binding by classical cadherins. Nat Struct Mol Biol. 2011;17:348–57.
Herold S, Gabrielli NM, Vadasz I. Novel concepts of acute lung injury and alveolar-capillary barrier dysfunction. Am J Physiol Lung Cell Mol Physiol. 2013;305:L665–L81.

Hicks K, O'Neil RG, Dubinsky WS, Brown RC. TRPC-mediated actin-myosin contraction is critical for BBB disruption following hypoxic stress. Am J Physiol Cell Physiol. 2010;298:C1583–C93.
Hirokawa N, Heuser JE. Quick-freeze, deep-etch visualization of the cytoskeleton beneath surface differentiations of intestinal epithelial cells. J Cell Biol. 1981;91:399–409.
Holinstat M, Knezevic N, Broman M, Samarel AM, Malik AB, Mehta D. Suppression of RhoA activity by focal adhesion kinase-induced activation of p190RhoGAP: role in regulation of endothelial permeability. J Biol Chem. 2006;281:2296–305.
Huveneers S, Oldenburg J, Spanjaard E, van der Krogt G, Grigoriev I, Akhmanova A, Rehmann H, de Rooij J. Vinculin associates with endothelial VE-cadherin junctions to control force-dependent remodeling. J Cell Biol. 2012;196:641–52.
Iden S, Misselwitz S, Peddibhotla SS, Tuncay H, Rehder D, Gerke V, Robenek H, Suzuki A, Ebnet K. aPKC phosphorylates JAM-A at Ser285 to promote cell contact maturation and tight junction formation. J Cell Biol. 2012;196:623–39.
Ikenouchi J, Furuse M, Furuse K, Sasaki H, Tsukita S. Tricellulin constitutes a novel barrier at tricellular contacts of epithelial cells. J Cell Biol. 2005;171:939–45.
Indra I, Hong S, Troyanovsky R, Kormos B, Troyanovsky S. The adherens junction: a mosaic of cadherin and nectin clusters bundled by actin filaments. J Invest Dermatol. 2013;133:2546–54.
Itoh M, Furuse M, Morita K, Kubota K, Saitou M, Tsukita S. Direct binding of three tight junction-associated MAGUKs, ZO-1, ZO-2, and ZO-3, with the COOH termini of claudins. J Cell Biol. 1999;147:1351–63.
Jacobson JR, Dudek SM, Singleton PA, Kolosova IA, Verin AD, Garcia JG. Endothelial cell barrier enhancement by ATP is mediated by the small GTPase Rac and cortactin. Am J Physiol Lung Cell Mol Physiol. 2006;291:L289–L95.
Jho D, Mehta D, Ahmmed G, Gao XP, Tiruppathi C, Broman M, Malik AB. Angiopoietin-1 opposes VEGF-induced increase in endothelial permeability by inhibiting TRPC1-dependent Ca2 influx. Circ Res. 2005;96:1282–90.
Katsube T, Takahisa M, Ueda R, Hashimoto N, Kobayashi M, Togashi S. Cortactin associates with the cell-cell junction protein ZO-1 in both Drosophila and mouse. J Biol Chem. 1998;273:29672–7.
Kouklis P, Konstantoulaki M, Vogel S, Broman M, Malik AB. Cdc42 regulates the restoration of endothelial barrier function. Circ Res. 2004;94:159–66.
Kowalczyk AP, Green KJ. Structure, function, and regulation of desmosomes. Prog Mol Biol Transl Sci. 2013;116:95–118.
Kruttgen A, Rose-John S. Interleukin-6 in sepsis and capillary leakage syndrome. J Interferon Cytokine Res. 2012;32:60–5.
Kussel-Andermann P, El-Amraoui A, Safieddine S, Nouaille S, Perfettini I, Lecuit M, Cossart P, Wolfrum U, Petit C. Vezatin, a novel transmembrane protein, bridges myosin VIIA to the cadherin-catenins complex. EMBO J. 2000;19:6020–9.
Lambert O, Taveau JC, Him JL, Al Kurdi R, Gulino-Debrac D, Brisson A. The basic framework of VE-cadherin junctions revealed by cryo-EM. J Mol Biol. 2005;346:1193–6.
Leach L, Lammiman MJ, Babawale MO, Hobson SA, Bromilou B, Lovat S, Simmonds MJ. Molecular organization of tight and adherens junctions in the human placental vascular tree. Placenta. 2000;21:547–57.
Lu Q, Sakhatskyy P, Grinnell K, Newton J, Ortiz M, Wang Y, Sanchez-Esteban J, Harrington EO, Rounds S. Cigarette smoke causes lung vascular barrier dysfunction via oxidative stress-mediated inhibition of RhoA and focal adhesion kinase. Am J Physiol Lung Cell Mol Physiol. 2011;301:L847–L57.
Macfarlane SR, Seatter MJ, Kanke T, Hunter GD, Plevin R. Proteinase-activated receptors. Pharmacol Rev. 2001;53:245–82.
Maekawa M, Ishizaki T, Boku S, Watanabe N, Fujita A, Iwamatsu A, Obinata T, Ohashi K, Mizuno K, Narumiya S. Signaling from Rho to the actin cytoskeleton through protein kinases ROCK and LIM-kinase. Science. 1999;285:895–8.
Maeng YS, Maharjan S, Kim JH, Park JH, Suk Y Yu, Kim YM, Kwon YG. Rk1, a ginsenoside, is a new blocker of vascular leakage acting through actin structure remodeling. PLoS One. 2013;8:e68659.

Maharjan S, Kim K, Agrawal V, Choi HJ, Kim NJ, Kim YM, Suh YG, Kwon YG. Sac-1004, a novel vascular leakage blocker, enhances endothelial barrier through the cAMP/Rac/cortactin pathway. Biochem Biophys Res Commun. 2013;435:420–7.

Martinez-Quiles N, Ho HY, Kirschner MW, Ramesh N, Geha RS. Erk/Src phosphorylation of cortactin acts as a switch on-switch off mechanism that controls its ability to activate N-WASP. Mol Cell Biol. 2004;24:5269–80.

Matthews BD, Thodeti CK, Tytell JD, Mammoto A, Overby DR, Ingber DE. Ultra-rapid activation of TRPV4 ion channels by mechanical forces applied to cell surface beta1 integrins. Integr Biol (Camb). 2010;2:435–42.

Mong PY, Petrulio C, Kaufman HL, Wang Q. Activation of Rho kinase by TNF-alpha is required for JNK activation in human pulmonary microvascular endothelial cells. J Immunol. 2008;180:550–8.

Murakami T, Felinski EA, Antonetti DA. Occludin phosphorylation and ubiquitination regulate tight junction trafficking and vascular endothelial growth factor-induced permeability. J Biol Chem. 2009;284:21036–46.

Nagar B, Overduin M, Ikura M, Rini JM. Structural basis of calcium-induced E-cadherin rigidification and dimerization. Nature. 1996;380:360–4.

Nagumo Y, Han J, Bellila A, Isoda H, Tanaka T. Cofilin mediates tight-junction opening by redistributing actin and tight-junction proteins. Biochem Biophys Res Commun. 2008;377:921–5.

Nilius B, Droogmans G. Ion channels and their functional role in vascular endothelium. Physiol Rev. 2001;81:1415–59.

Nomme J, Fanning AS, Caffrey M, Lye MF, Anderson JM, Lavie A. The Src homology 3 domain is required for junctional adhesion molecule binding to the third PDZ domain of the scaffolding protein ZO-1. J Biol Chem. 2011;286:43352–60.

Nwariaku FE, Liu Z, Zhu X, Turnage RH, Sarosi GA, Terada LS. Tyrosine phosphorylation of vascular endothelial cadherin and the regulation of microvascular permeability. Surgery. 2002;132:180–5.

Ooshio T, Irie K, Morimoto K, Fukuhara A, Imai T, Takai Y. Involvement of LMO7 in the association of two cell-cell adhesion molecules, nectin and E-cadherin, through afadin and alpha-actinin in epithelial cells. J Biol Chem. 2004;279:31365–73.

Orsenigo F, Giampietro C, Ferrari A, Corada M, Galaup A, Sigismund S, Ristagno G, Maddaluno L, Koh GY, Franco D, et al. Phosphorylation of VE-cadherin is modulated by haemodynamic forces and contributes to the regulation of vascular permeability in vivo. Nat Commun. 2012;3:1208.

Petreaca ML, Yao M, Liu Y, Defea K, Martins-Green M. Transactivation of vascular endothelial growth factor receptor-2 by interleukin-8 (IL-8/CXCL8) is required for IL-8/CXCL8-induced endothelial permeability. Mol Biol Cell. 2007;18:5014–23.

Pirot N, Delpech H, Deleuze V, Dohet C, Courtade-Saidi M, Basset-Leobon C, Chalhoub E, Mathieu D, Pinet V. Lung endothelial barrier disruption in Lyl1-deficient mice. Am J Physiol Lung Cell Mol Physiol. 2014;306:L775–L85.

Qiao J, Huang F, Lum H. PKA inhibits RhoA activation: a protection mechanism against endothelial barrier dysfunction. Am J Physiol Lung Cell Mol Physiol. 2003;284:L972–L80.

Rajput C, Kini V, Smith M, Yazbeck P, Chavez A, Schmidt T, Zhang W, Knezevic N, Komarova Y, Mehta D. Neural Wiskott-Aldrich syndrome protein (N-WASP)-mediated p120-catenin interaction with Arp2-Actin complex stabilizes endothelial adherens junctions. J Biol Chem. 2013;288:4241–50.

Rakshit S, Zhang Y, Manibog K, Shafraz O, Sivasankar S. Ideal, catch, and slip bonds in cadherin adhesion. Proc Natl Acad Sci U S A. 2012;109:18815–20.

Ramchandran R, Mehta D, Vogel SM, Mirza MK, Kouklis P, Malik AB. Critical role of Cdc42 in mediating endothelial barrier protection in vivo. Am J Physiol Lung Cell Mol Physiol. 2008;295:L363–L9.

Rikitake Y, Mandai K, Takai Y. The role of nectins in different types of cell-cell adhesion. J Cell Sci. 2012;125:3713–22.

Saito M, Tucker DK, Kohlhorst D, Niessen CM, Kowalczyk AP. Classical and desmosomal cadherins at a glance. J Cell Sci. 2012;125:2547–52.

Samanta D, Ramagopal UA, Rubinstein R, Vigdorovich V, Nathenson SG, Almo SC. Structure of Nectin-2 reveals determinants of homophilic and heterophilic interactions that control cell-cell adhesion. Proc Natl Acad Sci U S A. 2012;109:14836–40.

Sheldon R, Moy A, Lindsley K, Shasby S, Shasby DM. Role of myosin light-chain phosphorylation in endothelial cell retraction. Am J Physiol. 1993;265:L606–L12.

Shen Q, Rigor RR, Pivetti CD, Wu MH, Yuan SY. Myosin light chain kinase in microvascular endothelial barrier function. Cardiovasc Res. 2010;87:272–80.

Shikata Y, Rios A, Kawkitinarong K, DePaola N, Garcia JG, Birukov KG. Differential effects of shear stress and cyclic stretch on focal adhesion remodeling, site-specific FAK phosphorylation, and small GTPases in human lung endothelial cells. Exp Cell Res. 2005;304:40–9.

Shiobara T, Usui T, Han J, Isoda H, Nagumo Y. The reversible increase in tight junction permeability induced by capsaicin is mediated via cofilin-actin cytoskeletal dynamics and decreased level of occludin. PLoS One. 2013;8:e79954.

Sidhaye VK, Schweitzer KS, Caterina MJ, Shimoda L, King LS. Shear stress regulates aquaporin-5 and airway epithelial barrier function. Proc Natl Acad Sci U S A. 2008;105:3345–50.

Simionescu N, Simionescu M, Palade GE. Open junctions in the endothelium of the postcapillary venules of the diaphragm. J Cell Biol. 1978;79:27–44.

Singh I, Knezevic N, Ahmmed GU, Kini V, Malik AB, Mehta D. Galphaq-TRPC6-mediated Ca2 + entry induces RhoA activation and resultant endothelial cell shape change in response to thrombin. J Biol Chem. 2007;282:7833–43.

Slee JB, Lowe-Krentz LJ. Actin realignment and cofilin regulation are essential for barrier integrity during shear stress. J Cell Biochem. 2013;114:782–95.

Spindler V, Schlegel N, Waschke J. Role of GTPases in control of microvascular permeability. Cardiovasc Res. 2010;87:243–53.

Steed E, Rodrigues NT, Balda MS, Matter K. Identification of MarvelD3 as a tight junction-associated transmembrane protein of the occludin family. BMC Cell Biol. 2009;10:95.

Sundivakkam PC, Freichel M, Singh V, Yuan JP, Vogel SM, Flockerzi V, Malik AB, Tiruppathi C. The Ca(2 + ) sensor stromal interaction molecule 1 (STIM1) is necessary and sufficient for the store-operated Ca(2 + ) entry function of transient receptor potential canonical (TRPC) 1 and 4 channels in endothelial cells. Mol Pharmacol. 2012;81:510–26.

Thodeti CK, Matthews B, Ravi A, Mammoto A, Ghosh K, Bracha AL, Ingber DE. TRPV4 channels mediate cyclic strain-induced endothelial cell reorientation through integrin-to-integrin signaling. Circ Res. 2009;104:1123–30.

Ting LH, Jahn JR, Jung JI, Shuman BR, Feghhi S, Han SJ, Rodriguez ML, Sniadecki NJ. Flow mechanotransduction regulates traction forces, intercellular forces, and adherens junctions. Am J Physiol Heart Circ Physiol. 2012;302:H2220–H9.

Tiruppathi C, Minshall RD, Paria BC, Vogel SM, Malik AB. Role of Ca2 + signaling in the regulation of endothelial permeability. Vascul Pharmacol. 2002;39:173–85.

Truffi M, Dubreuil V, Liang X, Vacaresse N, Nigon F, Han SP, Yap AS, Gomez GA, Sap J. Receptor protein tyrosine phosphatase RPTPalpha controls epithelial adherens junctions, linking E-cadherin engagement to c-Src signaling to cortactin. J Cell Sci. 2014;127:2420–32.

Tsicopoulos A, de Nadai P, Glineur C. Environmental and genetic contribution in airway epithelial barrier in asthma pathogenesis. Curr Opin Allergy Clin Immunol. 2013;13:495–9.

Van Itallie CM, Aponte A, Tietgens AJ, Gucek M, Fredriksson K, Anderson JM. The N and C termini of ZO-1 are surrounded by distinct proteins and functional protein networks. J Biol Chem. 2013;288:13775–88.

van Nieuw Amerongen GP, Vermeer MA, van Hinsbergh VW. Role of RhoA and Rho kinase in lysophosphatidic acid-induced endothelial barrier dysfunction. Arterioscler Thromb Vasc Biol. 2000;20:E127–E33.

Vandenbroucke E, Mehta D, Minshall R, Malik AB. Regulation of endothelial junctional permeability. Ann N Y Acad Sci. 2008;1123:134–45.

Vandenbroucke St Amant E, Tauseef M, Vogel SM, Gao XP, Mehta D, Komarova YA, Malik AB. PKCalpha activation of p120-catenin serine 879 phospho-switch disassembles VE-cadherin junctions and disrupts vascular integrity. Circ Res. 2012;111:739–49.

Vogel SM, Gao X, Mehta D, Ye RD, John TA, Andrade-Gordon P, Tiruppathi C, Malik AB. Abrogation of thrombin-induced increase in pulmonary microvascular permeability in PAR-1 knockout mice. Physiol Genomics. 2000;4:137–45.

Wang L, Chiang ET, Simmons JT, Garcia JG, Dudek SM. FTY720-induced human pulmonary endothelial barrier enhancement is mediated by c-Abl. Eur Respir J. 2011a;38:78–88.

Wang Y, Minshall RD, Schwartz DE, Hu G. Cyclic stretch induces alveolar epithelial barrier dysfunction via calpain-mediated degradation of p120-catenin. Am J Physiol Lung Cell Mol Physiol. 2011b;301:L197–L206.

Wang T, Wang L, Moreno-Vinasco L, Lang GD, Siegler JH, Mathew B, Usatyuk PV, Samet JM, Geyh AS, Breysse PN, et al. Particulate matter air pollution disrupts endothelial cell barrier via calpain-mediated tight junction protein degradation. Part Fibre Toxicol. 2012;9:35.

Weis WI, Nelson WJ. Re-solving the cadherin-catenin-actin conundrum. J Biol Chem. 2006;281:35593–7.

West JB. How well designed is the human lung? Am J Respir Crit Care Med. 2006;173:583–4.

Wojciak-Stothard B, Potempa S, Eichholtz T, Ridley AJ. Rho and Rac but not Cdc42 regulate endothelial cell permeability. J Cell Sci. 2001;114:1343–55.

Wolfson RK, Mapes B, Garcia JG. Excessive mechanical stress increases HMGB1 expression in human lung microvascular endothelial cells via STAT3. Microvasc Res. 2014;92:50–5.

Xing J, Wang Q, Coughlan K, Viollet B, Moriasi C, Zou MH. Inhibition of AMP-activated protein kinase accentuates lipopolysaccharide-induced lung endothelial barrier dysfunction and lung injury in vivo. Am J Pathol. 2013;182:1021–30.

Yamada H, Abe T, Satoh A, Okazaki N, Tago S, Kobayashi K, Yoshida Y, Oda Y, Watanabe M, Tomizawa K, et al. Stabilization of actin bundles by a dynamin 1/cortactin ring complex is necessary for growth cone filopodia. J Neurosci. 2013;33:4514–26.

Yano T, Matsui T, Tamura A, Uji M, Tsukita S. The association of microtubules with tight junctions is promoted by cingulin phosphorylation by AMPK. J Cell Biol. 2013;203:605–14.

Yerrapureddy A, Tobias J, Margulies SS. Cyclic stretch magnitude and duration affect rat alveolar epithelial gene expression. Cell Physiol Biochem. 2010;25:113–22.

Yonemura S, Wada Y, Watanabe T, Nagafuchi A, Shibata M. alpha-Catenin as a tension transducer that induces adherens junction development. Nat Cell Biol. 2010;12:533–42.

Yuan D, He P. Vascular remodeling alters adhesion protein and cytoskeleton reactions to inflammatory stimuli resulting in enhanced permeability increases in rat venules. J Appl Physiol. 2012;(1985) 113:1110–20.

Zebda N, Tian Y, Tian X, Gawlak G, Higginbotham K, Reynolds AB, Birukova AA, Birukov KG. Interaction of p190RhoGAP with C-terminal domain of p120-catenin modulates endothelial cytoskeleton and permeability. J Biol Chem. 2013;288:18290–9.

Zhao J, Singleton PA, Brown ME, Dudek SM, Garcia JG. Phosphotyrosine protein dynamics in cell membrane rafts of sphingosine-1-phosphate-stimulated human endothelium: role in barrier enhancement. Cell Signal. 2009;21:1945–60.

# Chapter 5
# Barrier Enhancing Signals

**Panfeng Fu and Viswanathan Natarajan**

**Abbreviations**

| | |
|---|---|
| AJs | Adherens junctions |
| AKAP9 | A-kinase anchoring protein 9 |
| ANP | Atrial natriuretic peptide |
| ARAP3 | ArfGAP, RhoGAP, ankyrin repeats and PH domain 3 |
| Arf | ADP ribosylation factor |
| ARM | Armadillo |
| C3G | Cyanidin 3-Glucoside |
| CAR | Coxsackie and adenovirus receptors |
| cAMP | Cyclic adenosine monophosphate |
| Cdc42 | Cell division cycle 42 GTP-binding protein |
| cGMP | Cyclic guanosine monophosphate |
| CNB | Cyclic nucleotide binding |
| DEP-1 | Density enhanced phosphatase-1 |
| EC | Extracellular repeat |
| ECM | Extracellular matrix |
| ECs | Endothelial cells |
| Epac | Exchange protein activated by cAMP |
| FAK | Focal adhesion kinase |
| FAT | Focal adhesion targeting |
| FERM | Four-point-one, ezrin, radixin, moesin binding domain |
| Gab1 | Grb2-associated binder 1 |
| GAP | GTPase activating protein |

V. Natarajan (✉) · P. Fu
Department of Pharmacology, University of Illinois at Chicago COMRB,
Rm. # 3137, 909 South Wolcott Ave., Chicago, IL 60612, USA
e-mail: visnatar@uic.edu

P. Fu
e-mail: pfu@uic.edu



A. N. Makanya (ed.), *The Vertebrate Blood-Gas Barrier in Health and Disease,*
DOI 10.1007/978-3-319-18392-3_5

| | |
|---|---|
| GDI | Guanine nucleotide dissociation inhibitor |
| GUK | Guanylate kinase-like homologues |
| ESAM | Endothelial cell-selective adhesion molecule |
| GEF | GTPase exchange factor |
| GIT1 | G-protein-coupled receptor kinase-interacting protein 1 |
| GJs | Gap junctions |
| GPCR | G-protein coupled receptor |
| Grb2 | Growth factor receptor-bound protein 2 |
| HGF | Hepatic growth factor |
| HPAEC | Human pulmonary arterial endothelial cell |
| IQGAP | IQ motif containing GTPase activating protein |
| JAM | Junctional adhesion molecule |
| KRIT1 | K-Rev1 interaction Trapped gene 1 |
| MDCK | Madin-Darby canine kidney |
| MLC | Myosin light chain |
| MLCK | Myosin light chain kinase |
| NPR | Natriuretic Peptide Receptor |
| PAF | Platelet-activating factor |
| PAK | P21 activated kinase |
| PI3K | Phosphatidylinositol 3-kinase |
| PTP | Protein tyrosine phosphatases |
| Rac1 | Ras-related C3 botulinum toxin substrate |
| Rap1 | Ras-related protein1 |
| RGD | Arg-Gly-Asp peptide |
| Rho | Ras homologue |
| S1P | Sphingosine-1- phosphate |
| S1P1 | S1P receptor 1 |
| SHP2 | Src Homology Phosphatase 2 |
| TGF-β | Tumor growth factor β |
| Tiam1 | T-lymphoma invasion and metastasis 1 |
| TIMP2 | Tissue inhibitor of metalloproteinase 2 |
| TJs | Tight junctions |
| TNF-α | Tumor necrosis factor-α |
| Vav2 | Vav2 guanine nucleotide exchange factor |
| VEGF | Vascular endothelial growth factor |
| WASP | Wiskott-Aldrich syndrome protein |
| WAVE | Wiskott-Aldrich syndrome protein verprolin homologous |
| ZO | Zonula occludens |
| βPIX | Beta-p21-activated kinase-interactive exchange factor |

## 5.1 Introduction

The continuous monolayers of endothelial and epithelial cells lining the luminal surface of pulmonary microvessels and the pulmonary alveoli, respectively, are vital for efficient gas exchange in the lung. Both monolayers are essential for minimizing the plasma leakage of blood (both cells and plasma) into pulmonary interstitium. Stability of the monolayer is highly regulated by a wide range of signaling pathways that ultimately enhance cytoskeleton rearrangement, cell–cell interactions, and cell–matrix attachment. Cell–cell interactions involve a complex network of adhesion proteins that bind to each other and are linked to intracellular cytoskeletal and signaling partners. These proteins are organized into distinct structures and can be categorized into three groups, namely, adherens junctions (AJs), tight junctions (TJs), and gap junctions (GJs). They provide structural support for intercellular connection and maintain membrane integrity. They also take part in actin cytoskeleton remodeling, signaling transportation, and transcriptional regulation. Various signaling proteins and second messengers involved in barrier function have been identified, including small GTPases, tyrosine kinases, serine/threonine kinases, and lipid mediators. In this chapter, we focus on the role of the barrier enhancement signaling pathways and their underlying mechanism. We also discuss their potential development of barrier protective therapeutics.

## 5.2 Role of Cell–Cell Adhesions Junctions in Regulating Endothelial/Epithelial Barrier Function

Endothelial cells (ECs) and epithelial cells have all three types of cell–cell junctions assembled at cell–cell adhesions that maintain the integrity of endothelium and alveoli (Fig. 5.1).

While AJs and TJs are essential for monolayer permeability, GJs allow changes in transmembrane potential and serve a portal for the selective and direct cell-to-cell transfer of signaling molecules and ions. Therefore, GJs may not directly regulate monolayer permeability. This chapter focuses on the nature of molecular compositions of AJs and TJs in ECs, which are similar to those in epithelial cells (Hartsock and Nelson 2008), with some exceptions.

### *5.2.1 Structure of AJs*

ECs and epithelial cells express different AJs proteins. ECs express mainly vascular endothelial-cadherin (VE-cadherin) and neural cadherin (N-cadherin), whereas epithelial cells harbor epithelial cadherin (E-cadherin). Each cadherin has a relatively small cytoplasmic domain, a transmembrane domain, and a bulky extracellular binding domain. Both VE-cadherin and E-cadherin tend to form homogeneous

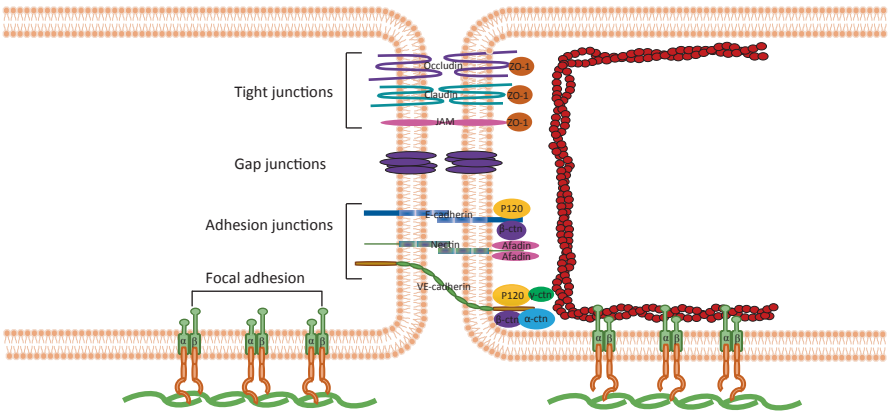


**Fig. 5.1** Intercellular and matrix structures maintaining cell barrier function. Typical cell–cell contacts include adhesions junctions, tight junctions, and gap junctions. Occludin, claudins, and JAMs are the backbones of tight junctions. VE-cadherin, E-cadherin, and nectin are components of adhesions junctions for endothelial and epithelial cells. Integrins mediate the interaction between cell and matrix. These structures utilize intracellular binding partners (ZO, p120 catenin, β-catenin, γ-catenin, α-catenin, afadin, vinculin, and talin) to stabilize their localization and interaction with cortical actin cytoskeleton. (*VE-cadherin* vascular endothelial cadherin, *E-cadherin* epithelial cadherin, *JAMs* junctional adhesion molecules, *ZO* zonula occludens )

clusters in a $Ca^{2+}$-dependent manner. VE-cadherin plays a key role in the maintenance of the vascular barrier function. Most barrier protective agonists promote cadherin stability and enhancement at AJs (Fig. 5.2), however, these agonists initiate distinct signaling pathways. Although both endothelial and epithelial cells play critical roles in maintaining pulmonary permeability, ECs are more intensively investigated for the mechanisms of pulmonary permeability. Therefore, we mainly focus on the mechanisms of barrier enhancement observed in ECs.

### *5.2.2 VE-Cadherin Structure*

Based on domain structure, genomic organization, and protein analysis, there exist five major groups of cadherins namely, the classical type I cadherins, atypical type II cadherin, desmogleins, desmocollins, and BS-cadherin (Nollet et al. 2000). VE-cadherin (CD144, cadherin 5, or type II cadherin) is encoded by the human gene CDH5. The protein is composed of five extracellular cadherin repeats (EC1–5), followed by a single transmembrane region, and a short cytoplasmic tail. It forms calcium-dependent *trans* homophilic interactions, through its EC, with VE-cadherins expressed on adjacent cells. The *trans* interaction is mediated by EC1 (Al-Kurdi et al. 2004; Hewat et al. 2007; Lambert et al. 2005). This is supported by the finding that antibodies to the EC1 region, but not EC3 and EC4, of VE-cadherin inhibit vessel formation and disrupt endothelial barrier function (Corada et al. 2001). *Trans* homophilic interaction is preceded by *cis* homophilic interaction of two adjacent

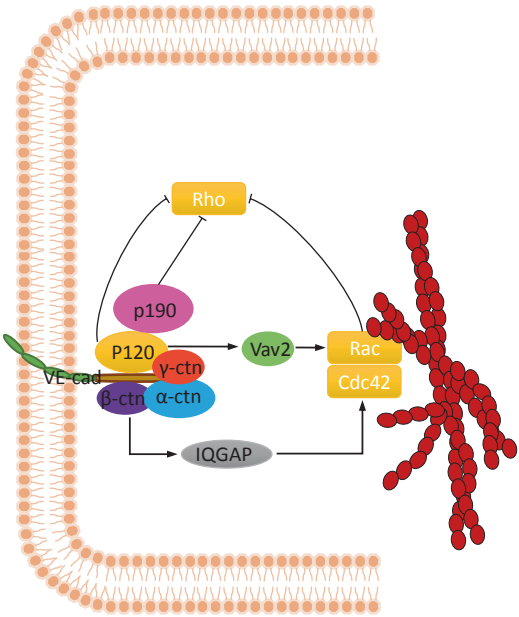


**Fig. 5.2** Model of adherens junction (AJ) complex. The AJ complex is formed by homotypic interactions of transmembrane VE-cadherin, which binds to p120 catenin at the juxtamembrane domain and either β-catenin or γ-catenin at the catenin-binding domain. Attachment of actin cytoskeleton to VE-cadherin is mediated by α-catenin. Interaction of VE-cadherin with these plakoglobin proteins conveys signals to activate small GTPases Rac1 and Cdc42, or inactivate Rho, resulting in formation of cortical actin ring and enhanced barrier function. (*VE-cadherin* vascular endothelial-cadherin, *Rac1* ras-related C3 botulinum toxin substrate, *Cdc42* cell division cycle 42 GTP-binding protein, *Rho* ras homologue)

VE-cadherin molecules within the plane of the plasma membrane of one cell. *Cis*-interaction is mediated by lateral interactions between EC1 repeats of VE-cadherin molecules that are on the same cell surface. This interaction occurs via insertion of the side chain of conserved Trp2 and Trp4 residue into a complementary hydrophobic pocket in its partner (Patel et al. 2006). Both *cis*- and *trans* interactions are dependent on the presence of $Ca^{2+}$.

In addition to homophilic interactions, VE-cadherin interacts directly with proteins of the Armadillo-repeat gene family, including p120 catenin, plakoglobin (γ-catenin), and β-catenin through its cytoplasmic domain. Moreover, VE-cadherin also indirectly associates with other adaptors, cytoskeletal and signaling proteins, such as α-catenin, actin, and p190RhoGAP.

The cytoplasmic domains of VE-cadherin, N-cadherin, and E-cadherin are highly homologous. All of them contain a juxtamembrane domain and a C-terminal catenin-binding domain. Both domains interact with the armadillo-repeat domain (ARM domain) of p120 catenin, β-catenin, and plakoglobin proteins. The ARM repeats create a tertiary structure consisting of a positively charged groove that binds to the negatively charged region of cadherins$^{8-}$ (Anastasiadis and Reynolds 2000). Similar

to p120 catenin, the binding of β-catenin and plakoglobin to VE-cadherin is also mediated through the ARM domains, and these two proteins bind to the CBD in a mutually exclusive fashion. β-catenin has 12 ARM repeats; each repeat is composed of three α-helices in close apposition, forming a superhelix. There is a 130-amino-acid N-terminal extension and a 100-amino-acid C-terminal extension. A 100-amino-acid region of cadherin, spanning residues 625–723, interacts across the entire 12 ARM motifs. The interaction between VE-cadherin and β-catenin occurs in early endoplasmic reticulum (ER) formation (Hinck et al. 1994) and VE-cadherin interacts with plakoglobin at a later stage of AJ formation (Schnittler et al. 1997).

## *5.2.3 Barrier Enhancement via VE-Cadherin*

### 5.2.3.1 p120 Catenin-Mediated VE-Cadherin Enhancement

VE-cadherin availability at the cell surface is a critical determinant for vascular barrier integrity, therefore, many barrier enhancement signaling pathways exert their roles by regulating the stability and availability of VE-cadherin at AJ. Binding of VE-cadherin with catenins provide structural basis for VE-cadherin stability at AJ. Earlier studies pointed out that manipulating p120 catenin availability exerted significant influence on intracellular VE-cadherin levels. Expression of VE-cadherin mutants that complete for β-catenin resulted in a decrease in endothelial barrier function and a dramatic downregulation of endogenous VE-cadherin (Iyer et al. 2004; Xiao et al. 2003). Further, downregulation of p120 catenin using specific small interfering RNA (siRNA) resulted in a corresponding loss of VE-cadherin (Iyer et al. 2004; Xiao et al. 2003), whereas, overexpression of p120 catenin inhibited VE-cadherin entry into endocytic compartments and caused a corresponding increase in cell surface levels of VE-cadherin (Iyer et al. 2004; Xiao et al. 2003). Interestingly, mutating the p120 catenin binding site on dominant negative VE-cadherin mutants abrogated the ability of the mutant to cause downregulation of the endogenous cadherin (Xiao et al. 2003). Later studies revealed that the direct binding of p120 catenin to VE-cadherin helps to retain VE-cadherin at the cell surface. Serine 879 of p120 catenin was recently identified to be phosphorylated by protein kinase C α in response to lipopolysaccharide (LPS) and thrombin. The phosphorylation of this site mediates p120 catenin binding affinity for VE-cadherin (Vandenbroucke St Amant et al. 2012). Meanwhile, a dual-function motif in VE-cadherin consisting of three highly conserved acidic residues has been identified to alternately serve as a p120 catenin-binding interface and an endocytic signal, and mutation of this motif resulted in resistance to endocytosis (Nanes et al. 2012). Clathrin-mediated endocytosis of VE-cadherin is inhibited as it interacts with the dileucine motif of VE-cadherin and precludes its binding to adaptor proteins of the endocytic machinery (Vaezi et al. 2002; Vasioukhin et al. 2000; Verma et al. 2004). Regulation of VE-cadherin by p120 catenin not only involves the stability of VE-cadherin at the cell surface but also their effects on Ras homologue (Rho) family GTPases. Rho family GTPases (including Ras homologue gene family, member

A (RhoA), Rac, and Cell division cycle 42 GTP-binding protein (Cdc42)) are key mediators of cytoskeletal dynamics. The interaction between p120 catenin with Rho GTPase activating protein (p190RhoGAP) promotes p190RhoGAP recruitment to cell periphery and local inhibition of Rho activity. The inhibition of Rho by p120 catenin interaction with p190GAP accounts for the barrier protective effects of oxidized phospholipids. It was further identified that the interaction between p120 catenin and p190RhoGAP is mediated by a 23-amino-acids stretch within the C-terminal domain of p120 catenin (amino acids 820–842; Zebda et al. 2013). Different mechanisms were proposed based on the cell types. p120 catenin was shown to interact preferentially with the GDP-bound of RhoA or Rho1 (the RhoA homology; Anastasiadis et al. 2000; Magie et al. 2002), as would be predicted for a protein acting as Guanine Nucleotide Dissociation Inhibitor (GDI). A study with highly purified proteins also implied a direct interaction between p120 catenin and RhoA (Anastasiadis et al. 2000). Alternatively, p120 catenin may exert its inhibitory effect on Rho through direct interaction with Vav2, Rho GTPase exchange factor (Rho GEF), which could account for the ability of p120 catenin to activate Ras-related C3 botulinum toxin substrate (Rac1) and Cdc42 because Rac1 can inhibit RhoA in some cells via a mechanism that involves reactive oxygen species, low molecular weight (LMW) phosphatase, and p190 RhoGAP (Nimnual et al. 2003).

#### 5.2.3.2 β-Catenin and Plakoglobin-Mediated VE-Cadherin Enhancement

Interaction of VE-cadherin with β-catenin also regulates the amount of VE-cadherin at AJ. The cytoplasmic C-terminus of VE-cadherin is prone to degradation due to the presence of proline, glutamic acid, serine, and threonine (PEST) domain that is targeted for ubiquitination. β-Catenin binding to this region prevents the exposure of cadherin C-terminal tail (Chen et al. 1999; Huber et al. 2001; Huber and Weis 2001). In addition to p120 catenin that regulates AJ stability by modulating GTPase activity, β-catenin also demonstrates such effect. It acts by recruiting IQRas GTP-activating protein 1 (IQGAP1) at AJ. IQGAP1, however, lacks GAP activity. It binds to Rac1 and Cdc42 and inhibits their intrinsic GTPase activity, thus stabilizing them in the active GTP-bound form (Briggs and Sacks 2003, 2006). A recent study revealed different roles for p120 catenin and β-catenin in AJ formation and its strengthening (Oas et al. 2013). P120 catenin appears to regulate adhesive contact area in a Rac1-dependent manner without affecting adhesion as such. In contrast, binding of VE-cadherin to β-catenin resulted in promoting strong steady-state adhesion strength. Plakoglobin also binds to a similar region in VE-cadherin, but it cannot compensate for β-catenin (Cattelino et al. 2003; Schnittler et al. 1997). Overexpression of plakoglobin in human microvascular endothelial cell increased endothelial barrier function (Venkiteswaran et al. 2002). The converse, inhibition of plakoglobin expression resulted in AJ disassembly in ECs exposed to shear stress (Schnittler et al. 1997). Cortical actin ring, which is characterized by actin accumulation at cell–cell contact area, is one of the architectural features of enhanced barrier function. VE-cadherin is anchored to cortical actin cytoskeleton through β-catenin and plakoglobin thus,

stabilizing VE-cadherin at AJ. Both β-catenin and plakoglobin play a key role in bridging VE-cadherin and actin skeleton through α-catenin and/or desmoplakin/vimentin. α-catenin lacks ARM domains and does not associate with VE-cadherin directly, but can interact with actin cytoskeleton through vinculin and α-actinin. Attachment of VE-cadherin to the actin cytoskeleton reduces the lateral mobility of VE-cadherin, thereby inducing VE-cadherin clustering and a subsequent increase in the strength of AJ (Baumgartner et al. 2003; Waschke et al. 2004a, b). However, a direct interaction of the cadherin-β-catenin–α-catenin complex with actin filament appears to be questionable as α-catenin cannot simultaneously bind to β-catenin and actin and therefore, cannot serve as a link between the actin cytoskeleton and the cadherin complex (Drees et al. 2005; Yamada et al. 2005). Unlike β-catenin, plakoglobin mediates attachment of VE-cadherin to intermediate filaments cytoskeleton through desmoplakin (Kowalczyk et al. 1998; Valiron et al. 1996).

## 5.3 Protein Tyrosine Phosphatases (PTPs)-Mediated AJ Enhancement

Phosphorylation of AJ complex proteins leads to destabilization of the AJ and increases cell monolayer permeability. Barrier disruptive factors, such as vascular endothelial growth factor (VEGF), tumor necrosis factor-α (TNF-α), platelet-activating factor (PAF), thrombin, and histamine induce tyrosine phosphorylation of VE-cadherin, p120 catenin, β-catenin, and plakoglobin, suggesting that phosphorylation of these AJ proteins promotes disruption of cell–cell contacts. Protein tyrosine phosphatases (PTPs) interact with AJ either directly or indirectly to regulate dephosphorylation of AJ proteins and maintain the stability of the AJ complex. Several phosphatases have been identified that regulate endothelial cell–cell junction, including PTPμ, Src Homology Phosphatase-2 (SHP-2), PTP1B, VE-PTP, and Density enhanced phosphatase-1 (DEP-1) (Nakamura et al. 2008; Nottebaum et al. 2008; Sui et al. 2005). PTPs are composed of 44 isoforms and can be grouped as the receptor and nonreceptor types. Among the five PTPs expressed in EC, PTPμ, VE-PTP, and DEP-1 belong to receptor-type PTP, and SHP-2 and PTPB1 belong to nonreceptor-type PTP. Receptor-type PTP consists of highly variable extracellular region and one or two intracellular phosphatase domains. PTPμ was observed almost exclusively at cell–cell contacts, bound directly to VE-cadherin and p120 catenin (Sui et al. 2005; Zondag et al. 2000). Overexpression of PTPμ decreased VE-cadherin tyrosine phosphorylation and permeability of the monolayer (Sui et al. 2005). In addition, downregulation of PTPμ by siRNA in ECs impaired the barrier function suggesting a critical role in the regulation of AJ integrity (Sui et al. 2005). It is interesting to note that prostate carcinoma cells lacking endogenous PTPμ show disability to form AJ, though, E-cadherin and the catenin proteins are present. Expression of catalytically dead PTPμ restored cadherin-mediated cell–cell adhesion (Hellberg et al. 2002). This finding suggests that PTPμ can maintain the stability of VE-cadherin-mediated AJ by recruiting regulatory proteins to sites of AJ by virtue

of a scaffold protein thereby, invoking an alternate mechanism. VE-PTP is expressed exclusively in the ECs (Baumer et al. 2006), interacts with the extracellular region in VE-cadherin (Nawroth et al. 2002), and maintains it in a dephosphorylated status. VE-PTP null mice show vascular defects (Dominguez et al. 2007) indicating a critical role for VE-PTP in the stabilization and remodeling of the vasculature. The dissociation of VE-PTP and VE-cadherin is a prerequisite for the destabilization of endothelial cell contacts, in response to VEGF and LPS challenge (Broermann et al. 2011) and leukocyte transmigration (Nottebaum et al. 2008). Nevertheless, VE-PTP maintains VE-cadherin integrity through plakoglobin, and not through β-catenin, as overexpression of VE-PTP leads to its increased association with plakoglobin, but not β-catenin in conjunction with VE-cadherin (Nottebaum et al. 2008). DEP-1 is another receptor-type PTP whose expression and activity are upregulated with increasing levels of cell confluence (Ostman et al. 1994). It indirectly associates with VE-cadherin by binding to p120 catenin, plakoglobin, and β-catenin. It also plays important roles in angiogenesis and vasculogenesis (Takahashi et al. 2006, 2003). On the contrary, DEP-1 may also play a barrier disruptive role. Phosphorylation of DEP-1 at Y1320 leads to Src activation and promotes Src-dependent endothelial permeability (Spring et al. 2012, 2014).

Cytosolic PTPs, PTP1B, and SHP2 also maintain AJ stability in a manner similar to receptor PTPs (Balsamo et al. 1996; Brady-Kalnay et al. 1993; Ukropec et al. 2000). Direct binding of PTPB1 to the cytoplasmic domain of N-cadherin promotes β-catenin recruitment to N-cadherin and cell membrane (Xu et al. 2002). SHP2 specifically associates with β-catenin (Ukropec et al. 2000). Loss of SHP2 from VE-cadherin complex accounts for the increase in phosphorylation of β-catenin, plakoglobin, and p120 catenin in response to thrombin treatment (Grinnell et al. 2010; Ukropec et al. 2000), in support of a key role in the stabilization of AJs. SHP2 is also involved in the recovery of endothelial AJs through control of β-catenin phosphorylation (Timmerman et al. 2012). SHP2-depleted cells showed prolonged elevation in tyrosine phosphorylation levels of VE-cadherin-associated β-catenin after thrombin treatment (Timmerman et al. 2012).

## 5.4 Small GTPases-Mediated Barrier Enhancement

Rho-GTPases have been the target of intense investigation due to their known roles in cytoskeleton organization and barrier function. This subfamily of Ras consists of 23 members that include well characterized members such as Rho, Rac, and Cdc42 (Wennerberg et al. 2005). Rho proteins share approximately 30% homology with the Ras subfamily of proteins and 80–90% homology with each other (Hall 1998). Rho GTPases cycle between an active GTP-bound and an inactive GDP-bound. The inactive GDP-bound Rho proteins are retained in the cytosol in complex with GDI and are activated by guanine nucleotide exchange factors (GEFs), which accelerate the exchange of GDP for GTP. Further, activated Rho proteins are subject to inactivation by GTPase-activating protein (GAPs) that promote hydrolysis GTP to GDP (Takai

et al. 2001). It is the general concept that Rho proteins affect cell adhesion and barrier function via the remodeling of actin (Jaffe and Hall 2005). On the contrary to the barrier disruptive effects of Rho, Rac and Cdc42 have barrier protective effects.

### *5.4.1 Rac1-Mediated Barrier Enhancement Signaling*

Rac1 is usually placed in the center of signaling pathways leading to barrier enhancement. Many barrier enhancement factors act through activation of Rac1 and its downstream target, p21 activated kinase (PAK). Basal Rac activation has been related to monolayer integrity and maintenance (Waschke et al. 2004a, 2004b; Wojciak-Stothard et al. 2001). However, several studies suggest that junctional stability requires a very fine tuning of Rac1 activity as both dominant-negative and constitutively active Rac1 increase endothelial permeability, and are associated with a loss of VE-cadherin at the cell–cell junction (van Wetering et al. 2002; Wojciak-Stothard et al. 2001). A number of barrier enhancement factors, such as sphingosine-1-phosphate (S1P), atrial natriuretic peptide (ANP), hepatic growth factor (HGF), angiopoietin-1, and prostaglandin D2, are known to regulate barrier integrity at least in part, through Rac- and/or Cdc42-dependent cytoskeleton remodeling. The mechanisms of Rac1 activation vary depending on the stimulants.

S1P generated by the activities of sphingosine kinase 1 or 2 on sphingosine. It is released from activated platelets, erythrocytes, and ECs. S1P is known to exert a diverse range of physiological and pathological effects via the activation of five G-protein coupled receptors, $S1P_1$–$S1P_5$. The barrier enhancement effects of S1P are mediated by $S1P_1$ receptor. $S1P_1$ is a 382-amino-acid protein that contains seven transmembrane spanning domains with significant structural similarities to other G-protein coupled receptors (GPCRs). Binding of S1P to $S1P_1$ stimulates mainly two signaling pathways, both of which contribute to enhanced barrier integrity. In one pathway, Rac1 plays a critical role and is characterized by a marked increase in polymerized cortical actin that represents a common and essential feature of barrier protection and also AJ assembly and stabilization. The other pathway involves focal adhesions and matrix interactions. S1P binding to $S1P_1$ receptor induces Gi signaling, which in turn, activates Rac1-specific GEF T-lymphoma invasion and metastasis 1 (Tiam-1) in caveolin-enriched lipid raft in a Phosphatidylinositol 3-kinase (PI3K)-dependent manner (Singleton et al. 2005). Activated Tiam-1 associates with and activates Rac1, resulting in Rac1 redistribution to areas of cell–cell contact (Lee et al. 1999).

ANP is a 28-amino-acid peptide, released mainly by cardiac myocytes of the atria of the heart and acts through three receptors—Natriuretic Peptide Receptor1 (NPR1), Natriuretic Peptide Receptor2 (NPR2), and Natriuretic Peptide Receptor3 (NRP3). Binding of ANP to its receptors induces intracellular Cyclic guanosine monophosphate (cGMP) and Cyclic adenosine monophosphate (cAMP) formation. Although most vascular effects of ANP are mediated by cGMP, barrier protective effect of ANP, however, appears to be mediated by cAMP, as both cGMP activator and inhibitor have no effects on thrombin-induced endothelial barrier permeability

(Birukova et al. 2008c). cAMP is the upstream effecter of ANP-initiated barrier protective response and induced Rac1 activation through PKA-dependent and PKA-independent pathways. In case of PKA-dependent pathway, PKA may regulate Rac1 through Rac1 GEFs, Tiam1, and Vav2 guanine nucleotide exchange factor (Vav2) as Tiam and Vav2 have consensus PKA phosphorylation sites (O'Connor and Mercurio 2001). Alternatively, PKA acts through direct phosphorylation of Rho resulting in the inhibition of this barrier disruptive signaling molecule (Dong et al. 1998; Lang et al. 1996). ANP achieves its barrier protective effects alternatively through PKA-independent and Epac/Rap1-dependent pathway. Epac functions as GEF for Rap1, which is also a small GTPase acting as GEF for Rac. Epa/Rap1 has emerged as a new mechanism for cAMP-mediated barrier protection that could not be attributed to the established target PKA. ANP-elevated cAMP preferentially binds to the N-terminal cyclic nucleotide binding (CNB) domain of Epac and facilitates the auto inhibitory regulatory domain to shift away from the catalytic region, thereby creating access to Rap1 and its activation (Gloerich and Bos 2010). Activated Rap1, in turn, activates the Rac-specific GEF, Vav2 and Tiam1, promoting Rac and Cdc42 activation (Birukova et al. 2007b, 2008c).

HGF, also known as scatter factor, has potent effects on cell proliferation, motility, morphogenesis, survival, and angiogenesis, in various cell types (Bussolino et al. 1992; Grant et al. 1993; Matsumoto and Nakamura 1996; Zhang et al. 2000). HGF is also known to enhance endothelial barrier function by remodeling cytoskeleton and stabilizing AJ complex (Birukova et al. 2007a; 2008b; Liu et al. 2002). The effects of HGF are mediated through the receptor tyrosine kinase c-Met, which is composed of a 50 kDa extracellular αsubunit and a 145 kDa transmembrane βsubunit (Bottaro et al. 1991). Binding of HGF with the receptor stimulates receptor kinase activity, leading to autophosphorylation of the receptor, followed by the recruitment of adaptor proteins, such as Grb2-associated binder-1 (Gab-1), Grb2, PI3K, phospholipase Cγ, Src, and SHP2 (Ponzetto et al. 1994; Schaeper et al. 2000). The effects of HGF on barrier enhancement also appear to be mediated through Rac1 activation (Birukova et al. 2007a, 2008b). HGF binding to the receptor activates Tiam1 via PI3K pathway. Then, Tiam1 activates Rac1. CD44 is also implicated in HGF-induced Rac1 activation as HGF treatment of EC resulted in c-Met association with CD44v10 and recruitment of c-Met into caveolin-enriched microdomains containing CD44. In addition, dynamin 2 is a vesicular regulator that is recruited into caveolin-enriched microdomains in response to HGF treatment. It also mediates Rac1 activation, as knockdown of dynamin 2 by siRNA reduced HGF-induced Rac1 activation (Singleton et al. 2007). Recently S1P1 and integrin β4 were identified to participate in HGF-induced endothelial barrier enhancement. HGF treatment of vascular ECs induced recruitment of c-Met, integrin β4 and S1P1 to caveolin-enriched lipid rafts and c-Met-dependent transactivation of S1P1 and integrin β4 (Ephstein et al. 2013).

As outlined above, Rac1 is a key common player in several signaling pathways and the signals downstream are common. PAK is the major downstream target of Rac1. Several downstream pathways of PAK have been proposed to mediate barrier integrity (Fig. 5.3).

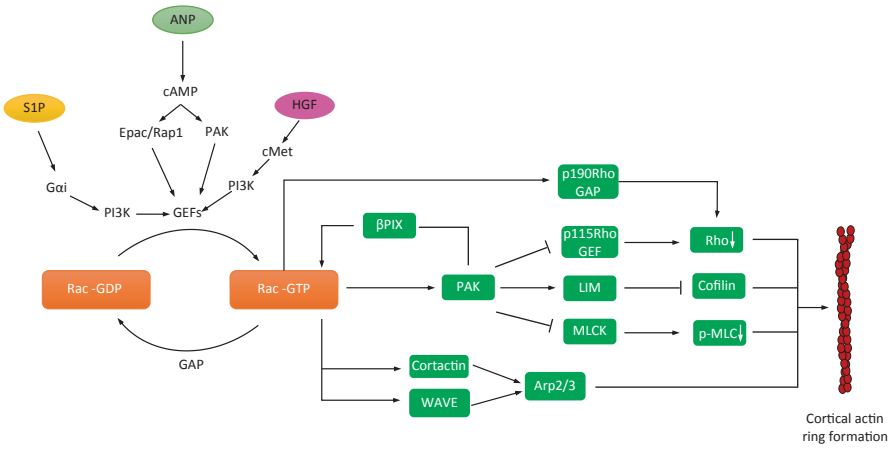


**Fig. 5.3** Rac1 plays central role in barrier enhancement signaling. Rac1 acts as molecular switches that stimulate downstream signals which control cellular processes. Barrier enhancement agonists, S1P, ANP, and HGF activate Rac1 through stimulation of Rac1 GEFs by various mechanisms. Activated Rac1 leads to cortical actin ring formation through either activation of cortactin/WAVE/Arp2/3 pathway to induced actin remodeling at cell peripheral or inactivation of Rho signaling to reduce stress fiber formation. (*Rac1* Ras-related C3 botulinum toxin substrate, *S1P* sphingosine-1-phosphate, *ANP* atrial natriuretic peptide, *HGF* hepatic growth factor, *GEF* GTPase exchange factor, *Rho* Ras homologue)

Activated PAK phosphorylates LIM kinase, which then inhibits cofilin activity in the cell periphery (Garcia et al. 2001). The direct consequence of cofilin inhibition is the stabilization of actin at the cell periphery. PAK can also inhibit p115RhoGEF, thus repressing RhoA activity (Rosenfeldt et al. 2006). Furthermore, PAK is known to inhibit myosin light chain kinase (MLCK) that mediates the phosphorylation of MLC in certain types of cells (Sanders et al. 1999). A model of positive feedback loop between Rac and PAK has been proposed. In this model, oxidized PAPC induces Rac1 activation leading to PAK-mediated phosphorylation of paxillin at Ser273, causes assembly of a GIT-Paxillin-PAK1-β-PIX signaling complex, and β-PIX further induces Rac activation (Birukova et al. 2008a). Rac activation is also associated with the translocation of cortactin, an actin-binding protein at AJ (Jacobson et al. 2006; Weed et al. 1998). Cortactin stimulates and stabilizes Arp2/3, an actin nucleator, mediating polymerization of branched actin filaments at peripheral sites (Uruno et al. 2001; Weaver et al. 2001). Alternatively, Rac may exert its effect on Arp2/3 via Wiskott-Aldrich syndrome protein verprolin homologous (WAVE), a protein with significant homology to verprolin, a member of the Wiskott–Aldrich syndrome protein (WASP). P190 Rho GAP plays a critical role in inhibition of RhoA at cell–cell adhesions where it is recruited by p120 catenin. Interestingly, its activity depends on p120 catenin (Wildenberg et al. 2006). Rac can inhibit Rho activity through p120 catenin (Herbrand and Ahmadian 2006; Wildenberg et al. 2006). Binding of Rac to p190RhoGAP results in a conformational change of p190RhoGAP that leads to its autoinhibition status. P190RhoGAP, in

turn, facilitates the hydrolysis of Rho-GTP to Rho-GDP that results in its inhibition at cell–cell adhesions.

### *5.4.2 Cdc42-Mediated Barrier Enhancement Signaling*

In many cases, agonists that activate Rac1 also activate Cdc42 (Baumer et al. 2009; Birukova et al. 2007b, 2008c; Waschke et al. 2006). Therefore, Cdc42 may be equally important for barrier maintenance and enhancement like Rac1. Cdc42 and Rac1 share common pathways leading to enhanced barrier integrity. Nevertheless, Cdc42 appears to be key GTPase that supports barrier restoration, indicating that Cdc42 is different from Rac1. In a thrombin-induced EC barrier dysfunction model, the activation of Cdc42 occurred during the recovery phase that follows loss in barrier integrity, whereas inactive Cdc42 was found only during the RhoA-mediated cell retraction phase (Kouklis et al. 2004). Transfection of EC with dominant-negative Cdc42 mutant delayed the restoration of EC barrier function after thrombin treatment in vivo. The mechanisms underlying Cdc42-mediated restoration of EC barrier function are likely to involve AJ proteins, VE-cadherin and catenins, and actin recruiting at sites in the plasma membrane. Cdc42 may interact with IQGAP1 and intersectin to promote the reannealing of AJs (Mehta and Malik 2006). Furthermore, Cdc42 stabilizes newly formed interactions by promoting actin remodeling through its downstream effector WASP (Mehta and Malik 2006). The mechanisms responsible for the delayed activation of Cdc42 are not well-defined. However, RhoA inactivation at AJ by p190RhoGAP and p120 complex may lead to Cdc42 activation, initiating the recovery phase and AJ reassembly.

#### 5.4.2.1 Rap1-Mediated Barrier Enhancement Signaling

Rap proteins, which include Rap1 (A and B) and Rap2 (A, B, and C) are members of the Ras super family of small GTPases. The landmark paper by Knox and Brown (2002) for the first time linked Rap1 to AJ formation (Knox and Brown 2002). The studies revealed that Rap1 is localized to the AJ. Rpa1 mutant cells displayed aberrant shapes and irregular connection with surrounding cells, indicating a defect in cell–cell adhesion. As Rap1 regulates Rac GEF, Tiam1 and Vav2, as illustrated above, signaling pathways regulated by Rac1 can explain Rap1-mediated barrier enhancement (Fig. 5.4).

ArfGAP, RhoGAP, ankyrin repeats and PH domain 3 (ARAP3), a member of the ARAP family of dual GAPs for ADP ribosylation factor (Arf) and Rho family GTPase, was identified from porcine neutrophils in a screen for PtdIns (3,4,5) P3-binding proteins (Krugmann et al. 2002; Miura et al. 2002). Rap proteins can bind directly to a neighboring Ras binding domain of ARAP3. This activation by Rap is GTP dependent and specific for Rap versus other Ras family members (Bos et al. 2001; Krugmann et al. 2004). Similar to Rho GAP, activated ARAP3 converts

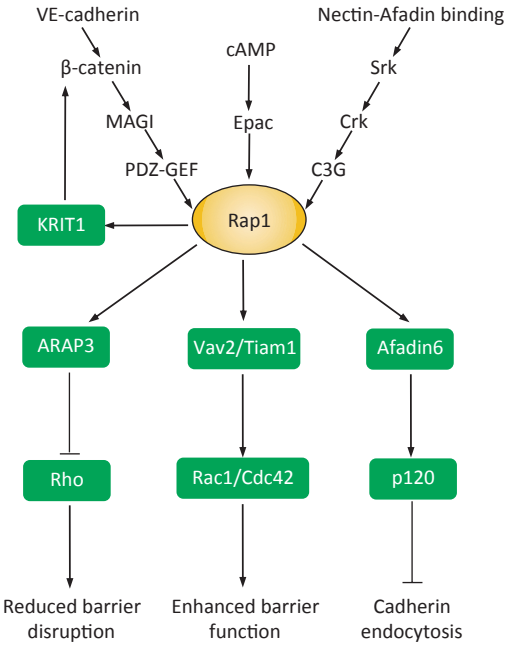


**Fig. 5.4** Rap1-mediated barrier enhancement signaling. Establishment of cell–cell contacts initiates signaling to activate Rap1, a small GTPase of Ras superfamily. Also, extracellular stimuli, including those that stimulate production of cAMP which activates Epac, induce Rap1 activation. Several Rap1 effecter proteins might mediate the effect on barrier function. Rap1 activates Rac1/Cdc42 via Vav2/Tiam1. Rap1 mediates the indirect binding of Afadin to p120 catenin, resulting in E-cadherin stabilization. In addition, Rap1 inactivates Rho through activation of Rho GAP ARAP3. (*Rap1* Ras-related protein1, *cAMP* Cyclic adenosine monophosphate, *Epac* Exchange protein activated by cAMP, *Rac1* Ras-related C3 botulinum toxin substrate, *Cdc42* Cell division cycle 42 GTP-binding protein, *Vav2* Vav2 guanine nucleotide exchange factor, *Tiam1* T-lymphoma invasion and metastasis 1, *Rho* Ras homologue, *GAP* GTPase activating protein, *ARAP3* ArfGAP, RhoGAP, ankyrin repeats and PH domain 3)

Rho-GTP into Rho-GDP, and thus downregulates Rho activity, resulting in enhanced barrier integrity. Afadin, an F-actin binding protein found to be a part of AJ, is composed of multiple functional domains, which mediate binding to various proteins. Of these binding partners, nectins are the most important partners that together contribute to cell–cell adhesion. The PDZ domain of afadin binds to the C-terminus of nectins (Aoki et al. 1997; Takai et al. 2008a). The *trans* interactions of nectins at the initial cell–cell contact sites induce the activation of Src (Fukuhara et al. 2004; Takai et al. 2008b) and then recruits Cyanidin 3-Glucoside (C3G), a GEF for Rap1, to nectins through adaptor protein Crk, resulting in the activation of Rap (Fukuyama et al. 2005). Rap1 subsequently binds to afadin and then, afadin indirectly binds to p120 catenin that is associated with *cis*-interacting E-cadherin and prevents the endocytosis of E-cadherin. Stabilized E-cadherin accumulates at the nectin-based cell–cell adhesion sites, leading to the establishment of AJ (Hoshino

et al. 2005; Sato et al. 2006). The Rap1 binding protein, K-Rev1 interaction Trapped gene 1 (KRIT1, also known as CCM1) was shown to be involved in Eapc1/Rap1-induced barrier enhancement of EC (Glading et al. 2007). In confluent EC monolayer, KRIT1 localizes to cell–cell contacts, where it forms a complex with VE-cadherin, p120 catenin, β-catenin, α-catenin, and afadin. Downregulation of KRIT1 by its siRNA-disabled Epac1/Rap1 to rescue thrombin-induced permeability, indicates that KRIT1 might be an effecter of Rap1. It remains to be elucidated how KRIT1 relays the Rap1 signal toward cell–cell contacts. KRIT1 associates with β-catenin and afadin in a Rap1-dependent manner and siRNA targeting KRIT1 disrupts junctional staining of β-catenin (Glading et al. 2007), suggesting KRIT1 might stabilize β-catenin at the AJ.

## 5.5 Tight Junction-Mediated Barrier Enhancement Signaling

TJs are the most apical structure of a junctional complex bordering the apico-basolateral membrane in both endothelial and epithelial cells. Within the lung tissue, TJs are the major structures that determine the permeability of epithelial cells, while lung vascular ECs rely more on AJs to regulate permeability. TJ is composed of strands of 10 nm fibrils that encircle the apical region of the cell. Three major transmembrane proteins, including occludin, claudin, and junctional adhesion molecule (JAM) are shown to constitute TJ. TJ clusters and cytosolic components form plaque of TJ, where they are associated with zonula occludens (ZO) proteins that link the intracellular domains of TJ with actin binding proteins and cytoskeleton including afadin, cingulin, β-catenin, and p120 catenin.

### *5.5.1 Occludins*

Occludin was the first identified transmembrane component of TJ and was originally isolated from chick livers (Furuse et al. 1993). It has two extracellular loops that appears to mediate localization of occluding to TJ and the paracellular permeability. Synthetic peptides corresponding to a 20-amino-acid sequence within the second extracellular loop of occluding increased barrier permeability and decreased occluding levels, as a result of increased protein turnover, suggesting this sequence mediates the association of occludins from adjacent cells (Wong and Gumbiner 1997). The expression of occluding correlates with barrier properties. The occluding expression from different vascular ECs presents a huge difference. For example, arterial ECs express 18-fold greater occluding protein levels than venous ECs and form a tighter solute barrier (Kevil et al. 1998). Similarly, occluding is highly expressed in brain endothelium which forms a very tight barrier, compared to ECs of non-neuronal tissue, which have lower occluding expression and barrier properties

than brain endothelium (Hirase et al. 1997). As predicted, increased expression of occludin correlates with enhanced barrier function. Hydrocortisone treatment of bovine retinal ECs resulted in increased occluding expression by twofold, and concomitant-enhanced barrier properties (Antonetti et al. 2002). Localization of this protein is also regulated by phosphorylation in both epithelial and ECs (Sakakibara et al. 1997). Non-phosphorylated occludin is localized to both the basolateral membrane and in cytoplasmic vesicles, whereas phosphorylated occluding is localized to TJ (Sakakibara et al. 1997). Specific phosphorylated residues within occludin have been investigated in terms of barrier function. T403 and T404 phosphorylation have been linked to enhanced occludin trafficking to the TJ and paracellular barrier function (Suzuki et al. 2009). In contrast, phosphorylation of Y398, Y402, and S490 is related to barrier disruption and attenuated interactions between occludin and ZO-1 (Elias et al. 2009; Sundstrom et al. 2009). Inhibition of S408 phosphorylation reduced paracellular cation flux by stabilizing occludin-ZO-1 interactions and enhanced subsequent association with claudin-1 and claudin-2, but not claudin-4 (Raleigh et al. 2011).

### *5.5.2 Claudins*

Claudins are a large family of transmembrane proteins that are components of TJs. Claudin-1 and claudin-2 are the first two identified members of the claudin family from chicken liver junctional fractions. So far 27 members of this family have been identified, with each showing a specific organ and tissue distribution (van Wetering et al. 2002). The structure of claudins is similar to occludin with four transmembrane domains, two extracellular loops, and cytoplasmic N- and C-termini. The C-terminal sequences of claudins all share a dipeptide sequence YV motif in the final two amino acids that is required for binding to the PDZ domain of ZO family members. Inhibition of this domain does not affect localization of claudin to TJ, but inhibits the association of ZO-1, -2, and -3 proteins (McCarthy et al. 2000). Extracellular loop regions determine ion selectivity as the regions are charged and exhibit a wide range of isoelectric points. This is, especially true in case of claudin-15, as it is sufficient to change the ion selectivity of the barrier (Colegio et al. 2002). In addition, mutating three positive charges to negative within the same region switched the ion selectivity of the claudin channel from $Na^{2+}$to $Cl^{-}$ (Colegio et al. 2002). Therefore, it seems that the first extracellular loop is sufficient to determine charge selectivity of the ion channel.

Different claudins are expressed throughout the respiratory tract. Claudin 1, 3, 4, 5, 7 have been reported to be expressed in human airway with different cellular localization (Coyne et al. 2003). The role of claudins in barrier integrity is a matter of debate. Some claudins increase paracellular permeability, for example, claudin 2, 3, and 5. IL-13-induced epithelial barrier dysfunction is attributed to claudin 2 induction (Rosen et al. 2013). Claudin 3 may serve as barrier disruptive claudin at baseline for type II alveolar epithelial cell (Mitchell et al. 2011). Human epithelial cell line (IB3.1) from cystic fibrosis airway presents enhanced permeability to different

size dextrans when claudin 5 is overexpressed in this cell line (Coyne et al. 2003). In contrast, claudin 1, 4, and 18 are known to enhance barrier integrity. Madin-Darby canine kidney (MDCK) cells transfected with mouse claudin 1 revealed increased expression of ZO-1 and exhibited enhanced barrier function (Inai et al. 1999). Expression of Claudin 4 is induced in acute lung injury and represents a mechanism to limit pulmonary edema (Mitchell et al. 2011; Wray et al. 2009). Claudin 18 is the only lung-specific TJ protein and the most abundant claudin in type 1 alveolar epithelial cells. Knockdown of claudin18 impaired alveolar epithelial barrier function in vivo and in vitro. Claudin 18 knockout mice developed postnatal lung injury and impaired alveolarization, indicating the importance of claudin 18 in lung epithelial barrier function and maturation (Lafemina et al. 2014). It is important to note that claudins might have different functions depending on the cellular and tissue context in which they are expressed. For example, although claudin 5 represents barrier disruptive property as described above, recent studies also demonstrated a crucial protective role for claudin 5 in lung microvascular ECs during influenza infection (Armstrong et al. 2012).

### *5.5.3 JAM*

JAM are IgG-like transmembrane proteins found at TJ. This family consists of the closely related members JAM-A, -B, and -C, and the more distantly related coxsackie and adenovirus receptors (CAR), endothelial cell-selective adhesion molecule (ESAM) and JAM-4 (Ebnet et al. 2004). JAMs have single pass transmembrane domain and extracellular region that contains two domains with V-type immunoglobin loops. JAMs appear to be important for TJ barrier function, as overexpression of JAM in CHO cells reduced paracellular permeability to 40 kDa dextran by 50 % in a calcium-dependent manner (Aurrand-Lions et al. 2001; Martin-Padura et al. 1998) and anti-JAM antibody reduced blood–brain barrier permeability (Del Maschio et al. 1999).

### *5.5.4 ZO Proteins*

Similar to AJ, TJ transmembrane proteins also require scaffolding molecules to connect with cytoskeleton proteins, such as actin. One important group of TJ scaffolding proteins is ZO proteins ZO-1, ZO-2, and ZO3. They bind directly to claudins via their PDZ1 domain and with occluding via their guanylate kinase-like homologues (GUK) domain, and the proline-rich C terminus mediates their binding to F-actin in vitro (Fanning et al. 2002; Schneeberger and Lynch 2004), and thus may serve to link ZO proteins to the cytoskeleton. As scaffold proteins, they facilitate claudin clustering, strand formation, and barrier function (Umeda et al. 2006). In addition to TJ proteins, ZO proteins also bind to the AJ protein, α-catenin, and the gap junction protein, connexin-43 (Giepmans and Moolenaar 1998; Itoh et al. 1999).

## 5.6 Focal Adhesion-Mediated Barrier Enhancement Signaling

Endothelial and epithelial cells attach to their underlying matrices through complex transmembrane structures termed focal adhesions (FAs) , which not only provide an anchor point for cells to adhere to the substratum but also selectively recruit various signaling molecules to the sites, allowing cells to monitor their immediate environment. Recent experimental evidence points to the importance of FAs in the regulation of barrier function.

### *5.6.1 Integrin-Mediated Barrier Enhancement*

Cell adhesion to the extracellular matrix (ECM) is mainly mediated by the integrin family of cell-surface receptors. Integrins are composed of noncovalently linked α and β subunits, each of which is a transmembrane glycoprotein with a single membrane-spanning segment and generally, a short cytoplasmic tail (Clark and Brugge 1995; Hynes 2002). In humans, a total of 18 integrin α chains and 8 β chains have been identified. They assemble in parallel arrays to form more than 24 heterodimers (Hynes 2002), each of which has a distinct, nonredundant function, binding to specific ECM components, and soluble protein ligands. Integrin-ECM interaction initiates the occupancy and clustering of integrins and in turn, promotes the recruitment of cytoskeletal and cytoplasmic proteins, such as talin, paxillin, and α-actinin to form focal complexes and focal adhesions (van der Flier and Sonnenberg 2001). As a bridge between ECM and cytoskeleton, integrins play essential roles in establishment and stabilization of barrier function. Synthetic peptides that compete for the Arg-Gly-Asp (RGD)-binding sequence (the targeting sequence in matrix proteins recognized by integrins) or antibodies against α5β1 induce a dramatic increase in barrier permeability (Curtis et al. 1995; Qiao et al. 1995; Wheatley et al. 1993). Integrin may also enhance barrier function through cell–cell adhesion. Several lines of evidence show that integrin participates in VE-cadherin mediated AJ. For instance, cAMP-activated Epac triggers the activation of A-kinase anchoring protein 9 (AKAP9), which plays a central role in microtube growth. AKAP9 promotes integrin $\alpha_v$ accumulation at the cell–cell border in ECs plated on fibronectin-coated plate, as $\alpha_v$ integrin has a relatively lower affinity for fibronectin than $\alpha_5$. Conversely, on collagen, $\alpha_5$ is enriched at the cell–cell interface. The ligand(s) at the cell–cell border for integrins are extracellular matrix proteins such as fibronectin, laminin, and collagen type IV, which are produced by the endothelium and concentrated at lateral cell–cell contacts (Sehrawat et al. 2011) . Integrin β4 is known to associate with S1P receptor 1 specifically in caveolin-enriched lipid rafts in human lung EC after HGF treatment. Reduced integrin β4 expression attenuated HGF-induced c-Met activation, c-Met/S1PR1 interaction, and decreased S1P- and HGF-induced EC barrier enhancement (Ephstein et al. 2013). Another study supports the protective role of simvastatin, a 3-hydroxy-3-methylglutaryl-coenzyme A-reductase inhibitor,

in LPS-induced pulmonary hyper-permeability and the injury that is mediated by integrin β4 (Chen et al. 2012). The protective effects of simvastatin are reversed by co-treatment with an integrin β4 blocking antibody. These results support a critical role for integrin β4 in regulating EC barrier integrity and function. Integrins regulate EC barrier function through cAMP as well (Kim et al. 2012). The mammalian tissue inhibitor of metalloproteinase 2 (TIMP2) binds to the surface of EC via interaction with the integrin α3β1. Treatment of EC with TIMP2 causes cytosolic cAMP elevation and increase in VE-cadherin association with actin cytoskeleton. α3β1 is revealed to mediate cAMP induction by TIMP2 as both α3- and β1-blocking antibodies abrogates TIMP2-mediated increase in cAMP production (Kim et al. 2012). The effects of integrin in barrier function are highly dependent on the subunit type and combination. Integrins β1 and β5 are known to regulate EC contractility and lung vascular permeability (Faurobert et al. 2013; Su et al. 2007) .

### *5.6.2 Focal Adhesion Kinase-Mediated Barrier Enhancement*

Focal adhesion kinase (FAK) is a critical non-receptor tyrosine kinase involved in the engagement of integrins and assembly of FA. It contains four principal regions mediating interactions with other adaptor and signaling proteins. The N-terminus contains a four-point-one, ezrin, radixin, moesin binding (FERM) domain, which acts as an auto inhibitory site by interacting with the kinase domain (Frame et al. 2010). The catalytic tyrosine kinase domain is localized in the middle. At the C-terminus is the C-terminal focal adhesion targeting (FAT) domain providing additional sites for FAK binding partners that include paxillin and members of the Rho family proteins. Between FAT and the central catalytic domain is the proline-rich region, which provides binding sites for FAK binding partners along with FAT domain (Schaller 2010).

Multiple studies have demonstrated an important role for FAK in modulating EC barrier function (Quadri et al. 2003; Yuan et al. 2012; Zebda et al. 2012). The importance of FAK in endothelial barrier function is highlighted by the fact that EC-specific deletion of murine FAK results in early embryonic lethality due to impaired vascular development (Braren et al. 2006; Shen et al. 2005). Furthermore, EC isolated from FAK knockout mice exhibit increased permeability as compared to wild type EC (Zhang et al. 2010). Similarly, reduction of FAK in human pulmonary artery EC (HPAEC) results in delayed barrier recovery after thrombin (Mehta et al. 2002). The underlying mechanism is that thrombin activates FAK via Gβγ and Fyn tyrosine kinase to associate with AJ complexes and stimulate their reassembly by phosphorylating p190RhoGAP to inhibit RhoA activity (Holinstat et al. 2006; Knezevic et al. 2009). Multiple tyrosine phosphorylation sites have been proposed to involve in S1P-induced barrier enhancement (Lee et al. 2000; Miura et al. 2000; Shikata et al. 2003a, b). Y576 of FAK, located in the activation loop of the catalytic domain, has been identified as the major phosphorylation target for S1P (Lee et al. 2000). The phosphorylation of Y576 is mediated by Src as inhibition of Src by PP2 blocks this event and attenuates S1P-induced translocation of FA proteins to the

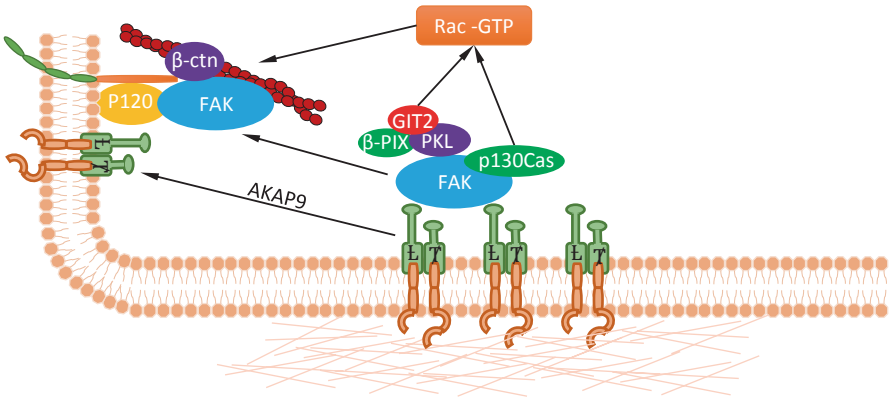


**Fig. 5.5** Focal adhesion protein complex cross talk with adhesions junctions (AJs). There is potential for crosstalk between cell–cell and cell–matrix adhesions through integrin shuttling between these distinct adhesion sites. AKAP9, which is activated by Epac, may mediate this process. FAK, a tyrosine kinase localized at FA, undergoes disassembly from FA after S1P treatment, dissociated FAK is then translocated to the EC periphery in association with the *PKL/GIT2*-paxillin complex, where cortical actin ring is facilitated by these proteins. (*AKAP9* A-kinase anchoring protein 9, *Epac* Exchange protein activated by cAMP, *FAK* Focal adhesion kinase, *S1P* Sphingosine-1-phosphate)

EC periphery (Shikata et al. 2003a, b). FAK-regulated barrier function may also be through its role in actin cytoskeleton reorganization via Rac activation (Fig. 5.5).

Evidence reveals that FAK translocates to EC periphery, where it may help regulate Rac activity. FAK activation leads to phosphorylation of the scaffolding protein, p130Cas, which can facilitate Rac activation (Chan et al. 2009; Tomar and Schlaepfer 2009). Alternatively, FAK phosphorylates the adaptor proteins β-PIX and PKL/GIT2 to form a complex and in turn, recruits and activates Rac (Chang et al. 2007; Yu et al. 2009). Additionally, FAK associates with AJ complexes to help cortical actin rearrangement. FAK localized at FA undergoes disassembly after S1P treatment, cytosolic FAK is then translocated to the EC periphery in association with PKL/GIT2-paxillin complex, where cortical actin ring is facilitated by these proteins (Shikata et al. 2003a, b). Furthermore, EC barrier enhancement coincides with increased association between FAK and AJ components. S1P significantly stimulates FAK association with VE-cadherin and β-catenin in HPAEC (Sun et al. 2009). In addition to S1P, thrombin treatment of EC also causes FAK redistribution to the cell peripheral where it interacts with p120 catenin in Y397/Y576 phosphorylation-dependent manner, leading to AJ reannealing during the time in which EC barrier function is restored (Knezevic et al. 2009).

Whether FAK functions to promote or disrupt endothelial barrier function is still a matter of debate, as depletion of FAK was observed to decrease response of S1P (Zhao et al. 2009). Furthermore, FAK phosphorylation and increased activity also occur in association with endothelial barrier-disrupting stimuli such as TGF-β (Lee et al. 2007), PMN (Guo et al. 2005), and VEGF (Wu et al. 2003). Thus, effects of FAK on EC barrier function depends on the stimulus involved.

## 5.7 Conclusions

As described in this chapter, normal barrier integrity is achieved by multiple cell structures. Most of the investigations have focused on cell–cell and cell–matrix contacts, and cytoskeleton remodeling as the major factors that regulate barrier integrity. Cell–cell contact may represent the most important regulation of barrier integrity as it is most dynamic. There are cross talks between cell-matrix components, however, the detailed mechanisms are unknown and therefore, represents an attractive future research direction. Regulation of barrier integrity by small GTPases is an active area of investigation. Many more GTPase regulators have been identified. In principle, direct targeting small GTPases using small molecular inhibitor would be a desirable approach to regulate barrier integrity for therapeutic purposes. Rho kinase inhibitor (HA-1077) has been used for the treatment of vascular disease. Mechanistic investigation of known barrier-enhancing agents are important areas for future research. These studies may lead to the discovery of new therapeutic targets and concepts for diseases associated with increase barrier permeability.

**Acknowledgment** We thank Dr. Prasad Kanteti for proofreading and editing. This work was supported in part by National Institutes of Health grant P01 HL58064 (Project 4) and P01 HL98050 to V.N.

## References

Al-Kurdi R, Gulino-Debrac D, Martel L, Legrand JF, Renault A, Hewat E, Venien-Bryan C. A soluble VE-cadherin fragment forms 2D arrays of dimers upon binding to a lipid monolayer. J Mol Biol. 2004;337:881–92.

Anastasiadis PZ, Reynolds AB. The p120 catenin family: complex roles in adhesion, signaling and cancer. J Cell Sci. 2000;113(8):1319–34.

Anastasiadis PZ, Moon SY, Thoreson MA, Mariner DJ, Crawford HC, Zheng Y, Reynolds AB. Inhibition of RhoA by p120 catenin. Nat Cell Biol. 2000;2:637–44.

Antonetti DA, Wolpert EB, DeMaio L, Harhaj NS, Scaduto RC Jr. Hydrocortisone decreases retinal endothelial cell water and solute flux coincident with increased content and decreased phosphorylation of occludin. J Neurochem. 2002;80:667–77.

Aoki J, Koike S, Asou H, Ise I, Suwa H, Tanaka T, Miyasaka M, Nomoto A. Mouse homolog of poliovirus receptor-related gene 2 product, mPRR2, mediates homophilic cell aggregation. Exp Cell Res. 1997;235:374–84.

Armstrong SM, Wang C, Tigdi J, Si X, Dumpit C, Charles S, Gamage A, Moraes TJ, Lee WL. Influenza infects lung microvascular endothelium leading to microvascular leak: role of apoptosis and claudin-5. PLoS One. 2012;7:e47323.

Aurrand-Lions M, Duncan L, Ballestrem C, Imhof BA. JAM-2, a novel immunoglobulin superfamily molecule, expressed by endothelial and lymphatic cells. J Biol Chem. 2001;276:2733–41.

Balsamo J, Leung T, Ernst H, Zanin MK, Hoffman S, Lilien J. Regulated binding of PTP1B-like phosphatase to N-cadherin: control of cadherin-mediated adhesion by dephosphorylation of beta-catenin. J Cell Biol. 1996;134:801–13.

Baumer S, Keller L, Holtmann A, Funke R, August B, Gamp A, Wolburg H, Wolburg-Buchholz K, Deutsch U, Vestweber D. Vascular endothelial cell-specific phosphotyrosine phosphatase (VE-PTP) activity is required for blood vessel development. Blood. 2006;107:4754–62.

Baumer Y, Spindler V, Werthmann RC, Bunemann M, Waschke J. Role of Rac 1 and cAMP in endothelial barrier stabilization and thrombin-induced barrier breakdown. J Cell Physiol. 2009;220:716–26.

Baumgartner W, Schutz GJ, Wiegand J, Golenhofen N, Drenckhahn D. Cadherin function probed by laser tweezer and single molecule fluorescence in vascular endothelial cells. J Cell Sci. 2003;116:1001–11.

Birukova AA, Alekseeva E, Mikaelyan A, Birukov KG. HGF attenuates thrombin-induced endothelial permeability by Tiam1-mediated activation of the Rac pathway and by Tiam1/Rac-dependent inhibition of the Rho pathway. FASEB J. 2007a;21:2776–86.

Birukova AA, Zagranichnaya T, Fu P, Alekseeva E, Chen W, Jacobson JR, Birukov KG. Prostaglandins PGE(2) and PGI(2) promote endothelial barrier enhancement via PKA- and Epac1/Rap1-dependent Rac activation. Exp Cell Res. 2007b;313:2504–20.

Birukova AA, Alekseeva E, Cokic I, Turner CE, Birukov KG. Cross talk between paxillin and Rac is critical for mediation of barrier-protective effects by oxidized phospholipids. Am J Physiol Lung Cell Mol Physiol. 2008a;295:L593–L602.

Birukova AA, Moldobaeva N, Xing J, Birukov KG. Magnitude-dependent effects of cyclic stretch on HGF- and VEGF-induced pulmonary endothelial remodeling and barrier regulation. Am J Physiol Lung Cell Mol Physiol. 2008b;295:L612–23.

Birukova AA, Zagranichnaya T, Alekseeva E, Bokoch GM, Birukov KG. Epac/Rap and PKA are novel mechanisms of ANP-induced Rac-mediated pulmonary endothelial barrier protection. J Cell Physiol. 2008c;215:715–24.

Bos JL, de Rooij J, Reedquist KA. Rap1 signalling: adhering to new models. Nat Rev Mol Cell Biol. 2001;2:369–77.

Bottaro DP, Rubin JS, Faletto DL, Chan AM, Kmiecik TE, Vande Woude GF, Aaronson SA. Identification of the hepatocyte growth factor receptor as the c-met proto-oncogene product. Science. 1991;251:802–4.

Brady-Kalnay SM, Flint AJ, Tonks NK. Homophilic binding of PTP mu, a receptor-type protein tyrosine phosphatase, can mediate cell–cell aggregation. J Cell Biol. 1993;122:961–72.

Braren R, Hu H, Kim YH, Beggs HE, Reichardt LF, Wang R. Endothelial FAK is essential for vascular network stability, cell survival, and lamellipodial formation. J Cell Biol. 2006;172:151–62.

Briggs MW, Sacks DB. IQGAP proteins are integral components of cytoskeletal regulation. EMBO Rep. 2003;4:571–4.

Broermann A, Winderlich M, Block H, Frye M, Rossaint J, Zarbock A, Cagna G, Linnepe R, Schulte D, Nottebaum AF, et al. Dissociation of VE-PTP from VE-cadherin is required for leukocyte extravasation and for VEGF-induced vascular permeability in vivo. J Exp Med. 2011;208:2393–401.

Brown MD, Sacks DB. IQGAP1 in cellular signaling: bridging the GAP. Trends Cell Biol. 2006;16:242–9.

Bussolino F, Di Renzo MF, Ziche M, Bocchietto E, Olivero M, Naldini L, Gaudino G, Tamagnone L, Coffer A, Comoglio PM. Hepatocyte growth factor is a potent angiogenic factor which stimulates endothelial cell motility and growth. J Cell Biol. 1992;119:629–41.

Cattelino A, Liebner S, Gallini R, Zanetti A, Balconi G, Corsi A, Bianco P, Wolburg H, Moore R, Oreda B, et al. The conditional inactivation of the beta-catenin gene in endothelial cells causes a defective vascular pattern and increased vascular fragility. J Cell Biol. 2003;162:1111–22.

Chan KT, Cortesio CL, Huttenlocher A. FAK alters invadopodia and focal adhesion composition and dynamics to regulate breast cancer invasion. J Cell Biol. 2009;185:357–70.

Chang F, Lemmon CA, Park D, Romer LH. FAK potentiates Rac1 activation and localization to matrix adhesion sites: a role for betaPIX. Mol Biol Cell. 2007;18:253–64.

Chen YT, Stewart DB, Nelson WJ. Coupling assembly of the E-cadherin/beta-catenin complex to efficient endoplasmic reticulum exit and basal-lateral membrane targeting of E-cadherin in polarized MDCK cells. J Cell Biol. 1999;144:687–99.

Chen W, Sammani S, Mitra S, Ma SF, Garcia JG, Jacobson JR. Critical role for integrin-beta4 in the attenuation of murine acute lung injury by simvastatin. Am J Physiol Lung Cell Mol Physiol. 2012;303:L279–85.

Clark EA, Brugge JS. Integrins and signal transduction pathways: the road taken. Science. 1995;268:233–9.
Colegio OR, van Itallie CM, McCrea HJ, Rahner C, Anderson JM. Claudins create charge-selective channels in the paracellular pathway between epithelial cells. Am J Physiol Cell Physiol. 2002;283:C142–7.
Corada M, Liao F, Lindgren M, Lampugnani MG, Breviario F, Frank R, Muller WA, Hicklin DJ, Bohlen P, Dejana E. Monoclonal antibodies directed to different regions of vascular endothelial cadherin extracellular domain affect adhesion and clustering of the protein and modulate endothelial permeability. Blood. 2001;97:1679–84.
Coyne CB, Gambling TM, Boucher RC, Carson JL, Johnson LG. Role of claudin interactions in airway tight junctional permeability. Am J Physiol Lung Cell Mol Physiol. 2003;285: L1166–78.
Curtis TM, McKeown-Longo PJ, Vincent PA, Homan SM, Wheatley EM, Saba TM. Fibronectin attenuates increased endothelial monolayer permeability after RGD peptide, anti-alpha 5 beta 1, or TNF-alpha exposure. Am J Physiol. 1995;269:L248–60.
Del Maschio A, de Luigi A, Martin-Padura I, Brockhaus M, Bartfai T, Fruscella P, Adorini L, Martino G, Furlan R, de Simoni, M. G, et al. Leukocyte recruitment in the cerebrospinal fluid of mice with experimental meningitis is inhibited by an antibody to junctional adhesion molecule (JAM). J Exp Med. 1999;190:1351–6.
Dominguez MG, Hughes VC, Pan L, Simmons M, Daly C, Anderson K, Noguera-Troise I, Murphy AJ, Valenzuela DM, Davis S, et al. Vascular endothelial tyrosine phosphatase (VE-PTP)-null mice undergo vasculogenesis but die embryonically because of defects in angiogenesis. Proc Natl Acad Sci U S A. 2007;104:3243–8.
Dong JM, Leung T, Manser E, Lim L. cAMP-induced morphological changes are counteracted by the activated RhoA small GTPase and the Rho kinase ROKalpha. J Biol Chem. 1998;273:22554–62.
Drees F, Pokutta S, Yamada S, Nelson WJ, Weis WI. Alpha-catenin is a molecular switch that binds E-cadherin-beta-catenin and regulates actin-filament assembly. Cell. 2005;123:903–15.
Ebnet K, Suzuki A, Ohno S, Vestweber D. Junctional adhesion molecules (JAMs): more molecules with dual functions? J Cell Sci. 2004;117:19–29.
Elias BC, Suzuki T, Seth A, Giorgianni F, Kale G, Shen L, Turner JR, Naren A, Desiderio DM, Rao R. Phosphorylation of Tyr-398 and Tyr-402 in occludin prevents its interaction with ZO-1 and destabilizes its assembly at the tight junctions. J Biol Chem. 2009;284:1559–69.
Ephstein Y, Singleton PA, Chen W, Wang L, Salgia R, Kanteti P, Dudek SM, Garcia JG, Jacobson JR. Critical role of S1PR1 and integrin beta4 in HGF/c-Met-mediated increases in vascular integrity. J Biol Chem. 2013;288:2191–200.
Fanning AS, Ma TY, Anderson JM. Isolation and functional characterization of the actin binding region in the tight junction protein ZO-1. FASEB J. 2002;16:1835–7.
Faurobert E, Rome C, Lisowska J, Manet-Dupe S, Boulday G, Malbouyres M, Balland M, Bouin AP, Keramidas M, Bouvard D, et al. CCM1-ICAP-1 complex controls beta1 integrin-dependent endothelial contractility and fibronectin remodeling. J Cell Biol. 2013;202:545–61.
van der Flier A, Sonnenberg A. Function and interactions of integrins. Cell Tissue Res. 2001;305:285–98.
Frame MC, Patel H, Serrels B, Lietha D, Eck MJ. The FERM domain: organizing the structure and function of FAK. Nat Rev Mol Cell Biol. 2010;11:802–14.
Fukuhara T, Shimizu K, Kawakatsu T, Fukuyama T, Minami Y, Honda T, Hoshino T, Yamada T, Ogita H, Okada M, et al. Activation of Cdc42 by trans interactions of the cell adhesion molecules nectins through c-Src and Cdc42-GEF FRG. J Cell Biol. 2004;166:393–405.
Fukuyama T, Ogita H, Kawakatsu T, Fukuhara T, Yamada T, Sato T, Shimizu K, Nakamura T, Matsuda M, Takai Y. Involvement of the c-Src-Crk-C3G-Rap1 signaling in the nectin-induced activation of Cdc42 and formation of adherens junctions. J Biol Chem. 2005;280:815–25.
Furuse M, Hirase T, Itoh M, Nagafuchi A, Yonemura S, Tsukita S. Occludin: a novel integral membrane protein localizing at tight junctions. J Cell Biol. 1993;123:1777–88.

Garcia JG, Liu F, Verin AD, Birukova A, Dechert MA, Gerthoffer WT, Bamberg JR, English D. Sphingosine 1-phosphate promotes endothelial cell barrier integrity by Edg-dependent cytoskeletal rearrangement. J Clin Invest. 2001;108:689–701.

Giepmans BN, Moolenaar WH. The gap junction protein connexin43 interacts with the second PDZ domain of the zona occludens-1 protein. Curr Biol. 1998;8:931–4.

Glading A, Han J, Stockton RA, Ginsberg MH. KRIT-1/CCM1 is a Rap1 effector that regulates endothelial cell cell junctions. J Cell Biol. 2007;179:247–54.

Gloerich M, Bos JL. Epac: defining a new mechanism for cAMP action. Annu Rev Pharmacol Toxicol. 2010;50:355–75.

Grant DS, Kleinman HK, Goldberg ID, Bhargava MM, Nickoloff BJ, Kinsella JL, Polverini P, Rosen EM. Scatter factor induces blood vessel formation in vivo. Proc Natl Acad Sci U S A. 1993;90:1937–41.

Grinnell KL, Casserly B, Harrington EO. Role of protein tyrosine phosphatase SHP2 in barrier function of pulmonary endothelium. Am J Physiol Lung Cell Mol Physiol. 2010;298:L361–70.

Guo M, Wu MH, Granger HJ, Yuan SY. Focal adhesion kinase in neutrophil-induced microvascular hyperpermeability. Microcirculation. 2005;12:223–32.

Hall A. Rho GTPases and the actin cytoskeleton. Science. 1998;279:509–14.

Hartsock A, Nelson WJ. Adherens and tight junctions: structure, function and connections to the actin cytoskeleton. Biochim Biophys Acta. 2008;1778:660–9.

Hellberg CB, Burden-Gulley SM, Pietz GE, Brady-Kalnay SM. Expression of the receptor protein-tyrosine phosphatase, PTPmu, restores E-cadherin-dependent adhesion in human prostate carcinoma cells. J Biol Chem. 2002;277:11165–73.

Herbrand U, Ahmadian MR. p190-RhoGAP as an integral component of the Tiam1/Rac1-induced downregulation of Rho. Biol Chem. 2006;387:311–7.

Hewat EA, Durmort C, Jacquamet L, Concord E, Gulino-Debrac D. Architecture of the VE-cadherin hexamer. J Mol Biol. 2007;365:744–51.

Hinck L, Nathke IS, Papkoff J, Nelson WJ. Dynamics of cadherin/catenin complex formation: novel protein interactions and pathways of complex assembly. J Cell Biol. 1994;125:1327–40.

Hirase T, Staddon JM, Saitou M, Ando-Akatsuka Y, Itoh M, Furuse M, Fujimoto K, Tsukita S, Rubin LL. Occludin as a possible determinant of tight junction permeability in endothelial cells. J Cell Sci. 1997;110(14):1603–13.

Holinstat M, Knezevic N, Broman M, Samarel AM, Malik AB, Mehta D. Suppression of RhoA activity by focal adhesion kinase-induced activation of p190RhoGAP: role in regulation of endothelial permeability. J Biol Chem. 2006;281:2296–305.

Hoshino T, Sakisaka T, Baba T, Yamada T, Kimura T, Takai Y. Regulation of E-cadherin endocytosis by nectin through afadin, Rap1, and p120ctn. J Biol Chem. 2005;280:24095–103.

Huber AH, Weis WI. The structure of the beta-catenin/E-cadherin complex and the molecular basis of diverse ligand recognition by beta-catenin. Cell. 2001;105:391–402.

Huber AH, Stewart DB, Laurents DV, Nelson WJ, Weis WI. The cadherin cytoplasmic domain is unstructured in the absence of beta-catenin. A possible mechanism for regulating cadherin turnover. J Biol Chem. 2001;276:12301–9.

Hynes RO. Integrins: bidirectional, allosteric signaling machines. Cell. 2002;110:673–87.

Inai T, Kobayashi J, Shibata Y. Claudin-1 contributes to the epithelial barrier function in MDCK cells. Eur J Cell Biol. 1999;78:849–55.

Itoh M, Morita K, Tsukita S. Characterization of ZO-2 as a MAGUK family member associated with tight as well as adherens junctions with a binding affinity to occludin and alpha catenin. J Biol Chem. 1999;274:5981–6.

Iyer S, Ferreri DM, DeCocco NC, Minnear FL, Vincent PA. VE-cadherin-p120 interaction is required for maintenance of endothelial barrier function. Am J Physiol Lung Cell Mol Physiol. 2004;286:L1143–53.

Jacobson JR, Dudek SM, Singleton PA, Kolosova IA, Verin AD, Garcia JG. Endothelial cell barrier enhancement by ATP is mediated by the small GTPase Rac and cortactin. Am J Physiol Lung Cell Mol Physiol. 2006;291:L289–95.

Jaffe AB, Hall A. Rho GTPases: biochemistry and biology. Annu Rev Cell Dev Biol. 2005;21:247–69.

Kevil CG, Okayama N, Trocha SD, Kalogeris TJ, Coe LL, Specian RD, Davis CP, Alexander JS. Expression of zonula occludens and adherens junctional proteins in human venous and arterial endothelial cells: role of occludin in endothelial solute barriers. Microcirculation. 1998;5:197–210.

Kim SH, Cho YR, Kim HJ, Oh JS, Ahn EK, Ko HJ, Hwang BJ, Lee SJ, Cho Y, Kim YK, et al. Antagonism of VEGF-A-induced increase in vascular permeability by an integrin alpha3beta1-Shp-1-cAMP/PKA pathway. Blood. 2012;120:4892–902.

Knezevic N, Tauseef M, Thennes T, Mehta D. The G protein betagamma subunit mediates reannealing of adherens junctions to reverse endothelial permeability increase by thrombin. J Exp Med. 2009;206:2761–77.

Knox AL, Brown NH. Rap1 GTPase regulation of adherens junction positioning and cell adhesion. Science. 2002;295:1285–8.

Kouklis P, Konstantoulaki M, Vogel S, Broman M, Malik AB. Cdc42 regulates the restoration of endothelial barrier function. Circ Res. 2004;94:159–66.

Kowalczyk AP, Navarro P, Dejana E, Bornslaeger EA, Green KJ, Kopp DS, Borgwardt JE. VE-cadherin and desmoplakin are assembled into dermal microvascular endothelial intercellular junctions: a pivotal role for plakoglobin in the recruitment of desmoplakin to intercellular junctions. J Cell Sci. 1998;111(Pt 20):3045–57.

Krugmann S, Anderson KE, Ridley SH, Risso N, McGregor A, Coadwell J, Davidson K, Eguinoa A, Ellson CD, Lipp P, et al. Identification of ARAP3, a novel PI3K effector regulating both Arf and Rho GTPases, by selective capture on phosphoinositide affinity matrices. Mol Cell. 2002;9:95–108.

Krugmann S, Williams R, Stephens L, Hawkins PT. ARAP3 is a PI3K- and rap-regulated GAP for RhoA. Curr Biol. 2004;14:1380–4.

Lafemina MJ, Sutherland KM, Bentley T, Gonzales LW, Allen L, Chapin CJ, Rokkam D, Sweerus KA, Dobbs LG, Ballard PL, et al. Claudin-18 deficiency results in alveolar barrier dysfunction and impaired alveologenesis in mice. Am J Respir Cell Mol Biol. 2014;51(4):550–8.

Lambert O, Taveau JC, Him JL, Al Kurdi R, Gulino-Debrac D, Brisson A. The basic framework of VE-cadherin junctions revealed by cryo-EM. J Mol Biol. 2005;346:1193–6.

Lang P, Gesbert F, Delespine-Carmagnat M, Stancou R, Pouchelet M, Bertoglio J. Protein kinase A phosphorylation of RhoA mediates the morphological and functional effects of cyclic AMP in cytotoxic lymphocytes. EMBO J. 1996;15:510–9.

Lee MJ, Thangada S, Claffey KP, Ancellin N, Liu CH, Kluk M, Volpi M, Sha'afi RI, Hla T. Vascular endothelial cell adherens junction assembly and morphogenesis induced by sphingosine-1-phosphate. Cell. 1999;99:301–12.

Lee OH, Lee DJ, Kim YM, Kim YS, Kwon HJ, Kim KW, Kwon YG. Sphingosine 1-phosphate stimulates tyrosine phosphorylation of focal adhesion kinase and chemotactic motility of endothelial cells via the G(i) protein-linked phospholipase C pathway. Biochem Biophys Res Commun. 2000;268:47–53.

Lee YH, Kayyali US, Sousa AM, Rajan T, Lechleider RJ, Day RM. Transforming growth factor-beta1 effects on endothelial monolayer permeability involve focal adhesion kinase/Src. Am J Respir Cell Mol Biol. 2007;37:485–93.

Liu F, Schaphorst KL, Verin AD, Jacobs K, Birukova A, Day RM, Bogatcheva N, Bottaro DP, Garcia JG. Hepatocyte growth factor enhances endothelial cell barrier function and cortical cytoskeletal rearrangement: potential role of glycogen synthase kinase-3beta. FASEB J. 2002;16:950–62.

Magie CR, Pinto-Santini D, Parkhurst SM. Rho1 interacts with p120ctn and alpha-catenin, and regulates cadherin-based adherens junction components in *Drosophila*. Development. 2002;129:3771–82.

Martin-Padura I, Lostaglio S, Schneemann M, Williams L, Romano M, Fruscella P, Panzeri C, Stoppacciaro A, Ruco L, Villa A, et al. Junctional adhesion molecule, a novel member of the immunoglobulin superfamily that distributes at intercellular junctions and modulates monocyte transmigration. J Cell Biol. 1998;142:117–27.

Matsumoto K, Nakamura T. Emerging multipotent aspects of hepatocyte growth factor. J Biochem. 1996;119:591–600.

McCarthy KM, Francis SA, McCormack JM, Lai J, Rogers RA, Skare IB, Lynch RD, Schneeberger EE. Inducible expression of claudin-1-myc but not occludin-VSV-G results in aberrant tight junction strand formation in MDCK cells. J Cell Sci. 2000;113(Pt 19):3387–98.

Mehta D, Malik AB. Signaling mechanisms regulating endothelial permeability. Physiol Rev. 2006;86:279–367.

Mehta D, Tiruppathi C, Sandoval R, Minshall RD, Holinstat M, Malik AB. Modulatory role of focal adhesion kinase in regulating human pulmonary arterial endothelial barrier function. J Physiol. 2002;539:779–89.

Mitchell LA, Overgaard CE, Ward C, Margulies SS, Koval M. Differential effects of claudin-3 and claudin-4 on alveolar epithelial barrier function. Am J Physiol Lung Cell Mol Physiol. 2011;301:L40–9.

Miura Y, Yatomi Y, Rile G, Ohmori T, Satoh K, Ozaki Y. Rho-mediated phosphorylation of focal adhesion kinase and myosin light chain in human endothelial cells stimulated with sphingosine 1-phosphate, a bioactive lysophospholipid released from activated platelets. J Biochem. 2000;127:909–14.

Miura K, Jacques KM, Stauffer S, Kubosaki A, Zhu K, Hirsch DS, Resau J, Zheng Y, Randazzo PA. ARAP1: a point of convergence for Arf and Rho signaling. Mol Cell. 2002;9:109–19.

Nakamura Y, Patrushev N, Inomata H, Mehta D, Urao N, Kim HW, Razvi M, Kini V, Mahadev K, Goldstein BJ, et al. Role of protein tyrosine phosphatase 1B in vascular endothelial growth factor signaling and cell-cell adhesions in endothelial cells. Circ Res. 2008;102:1182–91.

Nanes BA, Chiasson-MacKenzie C, Lowery AM, Ishiyama N, Faundez V, Ikura M, Vincent PA, Kowalczyk AP. p120-catenin binding masks an endocytic signal conserved in classical cadherins. J Cell Biol. 2012;199:365–80.

Nawroth R, Poell G, Ranft A, Kloep S, Samulowitz U, Fachinger G, Golding M, Shima DT, Deutsch U, Vestweber D. VE-PTP and VE-cadherin ectodomains interact to facilitate regulation of phosphorylation and cell contacts. EMBO J. 2002;21:4885–95.

Nimnual AS, Taylor LJ, Bar-Sagi D. Redox-dependent downregulation of Rho by Rac. Nat Cell Biol. 2003;5:236–41.

Nollet F, Kools P, van Roy F. Phylogenetic analysis of the cadherin superfamily allows identification of six major subfamilies besides several solitary members. J Mol Biol. 2000;299:551–72.

Nottebaum AF, Cagna G, Winderlich M, Gamp AC, Linnepe R, Polaschegg C, Filippova K, Lyck R, Engelhardt B, Kamenyeva O, et al. VE-PTP maintains the endothelial barrier via plakoglobin and becomes dissociated from VE-cadherin by leukocytes and by VEGF. J Exp Med. 2008;205:2929–45.

Oas RG, Nanes BA, Esimai CC, Vincent PA, Garcia AJ, Kowalczyk AP. p120-catenin and beta-catenin differentially regulate cadherin adhesive function. Mol Biol Cell. 2013;24:704–14.

O'Connor KL, Mercurio AM. Protein kinase A regulates Rac and is required for the growth factor-stimulated migration of carcinoma cells. J Biol Chem. 2001;276:47895–900.

Ostman A, Yang Q, Tonks NK. Expression of DEP-1, a receptor-like protein-tyrosine-phosphatase, is enhanced with increasing cell density. Proc Natl Acad Sci U S A. 1994;91:9680–4.

Patel SD, Ciatto C, Chen CP, Bahna F, Rajebhosale M, Arkus N, Schieren I, Jessell TM, Honig B, Price SR, et al. Type II cadherin ectodomain structures: implications for classical cadherin specificity. Cell. 2006;124:1255–68.

Ponzetto C, Bardelli A, Zhen Z, Maina F, dalla Zonca P, Giordano S, Graziani A, Panayotou G, Comoglio PM. A multifunctional docking site mediates signaling and transformation by the hepatocyte growth factor/scatter factor receptor family. Cell. 1994;77:261–71.

Qiao RL, Yan W, Lum H, Malik AB. Arg-Gly-Asp peptide increases endothelial hydraulic conductivity: comparison with thrombin response. Am J Physiol. 1995;269:C110–7.

Quadri SK, Bhattacharjee M, Parthasarathi K, Tanita T, Bhattacharya J. Endothelial barrier strengthening by activation of focal adhesion kinase. J Biol Chem. 2003;278:13342–9.

Raleigh DR, Boe DM, Yu D, Weber CR, Marchiando AM, Bradford EM, Wang Y, Wu L, Schneeberger EE, Shen L, et al. Occludin S408 phosphorylation regulates tight junction protein interactions and barrier function. J Cell Biol. 2011;193:565–82.

Rosen MJ, Chaturvedi R, Washington MK, Kuhnhein LA, Moore PD, Coggeshall SS, McDonough EM, Weitkamp JH, Singh AB, Coburn LA et al. STAT6 deficiency ameliorates severity of oxazolone colitis by decreasing expression of claudin-2 and Th2-inducing cytokines. J Immunol. 2013;190:1849–58.

Rosenfeldt H, Castellone MD, Randazzo PA, Gutkind JS. Rac inhibits thrombin-induced Rho activation: evidence of a Pak-dependent GTPase crosstalk. J Mol Signal. 2006;1:8.

Sakakibara A, Furuse M, Saitou M, Ando-Akatsuka Y, Tsukita S. Possible involvement of phosphorylation of occludin in tight junction formation. J Cell Biol. 1997;137:1393–401.

Sanders LC, Matsumura F, Bokoch GM, de Lanerolle P. Inhibition of myosin light chain kinase by p21-activated kinase. Science. 1999;283:2083–5.

Sato T, Fujita N, Yamada A, Ooshio T, Okamoto R, Irie K, Takai Y. Regulation of the assembly and adhesion activity of E-cadherin by nectin and afadin for the formation of adherens junctions in Madin-Darby canine kidney cells. J Biol Chem. 2006;281:5288–99.

Schaeper U, Gehring NH, Fuchs KP, Sachs M, Kempkes B, Birchmeier W. Coupling of Gab1 to c-Met, Grb2, and Shp2 mediates biological responses. J Cell Biol. 2000;149:1419–32.

Schaller MD. Cellular functions of FAK kinases: insight into molecular mechanisms and novel functions. J Cell Sci. 2010;123:1007–13.

Schneeberger EE, Lynch RD. The tight junction: a multifunctional complex. Am J Physiol Cell Physiol. 2004;286:C1213–28.

Schnittler HJ, Puschel B, Drenckhahn D. Role of cadherins and plakoglobin in interendothelial adhesion under resting conditions and shear stress. Am J Physiol. 1997;273:H2396–405.

Sehrawat S, Ernandez T, Cullere X, Takahashi M, Ono Y, Komarova Y, Mayadas TN. AKAP9 regulation of microtubule dynamics promotes Epac1-induced endothelial barrier properties. Blood. 2011;117:708–18.

Shen TL, Park AY, Alcaraz A, Peng X, Jang I, Koni P, Flavell RA, Gu H, Guan JL. Conditional knockout of focal adhesion kinase in endothelial cells reveals its role in angiogenesis and vascular development in late embryogenesis. J Cell Biol. 2005;169:941–52.

Shikata Y, Birukov KG, Birukova AA, Verin A, Garcia JG. Involvement of site-specific FAK phosphorylation in sphingosine-1 phosphate- and thrombin-induced focal adhesion remodeling: role of Src and GIT. FASEB J. 2003a;17:2240–9.

Shikata Y, Birukov KG, Garcia JG. S1P induces FA remodeling in human pulmonary endothelial cells: role of Rac, GIT1, FAK, and paxillin. J Appl Physiol (1985). 2003b;94:1193–203.

Singleton PA, Dudek SM, Chiang ET, Garcia JG. Regulation of sphingosine 1-phosphate-induced endothelial cytoskeletal rearrangement and barrier enhancement by S1P1 receptor, PI3 kinase, Tiam1/Rac1, and alpha-actinin. FASEB J. 2005;19:1646–56.

Singleton PA, Salgia R, Moreno-Vinasco L, Moitra J, Sammani S, Mirzapoiazova T, Garcia JG. CD44 regulates hepatocyte growth factor-mediated vascular integrity. Role of c-Met, Tiam1/Rac1, dynamin 2, and cortactin. J Biol Chem. 2007;282:30643–57.

Spring K, Chabot C, Langlois S, Lapointe L, Trinh NT, Caron C, Hebda JK, Gavard J, Elchebly M, Royal I. Tyrosine phosphorylation of DEP-1/CD148 as a mechanism controlling Src kinase activation, endothelial cell permeability, invasion, and capillary formation. Blood. 2012;120:2745–56.

Spring K, Lapointe L, Caron C, Langlois S, Royal I. Phosphorylation of DEP-1/PTPRJ on threonine 1318 regulates Src activation and endothelial cell permeability induced by vascular endothelial growth factor. Cell Signal. 2014;26:1283–93.

Su G, Hodnett M, Wu N, Atakilit A, Kosinski C, Godzich M, Huang XZ, Kim JK, Frank JA, Matthay MA, et al. Integrin alphavbeta5 regulates lung vascular permeability and pulmonary endothelial barrier function. Am J Respir Cell Mol Biol. 2007;36:377–86.

Sui XF, Kiser TD, Hyun SW, Angelini DJ, Del Vecchio RL, Young BA, Hasday JD, Romer LH, Passaniti A, Tonks NK, et al. Receptor protein tyrosine phosphatase micro regulates the paracellular pathway in human lung microvascular endothelia. Am J Pathol. 2005;166:1247–58.

Sun X, Shikata Y, Wang L, Ohmori K, Watanabe N, Wada J, Shikata K, Birukov KG, Makino H, Jacobson JR, et al. Enhanced interaction between focal adhesion and adherens junction

proteins: involvement in sphingosine 1-phosphate-induced endothelial barrier enhancement. Microvasc Res. 2009;77:304–13.
Sundstrom JM, Tash BR, Murakami T, Flanagan JM, Bewley MC, Stanley BA, Gonsar KB, Antonetti DA. Identification and analysis of occludin phosphosites: a combined mass spectrometry and bioinformatics approach. J Proteome Res. 2009;8:808–17.
Suzuki T, Elias BC, Seth A, Shen L, Turner JR, Giorgianni F, Desiderio D, Guntaka R, Rao R. PKC eta regulates occludin phosphorylation and epithelial tight junction integrity. Proc Natl Acad Sci U S A. 2009;106:61–6.
Takahashi T, Takahashi K, St John PL, Fleming PA, Tomemori T, Watanabe T, Abrahamson DR, Drake CJ, Shirasawa T, Daniel TO. A mutant receptor tyrosine phosphatase, CD148, causes defects in vascular development. Mol Cell Biol. 2003;23:1817–31.
Takahashi T, Takahashi K, Mernaugh RL, Tsuboi N, Liu H, Daniel TO. A monoclonal antibody against CD148, a receptor-like tyrosine phosphatase, inhibits endothelial-cell growth and angiogenesis. Blood. 2006;108:1234–42.
Takai Y, Sasaki T, Matozaki T. Small GTP-binding proteins. Physiol Rev. 2001;81:153–208.
Takai Y, Ikeda W, Ogita H, Rikitake Y. The immunoglobulin-like cell adhesion molecule nectin and its associated protein afadin. Annu Rev Cell Dev Biol. 2008a;24:309–42.
Takai Y, Miyoshi J, Ikeda W, Ogita H. Nectins and nectin-like molecules: roles in contact inhibition of cell movement and proliferation. Nat Rev Mol Cell Biol. 2008b;9:603–15.
Timmerman I, Hoogenboezem M, Bennett AM, Geerts D, Hordijk PL, van Buul JD. The tyrosine phosphatase SHP2 regulates recovery of endothelial adherens junctions through control of beta-catenin phosphorylation. Mol Biol Cell. 2012;23:4212–25.
Tomar A, Schlaepfer DD. Focal adhesion kinase: switching between GAPs and GEFs in the regulation of cell motility. Curr Opin Cell Biol. 2009;21:676–83.
Ukropec JA, Hollinger MK, Salva SM, Woolkalis MJ. SHP2 association with VE-cadherin complexes in human endothelial cells is regulated by thrombin. J Biol Chem. 2000;275:5983–6.
Umeda K, Ikenouchi J, Katahira-Tayama S, Furuse K, Sasaki H, Nakayama M, Matsui T, Tsukita S, Furuse M. ZO-1 and ZO-2 independently determine where claudins are polymerized in tight-junction strand formation. Cell. 2006;126:741–54.
Uruno T, Liu J, Zhang P, Fan Y, Egile C, Li R, Mueller SC, Zhan X. Activation of Arp2/3 complex-mediated actin polymerization by cortactin. Nat Cell Biol. 2001;3:259–66.
Vaezi A, Bauer C, Vasioukhin V, Fuchs E. Actin cable dynamics and Rho/Rock orchestrate a polarized cytoskeletal architecture in the early steps of assembling a stratified epithelium. Dev Cell. 2002;3:367–81.
Valiron O, Chevrier V, Usson Y, Breviario F, Job D, Dejana E. Desmoplakin expression and organization at human umbilical vein endothelial cell-to-cell junctions. J Cell Sci. 1996;109(Pt 8):2141–9.
Vandenbroucke St Amant E, Tauseef M, Vogel SM, Gao XP, Mehta D, Komarova YA, Malik AB. PKCalpha activation of p120-catenin serine 879 phospho-switch disassembles VE-cadherin junctions and disrupts vascular integrity. Circ Res. 2012;111:739–49.
Vasioukhin V, Bauer C, Yin M, Fuchs E. Directed actin polymerization is the driving force for epithelial cell-cell adhesion. Cell. 2000;100:209–19.
Venkiteswaran K, Xiao K, Summers S, Calkins CC, Vincent PA, Pumiglia K, Kowalczyk AP. Regulation of endothelial barrier function and growth by VE-cadherin, plakoglobin, and beta-catenin. Am J Physiol Cell Physiol. 2002;283:C811–21.
Verma S, Shewan AM, Scott JA, Helwani FM, den Elzen NR, Miki H, Takenawa T, Yap AS. Arp2/3 activity is necessary for efficient formation of E-cadherin adhesive contacts. J Biol Chem. 2004;279:34062–70.
Waschke J, Baumgartner W, Adamson RH, Zeng M, Aktories K, Barth H, Wilde C, Curry FE, Drenckhahn D. Requirement of Rac activity for maintenance of capillary endothelial barrier properties. Am J Physiol Heart Circ Physiol. 2004a;286:H394–H401.
Waschke J, Drenckhahn D, Adamson RH, Curry FE. Role of adhesion and contraction in Rac 1-regulated endothelial barrier function in vivo and in vitro. Am J Physiol Heart Circ Physiol. 2004b;287:H704–11.

Waschke J, Burger S, Curry FR, Drenckhahn D, Adamson RH. Activation of Rac-1 and Cdc42 stabilizes the microvascular endothelial barrier. Histochem Cell Biol. 2006;125:397–406.
Weaver AM, Karginov AV, Kinley AW, Weed SA, Li Y, Parsons JT, Cooper JA. Cortactin promotes and stabilizes Arp2/3-induced actin filament network formation. Curr Biol. 2001;11:370–4.
Weed SA, Du Y, Parsons JT. Translocation of cortactin to the cell periphery is mediated by the small GTPase Rac1. J Cell Sci. 1998;111(Pt 16):2433–43.
Wennerberg K, Rossman KL, Der CJ. The Ras superfamily at a glance. J Cell Sci. 2005;118:843–6.
van Wetering S, van Buul JD, Quik S, Mul FP, Anthony EC, ten Klooster JP, Collard JG, Hordijk PL. Reactive oxygen species mediate Rac-induced loss of cell-cell adhesion in primary human endothelial cells. J Cell Sci. 2002;115:1837–46.
Wheatley EM, McKeown-Longo PJ, Vincent PA, Saba TM. Incorporation of fibronectin into matrix decreases TNF-induced increase in endothelial monolayer permeability. Am J Physiol. 1993;265:L148–57.
Wildenberg GA, Dohn MR, Carnahan RH, Davis MA, Lobdell NA, Settleman J, Reynolds AB. p120-catenin and p190RhoGAP regulate cell-cell adhesion by coordinating antagonism between Rac and Rho. Cell. 2006;127:1027–39.
Wojciak-Stothard B, Potempa S, Eichholtz T, Ridley AJ. Rho and Rac but not Cdc42 regulate endothelial cell permeability. J Cell Sci. 2001;114:1343–55.
Wong V, Gumbiner BM. A synthetic peptide corresponding to the extracellular domain of occludin perturbs the tight junction permeability barrier. J Cell Biol. 1997;136:399–409.
Wray C, Mao Y, Pan J, Chandrasena A, Piasta F, Frank JA. Claudin-4 augments alveolar epithelial barrier function and is induced in acute lung injury. Am J Physiol Lung Cell Mol Physiol. 2009;297:L219–27.
Wu MH, Guo M, Yuan SY, Granger HJ. Focal adhesion kinase mediates porcine venular hyperpermeability elicited by vascular endothelial growth factor. J Physiol. 2003;552:691–9.
Xiao K, Allison DF, Buckley KM, Kottke MD, Vincent PA, Faundez V, Kowalczyk AP. Cellular levels of p120 catenin function as a set point for cadherin expression levels in microvascular endothelial cells. J Cell Biol. 2003;163:535–45.
Xu G, Arregui C, Lilien J, Balsamo J. PTP1B modulates the association of beta-catenin with N-cadherin through binding to an adjacent and partially overlapping target site. J Biol Chem. 2002;277:49989–97.
Yamada S, Pokutta S, Drees F, Weis WI, Nelson WJ. Deconstructing the cadherin-catenin-actin complex. Cell. 2005;123:889–901.
Yu JA, Deakin NO, Turner CE. Paxillin-kinase-linker tyrosine phosphorylation regulates directional cell migration. Mol Biol Cell. 2009;20:4706–19.
Yuan SY, Shen Q, Rigor RR, Wu MH. Neutrophil transmigration, focal adhesion kinase and endothelial barrier function. Microvasc Res. 2012;83:82–8.
Zebda N, Dubrovskyi O, Birukov KG. Focal adhesion kinase regulation of mechanotransduction and its impact on endothelial cell functions. Microvasc Res. 2012;83:71–81.
Zebda N, Tian Y, Tian X, Gawlak G, Higginbotham K, Reynolds AB, Birukova AA, Birukov KG. Interaction of p190RhoGAP with C-terminal domain of p120-catenin modulates endothelial cytoskeleton and permeability. J Biol Chem. 2013;288:18290–9.
Zhang L, Himi T, Morita I, Murota S. Hepatocyte growth factor protects cultured rat cerebellar granule neurons from apoptosis via the phosphatidylinositol-3 kinase/Akt pathway. J Neurosci Res. 2000;59:489–96.
Zhang G, Xu S, Qian Y, He P. Sphingosine-1-phosphate prevents permeability increases via activation of endothelial sphingosine-1-phosphate receptor 1 in rat venules. Am J Physiol Heart Circ Physiol. 2010;299:H1494–504.
Zhao J, Singleton PA, Brown ME, Dudek SM, Garcia JG. Phosphotyrosine protein dynamics in cell membrane rafts of sphingosine-1-phosphate-stimulated human endothelium: role in barrier enhancement. Cell Signal. 2009;21:1945–60.
Zondag GC, Reynolds AB, Moolenaar WH. Receptor protein-tyrosine phosphatase RPTPmu binds to and dephosphorylates the catenin p120(ctn). J Biol Chem. 2000;275:11264–9.

# Chapter 6
# Transbarrier Ion and Fluid Transport

**Charles A. Downs and My N. Helms**

**Abbreviations**

| | |
|---|---|
| β-AR | $\beta_2$-adrenergic receptor |
| ABC | ATP-binding cassette |
| ACM | alveolar capillary membrane |
| ARDS | acute respiratory distress syndrome |
| ATP | adenosine triphosphate |
| cAMP | cyclic adenosine monophosphate |
| cGMP | cyclic guanosine monophosphate |
| CF | cystic fibrosis |
| CFTR | cystic fibrosis transmembrane conductance regulator |
| COPD | chronic obstructive pulmonary disease |
| ELF | epithelial lining fluid |
| ENaC | epithelial sodium channel |
| EPC | endothelial progenitor cell |
| GSH | glutathione |
| GSSG | glutathione disulfide |
| HGF | hepatocyte growth factor |
| HSC | highly selective cation |
| ICAM-1 | intercellular adhesion molecule-1 |
| IL | interleukin |
| MAPK | mitogen activated protein kinase |

M. N. Helms (✉)
Department of Pediatrics, School of Medicine, Emory University, Atlanta, GA 30322, USA
e-mail: mhelms@emory.edu

Department of Pediatrics and Center for Cystic Fibrosis and Airways Disease Research at Children's Healthcare of Atlanta Hospital, Emory Children's Center, 2015 Uppergate Drive, Suite 314, Atlanta, GA 30322, USA

C. A. Downs
Nell Hodgson Woodruff School of Nursing and Department of Physiology, Emory University, 1520 Clifton Rd NE Suite 238, Atlanta, GA 30322, USA



A. N. Makanya (ed.), *The Vertebrate Blood-Gas Barrier in Health and Disease,*
DOI 10.1007/978-3-319-18392-3_6

| | |
|---|---|
| MMP-9 | matrix metalloproteinase 9 |
| MSC | mesenchymal stem cell |
| NADPH | nicotinamide adenine dinucleotide phosphate |
| NO | nitric oxide |
| NSC | nonselective cation |
| RAGE | receptor for advanced glycation end products |
| ROS | reactive oxygen species |
| T1 | alveolar epithelial type 1 |
| T2 | alveolar epithelial type 2 |
| TGF | transforming growth factor |
| TNFα | tumor necrosis factor alpha |

## 6.1 Introduction

The vertebrate blood–gas barrier performs the important task of passive gas exchange between the alveolar airspace and pulmonary capillaries. The ability to effectively exchange oxygen for carbon dioxide between the blood–gas barrier depends in large part on precise regulation of the amount of fluid lining the alveolar airspace. Although all segments of the nasal and pulmonary epithelium have the capacity to transport ions (and thereby alter secretion or reabsorbtion of lung fluid), transbarrier ion and fluid transport across the alveolar epithelium directly affects oxygenation of the blood. Therefore, this chapter focuses on the mechanisms that regulate transbarrier ion transport in the alveolar epithelium, thereby altering net fluid transport in the distal lung. Since the epithelial lining fluid (ELF) contains high amounts of glutathione (GSH), and the lung epithelium is directly exposed to prooxidants, redox regulation of ion transport in the lung may be critically important in understanding fluid dynamics in the lungs. Loss of normal transport properties in the alveolar epithelium can lead to severe pulmonary disorders such as acute respiratory distress syndrome (ARDS), cystic fibrosis (CF), and chronic obstructive pulmonary disease (COPD).

### *6.1.1 Overview of the Structure and Function of the Alveolar Epithelium*

The alveolar epithelium is the major barrier to the movement of ion and fluid into and out of the alveolus and is composed of two morphologically distinct cell types: alveolar epithelial type 1 (T1) and type 2 (T2) cells. Since the pulmonary alveoli at the terminal ends of the respiratory tree play a critically important role in the diffusion of carbon dioxide and oxygen, much of our discussion centers on transbarrier ion transport across T1 and T2 cells (as opposed to epithelium of the upper and bronchial airways). T1 cells make up approximately 96% of the alveolar surface area and are characterized by attenuated cytoplasm lacking organelles. The T1 cells are uniquely thin (between 25 and 200 nm except for the nuclear region),

which facilitates gaseous exchange across the blood–gas barrier. T2 cells are cuboidal, cover ~4% of the remaining alveolar surface area, and are typically found in the angulated portion of an alveolus. Compared to T1 cells, the cytoplasm of T2 cells contains mitochondria, Golgi complexes, and large lamellar bodies that play a critical role in T2 cell production, storage, and secretion of surfactant. Activation of apical and basolateral ion channels, transporters, and pumps (discussed below) expressed in T1 and T2 cells are responsible for maintaining lung fluid balance, and thus integrity of the blood–gas barrier between epithelial and capillary cells.

Tight junctions form between T1 and T2 cells during the early stages of lung development and provide a barrier between the internal vascular compartment and a fluid-lined airspace throughout life. In healthy lung, the tight junctions that form between T1 and T2 cells are virtually impermeable to proteins and solutes. Since the tight junctions formed are impermeable to macromolecules, alveolar macrophages are primarily responsible for removing any particulate matter or bacterium that is not removed by the mucosal escalator in the conducting airways. Passage of molecules, fluid, and ions rely on active transport across alveolar epithelial cells by diffusion or active transport in order to traverse the epithelial barrier formed between the airspace and basolateral compartments. Figure 6.1 is an electron micrograph

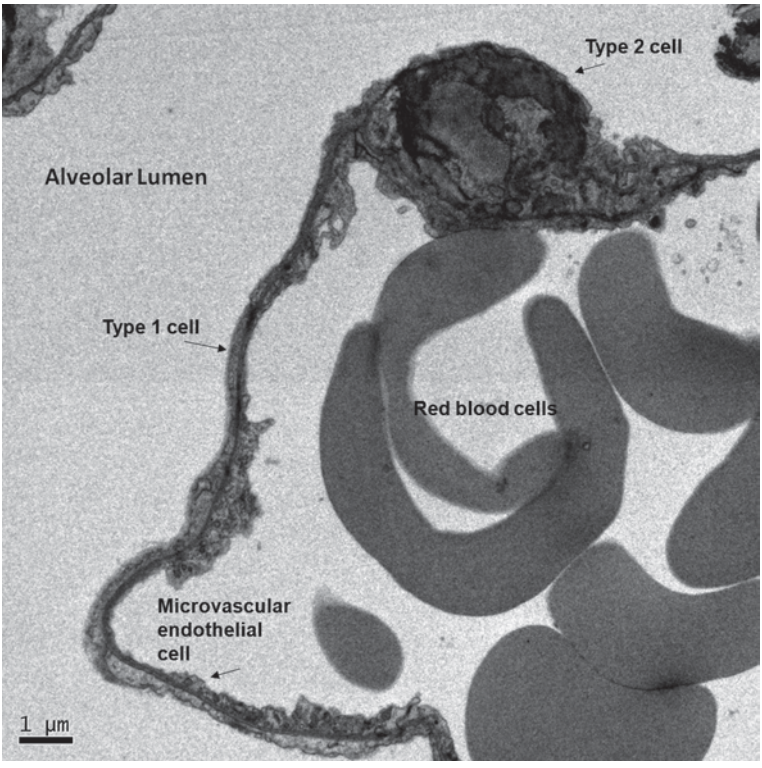


**Fig. 6.1** Electron micrograph of the pulmonary alveolus. T1 cells are in close apposition with microvascular endothelial cells to facilitate gas exchange between red blood cells and the alveolar lumen. T2 cells can be seen with many small vesicles in the cytoplasm. Original magnification 1500×, bar = 1 µm

depicting mouse T1 and T2 cells, microvascular endothelial cells, and red blood cells in relation to the alveolar lumen.

### 6.1.2 *Generalized Paradigm for Transbarrier Ion and Fluid Transport*

With little exception, the rate of fluid absorption depends upon the rate of ion transport across a tight epithelium. Figure 6.2 illustrates a generalized schematic for salt and water reabsorption across lung epithelia that primarily serve to maintain an appropriately moist airspace. Unlike renal transport processes that occur along distinct portions of the nephron against sizable concentration gradients and filtrate volume, net ion transport occurs across a single alveolar unit (composed of T1 and T2 cells with similar transport abilities) with very low volume of luminal surface fluid. Generally speaking, salt and water transport across the alveolar epithelium occurs as a result of a multistep process. As a starting point, the apical membrane of the alveolar epithelium is highly permeable to $Na^+$, with the basolateral membrane conferring high permeability to $K^+$ (step 1). The electrogenic Na/K ATPase pumps serve to recycle $K^+$ and maintain low intracellular $Na^+$ content needed for movement of cations across the inner and outer membrane. Since amiloride sensitive epithelial sodium channels (ENaC) are located at the apical membrane, activation

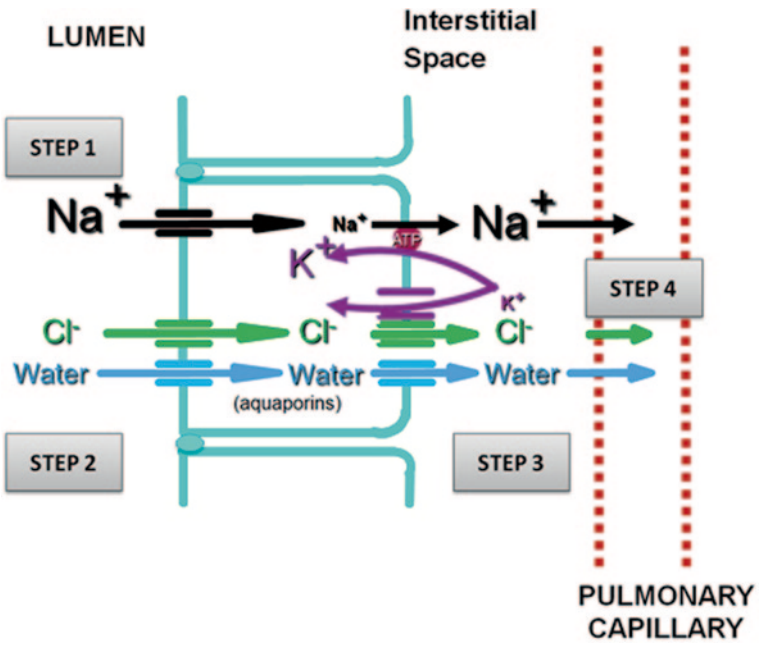


**Fig. 6.2** Generalized schema for net salt and water movement across the alveolar epithelium

of these channels is often regarded as the rate-limiting step in transbarrier ion transport. Anions accompany net $Na^+$ movement from the outside to the inside of the cell to sustain electroneutrality (step 2). The accumulation of anions and cations generates an osmotic gradient that drives water movement from luminal to serosal compartments. The accumulation of both salt and water in the interstitium (step 3) and Starling's forces promote bulk flow of water and salt into the alveolar capillary network (step 4).

The generalized transport of salt and water out of the airways depicted in Fig. 6.2 is a critically important function of the alveolar epithelium since passive movement of fluid driven by hydrostatic pressure of pulmonary capillaries lining the lung continually inundates the airspace with extravascular fluid. Alveolar pulmonary edema is most effectively resolved via the absorptive properties of T1 and T2 cells alongside attenuation of secretory processes. Inflammation and injury to the epithelial tight junctions can significantly alter the volume of fluid lining the lungs.

## *6.1.3 Bioelectric Properties of the Alveolar Epithelium*

### 6.1.3.1 Epithelial Sodium Channel (ENaC)

Lung ENaC is expressed in the upper and lower airways. Most recently, all cells comprising the alveolar epithelium have been identified to express functional ENaC in the apical membrane (Helms et al. 2008). ENaC is a member of the Degenerin family of ion channels and is made up of α-, β-, and γ- subunits which make up either the highly selective cation *(HSC)* or nonselective cation *(NSC)* channel isoforms of ENaC. HSCs are smaller conducting channels, made up of all 3 subunits, and is responsible for the unidirectional reabsorption of $Na^+$ ions from the airways back into serosal compartments (with the aid of basolateral Na/K ATPases discussed below) because it favors $Na^+$ transport over other cations (e.g., $K^+$, 40:1). As such, HSC-ENaC generates an osmotic gradient for water reabsorption out of the airspace and is regarded as the rate limiting step in alveolar fluid clearance. The NSC variety of $Na^+$ channels, however, has a larger conducting pore with low selectivity for $Na^+$ entry over $K^+$ secretion into the lumen ($Na^+/K^+$ 1:1.1). For this reason, NSCs are proposed to serve primarily to maintain airway fluid homeostasis via its secretory and absorptive properties. The molecular identity of HSC and NSC channels, however, remain unclear. In overexpression models, the α-subunit has been shown to produce amiloride-sensitive current (alone or in combination with β- or γ-ENaC subunits (Konstas and Korbmacher 2003)). Neither β-ENaC nor γ-ENaC has been shown to produce significantly large amiloride-sensitive current when over-expressed alone. The importance of α-ENaC in regulating lung fluid balance is highlighted by studies that show α-ENaC knockout mice die within 20 h of birth due to an inability to remove lung fluid (Hummler et al. 1996). Moreover, normalized expression of all classical subunits in human respiratory epithelial cells (trachea, bronchi, and lung) indicates significantly higher levels of α-ENaC subunit expression (Ji et al. 2012).

Recently a δ-ENaC subunit was discovered in the human lung, which also expresses the alpha, beta, and gamma subunits (Haerteis et al. 2009; Zhao et al. 2012). Sodium channels composed of δ-, β-, and γ-hENaC subunits are less sensitive to proteolytic cleavage and exhibit larger single conductances than α-, β-, and γ-subunits comprising HSC channels (Haerteis et al. 2009). Despite extensive biophysiological characterization of the δ-ENaC subunit, its role in lung disorders remains largely unknown (reviewed in Ji et al. 2012).

#### 6.1.3.2 Na/K ATPases

Basolateral Na/K ATPases are antiporter enzymes and play an important role in active transbarrier transport of $Na^+$across lung epithelia. The sodium pump is made up of two major subunits, α and β, that combine to form a heterodimer in the plasma membrane in which three $Na^+$ions are extruded in exchange for 2 $K^+$ions. The catalytic α-subunit undergoes ion- and adenosine triphosphate (ATP) coupling needed for the uphill transport of ions. The β-subunit is responsible for the assembly and normal insertion of the enzyme into the plasma membrane. Above and beyond transporting $Na^+$ from the apical to basolateral compartment while recycling $K^+$, Na/K ATPases play important roles in maintaining the cellular resting membrane potential and controlling cell volume, and they serve as important signal transducers. Under basal conditions, 4–10% of total cellular energy turnover is estimated to be utilized for active Na/K ATPase transport, albeit in muscle fiber (Clausen et al. 1991). In patients with CF (and hence hyperactive $Na^+$ reabsorption) energy expenditure for Na/K ATPase can increase to as much as two thirds of the cell's total energy expenditure (Stutts et al. 1986).

#### 6.1.3.3 Chloride Channels

The cystic fibrosis transmembrane conductance regulator (CFTR) is made up of two, six-span membrane-bound regions, each connected to a nuclear binding factor that binds ATP. Only 4% on the CFTR protein is found in the extracellular loops, and 19% of the chloride channel makes up the transmembrane domains. CFTR belongs to the ATP-binding cassette (ABC) transporter-type family of proteins and is found throughout the upper and lower airways. Although western and northern blot studies provide evidence for the expression of CFTR in the alveolar epithelium (Johnson et al. 2006), the physiological role of CFTR in T1 and T2 cells of the mature lung remains unclear. In utero, CFTR in the developing lung plays an important role in actively secreting $Cl^-$ into the luminal space, which promotes both fluid secretion and continued lung growth (Kitterman 1984). Since airspace fluid is quickly absorbed immediately after birth in the lungs, it remains controversial whether CFTR plays an important role as an anion transporter in T1 and T2 cells of adult lungs. Although very small percentages of alveolar cells have been shown to exhibit $Cl^-$ channel activation following cyclic adenosine monophosphate (cAMP)

stimulation (Zhu et al. 1996), there are many experimental studies that implicate $Cl^-$ channel activation in the resolution of alveolar edema (reviewed in O'Grady and Lee 2003). Based on these studies, and the biophysical characterization of CFTR, it is possible that CFTR is present in the alveolar epithelium and modulates bidirectional $Cl^-$ flux (into and out of the alveolar airspace) to regulate lung fluid volumes.

Classically, the anion selectivity sequence of CFTR is found to be $BR^- \geq Cl^- > I^- > F^-$. Additional evidence, however, indicates that CFTR may be a novel transbarrier pathway by which the anionic antioxidant tripeptide GSH and its oxidized form (glutathione disulfide; GSSG) are released into the airway surface lining fluid (Gao et al. 1999; Gould et al. 2012; Hudson 2001; Kariya et al. 2007; Kogan et al. 2003). Since the GSH/GSSG redox couple is the most important pair in controlling cellular oxidative states, transporters of reduced and oxidized GSH play critically important roles in the vertebrate blood–gas barrier.

The relationship between $Cl^-$ channel activation and transbarrier movement of $Na^+$ in adult alveolar cells is also widely debated. In line with the clinical manifestations of CF patients, the low-volume hypothesis suggests that loss of CFTR function fails to inhibit ENaC activity (reviewed in (Collawn 2012). Hyperactive ENaC indeed promotes increased sodium and water absorption and therefore causes a corresponding decrease in airway surface fluid and increased susceptibility for infection and inflammation. The airway cells and bronchoalveolar lavage fluid of CF patients, however, are also depleted of antioxidants, lending further credence for the importance of the transbarrier transport of GSH via CFTR.

#### 6.1.3.4 Potassium Channels

Transcript studies reveal more than 30 different $K^+$ channels in the respiratory epithelium lining the airways and alveoli (reviewed in Bardou et al. 2009). In $Cl^-$ secreting cells, $K^+$ efflux through basolateral $K^+$ channels is essential in preventing depolarization and in maintaining the electrochemical driving force for continued $Cl^-$ secretion. Apically located $K^+$ channels contribute to the high $K^+$ content in the airway surface liquid and influences the apical resting membrane potential (Valeyre et al. 1991). Alternatively, $K^+$ channels have also been shown to play key roles in oxygen sensing and respiratory repair after injury (reviewed in O'Grady and Lee 2003).

#### 6.1.3.5 Aquaporins

Water transport across the alveolar epithelium occurs in response to the development of osmotic gradients created by the unidirectional transport of $Na^+$ and $Cl^-$, as illustrated in Fig 6.2. Aquaporins are made up of six transmembrane α-helices with the amino and carboxy termini located intracellularly. Importantly, aquaporins form tetramers in the cell membrane, with each unit acting as a water channel. An aromatic/arginine selectivity filter allows water molecules to pass and excludes other

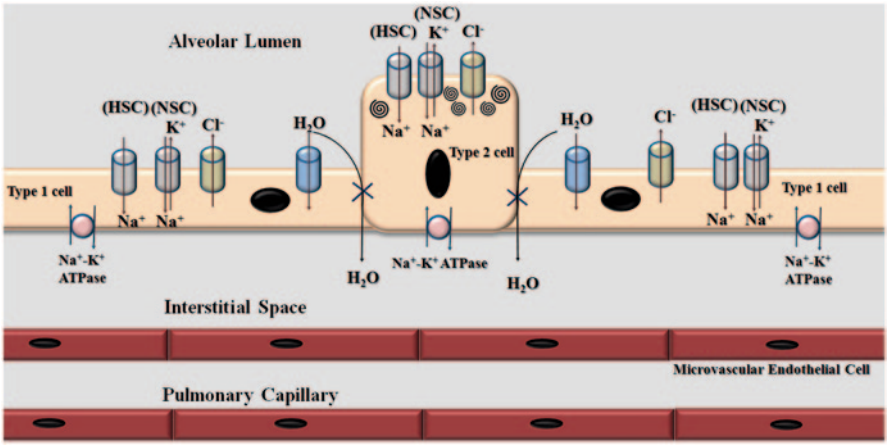


**Fig. 6.3** Schematic diagram of the major channels, pumps, and transporters for ion and water movement across the alveolar and airway epithelium

molecules from entering the pore. There are 13 known types of aquaporins (and many more are suspected to exist). Aquaporin 5 is primarily expressed in alveolar T1 cells, where the majority of water is transported across the alveolar epithelium.

### *6.1.4 Summary of Transbarrier Transport of Salt and Water*

Transepithelial movement of fluid relies on the osmotic gradient generated by unidirectional transport of $Na^+$ across lung epithelia. The transport of $Cl^-$ and $K^+$ maintains electroneutrality and prevents significant depolarization of the cell membrane. Pnuemocytes also have specific transbarrier water transporters that play an important role in the movement of water across the alveolar and airway epithelia. Figure 6.3 illustrates the major pathways for ion and water transport across airway and alveolar epithelium. Other known membrane transporters that are not directly involved in net fluid transport are not shown.

### *6.1.5 Transbarrier Transport in Lung Disease*

Maintaining the integrity of the alveolar capillary membrane (ACM) is critical for optimal physiologic function of the lung. Disruption in the barrier or activity of the ion channels, pumps, and pores that regulate lung fluid balance results in disease. Severe disruption in the barrier properties of the alveolar capillary membrane occurs in ARDS, while alterations in the regulation of ion channels occur in CF and COPD.

#### 6.1.5.1 The Importance of Oxidative Stress in Lung Disease

Oxidative stress is defined as an imbalance in oxidants and antioxidants that results in a disruption in redox signaling and control (Jones 2006). Redox signaling can occur via oxidation and reduction reactions involving oxidants and antioxidants, and a delicate balance must be maintained to ensure appropriate signaling. However, in many pulmonary disease states, there is considerable oxidative stress that can affect transbarrier transport in the lung. Therefore, an overview of the processes governing impaired or altered transbarrier transport in pulmonary disease, with an emphasis on oxidant-mediated signaling and oxidative stress, is provided below.

#### 6.1.5.2 Acute Respiratory Distress Syndrome (ARDS)

ARDS is a life-threatening form of hypoxemic respiratory failure characterized by non-cardiogenic pulmonary edema and refractory hypoxemia (Matthay and Zemans 2011; Matthay et al. 2012). Pathological features of ARDS include a disruption in the integrity of the ACM and an overwhelming inflammatory response. The ACM is composed of two distinct barriers: the microvascular endothelium that lines the capillaries and the alveolar epithelium that lines the alveolar surface (see Fig 6.1). Early in the pathogenesis of ARDS, there is an influx of protein-rich edema fluid into the airspaces. Alterations to the integrity of the microvascular endothelium and the alveolar epithelium leads to the accumulation of edema fluid—primarily through increased vascular permeability coupled with dysregulation of epithelial ion transport. These processes disrupt the transbarrier properties of the ACM leading to impaired gas exchange and critical illness. Therefore, survival is necessarily dependent upon reestablishing an intact and fully functional ACM (Matthay and Wiener-Kronish 1990).

#### 6.1.5.3 Pulmonary Edema in ARDS

Alveolar T1 and T2 cells contain a full complement of ion channels, enzymes, and pores important for resolution of pulmonary edema. The importance of transbarrier transport of $Na^+$ across T1 and T2 cells in resolving pulmonary edema is readily appreciated in studies showing that α-ENaC-deficient mice die shortly after birth due to flooded airways (Hummler et al. 1996). Additionally, pharmacological stimulation of ENaC, the rate-limiting factor in the absorption of $Na^+$ and ultimately water, facilitates recovery from lung injury in several experimental models of lung injury (Downs et al. 2012). Therefore, understanding the factors leading to the dysregulation of ENaC is critically important in understanding the pathogenesis of ARDS.

Pneumonia and systemic infections (e.g., sepsis) are primary causes of ARDS, and both are associated with oxidative stress (Cross et al. 1990; Cross et al. 1994; Trefler et al. 2014). Physiologic levels of reactive oxygen species (ROS) are necessary for cell signaling and oxidants to regulate a variety of ion channels and pumps

including ENaC, CFTR, and Na/K ATPases (Dong et al. 1995; Downs et al. 2013a; Guo et al. 1998; Helms et al. 2008). However, as oxidative stress ensues, there is a disruption in physiologic redox signaling that results in the altered regulation of ion channels and enzymatic pumps, thus impacting transbarrier fluid transport in the lung (Barlow et al. 2006; Eaton et al. 2009; Takemura et al. 2010). Delineating the specific mechanisms of ion channel and transporter disruption is currently an area of intense research.

It is clear that T1 and T2 cells play an active role in the regulation of lung fluid balance and in the resolution of pulmonary edema in ARDS patients (Downs et al. 2013a; Helms et al. 2008; Downs et al. 2013b; Downs et al. 2013c; Downs et al. 2015). A new role for the receptor for advanced glycation end products (RAGE), a transmembrane protein of the immunoglobulin superfamily (Schmidt et al. 2000; Schmidt et al. 2001; Schmidt and Stern 2001) expressed in T1 and T2 cells is emerging as an important determinant of lung ENaC activity (Downs et al. 2015). Additionally, RAGE is a multi-ligand receptor that functions to amplify and perpetuate the inflammatory response, and its activity has been found to be upregulated in ARDS (Uchida et al. 2006). The full-length membrane-bound form of RAGE may be enzymatically cleaved through activity of the matrix metalloproteinase 9 (MMP-9), or an endogenously secreted form may be produced through splice variant (Schmidt et al. 2000; Schmidt et al. 2001; Schmidt and Stern 2001). Collectively these proteins yield a soluble form of RAGE (sRAGE), which binds RAGE ligands but lacks the critical intracellular domain needed for cell signaling, thereby effectively serving as an antagonist of RAGE signaling. The elevated levels of sRAGE that have been documented in the edema fluid of individuals with ARDS (Uchida et al. 2006) suggest that RAGE signaling may be involved in transbarrier solute transport. Furthermore, increasing levels of sRAGE are thought to indicate greater damage to the alveolar epithelium—and more directly reflect injury of T1 cells (Uchida et al. 2006).

The concentrations of several biologically active substances have been collected from the pulmonary edema fluid of individuals with ARDS and compared to controls with hydrostatic pulmonary edema. In addition to elevated concentrations of sRAGE, the pulmonary edema fluid of ARDS patients differentially contain greater concentrations of intercellular adhesion molecule-1 (ICAM-1; Conner et al. 1999), hepatocyte growth factor (HGF; Verghese et al. 1998), soluble transforming growth factor-α (TGF-α; Chesnutt et al.1997), transforming growth factor-β (TGF-β; Frank and Matthay 2014), Leukotriene $B_4$, substance P, interleukin-6 (IL-), and IL-8 (Pittet et al. 1997; Pittet et al. 2001). The significance of these molecules remains unclear. However, TGF-α as well as several of the ILs are potent regulators of alveolar epithelial sodium transport and alveolar epithelial cell mobility (Frank and Matthay 2014; Pittet et al. 2001; Peters et al. 2014). Collectively, these observations suggest that these proteins and the signaling pathways in which they are involved could be important mediators of transepithelial $Na^+$ transport in the ARDS lung.

Reduced GSH is an abundant antioxidant in the lung (Jones 2006; Jones 2011; Rahman and McNee 2000). The oxidized form of GSH, GSSG, is formed through the formation of disulfide bonds between two oxidized GSH molecules and

participates in the posttranslational modification of proteins in a process termed S-glutathionylation, in which protein Cys residues form disulfide bonds with GSSG. Both GSH and GSSG can modify $K^+$-channel activity in the pulmonary vasculature (Jerng and Pfaffinger 2014), and emerging evidence suggests that ENaC and chloride channels may also be S-glutathionylated leading to a downregulation in their function. Clinically, elevated levels of GSSG occur in the lungs of individuals with ARDS (Fremont et al. 2010), indicating that S-glutathionylation of ion channels and transporters may serve as an important posttranslational modifier of transbarrier movement of solutes in the lung.

$\beta_2$-Adrenergic receptor (β-AR) agonists are frequently prescribed clinically to treat and/or prevent bronchoconstriction in individuals hospitalized with ARDS. Bronchoconstriction and mucous accumulation produce hypoxia, as does the pulmonary edema that occurs in ARDS. Hypoxia, regardless of the etiology, affects respiratory epithelial function and inhibits transepithelial sodium transport (Bhalla and Hallows 2008; Carpenter et al. 2003). Specifically, prolonged hypoxia reduces ENaC activity and activity of the Na/K ATPase. $\beta_2$-AR agonists are often used to improve oxygenation in the lung. In addition, $\beta_2$-AR agonists also increase cAMP levels to then activate ENaC (Downs et al. 2012). However, in large randomized controlled trials, inhaled $\beta_2$-AR agonists have not been shown to be effective in promoting lung fluid clearance (Gates et al. 2013; Perkins et al. 2014). There are a variety of purported reasons. $\beta_2$-AR can become desensitized and, as a result of continued use, are therefore less capable of responding to an agonist. Indeed, individuals being treated for sepsis often require intravenous infusions of catecholamines to support cardiovascular function which contribute to desensitization of the receptors (Shi et al. 2013) and may explain their lack of effectiveness.

Inflammation is also a key feature of ARDS. Many cytokines (e.g., IL-1, IL-6, IL-10, and tumor necrosis factor alpha (TNFα)) are secreted by activated immune cells such as neutrophils and macrophages during the inflammatory response. IL-1β and TNF-α increase permeability of the capillary membrane (Puhlmann et al. 2005). In addition, cytokines have been shown to affect ion transport in the lung. IL-1β decreases ENaC activity through the p38 mitogen activated protein kinase (MAPK) pathway and decreases mRNA expression of α-, β-, and γ-ENaC (Al-Sadi and Kreydiyyeh 2003; Al-Sadi and Ma 2007). The significance of this observation is highlighted by studies in humans showing that elevated levels of IL-1β correlate with a poor prognosis in individuals with ARDS (Meduri et al. 1995a,b).

Activity of the basolaterally located Na/K ATPases are also affected in ARDS. Oxidative stress and ischemia decrease activity of the pump, leading to a reduction in the vectorial transport of $Na^+$ from the apical membrane to the interstitial space (Cross et al. 1995).

The barrier integrity can be assessed clinically in individuals with ARDS. Since the epithelial barrier is normally impermeable to protein, the ratio of protein concentration in edema fluid to plasma provides an index of epithelial permeability. Consequently, changes in the net concentration of protein in the edema fluid can be assessed over time to provide an estimate of alveolar fluid removal. Alveolar fluid clearance can occur early and is often apparent within the first few hours of

establishing mechanical ventilation in patients with either hydrostatic or increased permeability edema (Calfee et al. 2007; Ware et al. 2010a, b). The precise mechanism by which mechanical ventilation resolves alveolar flooding is not clear; it may be feasible that oxygen-mediated signaling may play an important role in activating apical Na+ channels responsible for generating the osmotic gradient necessary for lung fluid clearance.

Repair of the integrity of the ACM is requisite for the reestablishment of homeostasis in the lung parenchyma. Denudation of the alveolar epithelium occurs because of damage to alveolar T1 cells and T2 cells (e.g., apoptosis and necrosis secondary to infection). Reformation of the alveolar barrier occurs as alveolar T2 cells differentiate into T1 cells, thereby restoring barrier integrity. Cell differentiation is tightly regulated. HGF and keratinocyte growth factor are major mitogens for alveolar T2 cells, and T2 cell differentiation occurs as ARDS resolves (Leslie et al. 1997; Portnoy et al. 2004). Mesenchymal stem cells (MSC) and endothelial progenitor cells (EPC) hold promise as potential therapeutic options to treat lung injury. MSCs offer considerable promise because of their potential to differentiate into lung cells and directly replace damaged cells and tissues (Matthay et al. 2010; Matthay et al. 2013). Additionally, during lung injury there is an intense immune response that MSCs can modulate by reprogramming the inflammatory response thereby effectively reducing inflammation and its associated damage.

Transbarrier transport in the ARDS lung initially occurs against a backdrop of increased permeability and an overwhelming inflammatory response. Over time and as the barrier integrity is restored, lung homeostasis is restored and physiologic transbarrier transport can resume.

#### 6.1.5.4 Cystic Fibrosis (CF)

CF is a heritable, autosomal recessive disorder involving the CFTR gene. The CFTR gene codes for the chloride channel necessary to promote appropriate lung fluid balance by secreting $Cl^-$ and maintaining electroneutrality. Indeed, impaired CFTR function occurs in individuals with CF that results in chronically dehydrated ELF and thick, tenacious mucous. Altered ELF volumes coupled with thick mucus promotes an environment that allows for colonization of the airways with pathogenic bacteria. Repeated bouts with respiratory infections promote oxidative stress that can further alter transbarrier transport in the CF lung.

It is believed that active CFTR inhibits ENaC activity, and that lack of CFTR function subsequently leads to excessive $Na^+$ reabsorption. Hyperactive ENaC activity ultimately dehydrates the ELF. Thus, altered CFTR function promotes the development of thick, viscous mucus that is difficult to expectorate via dysregulation of apical $Na^+$ channels.

Oxidants and reactive nitrogen species also affect CFTR function (Dong et al. 1995; Chao et al. 1994; Steagall et al. 2000). In CF patients, airway epithelial cells are more susceptible to bacterial and viral infection due, in part, to impaired host nitric oxide (NO) defense pathway. NO mediates many effects through production

of cyclic guanosine monophosphate (cGMP) by NO-sensitive guanylate cyclase. cGMP activates cGMP protein kinase G2, which phosphorylates CFTR and increases its activity (Dong et al. 1995). In the normal lung, NO and cGMP stimulate CFTR activity and can downregulate amiloride-sensitive epithelial sodium absorption. However, in CF there is a reduction in NO production which could further hinder CFTR's ability to regulate ENaC activity (Michl et al. 2013).

Chloride channels including CFTR are also regulated through purinergic activators. Specifically, ATP serves as an autocrine signaling pathway for CFTR,that is, ATP increases the activity of CFTR and promotes the recruitment of CFTR, thereby governing airway epithelial cell volume (Braunstein et al. 2001; Braunstein et al. 2004; Schwiebert et al. 2002; Zsembery et al. 2004). The gating properties of CFTR $Cl^-$ channel is regulated by the interaction of ATP with its two cytoplasmic nucleotide-binding domains. Moreover, the cAMP-dependent phosphorylation of the CFTR regulatory domains is a prerequisite for ATP-dependent activity (Berger et al. 2005; Ikuma and Welsh 2000).

In CF, there is also an increase in immune cell infiltration coupled with oxidative stress. Interestingly, oxidative stress, at least early on, appears to increase EnaC-gating properties as well as promoting retention of the active channel in the plasma membrane (Downs et al. 2013a,b). However, oxidative stress promotes internalization of CFTR and decreases CFTR activity (Clunes et al. 2012; Cantin et al. 2006a, b). CF exacerbations typically occur in response to infections. Infection promotes the migration of macrophages and recruits neutrophils into the airways. The increase in immune cells promotes greater oxidant production, further impairing CFTR function, leading to further dehydration of the ELF. The impact of oxidants and oxidative stress in the CF lung is further exacerbated because individuals with CF are deficient in the antioxidant GSH (Rahman and Macn 2000). In summary, oxidative stress and impaired NO production significantly impair CFTR function leading to thick, tenacious mucus that is the phenotypical feature of CF. Furthermore this process is worsened during periods of infection as greater oxidative stress occurs.

#### 6.1.5.5 Chronic Lung Disease

COPD is a heterogeneous disease composed of varying degrees of chronic bronchitis, emphysema, and, at times, asthma (Mannino 2002). COPD is characterized by a persistent and abnormal inflammatory response that culminates in airflow limitation that is not fully reversible. Impaired transbarrier transport occurs in COPD, although the significance to disease development remains unclear. Mice overexpressing β-ENaC spontaneously develop a phenotype consistent with chronic bronchitis and emphysema, suggesting that altered ion transport likely plays a central role in the pathogenesis of COPD (Mall et al. 2004).

Cigarette smoke is the primary etiology of COPD. Cigarette smoke has been shown to decrease mRNA for α-, β-, and γ-ENaC (Downs et al. 2013b; Xu and Chu 2007). However, acute exposure to an aqueous form of cigarette smoke increased

ENaC activity in alveolar T1 and T2 cells through an oxidant-mediated signaling pathway (Downs et al. 2013b). Cigarette smoke also promotes internalization of the CFTR $Cl^-$ channel, suggesting that acutely cigarette smoke promotes $Na^+$ absorption (Clunes et al. 2012). In mice, instillation of an aqueous form of cigarette smoke accelerated removal of the instillate, while inhibition of the NADPH oxidases attenuated the effect (Downs et al. 2013b). In humans, studies show that smokers have lower volumes of the antioxidant-rich ELF compared to nonsmokers (Downs et al. 2015), suggesting that cigarette smoke activates Na+ absorption to affect lung fluid homeostasis and transbarrier solute transport.

Cigarette smoke is a complex mixture of over 4000 chemicals and noxious compounds, many of which are known carcinogens (Church et al. 1990; Pryor 1992). Smoking impairs the integrity of the ACM through apoptosis or programmed cell death as well as necrosis (Barlow et al. 2006; Asano et al. 2012). Cigarette smoke has been shown to be cytotoxic to alveolar cells (Hoshino et al. 2001). In humans with COPD, there is evidence of increased apoptosis of bronchial and alveolar epithelial cells compared to persons without COPD (Bracke et al. 2007; Demedts et al. 2006). Loss of the alveolar surface area occurs in emphysema; this loss, by definition, demonstrates that cigarette smoke impairs the integrity of the alveolar epithelial barrier. Therefore, the loss of alveolar surface area likely impacts net transbarrier transport, while concurrently effecting gas exchange.

An abnormal and persistent inflammatory response also occurs in COPD. Specifically, there is an increase in macrophages and an accumulation of neutrophils in the airways. These immune cells produce large quantities of ROS that may induce necrosis and increase cytokine production. Necrotic cells secrete a variety of noxious proteins and molecules that can affect lung integrity and impact the integrity of the airway and alveolar epithelium. TNF-α is secreted by activated immune cells such as alveolar macrophages and neutrophils and is a potent regulator of ENaC function. Studies show an increase in TNF-α expression in the airways and lung parenchyma of individuals with COPD. As disease progression ensues, there is a further increase in TNF-α levels such that TNF-α levels often correlate with disease severity.

### *6.1.6 Summary of Transbarrier Transport in Lung Disease*

Transbarrier transport across the alveolar capillary membrane is critical for effective gas exchange. Solute transport is the direct effect of a series of coordinated events involving ion channels, enzymatic pumps and pores. Disruption in the integrity of the ACM or dysregulation of these proteins is involved in disease development and progression and remains a source of active investigation and potential target for pharmacological interventions to treat a variety of lung diseases.

**Acknowledgments** The authors acknowledge the assistance of Elizabeth M. Brewer and Phi T. Trac in the preparation of this chapter.

## References

Al-Sadi RM, Kreydiyyeh SI. Mediators of interleukin-1 beta action Na(+)-K(+)ATPase in Caco-2 cells. Eur Cytokine Netw. 2003;14:83–90.

Al-Sadi RM, Ma TY. IL-1beta causes an increase in intestinal epithelial tight junction permeability. J Immunol. 2007;178:4641–9.

Asano H, Horinouchi T, Mai Y, Sawada O, Fujii S, Nishiya T, et al. Nicotine- and tar-free cigarette smoke induces cell damage through reactive oxygen species newly generated by PKC-dependent activation of NADPH oxidase. J Pharmacol Sci. 2012;118:275–87.

Bardou O, Trinh NT, Brochiero E. Molecular diversity and function of K + channels in airway and alveolar epithelial cells. Am J Physiol Lung Cell Mol Physiol. 2009;296:L145–L55.

Barlow CA, Shukla A, Mossman BT, Lounsbury KM. Oxidant-mediated cAMP response element binding protein activation: calcium regulation and role in apoptosis of lung epithelial cells. Am J Respir Cell Mol Biol. 2006;34:7–14.

Berger AL, Ikuma M, Welsh MJ. Normal gating of CFTR requires ATP binding to both nucleotide-binding domains and hydrolysis at the second nucleotide-binding domain. Proc Natl Acad Sci U S A. 2005;102:455–60.

Bhalla V, Hallows KR. Mechanisms of ENaC regulation and clinical implications. J Am Soc Nephrol. 2008;19:1845–54.

Bracke KR, D'hulst AI, Maes T, Demedts IK, Moerloose KB, Kuziel WA, et al. Cigarette smoke-induced pulmonary inflammation, but not airway remodelling, is attenuated in chemokine receptor 5-deficient mice. Clin Exp Allergy. 2007;37:1467–79.

Braunstein GM, Roman RM, Clancy JP, Kudlow BA, Taylor AL, Shylonsky VG, et al. Cystic fibrosis transmembrane conductance regulator facilitates ATP release by stimulating a separate ATP release channel for autocrine control of cell volume regulation. J Biol Chem. 2001;276:6621–30.

Braunstein GM, Zsembery A, Tucker TA, Schwiebert EM. Purinergic signaling underlies CFTR control of human airway epithelial cell volume. J Cyst Fibros. 2004;3:99–117.

Calfee CS, Eisner MD, Ware LB, Thompson BT, Parsons PE, Wheeler AP, et al. Trauma-associated lung injury differs clinically and biologically from acute lung injury due to other clinical disorders. Crit Care Med. 2007;35:2243–50.

Cantin AM, Bilodeau G, Ouellet C, Liao J, Hanrahan JW. Oxidant stress suppresses CFTR expression. Am J Physiol Cell Physiol. 2006a;290:C262–C70.

Cantin AM, Hanrahan JW, Bilodeau G, Ellis L, Dupuis A, Liao J, et al. Cystic fibrosis transmembrane conductance regulator function is suppressed in cigarette smokers. Am J Respir Crit Care Med. 2006b;173:1139–44.

Carpenter TC, Schomberg S, Nichols C, Stenmark KR, Weil JV. Hypoxia reversibly inhibits epithelial sodium transport but does not inhibit lung ENaC or Na-K-ATPase expression. Am J Physiol Lung Cell Mol Physiol. 2003;284:L77–L83.

Chao AC, de Sauvage FJ, Dong YJ, Wagner JA, Goeddel DV, Gardner P. Activation of intestinal CFTR $Cl^-$ channel by heat-stable enterotoxin and guanylin via cAMP-dependent protein kinase. EMBO J. 1994;13:1065–72.

Chesnutt AN, Matthay MA, Tibayan FA, Clark JG. Early detection of type III procollagen peptide in acute lung injury. Pathogenetic and prognostic significance. Am J Respir Crit Care Med. 1997;156:840–5.

Church DF, Burkey TJ, Pryor WA. Preparation of human lung tissue from cigarette smokers for analysis by electron spin resonance spectroscopy. Methods Enzymol. 1990;186:665–9.

Clausen T, Van HC, Everts ME. Significance of cation transport in control of energy metabolism and thermogenesis. Physiol Rev. 1991;71:733–74.

Clunes LA, Davies CM, Coakley RD, Aleksandrov AA, Henderson AG, Zeman KL, et al. Cigarette smoke exposure induces CFTR internalization and insolubility, leading to airway surface liquid dehydration. FASEB J. 2012;26:533–45.

Collawn JF, Lazrak A, Bebok Z, Matalon S. The CFTR and ENaC debate: how important is ENaC in CF lung disease? Am J Physiol Lung Cell Mol Physiol. 2012;302:L1141–L6.

Conner ER, Ware LB, Modin G, Matthay MA. Elevated pulmonary edema fluid concentrations of soluble intercellular adhesion molecule-1 in patients with acute lung injury: biological and clinical significance. Chest. 1999;116 (Suppl:83):S–4S.

Cross CE, Frei B, Louie S. The adult respiratory distress syndrome (ARDS) and oxidative stress: therapeutic implications. Adv Exp Med Biol. 1990;264:435–48.

Cross CE, van d, V, O'Neill CA, Louie S, Halliwell B. Oxidants, antioxidants, and respiratory tract lining fluids. Environ Health Perspect. 1994;102 (Suppl 10):185–91.

Cross HR, Radda GK, Clarke K. The role of Na+/K+ATPase activity during low flow ischemia in preventing myocardial injury: a 31P, 23Na and 87Rb NMR spectroscopic study. Magn Reson Med. 1995;34:673–85.

Demedts IK, Demoor T, Bracke KR, Joos GF, Brusselle GG. Role of apoptosis in the pathogenesis of COPD and pulmonary emphysema. Respir Res. 2006;7:53.

Dong YJ, Chao AC, Kouyama K, Hsu YP, Bocian RC, Moss RB, et al. Activation of CFTR chloride current by nitric oxide in human T lymphocytes. EMBO J. 1995;14:2700–7.

Downs CA, Kriener LH, Yu L, Eaton DC, Jain L, Helms MN. β-Adrenergic agonists differentially regulate highly selective and nonselective epithelial sodium channels to promote alveolar fluid clearance in vivo. Am J Physiol Lung Cell Mol Physiol. 2012;302:L1167–L78.

Downs CA, Trac DQ, Kreiner LH, Eaton AF, Johnson NM, Brown LA, et al. Ethanol alters alveolar fluid balance via Nadph oxidase (NOX) signaling to epithelial sodium channels (ENaC) in the lung. PLoS ONE. 2013a;8:e54750.

Downs CA, Kreiner LH, Trac DQ, Helms MN. Acute effects of cigarette smoke extract on alveolar epithelial sodium channel activity and lung fluid clearance. Am J Respir Cell Mol Biol. 2013b;49:251–9.

Downs CA, Kumar A, Kreiner LH, Johnson NM, Helms MN. H2O2 regulates lung epithelial sodium channel (ENaC) via ubiquitin-like protein Nedd8. J Biol Chem. 2013c;288:8136–45.

Downs CA, Kreiner LH, Johnson NM, Brown LA, Helms MN. RAGE regulates lung fluid balance via PKC-gp91 signaling to epithelial sodium channels (ENaC). Am J Respir Cell Mol Biol. 2015;52(1):75–87.

Eaton DC, Helms MN, Koval M, Bao HF, Jain L. The contribution of epithelial sodium channels to alveolar function in health and disease. Annu Rev Physiol. 2009;71:403–23.

Frank JA, Matthay MA. TGF-beta and lung fluid balance in ARDS. Proc Natl Acad Sci U S A. 2014;111:885–6.

Fremont RD, Koyama T, Calfee CS, Wu W, Dossett LA, Bossert FR, et al. Acute lung injury in patients with traumatic injuries: utility of a panel of biomarkers for diagnosis and pathogenesis. J Trauma. 2010;68:1121–7.

Gao L, Kim KJ, Yankaskas JR, Forman HJ. Abnormal glutathione transport in cystic fibrosis airway epithelia. Am J Physiol. 1999;277:L113–L8.

Gates S, Perkins GD, Lamb SE, Kelly C, Thickett DR, Young JD, et al. Beta-Agonist Lung injury TrIal-2 (BALTI-2): a multicentre, randomised, double-blind, placebo-controlled trial and economic evaluation of intravenous infusion of salbutamol versus placebo in patients with acute respiratory distress syndrome. Health Technol Assess. 2013;17:v–87.

Gould NS, Min E, Martin RJ, Day BJ. CFTR is the primary known apical glutathione transporter involved in cigarette smoke-induced adaptive responses in the lung. Free Radic Biol Med. 2012;52:1201–6.

Guo Y, Duvall MD, Crow JP, Matalon S. Nitric oxide inhibits Na + absorption across cultured alveolar type II monolayers. Am J Physiol. 1998;274:L369–L77.

Haerteis S, Krueger B, Korbmacher C, Rauh R. The delta-subunit of the epithelial sodium channel (ENaC) enhances channel activity and alters proteolytic ENaC activation. J Biol Chem. 2009;284:29024–40.

Helms MN, Jain L, Self JL, Eaton DC. Redox regulation of epithelial sodium channels examined in alveolar type 1 and 2 cells patch-clamped in lung slice tissue. J Biol Chem. 2008;283:22875–83.

Hoshino Y, Mio T, Nagai S, Miki H, Ito I, Izumi T. Cytotoxic effects of cigarette smoke extract on an alveolar type II cell-derived cell line. Am J Physiol Lung Cell Mol Physiol. 2001;281:L509–L16.

Hudson VM. Rethinking cystic fibrosis pathology: the critical role of abnormal reduced glutathione (GSH) transport caused by CFTR mutation. Free Radic Biol Med. 2001;30:1440–61.

Hummler E, Barker P, Gatzy J, Beermann F, Verdumo C, Schmidt A, et al. Early death due to defective neonatal lung liquid clearance in alpha-ENaC-deficient mice. Nat Genet. 1996;12:325–8.

Ikuma M, Welsh MJ. Regulation of CFTR $Cl^-$ channel gating by ATP binding and hydrolysis. Proc Natl Acad Sci U S A. 2000;97:8675–80.

Jerng HH, Pfaffinger PJ. S-glutathionylation of an auxiliary subunit confers redox sensitivity to Kv4 channel inactivation. PLoS ONE. 2014;9:e93315.

Ji HL, Zhao RZ, Chen ZX, Shetty S, Idell S, Matalon S. delta ENaC: a novel divergent amiloride-inhibitable sodium channel. Am J Physiol Lung Cell Mol Physiol. 2012;303:L1013–L26.

Johnson MD, Bao HF, Helms MN, Chen XJ, Tigue Z, Jain L, et al. Functional ion channels in pulmonary alveolar type I cells support a role for type I cells in lung ion transport. Proc Natl Acad Sci U S A. 2006;103:4964–9.

Jones DP. Redefining oxidative stress. Antioxid Redox Signal. 2006;8:1865–79.

Jones DP. The Health Dividend of Glutathione. Nat Med J 2011;3(2).

Kariya C, Leitner H, Min E, van HC, van HA, Day BJ. A role for CFTR in the elevation of glutathione levels in the lung by oral glutathione administration. Am J Physiol Lung Cell Mol Physiol. 2007;292:L1590–L7.

Kitterman JA. Fetal lung development. J Dev Physiol. 1984;6:67–82.

Kogan I, Ramjeesingh M, Li C, Kidd JF, Wang Y, Leslie EM, et al. CFTR directly mediates nucleotide-regulated glutathione flux. EMBO J. 2003;22:1981–9.

Konstas AA, Korbmacher C. The gamma-subunit of ENaC is more important for channel surface expression than the beta-subunit. Am J Physiol Cell Physiol. 2003;284:C447–C56.

Leslie CC, McCormick-Shannon K, Shannon JM, Garrick B, Damm D, Abraham JA, et al. Heparin-binding EGF-like growth factor is a mitogen for rat alveolar type II cells. Am J Respir Cell Mol Biol. 1997;16:379–87.

Mall M, Grubb BR, Harkema JR, O"Neal WK, Boucher RC. Increased airway epithelial Na + absorption produces cystic fibrosis-like lung disease in mice. Nat Med. 2004;10:487–93.

Mannino DM. COPD: epidemiology, prevalence, morbidity and mortality, and disease heterogeneity. Chest. 2002;121 Suppl 5:121S–6S.

Matthay MA, Wiener-Kronish JP. Intact epithelial barrier function is critical for the resolution of alveolar edema in humans. Am Rev Respir Dis. 1990;142:1250–7.

Matthay MA, Zemans RL. The acute respiratory distress syndrome: pathogenesis and treatment. Annu Rev Pathol. 2011;6:147–63.

Matthay MA, Thompson BT, Read EJ, McKenna DH Jr, Liu KD, Calfee CS, et al. Therapeutic potential of mesenchymal stem cells for severe acute lung injury. Chest. 2010;138:965–72.

Matthay MA, Ware LB, Zimmerman GA. The acute respiratory distress syndrome. J Clin Invest. 2012;122:2731–40.

Matthay MA, Anversa P, Bhattacharya J, Burnett BK, Chapman HA, Hare JM, et al. Cell therapy for lung diseases. Report from an NIH-NHLBI workshop, November 13–14, 2012b. Am J Respir Crit Care Med. 2013;188:370–5.

Meduri GU, Headley S, Tolley E, Shelby M, Stentz F, Postlethwaite A. Plasma and BAL cytokine response to corticosteroid rescue treatment in late ARDS. Chest. 1995a;108:1315–25.

Meduri GU, Kohler G, Headley S, Tolley E, Stentz F, Postlethwaite A. Inflammatory cytokines in the BAL of patients with ARDS. Persistent elevation over time predicts poor outcome. Chest. 1995b;108:1303–14.

Michl RK, Hentschel J, Fischer C, Beck JF, Mainz JG. Reduced nasal nitric oxide production in cystic fibrosis patients with elevated systemic inflammation markers. PLoS ONE. 2013;8:e79141.

O'Grady SM, Lee SY. Chloride and potassium channel function in alveolar epithelial cells. Am J Physiol Lung Cell Mol Physiol. 2003;284:L689–L700.

Perkins GD, Gates S, Park D, Gao F, Knox C, Holloway B, et al. The beta agonist lung injury trial prevention. A randomized controlled trial. Am J Respir Crit Care Med. 2014;189:674–83.

Peters DM, Vadasz I, Wujak L, Wygrecka M, Olschewski A, Becker C, et al. TGF-beta directs trafficking of the epithelial sodium channel ENaC which has implications for ion and fluid transport in acute lung injury. Proc Natl Acad Sci U S A. 2014;111:E374–E83.

Pittet JF, Mackersie RC, Martin TR, Matthay MA. Biological markers of acute lung injury: prognostic and pathogenetic significance. Am J Respir Crit Care Med. 1997;155:1187–205.

Pittet JF, Griffiths MJ, Geiser T, Kaminski N, Dalton SL, Huang X, et al. TGF-beta is a critical mediator of acute lung injury. J Clin Invest. 2001;107:1537–44.

Portnoy J, Curran-Everett D, Mason RJ. Keratinocyte growth factor stimulates alveolar type II cell proliferation through the extracellular signal-regulated kinase and phosphatidylinositol 3-OH kinase pathways. Am J Respir Cell Mol Biol. 2004;30:901–7.

Pryor WA. Biological effects of cigarette smoke, wood smoke, and the smoke from plastics: the use of electron spin resonance. Free Radic Biol Med. 1992;13:659–76.

Puhlmann M, Weinreich DM, Farma JM, Carroll NM, Turner EM, Alexander HR, Jr. Interleukin-1beta induced vascular permeability is dependent on induction of endothelial tissue factor (TF) activity. J Transl Med. 2005;30(3):37.

Rahman I, Macnee W. Oxidative stress and regulation of glutathione in lung inflammation. Eur Respir J. 2000;16:534–54.

Schmidt AM, Stern DM. Receptor for age (RAGE) is a gene within the major histocompatibility class III region: implications for host response mechanisms in homeostasis and chronic disease. Front Biosci. 2001;6:D1151–D60.

Schmidt AM, Yan SD, Yan SF, Stern DM. The biology of the receptor for advanced glycation end products and its ligands. Biochim Biophys Acta. 2000;1498:99–111.

Schmidt AM, Yan SD, Yan SF, Stern DM. The multiligand receptor RAGE as a progression factor amplifying immune and inflammatory responses. J Clin Invest. 2001;108:949–55.

Schwiebert EM, Wallace DP, Braunstein GM, King SR, Peti-Peterdi J, Hanaoka K, et al. Autocrine extracellular purinergic signaling in epithelial cells derived from polycystic kidneys. Am J Physiol Renal Physiol. 2002;282:F763–F775.

Shi M, Yang Z, Hu M, Liu D, Hu Y, Qian L, et al. Catecholamine-Induced beta2-adrenergic receptor activation mediates desensitization of gastric cancer cells to trastuzumab by upregulating MUC4 expression. J Immunol. 2013;190:5600–8.

Steagall WK, Elmer HL, Brady KG, Kelley TJ. Cystic fibrosis transmembrane conductance regulator-dependent regulation of epithelial inducible nitric oxide synthase expression. Am J Respir Cell Mol Biol. 2000;22:45–50.

Stutts MJ, Knowles MR, Gatzy JT, Boucher RC. Oxygen consumption and ouabain binding sites in cystic fibrosis nasal epithelium. Pediatr Res. 1986;120:1316–20.

Takemura Y, Goodson P, Bao HF, Jain L, Helms MN. Rac1-mediated NADPH oxidase release of O2- regulates epithelial sodium channel activity in the alveolar epithelium. Am J Physiol Lung Cell Mol Physiol. 2010;298:L509–L20.

Trefler S, Rodriguez A, Martin-Loeches I, Sanchez V, Marin J, Llaurado M, et al. Oxidative stress in immunocompetent patients with severe community-acquired pneumonia. A pilot study. Med Intensiva. 2014;38:73–82.

Uchida T, Shirasawa M, Ware LB, Kojima K, Hata Y, Makita K, et al. Receptor for advanced glycation end-products is a marker of type I cell injury in acute lung injury. Am J Respir Crit Care Med. 2006;173:1008–15.

Valeyre D, Soler P, Basset G, Loiseau P, Pre J, Turbie P, et al. Glucose, K +, and albumin concentrations in the alveolar milieu of normal humans and pulmonary sarcoidosis patients. Am Rev Respir Dis. 1991;143:1096–101.

Verghese GM, McCormick-Shannon K, Mason RJ, Matthay MA. Hepatocyte growth factor and keratinocyte growth factor in the pulmonary edema fluid of patients with acute lung injury. Biologic and clinical significance. Am J Respir Crit Care Med. 1998;158:386–94.

Ware LB, Fremont RD, Bastarache JA, Calfee CS, Matthay MA. Determining the aetiology of pulmonary oedema by the oedema fluid-to-plasma protein ratio. Eur Respir J. 2010a;35:331–7.

Ware LB, Koyama T, Billheimer DD, Wu W, Bernard GR, Thompson BT, et al. Prognostic and pathogenetic value of combining clinical and biochemical indices in patients with acute lung injury. Chest. 2010b;137:288–96.

Xu H, Chu S. ENaC alpha-subunit variants are expressed in lung epithelial cells and are suppressed by oxidative stress. Am J Physiol Lung Cell Mol Physiol. 2007;293:L1454–L62.

Zhao RZ, Nie HG, Su XF, Han DY, Lee A, Huang Y, et al. Characterization of a novel splice variant of delta ENaC subunit in human lungs. Am J Physiol Lung Cell Mol Physiol. 2012;302:L1262–L72.

Zhu S, Yue G, Shoemaker RL, Matalon S. Adult alveolar type II cells lack cAMP and Ca(2 + )-activated $Cl^-$ channels. Biochem Biophys Res Commun. 1996;218:302–8.

Zsembery A, Fortenberry JA, Liang L, Bebok Z, Tucker TA, Boyce AT, et al. Extracellular zinc and ATP restore chloride secretion across cystic fibrosis airway epithelia by triggering calcium entry. J Biol Chem. 2004;279:10720–9.

# Chapter 7
# Stress Failure of the Pulmonary Blood–Gas Barrier

**John B. West**

## 7.1 Introduction

This chapter is devoted to the mechanical failure of the pulmonary blood–gas barrier and includes discussions of its ultrastructure, strength, and modes of failure under various conditions. However, it is salutary to begin by noting how long it took for physiologists and physicians to recognize the vulnerability of the barrier. Its ultrastructure remained unknown until the advent of electron microscopy because its dimensions are beyond the resolution of the light microscope. However, when Frank Low published the first electron micrograph of the human blood–gas barrier in 1953, it immediately became clear that only about 0.2 μm of tissue separated the capillary endothelium of the pulmonary capillaries from the alveolar space over much of the area. This vanishingly small amount of tissue might have been expected to alert people to the vulnerability of the barrier. No other capillaries in the human body find themselves in this predicament. Yet, it was not until 40 years later that stress failure of the barrier was recognized and its mechanical behavior was analyzed.

## 7.2 Ultrastructure of the Blood–Gas Barrier

The structure of the blood–gas barrier was a mystery for many years simply because its components are beyond the resolution of the light microscope. However, this did not prevent pathologists and others from speculating about its makeup. By the end of the nineteenth century there were two schools of thought. One was that the pulmonary capillaries were essentially naked in the sense that there was nothing between

J. B. West (✉)
Department of Medicine, University of California San Diego, 9500 Gilman Drive, La Jolla, CA 92093-0623, USA
e-mail: jwest@ucsd.edu



A. N. Makanya (ed.), *The Vertebrate Blood-Gas Barrier in Health and Disease,*
DOI 10.1007/978-3-319-18392-3_7

them and the alveolar gas. For example, the French physician Policard (1929) stated "La surface respiratoire est assimilable à une plaie à vif" (the respiratory surface is like the flesh of an open wound). The other school argued that there was an epithelium, although it could not be clearly imaged. In fact, Kölliker (1881) asserted that much of the epithelial surface consisted of "nonnucleated plates" ("kernlose Platten"), because he could not find nuclei. We now realize that this misconception arose because the cytoplasm of the type I alveolar epithelial cells spreads over a very wide area, and so it would be easy to conclude that some of the cells had no nuclei at all. For a fuller discussion of these early ideas, see Weibel (1996).

However, everything changed when Low (1953) published the first electron micrograph of the blood–gas barrier in the human lung in 1953 (Fig. 7.1).

This immediately resolved many of the arguments that had been so heated. Although the micrograph does not have the resolution of modern images such as Fig. 7.2, the important features of the blood–gas barrier are clearly seen. In the lower left there is a red blood cell (RBC), then the lumen of the capillary (CAP), and then the capillary endothelial cell labeled 2. The next layer labeled 3 is only partly seen. In the region where the arrow of the label is placed, the structure is clearly visible but further to the left in the region labeled 4, this layer has apparently disappeared. However, later electron micrographs with better resolution such as Fig. 7.2 showed that this extracellular matrix is a continuous structure.

Figure 7.1 also clearly shows the alveolar epithelial layer labeled 1. This is contiguous with the large nucleus of the type I alveolar epithelial cell with its prominent

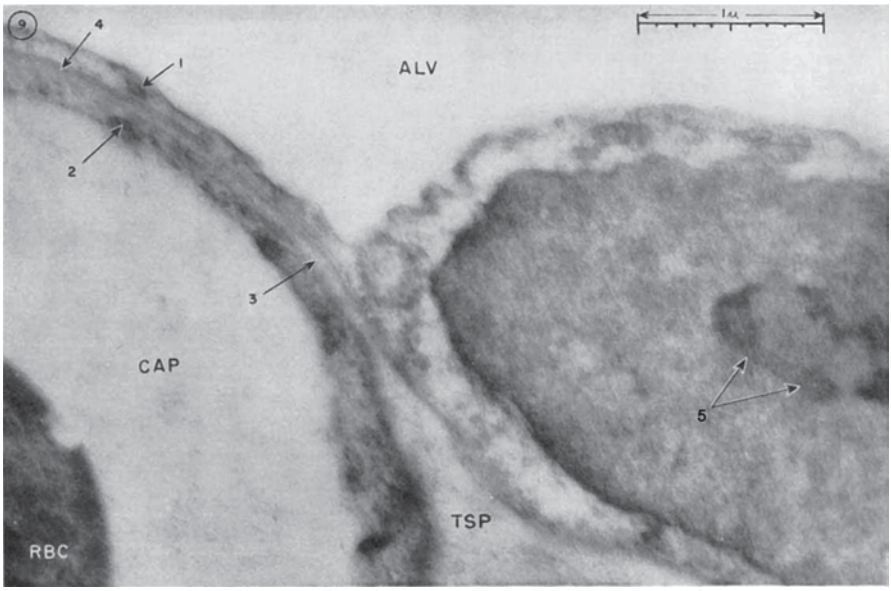


**Fig. 7.1** First published electron micrograph of the blood–gas barrier in the human lung. Note that the total thickness is about 0.3 μm. See text for details. *ALV* alveolar gas space, *CAP* capillary lumen, *RBC* red blood cell, *TSP* tissue space. (From Low 1953)

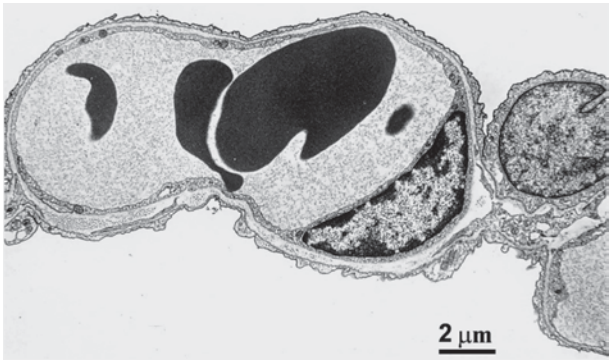


**Fig. 7.2** Modern electron micrograph of a pulmonary capillary showing excellent resolution. Note that the appearances on the *right* are similar to those in Fig. 7.1. (From Weibel 1973)

nucleolus labeled 5. Above this is the alveolar gas space (ALV), and finally there is the calibrating scale with a total length of 1 µm. Note that in comparison with the depicted scale, the total thickness of the blood–gas barrier is about 0.3 µm. Below the nucleus, the extracellular matrix widens to show part of the interstitium labeled (TSP for tissue space).

This iconic micrograph has revolutionized the thinking about the ultrastructure of the blood–gas barrier. It would be satisfying to state that Low's discovery was greeted with acclamation and that he received numerous accolades as a result. Unfortunately, this does not appear to be the case for reasons that are not clear.

A splendid example of a modern electron micrograph is shown in Fig. 7.2. Note the similarity of the right-hand part of the image to the appearances shown in Fig. 7.1. The transition from the nucleus of the type I alveolar epithelial cell to its cytoplasmic extension is clearly seen in both images. However, Fig. 7.2 also shows that the layer of extracellular matrix that Low thought disappeared at one stage is now clearly seen around the whole of the capillary. Figure 7.2 also nicely shows that the structure of the blood–gas barrier is "polarized" in the sense that it is typically very thin on one side of the capillary and much thicker on the other. In fact, on the lower thick side we can see fibrils of type I collagen on the left, and also the prolongations of a fibroblast on the right below the nucleus. The thin part of the blood–gas barrier is the most important region for pulmonary gas exchange which occurs by passive diffusion, while the thick part of the barrier has an important mechanical function and is also important for fluid exchange. It is believed that there is a small but constant loss of fluid from the lumen of the capillary into the interstitium under normal resting conditions and that this rapidly increases when the capillary pressure is raised as in exercise (Staub 1970).

Part of the reason for the "polarization" of the blood–gas barrier is due to the mechanical support required to maintain the integrity of the alveolar wall. In the mammalian lung, the pulmonary capillaries are strung out along the alveolar wall much like a string of beads. The capillaries therefore receive little support at right angles to the wall and some is provided by the long cable composed of type I collagen that snakes its way along the alveolar wall moving from one side of the capillary to the other as shown in Fig. 7.3. In addition, the alveolar wall itself presumably requires

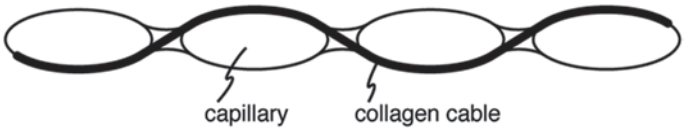


**Fig. 7.3** Diagram showing how the type I collagen cable snakes its way along the alveolar wall moving from the one side to another of the capillaries. This cable is apparently important in the mechanical support of the capillaries and the whole alveolar wall. (From West 2009; modified from West et al. 2007)

a network of collagen fibers to maintain its strength. The collagen cable seen in Fig. 7.3 is an inevitable consequence of the relatively large alveoli in the mammalian lung with the consequently extensive alveolar walls.

As discussed later, the situation is different in the avian parabronchi where gas exchange occurs in the bird lung. Here, the pulmonary capillaries are embedded within a honeycomb-like structure of air capillaries that give support to the pulmonary capillaries through a series of epithelial bridges. The happy result of this additional support is that the blood–gas barrier in the avian lung is uniform in thickness and does not show the polarization that occurs in the mammalian lung. An added advantage of the different means of support of the pulmonary capillaries is that the blood–gas barrier can also be generally thinner in the bird than in the mammal with obvious advantages for diffusive gas exchange (Maina and West 2005).

## 7.3 The Structural Dilemma of the Blood–Gas Barrier

Figures 7.1 and 7.2 clearly show the extreme thinness of the blood–gas barrier and this exists over much of its area. Of course the reason for this is that the transfer of gases across the barrier occurs by passive diffusion. Fick's law states that the volume of gas per unit time diffusing across a tissue sheet is proportional to the area of the sheet, inversely proportional to its thickness, proportional to a constant D, and proportional to the partial pressure difference between the two sides. In symbols:

$$V_{gas} = \frac{A}{T} D(P_1 - P_2).$$

The area of the blood–gas barrier in the human lung is very large being about 50–100 $m^2$ (Weibel 1963). This prodigious area is brought about by having some 500 million alveoli each with many capillaries in the alveolar walls. In fact, the alveolar wall is essentially composed of a network of capillaries. In addition, as already stated, the thickness of the blood–gas barrier over much of its area is only about 0.3 μm. This means that the dimensions are extremely well suited for gas exchange by passive diffusion.

However, this also means that the barrier is potentially vulnerable to mechanical failure because of its extreme thinness. In other words, the selection pressure for a very thin barrier is extremely strong because of the requirements for diffusion, but at the same time the integrity of the barrier must be preserved. The blood–gas barrier is the wall of the pulmonary capillary and if this is breached, the contents of the capillary will spill into the alveolar spaces with disastrous consequences for gas exchange. Thus, the blood–gas barrier has a dilemma in that it is not only necessary that it is extremely thin but also essential that it is very strong.

## 7.4 What Component of the Blood–Gas Barrier is Responsible for Its Strength?

Figure 7.4a and b show very high-power views of the barrier. Both the epithelial and endothelial layers are clearly seen, and between these is the extracellular matrix. However, the matrix is not uniform in appearance. In the center is an electron-

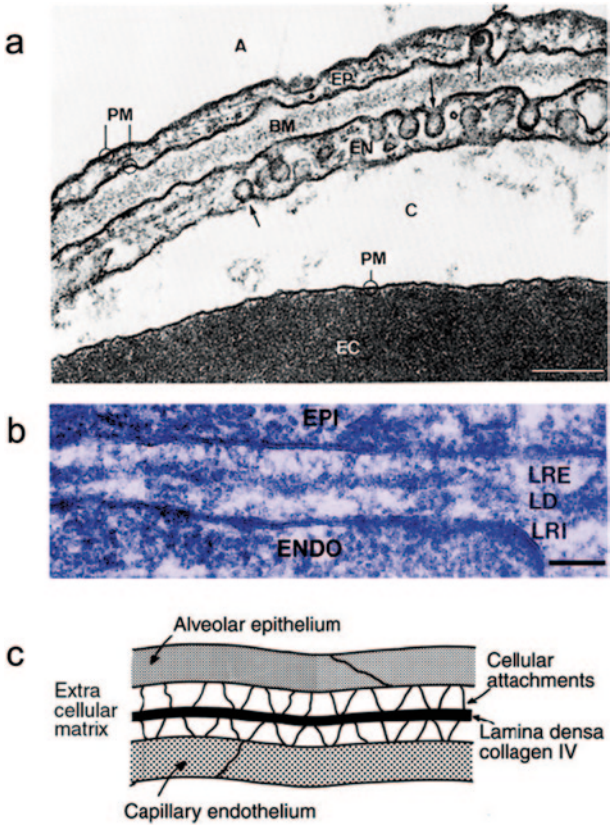


**Fig. 7.4** **a** High-power electron micrograph of the blood–gas barrier. Note that the extracellular matrix contains a band of electron-dense material which is believed to be type IV collagen. Calibration bar is 0.2 µm (from Weibel 1984). **b** Electron micrograph of part of the blood–gas barrier showing the electron-dense band called the LD in the center of the extracellular matrix. *EPI* epithelium, *ENDO* endothelium, *LRE* lamina rara externa, *LRI* lamina rara interna, *LD* lamina densa. Calibration bar is 0.1 µm. (from (Maina and West; modified from Vaccaro and Brody 1981). **c** Diagram of the thin side of the blood–gas barrier. (Modified from West and Mathieu-Costello 1992)

dense band that is believed to represent the type IV collagen, that is a key component of basement membranes. In fact, the extracellular matrix on the thin side of the blood–gas barrier is formed by the fusion of the basement membranes of the two cellular layers which is the reason why the dense band is seen in the middle. This appearance is well seen in Fig. 7.4b where the central electron-dense band is called the lamina densa (LD), and this is flanked on the epithelial side by the lamina rara externa (LRE) and on the endothelial side by the lamina rara interna (LRI). Evidence that this dense band is the site of the type IV collagen was provided by studies by Crouch et al. (1997) who used antihuman type IV collagen antibody and showed that the distribution of this was associated with the LD as seen by electron microscopy.

Basement membranes contain a variety of other molecules including laminin, entactin/nidogen, heparan sulfate proteoglycans, tenascin, and integrins. Some of these form the anchoring fibers that can be seen in Fig. 7.4c. However, type IV collagen appears to be the most important constituent for the strength of the blood–gas barrier.

Type IV collagen is an interesting molecule. It is composed of three peptide chains, two alpha 1 (IV) with one alpha 2 (IV), and these form a triple helix (Fig. 7.5a). Figure 7.5b shows that each molecule is about 400 nm long. At one end, there is a large COOH-terminal globular domain (NC1) and at the other end there is a distinctive collagenous $NH_2$-terminal (7S) that promotes cross-linking. Two of the type IV collagen molecules link at the COOH terminus to give a doublet 800 nm long. Then four molecules link at the $NH_2$ terminus to give a chicken-wire type of structure as shown in Fig. 7.5b and c.

Because the layer of type IV collagen shown in Fig. 7.4a and b is only about 50 nm thick while the doublet shown in Fig. 7.5b is 800 nm-long. It is clear that the sheets shown in Fig. 7.5c must lie parallel to the CAP. Presumably, several sheets lie on top of each other like sheets of chicken wire. Since a collagen IV molecule is only about 1.5 nm thick, there would be space for some 30 sheets like those shown in Fig. 7.5c to be accommodated in the 50 nm available.

A feature of human type IV collagen is that it has regions that apparently allow bending of the molecule (Takami et al. 1994). This may mean that the matrix shown in Fig. 7.5b and c can lengthen under tension just as a chicken wire does. This could explain the appearances in Fig. 7.6a and b, where the extracellular matrix remains intact but the epithelial or endothelial layers or both disrupt and separate.

There is strong though indirect evidence that the strength of the blood–gas barrier can be attributed to the extracellular matrix, and in particular to the type IV collagen within this. First, as it is discussed below, animal experiments in which the barrier shows structural failure as a result of being exposed to high stresses frequently show that both the epithelial and endothelial layers break but the extracellular matrix remains intact. This observation suggests that the endothelial and epithelial cell layers themselves are not strong in tension. Additional evidence comes from studies of the mechanical properties of basement membrane in other structures. For example, Fisher and Wakely (1976) made measurements on the basement membrane of the lens capsule of cat and reported an ultimate tensile strength of

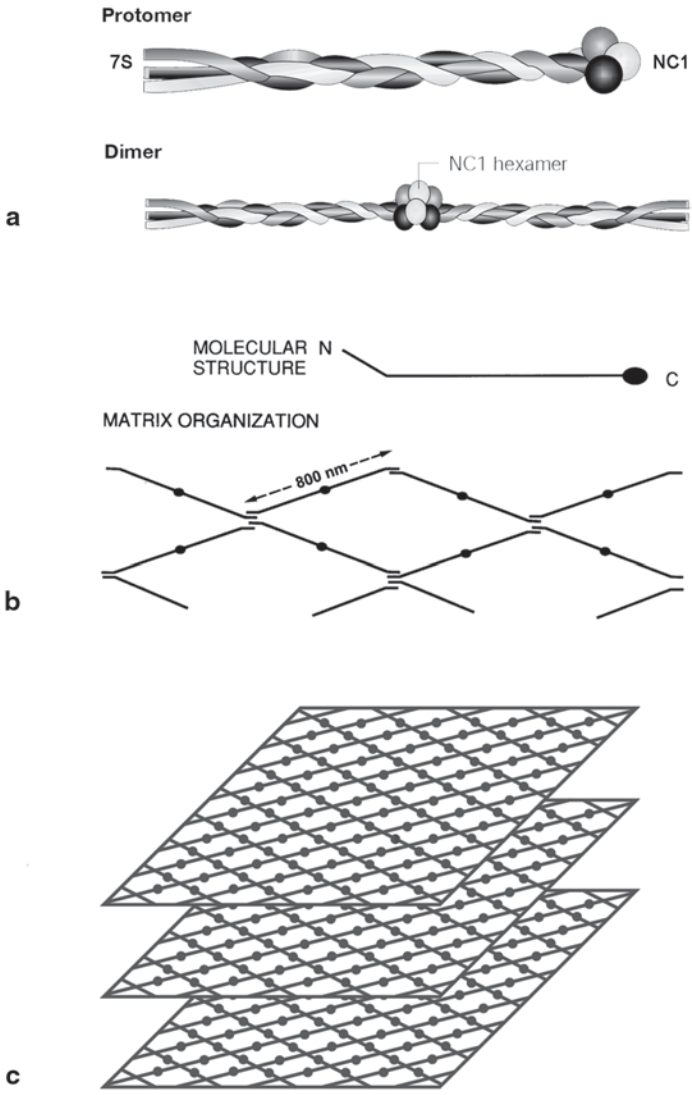


**Fig. 7.5** **a** shows a type IV collagen molecule with its three peptide chains, **b** shows how two molecules join at the NC-1 domain and four molecules join at the $NH_2$ terminal. **c** The matrix layers lie on top of each other in the middle of the extracellular matrix as shown in Fig. 7.4. (From West 2013)

$1.74 \pm 0.16 \times 10^6$ N · m$^{-2}$, a very high value. Interestingly, this value is comparable with that reported for cow ligamentum nuchae which is composed mainly of type I collagen, a material which is known to be very strong (Skalak and Chien 1987). Additional information on the ultimate tensile strength of basement membrane was provided by Welling and Grantham (1972) who measured the pressure–volume

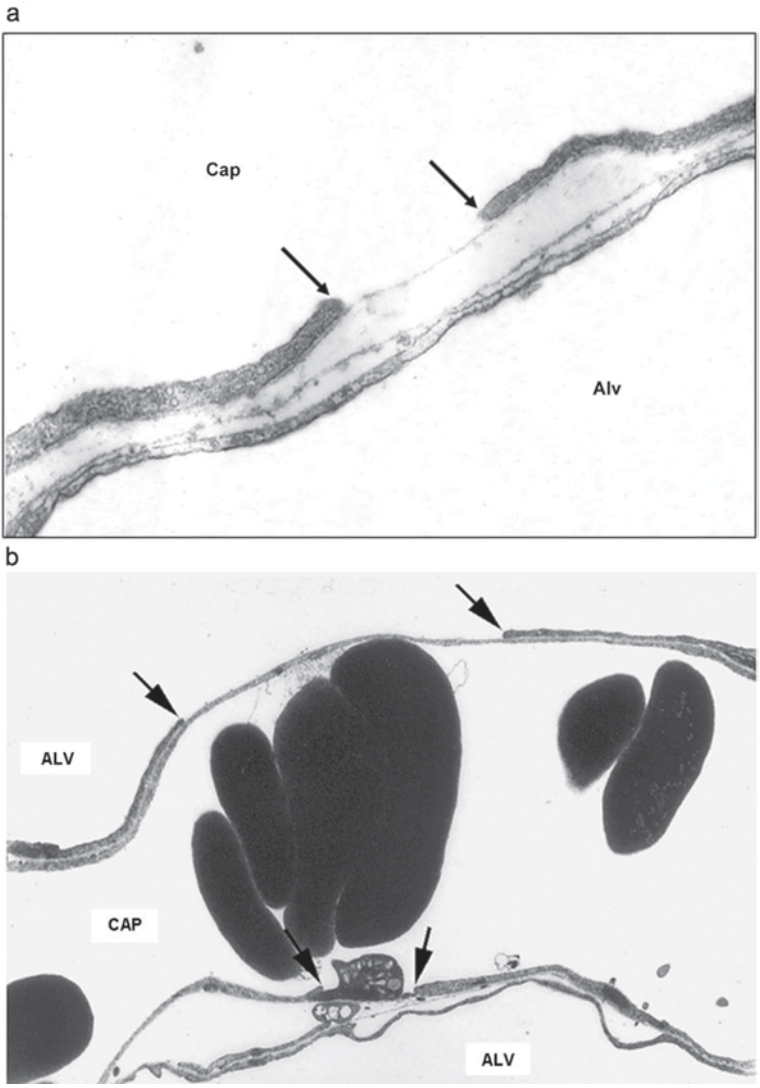


**Fig. 7.6** **a** shows disruption of the capillary endothelial layer while the alveolar epithelium and two basement membranes remain intact. **b** shows disruption of the alveolar epithelial layer at the top and the capillary endothelial layer at the bottom. A blood platelet is adhering to the exposed basement membrane. *ALV* alveolus, *CAP* capillary. (From West et al. 1991)

behavior of isolated rabbit renal tubules. Calculations from their data show that the ultimate tensile strength exceeded $5 \times 10^5$ N $m^{-2}$. Furthermore, in these studies where the tubules were composed of only a single epithelial layer and its basement membrane, it was shown that the mechanical behavior of the tubules in tension was the same whether the epithelial layer was present or not, strongly supporting the conclusion that the strength of the tubules came from the basement membrane. In

another study, Swayne et al. (1989) showed that the degree of distention of capillaries in frog mesentery could be explained by the elastic properties of basement membrane.

## 7.5 What Stress Is Required to Produce Failure of the Blood–Gas Barrier?

The simplest way to increase the stress in the blood–gas barrier of pulmonary capillaries is to raise the transmural pressure. Several years ago, we carried out experiments on anesthetized rabbits to study this. The chest was opened, cannulas were inserted into the pulmonary artery and left atrium, and the lung was perfused with the rabbit's own blood at known capillary transmural pressures. After a short time, the blood was washed out with a saline/dextran mixture and the lungs were fixed for electron microscopy with buffered glutaraldehyde, this perfusion being made at the same pressures. The composition of the perfusates and fixatives were based on the work of Bachofen et al. (1982) who showed that these procedures accurately preserved the ultrastructure of the lung. Perfusions were carried out using pulmonary artery pressures of 20, 40, 60, and 80 cm $H_2O$ with the pulmonary venous pressure kept at 5 cm $H_2O$ below the arterial pressure. Because the difference between arterial and venous pressures was only 5 cm $H_2O$, this allowed the capillary pressure to be estimated within 2.5 cm $H_2O$. The alveolar pressure was kept constant at 5 cm $H_2O$ thus allowing the capillary transmural pressure to be calculated.

Typical ultrastructural appearances from those experiments are shown in Fig. 7.6a and b. In Fig. 7.6a, we can see a disruption of the capillary endothelial layer while the alveolar epithelium and the two basement membranes remain intact. In Fig. 7.6b, there is a disruption of the alveolar epithelium near the top of the image, while near the bottom the capillary endothelium shows a break with the ends indicated by arrows. A blood platelet is adhering to the exposed basement membrane below. In these preparations, the first indications of failure were seen at a capillary transmural pressure of 24 mmHg. However, the number of breaks was much increased at a transmural pressure of 39 mmHg, and the frequency was even greater at a pressure of 53 mmHg.

It is interesting to calculate the tensile stress in the layer of type IV collagen shown in Fig. 7.4 in this rabbit preparation although admittedly the calculations can only be approximate. The hoop stress S is given by the Laplace relationship: $S = P \cdot r/t$, where P is the transmural pressure, r is the radius of curvature, and t is the thickness of the load-bearing structure. For a transmural pressure of 39 mmHg, radius of curvature of 3.5 μm (Birks et al. 1994), and thickness of the type IV collagen layer of 50 nm, the calculated stress is about $3 \times 10^5\ N \cdot m^{-2}$. This is of the same order of magnitude as the ultimate tensile stress of collagen IV as discussed earlier. This means that the assumptions that the stress is borne by the type IV collagen, and that its layer is about 50 nm thick, seem reasonable based on the experimental results although as indicated, the calculations are approximate.

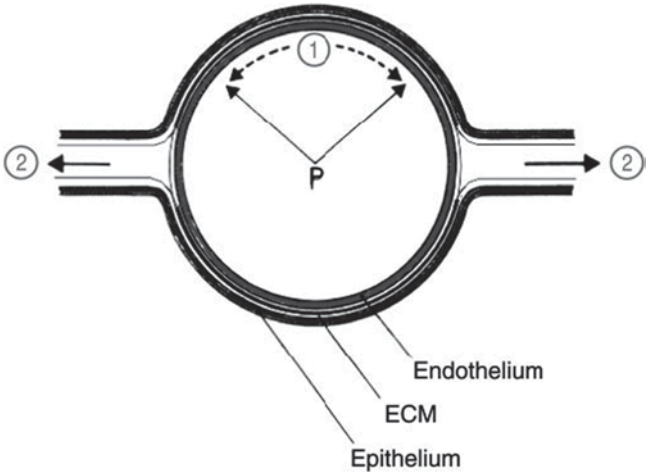


**Fig. 7.7** Diagram showing two mechanisms that can increase the stress in the blood–gas barrier. Mechanism *1* shows how the hoop or circumferential stress is raised by increasing the capillary transmural pressure according to the Laplace relationship. In *2*, the increased linear tension in the alveolar wall caused by lung inflation is transmitted to the capillary wall. *P* is the capillary hydrostatic pressure. (Modified from West et al. 1991)

Up to now, we have discussed raising the stress in the blood–gas barrier by increasing the transmural pressure of the capillaries. However, Fig. 7.7 shows that there is an additional way of increasing the stress in the barrier that is by increasing the volume of the lung.

This maneuver increases the tension in the alveolar walls and some of this tension is transmitted to the capillary walls. In this context, we can think of the alveolar wall as basically made up of a string of capillaries as shown in Fig. 7.3. Evidence that the stress in the capillary wall is increased at high lung volumes is that if the diameter of the capillaries orthogonal to the alveolar wall is measured, this is markedly reduced at high lung volumes even if the transmural pressure of the capillaries remains constant (Glazier et al. 1969). Consistent with this, we have shown that the frequency of stress failure of the blood–gas barrier is greatly increased at high lung volumes for a given capillary transmural pressure (Fu et al. 1992). This finding is important in the clinical setting when patients are treated with high levels of positive end-expiratory pressure in the intensive care unit. If the lung volume is greatly increased, damage to the capillaries occurs.

A remarkable feature of the cellular disruptions is that many of these are rapidly reversible when the capillary transmural pressure is reduced. For example, in experiments where the pressure was first raised to a high level sufficient to damage the capillaries, and then the pressure was reduced to a low level and the lung was fixed for microscopy, it was found that about 70 % of both the endothelial and epithelial disruptions had closed within a few minutes (Elliot et al. 1992). A possible mechanism for this behavior would be elastic deformation of the extracellular matrix as was referred to earlier because of the presence of bending sites in the type IV collagen molecule. In other words, at high capillary pressures the extracellular

matrix stretches resulting in disruption of the cellular layers, but when the pressure is reduced, the matrix resumes its original length and the breaks close.

## 7.6 Stress Failure of the Blood–Gas Barrier Under Physiological Conditions

As discussed earlier, there is strong selective pressure to make the blood–gas barrier as thin as possible to allow sufficient gas exchange to occur by passive diffusion under demanding conditions such as heavy exercise. On the other hand, thinning the barrier means that it becomes increasingly fragile and disruption of the barrier may occur. This could be very deleterious because it allows the contents of the pulmonary capillaries to spill into the alveolar spaces and thus impair pulmonary gas exchange. It is therefore not surprising that failure of the barrier is only seen under exceptional conditions in the normal lung. This conforms to the usual evolutionary pattern that the strength of a part of the body, for example, a bone or joint, is sufficient to withstand almost all the normal stresses that are encountered, but under exceptional conditions, failure may occur.

There is evidence that in the human lung, both the strength and the thinness (i.e., diffusion properties) of the blood–gas barrier are inadequate to cope with the exceptional conditions associated with the high levels of exercise. First consider the strength. In a study of elite cyclists who sprinted uphill at maximal effort for several minutes, there was evidence of damage to the blood–gas barrier. In this experiment, the mean heart rate was 177 beats $\cdot$ min$^{-1}$ indicating a very high aerobic activity. The subjects underwent bronchoalveolar lavage (BAL) shortly after the exercise, and it was found that the BAL fluid had higher concentrations of red cells, total protein, albumin, and leukotriene B4 than control subjects (Hopkins et al. 1997). The controls were sedentary volunteers who did not exercise. Leukotriene B4 was measured because elevated levels of this were found in the BAL fluid of patients with high altitude pulmonary edema which is another condition where the blood–gas barrier fails (see later). The results of this study of extreme exercise strongly support the hypothesis that abnormal changes occur in the blood–gas barrier under these exceptional conditions.

In order to determine whether the very high level of exercise was the culprit, another study was carried out on a similar group of six elite cyclists who exercised for 1 h at a submaximal level (77% of their maximal oxygen consumption) and subsequently underwent BAL. Again the controls were eight normal nonathletes who did not exercise before BAL. In contrast to the results found following maximal exercise, the concentrations of RBCs, total protein, and leukotriene B4 in the BAL fluid of the exercising cyclists were no different from those of the control group (Hopkins et al. 1998). Therefore, it was concluded that the integrity of the blood–gas barrier was only altered at the extreme levels of exercise consistent with the evolutionary considerations mentioned above. These studies are also consistent with a number of reports in the literature of lung bleeding in human athletes during very high levels of exercise including swimmers and runners (McKechnie et al. 1979; Weiler-Ravell et al. 1995).

The above studies show that the human pulmonary blood–gas barrier is so thin that it is damaged under exceptional physiological conditions. The question then arises as to why the barrier is so thin. The answer is that during some challenging physiological states, for example, high levels of exercise, there is good evidence that the diffusion properties of the lung limit pulmonary gas exchange which is crucial in conditions of severe exercise. Specifically, the $P_{O2}$ in the pulmonary capillary blood does not reach that of alveolar gas with the result that there is arterial hypoxemia. Evidence for this comes from the studies of Wagner et al. (1986) when normal subjects were studied at increasing levels of exercise at sea level. The degree of ventilation–perfusion ratio inequality was measured so that its role in the arterial hypoxemia could be determined. It was then found that when the oxygen consumption exceeded 2.7 $L \cdot min^{-1}$, there was clear evidence that part of the hypoxemia was caused by inadequate diffusion of oxygen across the blood–gas barrier. In another study (Wagner et al. 1987), at simulated high altitudes in a low pressure chamber, depression of the arterial $P_{O2}$ caused by diffusion limitation was seen at an oxygen consumption of less than 1 $L \cdot min^{-1}$ at altitudes of 7620 and 8840 m. The fact that diffusion limitation was seen at much lower levels of exercise at high altitude compared with the sea level is consistent with the fact that lowering the alveolar $P_{O2}$ challenges the diffusion process. This is a well-known way of causing diffusion-limited hypoxemia.

Elite human athletes are capable of very high levels of exercise but for even higher levels we need to go to other animals. The best example is the Thoroughbred racehorse that has been bred for racing over several hundred years. Remarkably there is strong evidence that all Thoroughbreds in training break their pulmonary capillaries.

There are reports dating back to the seventeenth century that some racehorses bleed through their nose after galloping. Various causes have been suggested for this including moldy hay, but in the 1980s it was found by bronchoscopy that some 70% of horses had frank blood in their airways after a race (Pascoe et al. 1981). Shortly after this, it was discovered that all Thoroughbred racehorses in training had hemosiderin-laden macrophages in their lungs (Whitwell and Greet 1984). The inevitable conclusion was that they all developed pulmonary hemorrhage.

To clarify the cause of the bleeding, pulmonary vascular pressures were measured while the horses were galloping on a treadmill (Erickson et al. 1992; Jones et al. 1992). Incidentally, some animal activists objected to this but the horses do everything they can to get the treadmill started because they love to run. Extraordinarily high pressures in the pulmonary circulation were measured. In one study, a catheter placed in the left atrium showed a mean pressure as high as 70 mmHg during galloping, while the mean pulmonary artery pressure was as high as 120 mmHg. The mean right atrial pressure was 40 mmHg. Pressures on the systemic side of the circulation were also very high with a mean arterial pressure up to 240 mmHg. (Jones et al. 1992; Erickson et al. 1992).

What is the mechanism for these amazingly high pressures? Thoroughbreds run very fast and they have been shown to have maximal oxygen consumptions of up to 180 $ml \cdot min^{-1}\ kg^{-1}$ and cardiac outputs as high as 750 $ml \cdot min^{-1} \cdot kg^{-1}$. This means that the filling pressures of the left ventricle are extremely high, and this apparently

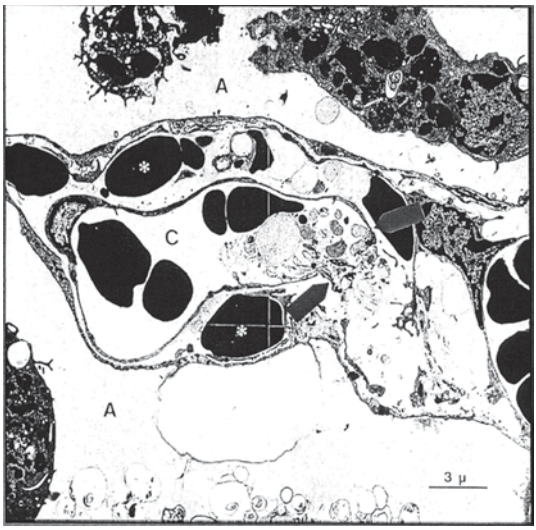


**Fig. 7.8** Electron micrograph showing a large break in a pulmonary capillary of a Thoroughbred horse lung. The animal galloped on a treadmill and shortly after this the horse was euthanized and the lung was fixed for microscopy. The *large arrows* show the site of the break. (From West et al. 1993)

accounts for the very high left atrial, pulmonary venous, and pulmonary capillary pressures. If the left atrial pressure is 70 mmHg and the pulmonary arterial pressure is 120 mmHg, the capillary pressure must be in the region of 100 mmHg. It is not surprising that the capillaries break under these conditions and indeed, it would be astonishing if they did not. We were able to examine the lungs of Thoroughbreds after they had been galloping on a treadmill and were able to see frank breaks in the blood–gas barrier (West et al. 1993). An example is shown in Fig. 7.8.

It is known that horses that repeatedly bleed develop pathological changes in their lungs, predominantly fibrosis. This is believed to impair their racing performance.

Do other fast-running animals bleed into their lungs? In general, the answer is not known because the appropriate measurements have not been made. It would be of great interest to have these, in the pronghorn antelope and cheetah, for example. There is some evidence that racing greyhounds bleed into their lungs (Poole and Erickson 2011).

## 7.7 Stress Failure Under Pathological Conditions

There are many pathological conditions that cause stress failure of the blood–gas barrier. They can be divided into three main causes: abnormally high capillary pressure, increased capillary wall stress caused by lung overinflation, and diseases in which the mechanical properties of the barrier are impaired.

An interesting condition where stress failure of the blood–gas barrier occurs as a result of an increased pulmonary capillary pressure is high altitude pulmonary edema (HAPE). This is seen from time to time in climbers, trekkers, and skiers at high altitude and can be life threatening. The pathogenesis was a mystery until

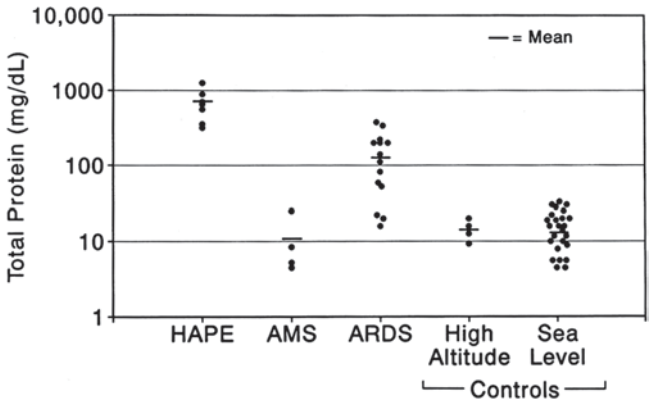


**Fig. 7.9** Total protein concentrations in the bronchoalveolar lavage fluid. Note that the concentrations in *HAPE* are even higher than in *ARDS* where substantial leakage of proteins through the pulmonary capillary walls is known to occur. *HAPE* high altitude pulmonary edema, *AMS* acute mountain sickness, *ARDS* adult respiratory distress syndrome. (From Schoene et al. 2001)

the 1980s. Initially, it was thought to be some form of left ventricular failure but this was ruled out when catheterization studies showed that the pulmonary arterial wedge pressure was normal. However, it was then gradually realized that there was a strong link between HAPE and pulmonary hypertension. People who developed the disease tended to have high pulmonary artery pressures, and furthermore, people who were susceptible to HAPE had an increased hypoxic pulmonary vasoconstriction response.

A critical advance was made when enterprising investigators set up a laboratory at high altitude on Mt. McKinley (Denali) and they studied climbers who were descending but had developed HAPE (Hackett et al. 1986; Schoene et al. 1986). Remarkably, the investigators were able to perform BAL on the climbers and the results showed that the edema fluid had a high concentration of cells and very high protein concentrations (Fig. 7.9). The inevitable conclusion was that some of the capillaries were being damaged, presumably because they were being exposed to a high blood pressure.

However, this was something of a mystery because hypoxic pulmonary vasoconstriction is believed to occur in the small arteries upstream of the capillaries. In this case, the capillaries would be protected from the high pulmonary artery pressure. But it had been suggested some years ago that the hypoxic vasoconstriction may be uneven (Hultgren 1969) and if this were true it would mean that some of the capillaries were not protected and would be exposed to a high pressure. Surprisingly, no one had raised the pressure in pulmonary capillaries in animal preparations and used electron microscopy to examine the ultrastructure of their walls. When this was done, as described earlier, clear breaks were seen in the capillary endothelium, alveolar epithelium, and in some cases the extracellular matrix as well (West et al. 1991; Tsukimoto et al. 1991). These ultrastructural changes provided a ready explanation for the increase in red cells and high-molecular weight proteins in the

BAL fluid. Subsequent studies of the pathogenesis of HAPE are consistent with this explanation.

There are other diseases in which the pulmonary capillary pressure rises to abnormally high levels and stress failure occurs resulting in bleeding into the alveolar spaces. An interesting disease from a historical point of view is mitral stenosis. In this condition, the mitral valve gradually narrows causing obstruction to flow. The result is increase in the pressures in the pulmonary veins and capillaries. This disease was common in the 1950s and articles at that time reported that hemoptysis was frequent and also that the lungs at autopsy showed marked hemosiderosis (Wood 1954a and b). This was correctly attributed to "multiple recurrent hemorrhages" but no one suspected that the capillaries were responsible. Instead, the site of the bleeding was attributed to the bronchopulmonary anastomoses in the terminal bronchioles. Since the extreme thinness of the blood–gas barrier had been described by Low in 1953 (Low 1953), it is difficult to understand why the capillaries received no attention. For some reason the fragility of the blood–gas barrier was a blind spot.

Similar changes occur in the pulmonary capillaries in left ventricular failure caused, for example, by myocardial infarction. It is now established that with small increases in capillary pressure, the pulmonary edema fluid is a transudate with a low protein concentration as explained by an imbalance of the Starling forces. However, with the higher pulmonary capillary pressures, the edema fluid has a large concentration of high-molecular weight proteins and is therefore of the high-permeability type implying damage to the capillary wall (Sprung et al. 1981).

As indicated in Fig. 7.7, an additional mechanism causing increased stress in the blood–gas barrier apart from raising the capillary transmural pressure is inflating the lung to an abnormally high volume. Here, the increased tension in the alveolar walls is partially transmitted to the walls of the capillaries because the alveolar wall is basically made up of a string of capillaries. The commonest clinical situation where stress failure occurs as a result of this mechanism is the use of high levels of positive end-expiratory pressure (PEEP) in the intensive care unit. A frequent problem is that patients with very severe lung disease have marked arterial hypoxemia and in an attempt to correct this, not only is the inspired oxygen concentration raised but high levels of PEEP also are employed. The hope is that this will open up atelectatic areas that are responsible for a shunt. However, inevitably some areas of the diseased lung are then overinflated. Unfortunately, the pathological changes in the lungs of patients with acute respiratory failure are so complicated that it is not possible to directly demonstrate stress failure of the capillaries.

However, in animal experiments where it is possible to keep the capillary transmural pressure constant but raise lung volume to abnormally high levels, increased disruptions of the alveolar epithelium and capillary endothelium in the capillaries can be documented (Fu et al. 1992). Other studies in rats have also shown that hyperinflation of the lung damages pulmonary capillaries (Dreyfuss et al. 1985). The recognition that high levels of PEEP can be damaging has led to a change in clinical practice and the recommendation of lower PEEP levels (Brower et al. 2000).

Another clinical situation where stress failure of the blood–gas barrier may occur is the infant respiratory distress syndrome. This is often accompanied by bleeding

into the alveolar spaces. In this condition, there is a deficiency of pulmonary surfactant, and it is possible that this increases the capillary transmural pressure. The mechanism is not an increased capillary pressure per se, or increased lung inflation. Instead, the increased surface tension in the alveolar lining layer because of the absence of surfactant reduces the pressure in the interstitial tissue around the capillaries. The result is an increase in capillary transmural pressure. This is a complicated mechanism but the abnormally high inward pull of the alveolar surface toward the center of the alveoli that exists on both sides of the alveolar wall effectively reduces the pressure outside the capillaries that lie in the wall. In fact, Pattle (1955) in his very early studies on pulmonary surfactant argued that its main purpose was to prevent pulmonary edema. However, the possible importance of this proposed mechanism for alveolar bleeding in the infant respiratory distress syndrome requires further study.

The last pathological cause of stress failure of the blood–gas barrier is diseases where the type IV collagen is abnormal. As indicated earlier, it is believed that the type IV collagen as shown in Figs. 7.4 and 7.5 is the principal component of the blood–gas barrier that is responsible for its strength. In Goodpasture's syndrome, an antibody attacks the NC1 globular domain of type IV collagen (Wieslander and Heinegard 1985). As a consequence, the strength of the blood–gas barrier is reduced and pulmonary hemorrhage is seen. A feature of this disease is that bleeding occurs both into the alveolar spaces of the lung and the glomerular spaces of the kidney. In fact, just as the type IV collagen layer in the capillary wall maintains its integrity, so does the type IV collagen in the basement membrane of the renal capillary wall prevent blood leaking into Bowman's capsule. Actually the situation for the kidney is more precarious because this organ is supplied by the systemic circulation, and the capillary transmural pressure of the glomerular capillaries is therefore, much higher than is the case for the pulmonary capillaries.

## 7.8 Remodeling of Pulmonary Capillaries

An important question is what regulates the thickness of the blood–gas barrier. As we have seen, it is normally extremely thin, but even so under some extreme physiological conditions the rate of diffusion of oxygen across it is not sufficient to prevent arterial hypoxemia. At the same time it is extraordinarily strong, but again under exceptional physiological situations mechanical failure can occur. It could be said that the structure of the barrier sits on a knife edge being just thin enough for adequate gas exchange and just strong enough to maintain its integrity. How is this balance obtained?

A reasonable explanation is that the structure of the barrier is regulated in response to the wall stress. In other words, some component of the capillary wall is sensing stress and then responding by regulating the amount of type IV collagen in the barrier. Some of the best evidence that this occurs is in patients with mitral stenosis where the capillary transmural pressure gradually rises over many weeks or months (Haworth et al. 1988). Figure 7.10 shows an electron micrograph of a

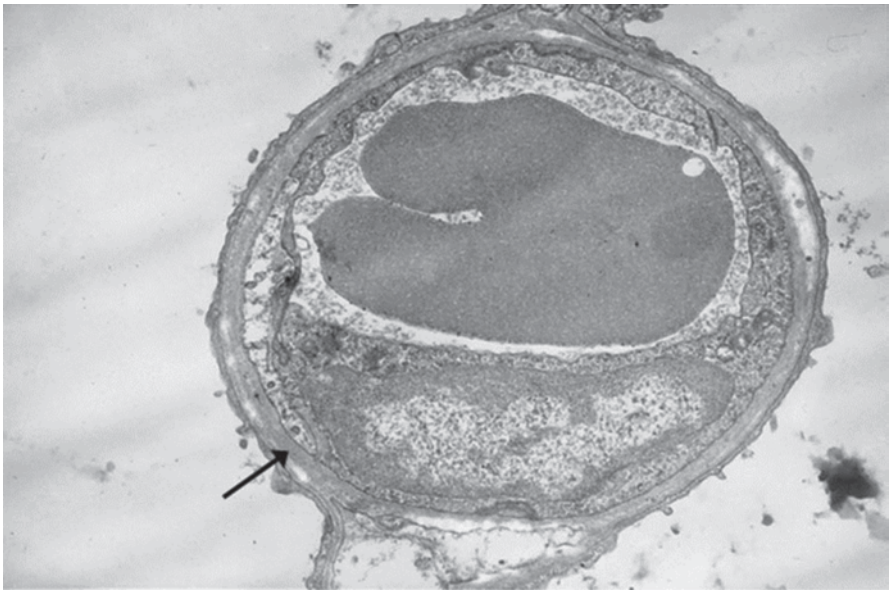

**Fig. 7.10** Electron micrograph of a pulmonary capillary from a young patient with mitral stenosis. There is obvious thickening of the extracellular matrix, and the *arrow* shows that the thickening is mainly associated with the basement membrane of the capillary endothelial. A scale bar is not available but the diameter of the capillary is about 10 μm. (Courtesy of Sheila Haworth; From West et al. 2003)

pulmonary capillary of a patient with severe mitral stenosis, and thickening of the extracellular matrix is clearly seen. As the arrow shows, the thickening seems to be mainly associated with the basement membrane of the capillary endothelial cell. Similar changes have been reported elsewhere (Asano 1964; Coalson et al. 1967; Kay and Edwards 1973).

There is an extensive literature on remodeling in larger pulmonary blood vessels associated with the pulmonary hypertension. A number of investigators have reported thickening of the vessel wall including both the smooth muscle and the interstitium in animals exposed to chronic hypoxia (Stenmark and Mecham 1997). A remarkable feature of this remodeling is how rapidly it can apparently occur. For example, Tozzi et al. (1989) studied explants of rings of rat pulmonary artery. They showed that when the rings were exposed to mechanical tension, increase in collagen and elastin synthesis began within 4 h. They also found that the changes depended on the presence of endothelium because the synthesis did not occur in the absence of this layer. This is interesting with respect to Fig. 7.10, where the increase in extracellular matrix appears to be associated with the endothelial cell rather than the epithelial cell as shown by the arrow.

A number of attempts have been made to identify the molecular factors that respond to increased stress in the capillary wall (Berg et al. 1997, 1998; Parker et al. 1997). Increased gene expression for alpha 1 (III) and alpha 2 (IV) procollagens, fibronectin, basic fibroblast growth factor, and transforming growth factor beta 1

have been identified. However, the situation is complicated and no clear picture has yet emerged. Part of the problem is that it is technically difficult to raise the wall stress of the capillaries without doing the same to the larger blood vessels in the lung. Whereas a great deal of research has been devoted to remodeling of larger pulmonary blood vessels, it is remarkable how little attention has been given to the capillaries.

## 7.9 Comparative Physiology of the Blood–Gas Barrier

So far we have been discussing the ultrastructure and function of the blood–gas barrier in humans and other mammals. As we have seen, the barrier is a tripartite structure consisting of the capillary endothelium, extracellular matrix, and alveolar epithelium. A fascinating feature is how this tripartite structure has been conserved over an extremely long period of time. Evolution apparently fixed on this structure very early after the transition of vertebrates to land and the adoption of air breathing, and the ultrastructure has changed little over the ensuing 400 million years or so. Figure 7.11 shows micrographs of the blood–gas barrier in the African lungfish *Protopterus aethiopicus*, an amphibian, the tree frog *Chiromantis petersii*, and a reptile, the black mamba snake *Dendroaspsis polylepsis*. The blood–gas barrier of the bird lung also shows the same ultrastructure as discussed below (Fig. 7.12).

Note that all three electron micrographs in Fig. 7.11 show the same basic structure with a capillary endothelial layer, extracellular matrix, and alveolar epithelial layer. The electron-dense layer of type IV collagen in the center of the extracellular matrix is particularly well seen in all three micrographs. Perhaps, it is not surprising that the tripartite pattern occurs in all examples since all blood vessels need an endothelium, and the gas-exchanging organ is exposed to the atmosphere and therefore needs an epithelium. However, the similarity of the ultrastructure along 400 million years or so of vertebrate evolution is striking indeed.

When we turn to the blood–gas barrier of the bird lung, an example of which is shown in Fig. 7.12, we are in for a surprise. When we compare this image which is from the domestic chicken *Gallus gallus domesticus* with Fig. 7.2 which is from the dog, we see striking differences. First the blood–gas barrier is clearly thinner in the bird than the mammal. Next, the dog has the typical "polarized" barrier in the sense that one side of the capillary wall is much thinner than the other, whereas this is not so in the chicken. Clearly, both these differences are advantageous for gas exchange in the bird. A thinner barrier is preferable for diffusive gas exchange, and in the mammalian example of Fig. 7.2, the bottom section of the barrier is so thick that its role in gas exchange must be small.

How is it that evolution has provided the bird with a better gas exchanger than the mammal? The answer lies in the very different anatomy of the bird lung compared with that of the mammals. In mammals, ventilation is reciprocating in that air is moved in and out of the alveolar regions during cyclical breathing. Typically, the tidal volume is small in relation to the volume of gas in the alveoli, and inspired gas

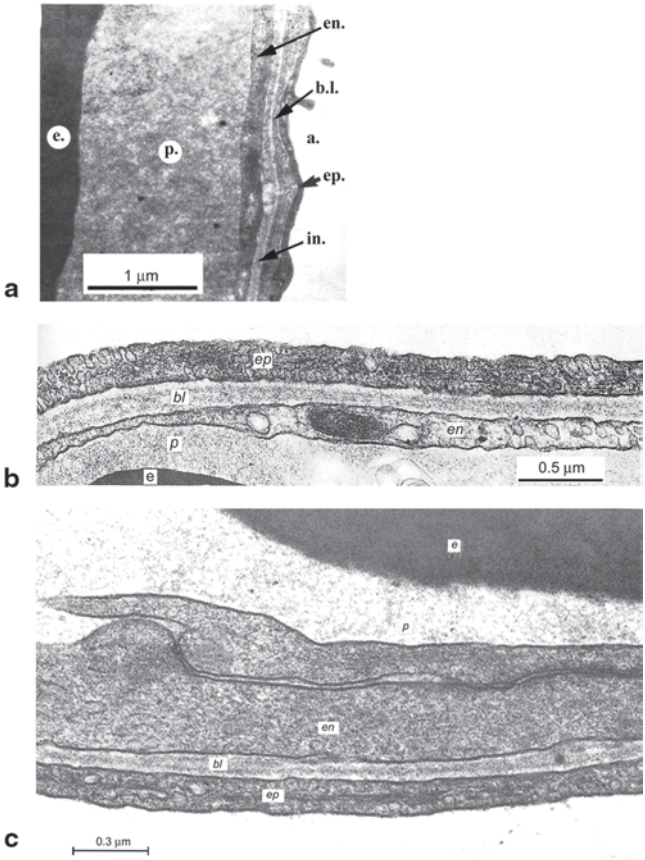


**Fig. 7.11** Electron micrographs showing the ultrastructure of the blood–gas barrier in three vertebrates. **a** is the African lungfish *Protopterus aethiopicus,* **b** is from the amphibian, the tree frog *Chiromantis petersii*. **c** is from a reptile, the black mamba snake *Dendroaspsis polylepsis*. All three images show striking similarities in the ultrastructure of the blood–gas barrier. See text for details. (From West 2003)

must reach the most distal parts of the lung by a complicated process of convection and diffusion. This necessitates having peripheral airways including alveoli with relatively large cross sections so that the final diffusion process can come to completion. The end result is that the alveoli in the mammalian lung are relatively large. For example, in humans the diameter of the alveoli is about 0.3 mm. A necessary result of this is that the capillaries are strung out along the extensive alveolar wall like a string of beads. As discussed earlier, this also means that there needs to be a collagen cable supporting the capillaries and adding strength to the alveolar wall as shown in Fig. 7.3. Obviously, this thickens one side of the capillary which interferes with the gas exchange.

The situation in the bird lung is very different. First, the bird has separated the ventilatory and gas exchange functions Ventilation is brought about by expansion

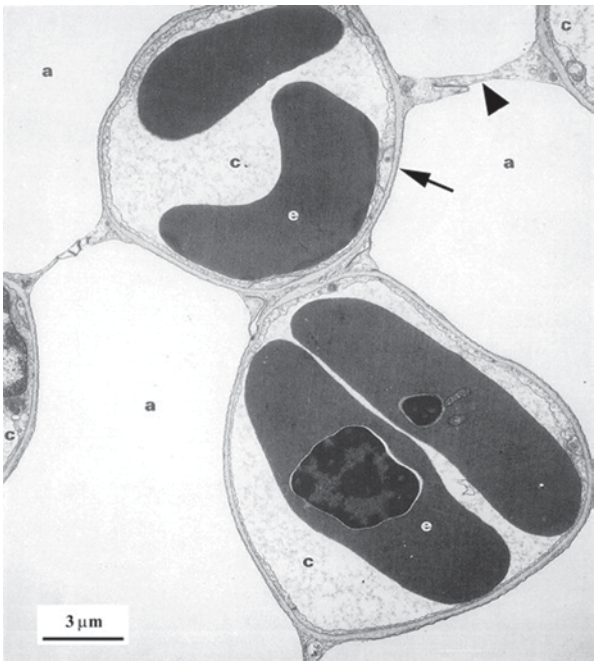


**Fig. 7.12** Electron micrographs from the lung of a domestic chicken *Gallus gallus* variant *domesticus* showing the blood–gas barrier. Note that this is very thin and uniform in thickness around the whole of the capillary. Epithelial bridges which are part of the air capillaries support the blood capillaries. ***a*** air capillary, ***c*** blood capillary, ***e*** erythrocyte. (From West 2003; modified from Maina 2002)

of nonvascular air sacs, and gas exchange is carried out in the parabronchi which consist of air capillaries adjacent to the blood capillaries. Air flow through the air capillaries is continuous by convection and this means that these structures can have a very small diameter of the order of 10–20 µm. This is some 20–30 times smaller than the diameter of human alveoli. In addition as Fig. 7.12 shows, the blood capillaries in the bird are supported by epithelial bridges that make up the walls of the air capillaries. This support means that the capillaries in the avian lung have no need of the collagen cable seen in the mammalian lung. The result is a much more efficient organ for gas exchange in the bird.

One feature of the avian lung that is still poorly understood is how it copes with fluid movement out of the pulmonary capillaries. As discussed earlier, the thick side of the blood–gas barrier in the mammalian lung shown in Fig. 7.2 not only accommodates the collagen cable but also allows the movement of fluid out of the CAP. This is seen in early pulmonary edema where the thick side of the blood–gas barrier widens whereas the thin side does not change its dimensions (Fishman 1972). Since the avian lung does not have a thick side of the blood–gas barrier it is not clear how it handles the movement of fluid out of the CAP. We know that there is swelling of the epithelial bridges (Weidner and Kinnison 2002) but how the fluid gets to them from the lumen of the capillary is not clear.

An unexpected feature of the avian lung is that the pulmonary capillaries behave like almost rigid tubes. Experiments show that when the diameters of the capillaries in chicken lungs are measured as the capillary transmural pressure is raised over a large range, little increase in diameter is seen. For example, in the chicken, the

diameter of the pulmonary capillaries increased by only 13 % when the pressure inside them was raised from 0 to 25 cm $H_2O$ (Watson et al. 2008). By contrast studies on the mean width of the pulmonary capillaries in dogs show that these increased by about 125 % for the same pressure change, and in the cat the figure was 128 %. In addition, raising the pressure by 35 cm $H_2O$ outside the capillaries of the chicken lung caused little change in diameter. This is in great contrast to the behavior of mammalian capillaries where under the same pressure conditions the capillaries are completely collapsed (Glazier et al. 1969).

The reason for this difference in behavior is apparently the support that the avian pulmonary capillaries receive from the epithelial bridges shown in Fig. 7.12. These increase the rigidity of the capillaries both when the pressure inside them is increased or the pressure outside them is raised. This unexpected behavior raises the question of what happens to the pulmonary artery pressure in avian lungs when the cardiac output increases greatly as, for example, during exercise. In mammals, there is only a modest increase in pulmonary artery pressure because of recruitment and distension of the capillaries. Since these changes in the capillaries do not occur in the avian lung it seems likely that the pulmonary artery pressure will rise substantially under the same conditions but no measurements are available as yet.

Very little is known about the strength of the blood–gas barrier in birds. However, Maina and Jimoh (2013) have lavaged the lungs of resting and exercising chickens and shown increase in the concentrations of RBCs and lactate in the lavage fluid as a result of exercise. Both the number of red cells and the lactate levels steadily increased when the birds were exercised on a treadmill and the belt speed was increased. It is interesting that even resting chickens showed about $3 \times 10^5$ red cells per cubic centimeter of lavage fluid. These unexpected results will presumably be clarified with further work.

In conclusion the pulmonary blood–gas barrier is fascinating from an evolutionary point of view because it has been so faithfully conserved since vertebrates graduated from water to air breathing. To quote the immortal Darwin “There is grandeur in this view of life, with its several powers, having been originally breathed into a few forms or into one; and that, while this planet has gone cycling on according to the fixed law of gravity, from so simple a beginning endless forms most beautiful and most wonderful have been, and are being, evolved” (Darwin 1859). But it could be argued that the features of the blood–gas barrier are constrained by simple laws of physics and chemistry. It must be extraordinarily thin to allow diffusion of gases on the one hand, and on the other, it must be immensely strong because of mechanical forces. While the organisms themselves have evolved into “endless forms most beautiful,” the blood–gas barrier has remained almost unchanged.

## References

Asano H. Pathohistological and electron-microscopical studies of the lung in mitral stenosis with special reference to the correlation between morphological changes and cardiopulmonary dynamics. Jap Circul J. 1964;28(10):801–16.

Bachofen H, Ammann A, Wangensteen D, Weibel ER. Perfusion fixation of lungs for structure-function analysis: credits and limitations. J Appl Physiol Respir Environ Exerc Physiol. 1982;53(2):528–33.

Berg JT, Fu Z, Breen EC, Tran HC, Mathieu-Costello O, West JB. High lung inflation increases MRNA levels of ECM components and growth factors in lung parenchyma. J Appl Physiol. 1997;83(1):120–8.

Berg JT, Breen EC, Fu Z, Mathieu-Costello O, West JB. Alveolar hypoxia increases gene expression of extracellular matrix proteins and platelet-derived growth factor-b in lung parenchyma. Am J Respir Crit Care Med. 1998;158(6):1920–8.

Birks EK, Mathieu-Costello O, Fu Z, Tyler WS, West JB. Comparative aspects of the strength of pulmonary capillaries in rabbit, dog, and horse. Respir Physiol. 1994;97(2):235–46.

Brower RG, Matthay MA, Morris A, Schoenfeld D, Thompson BT, Wheeler A. Ventilation with lower tidal volumes as compared with traditional tidal volumes for acute lung injury and the acute respiratory distress syndrome. N Engl J Med. 2000;342(18):1301–8.

Coalson JJ, Jaques WE, Campbell GS, Thompson WM. Ultrastructure of the alveolar-capillary membrane in congenital and acquired heart disease. Arch Pathol. 1967;83(4):377–91.

Crouch EC, Martin GR, Jerome BS, Laurie GW. Basement membranes. In: Crystal RG, West JB, Weibel ER, Barnes PJ, editors. The lung: Scientific foundations. Vol. 1. Philadelphia: Lippincott-Raven; 1997. p. 769–91.

Darwin C. On the origin of species by means of natural selection. London: J. Murray; 1859.

Dreyfuss D, Basset G, Soler P, Saumon G. Intermittent positive-pressure hyperventilation with high inflation pressures produces pulmonary microvascular injury in rats. Am Rev Respir Dis. 1985;132(4):880–4.

Elliott AR, Fu Z, Tsukimoto K, Prediletto R, Mathieu-Costello O, West JB. Short-term reversibility of ultrastructural changes in pulmonary capillaries caused by stress failure. J Appl Physiol. 1992;73(3):1150–8.

Erickson BK, Erickson HH, Coffman JR. Pulmonary artery and aortic pressure changes during high intensity treadmill exercise in the horse: effect of furosemide and phentolamine. Equine Vet J. 1992;24(3):215–9.

Fisher RF, Wakely J. The elastic constants and ultrastructural organization of a basement membrane (lens capsule). Proc R Soc Lond B Biol Sci. 1976;193(1113):335–58.

Fishman AP. Pulmonary edema the water-exchanging function of the lung. Circulation. 1972;46(2):390–408.

Fu Z, Costello ML, Tsukimoto K, Prediletto R, Elliott AR, Mathieu-Costello O, West JB. High lung volume increases stress failure in pulmonary capillaries. J Appl Physiol. 1992;73(1):123–33.

Glazier JB, Hughes JM, Maloney JE, West JB. Measurements of capillary dimensions and blood volume in rapidly frozen lungs. J Appl Physiol. 1969;26(1):65–76.

Hackett PH, Bertman J, Rodriguez G, Tenney J. Pulmonary edema fluid protein in high-altitude pulmonary edema. JAMA. 1986;256(1):36-.

Haworth SG, Hall SM, Panja M, Patel M. Peripheral pulmonary vascular and airway abnormalities in adolescents with rheumatic mitral stenosis. Int J Cardiol. 1988;18(3):405–16.

Hopkins SR, Schoene RB, Henderson WR, Spragg RG, Martin TR, West JB. Intense exercise impairs the integrity of the pulmonary blood–gas barrier in elite athletes. Am J Respir Crit Care Med. 1997;155(3):1090–4.

Hopkins SR, Schoene RB, Henderson WR, Spragg RG, West JB. Sustained submaximal exercise does not alter the integrity of the lung blood-gas barrier in elite athletes. J Appl Physiol. 1998;84(4):1185–9.

Hultgren HN. High altitude pulmonary edema. In: Hegnauer AH, editor. Biomedicine problems of high terrestrial altitude. New York: Springer; 1969. p. 131–41.

Jones JH, Smith BL, Birks EK, Pascoe JR, Hughes TR. Left atrial and pulmonary arterial pressures in exercising horses. FASEB J. 1992;6:A2020.

Kay JM, Edwards FR. Ultrastructure of the alveolar-capillary wall in mitral stenosis. J Pathol. 1973;111(4):239–45.

Kölliker A. Zur Kenntnis des Baues der Lunge des Menschen. Verb D Physik Med Gesellschaft Würzburg. 1881;16:1–24.

Low FN. The pulmonary alveolar epithelium of laboratory mammals and man. Anat Rec. 1953; 117(2):241–63.
Maina JN. Functional morphology of the vertebrate respiratory systems. Enfield: Science Publishers; 2002.
Maina JN, Jimoh SA. Structural failures of the blood-gas barrier and the epithelial-epithelial cell connections in the different vascular regions of the lung of the domestic fowl, gallus gallus variant domesticus, at rest and during exercise. Biol Open. 2013;2(3):267–76.
Maina JN, West JB. Thin and strong! The bioengineering dilemma in the structural and functional design of the blood-gas barrier. Physiol Rev. 2005;85(3):811–44.
McKechnie JK, Leary WP, Noakes TD, Kallmeyer JC, MacSearraigh ET, Olivier LR. Acute pulmonary oedema in two athletes during a 90-km running race. S Afr Med J. 1979;56(7):261–5.
Parker JC, Breen EC, West JB. High vascular and airway pressures increase interstitial protein mRNA expression in isolated rat lungs. J Appl Physiol. 1997;83(5):1697–705.
Pascoe JR, Ferraro GL, Cannon JH, Arthur RM, Wheat JD. Exercise-induced pulmonary hemorrhage in racing thoroughbreds: a preliminary study. Am J Vet Res. 1981;42(5):703–7.
Pattle RE. Properties, function and origin of the alveolar lining layer. Nature. 1955;175(4469):1125–6.
Policard A Les nouvelles idées sur la disposition de la surface respiratoire pulmonaire. Presse Méd. 1929;37:1293–5.
Poole DC, Erickson HH. Highly athletic terrestrial mammals: horses and dogs. Compr Physiol. 2011;1(1):1–37.
Schoene RB, Hackett PH, Henderson WR, Sage EH, Chow M, Roach RC, et al. High-altitude pulmonary edema. Characteristics of lung lavage fluid. JAMA. 1986;256(1):63–9.
Schoene RB, Swenson ER, Hultgren HN. High-altitude pulmonary edema. In: Hornbein TF, Schoene RB, editors. High altitude: an exploration of human adaptation. New York: Marcel Dekker; 2001.
Skalak R, Chien S. Handbook of bioengineering. New York: McGraw-Hill; 1987.
Sprung CL, Rackow EC, Fein IA, Jacob AI, Isikoff SK. The spectrum of pulmonary edema: differentiation of cardiogenic, intermediate, and noncardiogenic forms of pulmonary edema. Am Rev Respir Dis. 1981;124(6):718–22.
Staub NC. The pathophysiology of pulmonary edema. Human Pathol. 1970;1(3):419–32.
Stenmark KR, Mecham RP. Cellular and molecular mechanisms of pulmonary vascular remodeling. Annu Rev Physiol. 1997;59(1):89–144.
Swayne GT, Smaje LH, Bergel DH. Distensibility of single capillaries and venules in the rat and frog mesentery. Int J Microcirc Clin Exp. 1989;8(1):25–42.
Takami H, Burbelo PD, Fukuda K, Chang HS, Phillips SL, Yamada Y. Molecular organization and gene regulation of type IV collagen. Contrib Nephrol. 1994;107:36.
Tozzi CA, Poiani GJ, Harangozo AM, Boyd CD, Riley DJ. Pressure-induced connective tissue synthesis in pulmonary artery segments is dependent on intact endothelium. J Clin Invest. 1989;84(3):1005–12.
Tsukimoto K, Mathieu-Costello O, Prediletto R, Elliott AR, West JB. Ultrastructural appearances of pulmonary capillaries at high transmural pressures. J Appl Physiol. 1991;71(2):573–82.
Vaccaro CA, Brody JS. Structural features of alveolar wall basement membrane in the adult rat lung. J Cell Biol. 1981;91(2 Pt 1):427–37.
Wagner PD, Gale GE, Moon RE, Torre-Bueno JR, Stolp BW, Saltzman HA. Pulmonary gas exchange in humans exercising at sea level and simulated altitude. J Appl Physiol. 1986;61(1):260–70.
Wagner PD, Sutton JR, Reeves JT, Cymerman A, Groves BM, Malconian MK. Operation Everest II: pulmonary gas exchange during a simulated ascent of Mt. Everest. J Appl Physiol. 1987;63(6):2348–59.
Watson RR, Fu Z, West JB. Minimal distensibility of pulmonary capillaries in avian lungs compared with mammalian lungs. Respir Physiol Neurobiol. 2008;160(2):208–14.
Weibel ER. Morphometry of the human lung. Berlin: Springer; 1963.
Weibel ER. Morphological basis of alveolar-capillary gas exchange. Physiol Rev. 1973;53(2):419–95.
Weibel ER. The pathway for oxygen: structure and function in the mammalian respiratory system. Cambridge: Harvard University Press; 1984.

Weibel ER. The structural basis of lung function. In: West JB, editor. Respiratory physiology: people and ideas. Oxford: Oxford University Press; 1996.
Weidner WJ, Kinnison JR. Effect of hydrostatic pulmonary edema on the interparabronchial septum of the chicken lung. Poult Sci. 2002;81(10):1563–6.
Weiler-Ravell D, Shupak A, Goldenberg I, Halpern P, Shoshani O, Hirschhorn G, Margulis A. Pulmonary oedema and haemoptysis induced by strenuous swimming. BMJ. 1995;311(7001):361–2.
Welling LW, Grantham JJ. Physical properties of isolated perfused renal tubules and tubular basement membranes. J Clin Invest. 1972;51(5):1063–75.
West JB. Thoughts on the pulmonary blood-gas barrier. Am J Physiol Lung Cell Mol Physiol. 2003;285(3):L501–13.
West JB. Comparative physiology of the pulmonary blood-gas barrier: the unique avian solution. Am J Physiol Regul Integr Comp Physiol. 2009;297(6):R1625–34.
West JB. Fragility of pulmonary capillaries. J Appl Physiol. 2013;115(1):1–15.
West JB, Mathieu-Costello O. Strength of the pulmonary blood-gas barrier. Respir Physiol. 1992;88(1):141–8.
West JB, Tsukimoto K, Mathieu-Costello O, Prediletto R. Stress failure in pulmonary capillaries. J Appl Physiol. 1991;70(4):1731–42.
West JB, Mathieu-Costello O, Jones JH, Birks EK, Logemann RB, Pascoe JR, Tyler WS. Stress failure of pulmonary capillaries in racehorses with exercise-induced pulmonary hemorrhage. J Appl Physiol. 1993;75(3):1097–109.
West JB, Watson RR, Fu Z. The human lung: did evolution get it wrong? Eur Respir J. 2007; 29(1):11–7.
Whitwell KE, Greet TR. Collection and evaluation of tracheobronchial washes in the horse. Equine Vet J. 1984;16(6):499–508.
Wieslander J, Heinegård D. The involvement of type IV collagen in Goodpasture's syndrome. Ann NY Acad Sci. 1985;460(1):363–74.
Wood P. An appreciation of mitral stenosis—I. Br Med J. 1954a;1:1051–63.
Wood P. An appreciation of mitral stenosis—II. Br Med J. 1954b;1:1113–24.

# Chapter 8
# The Lung Endothelial Barrier in Acute Inflammation

**Holger C. Müller-Redetzky, Jasmin Lienau and Martin Witzenrath**

**Non-Standard Abbreviations**

| | |
|---|---|
| $[Ca^{2+}]_i$ | Intracellular calcium concentration |
| ALI | Acute lung injury |
| AM | Adrenomedullin |
| Ang | Angiopoietin |
| ARDS | Acute respiratory distress syndrome |
| COX | cyclooxygenase |
| DAMP | Danger-associated molecular pattern |
| eNOS | Endothelial nitric oxide synthase |
| HMGB1 | High mobility group box-1 |
| ICAM-1 | Intercellular adhesion molecule 1 |
| IL | Interleukin |
| iNOS | Inducible nitric oxide synthase |
| LPS | Lipopolysaccharide |
| MAPK | Mitogen-activated protein kinase |
| MLC | Myosin light chain |
| MLCK | Myosin light chain kinase |
| NF-κB | Nuclear factor-kappa B |
| PAF | Platelet activating factor |
| PAMP | Pathogen-associated molecular pattern |
| PMN | Polymorphonuclear leukocyte |

Author's note: This chapter is based on, and an update of our recent review (Muller-Redetzky et al. 2014a) with kind permission of the publisher.

M. Witzenrath (✉) · H. C. Müller-Redetzky · J. Lienau
Department of Infectious Diseases and Pulmonary Medicine, Charity University of Medicine Berlin, Charitéplatz 1, 10117 Berlin, Germany
e-mail: martin.witzenrath@charite.de

H. C. Müller-Redetzky
e-mail: Holger.Mueller-Redetzky@charite.de

J. Lienau
e-mail: Jasmin.Lienau@charite.de



A. N. Makanya (ed.), *The Vertebrate Blood-Gas Barrier in Health and Disease,*
DOI 10.1007/978-3-319-18392-3_8

| | |
|---|---|
| PRR | Pathogen recognition receptor |
| RNS | Reactive nitrogen species |
| ROS | Reactive oxygen species |
| S1P | Sphingosine-1-phosphate |
| S1P1−5 | S1P receptor 1–5 |
| S1PL | S1P lyase |
| SM | Sphingomyelin |
| Sph | Sphingosine |
| SphK | Sphingosine kinase |
| TLR | Toll-like receptor |
| TNFα | Tumour necrosis factor alpha |
| TRPC | Transient receptor potential canonical |
| TX | Thromboxane |
| TXR | Thromboxane receptor |
| VE-cadherin | Vascular endothelial cadherin |
| VEGF | Vascular endothelial growth factor |
| VILI | Ventilator-induced lung injury |

## 8.1 Introduction

Blood vessels are lined on their inner surface by a continuous layer of endothelial cells, closely connected by interendothelial junctions, thereby forming a semipermeable barrier between blood and interstitium. Transcellular transport mechanisms and paracellular extravasation of solutes and proteins is actively regulated by endothelial cells, thereby controlling tissue fluid homeostasis. Adherent junctions consisting of vascular endothelial (VE)-cadherin and catenin maintain the tight interendothelial connections (Predescu et al. 2007).

In the lungs, alveolar endo- and epithelial cells and their merged basal laminae form a less than 1 μm-thin membrane, which allows rapid and effective gas exchange between the alveolar and vascular compartment. Nevertheless, this extremely thin structure provides a barrier against inhaled particles and pathogens and importantly contributes to pulmonary metabolic and immunologic functions.

Pulmonary endothelial barrier function may be affected by infectious or sterile inflammatory stimulation via either the alveolar (e.g. in pneumonia, mechanical ventilation) or the vascular lumen (e.g. in bacteremia and sepsis). This may lead to increased permeability with protein-rich fluid extravasation, lung edema, and finally acute respiratory distress syndrome (ARDS; reviewed in Muller-Redetzky et al. 2014a; Fig. 8.1). Depending on severity, ARDS is associated with mortality rates ranging from 27 to 45 % (Ranieri et al. 2012).

Pneumonia is the most common infectious disease worldwide, and the third most common cause of death (World-Health-Organisation 2013). Further, pneumonia is the most frequent cause of sepsis, a systemic inflammatory response to infection

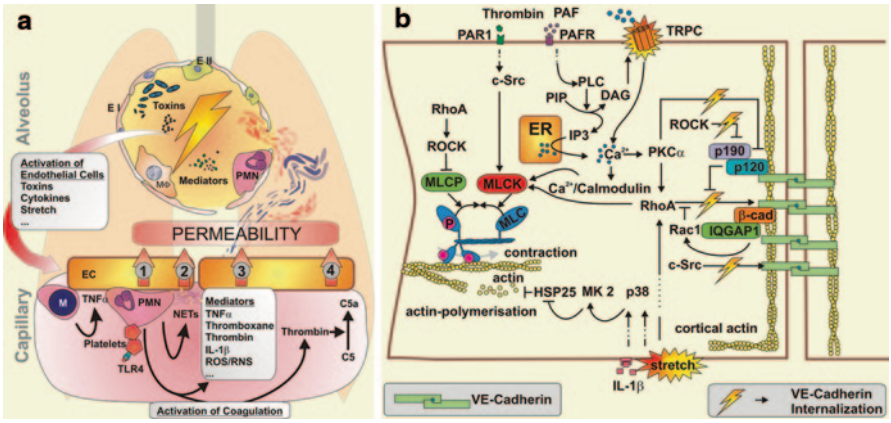


**Fig. 8.1** **a** Airspace-derived activation of the endothelium by mediators, bacterial toxins or physical stress due to mechanical ventilation starts a complex interplay of various inflammatory cascades resulting in vascular permeability. Monocytes (*M*) are recruited to the endothelium (*EC*) and facilitate its further activation by secretion of *TNFα*, thereby augmenting the recruitment of neutrophils (*PMN*). Activated platelets stimulate *PMN*. Endothelium-*PMN* contact leads to permeability (*1*). Upon stimulation *PMN* undergo netosis, liberating neutrophil extracellular traps (*NETs*) consisting of DNA and histones that cause endothelial toxicity and barrier breakdown (*2*). Specific soluble mediators also increase permeability (*3*). Neutrophil–platelet complexes activate blood coagulation. Central effector proteases like thrombin directly mediate vascular permeability. Further, *thrombin* activates complement factor *C5* to *C5a*—a permeability increasing anaphylatoxin (*4*). TNF tumour necrosis factor; *IL-1β* Interleukin-1β; *ROS/RNS* reactive oxygen and nitrogen species. **b** Intracellular signalling regulates endothelial permeability. Endothelial contraction results from actin myosin interaction after *MLC* phosphorylation, which is regulated by myosin light chain kinase (*MLCK*) and myosin light chain phosphatase (*MLCP*). *MLCP* is inhibited by *RhoA–ROCK* signalling while *MLCK* is activated by *c-Src*, *RhoA* and $Ca^{2+}$/*calmodulin*. $Ca^{2+}$ enters the cytosol from endoplasmatic reticulum (*ER*) or extracellular space. Downstream of platelet activating factor (*PAF*) and *PAF* receptor (*PAFR*), phospholipase C (*PLC*) hydrolyses posphatidyl inositol bisphosphate (*PIP*) into inositol 1,4,5-triphosphate (*IP3*) and diacylglycerol (*DAG*). *IP3* mediates $Ca^{2+}$ liberation from the *ER* while *DAG* opens transient receptor potential canonical (*TRPC*) channels in the cellular membrane. The resulting increase of intracellular $Ca^{2+}$ leads to the activation of protein kinase C (*PKC*) *α*, to further *RhoA* activation and to $Ca^{2+}$/calmodulin complexes, altogether finally leading to *MLCK* activation. Actin polymerization forms stress fibres associated with endothelial contraction. Various stimuli like *IL-1β* or mechanical force activate mitogen-activated protein kinase (*MAPK*) *p38* (*p38*), which activates *MAPK* activated protein kinase 2 *(MK2*), which phosphorylates heat shock protein 25 (*HSP25*) leading to actin polymerization. Adherence junctions (*AJ*) are mandatory for the sealing of intercellular contacts. *VE-cadherin* is anchored in peripheral cortical actin to the cytoskeleton. *VE-cadherin* phosphorylation leads to *VE-cadherin* internalization and thereby to increased endothelial permeability. *RhoA* and *c-Src* phosphorylate *VE-cadherin*. *Rac-1* and 190RhoAGAP (*p190*) functionally antagonize *RhoA* activity. p190RhoAGAP is recruited to the AJ by p120-catenin (*p120*), which itself inhibits *VE-cadherin* internalization. *ROCK* inhibits p190RhoAGAP and *PKCα* inactivates *p120*-catenin, thereby augmenting destabilization of *AJ*. *IQ* domain GTPase-activating protein 1 (*IQGAP1*) recruits and stabilizes *Rac-1*, protecting against *VE-cadherin* internalization. (reprinted from Müller-Redetzky et al., Cell Tissue Res (2014) 355:657–673 with kind permission of the publisher)

(Matthay et al. 2012). Both pneumonia and sepsis originate due to an innate immune reaction to invading pathogens. Host–pathogen interactions lead to complex inflammatory responses including secretion of inflammatory mediators, leukocyte recruitment and activation, as well as activation of complement and coagulation cascades that may contribute to pulmonary hyperpermeability and development of ARDS.

Mechanical ventilation is an essential component of the care of patients with ARDS, but it may also perpetuate the inflammatory response and further aggravate pulmonary endothelial barrier dysfunction (Verbrugge et al. 2007). Currently, there are no specific pharmacologic therapies improving endothelial barrier function in patients with pneumonia, sepsis and/or ARDS. However, recent experimental studies unraveled endothelial pathomechanisms, which contribute to the development of ARDS, thereby providing the basis for the development of novel therapeutic strategies (reviewed in Muller-Redetzky et al. 2014a). This chapter gives an overview on recent insights into the mechanisms of pulmonary endothelial barrier dysfunction in acute inflammation.

## 8.2 Pulmonary Endothelial Barrier Disruption

Pathogens that enter the alveolar compartment and liberated pathogenic factors are detected by pattern recognition receptors (PRRs). The recognition constitutes a crucial step of host defence during infection. PRRs include Toll-like receptors (TLRs), cytosolic NOD-like receptors (NLRs), RIG-I-like RNA receptors (RLRs), and DNA sensors (Opitz et al. 2010). PRRs sense evolutionarily conserved structures on pathogens called pathogen-associated molecular patterns (PAMPs), and specific endogenous molecules released after cell injury called danger-associated molecular patterns (DAMPs). In the alveolar compartment, PRRs are expressed in macrophages, epithelial and endothelial cells, dendritic cells and in recruited immune cells. PRRs play a key role in the inflammatory response to microbial infection and sterile tissue injury. PRR activation triggers production of inflammatory cytokines, interferons and chemokines on transcriptional and post-translational levels (Opitz et al. 2010), leading to the activation of local cells and recruitment of macrophages and neutrophils. At best, these inflammatory cascades will lead to pathogen clearance and finally survival. However, ongoing PAMP and DAMP release from dying bacteria and injured cells, respectively, may lead to an over-activation of the immune response. This over-activation results in uncontrolled production of cytokines, chemokines and lipid mediators, accumulation and activation of leukocytes, inappropriate activation of complement and coagulation cascades and eventually, endothelial barrier disruption.

In addition to host-dependent inflammatory mechanisms, pathogens may also directly induce endothelial injury resulting in pulmonary hyperpermeability. As one of many examples, the pneumococcal exotoxin pneumolysin may induce calcium influx as well as secretion of platelet activating factor (PAF) followed by thromboxane (TX) release (Witzenrath et al. 2007; Lucas et al. 2012). Both increased

intracellular calcium concentration ($[Ca^{2+}]_i$) and TX receptor (TXR) ligation lead to activation of myosin light chain kinase (MLCK) via protein kinase C (PKC) alpha- and Rho-kinase-dependent signalling (Hippenstiel et al. 1997; Witzenrath et al. 2007; Lucas et al. 2012). Phosphorylation of MLC induces actomyosin contractility leading to disruption of adherens junctions, interendothelial gap formation and paracellular permeability (Shen et al. 2010). Furthermore, pneumolysin belongs to the cholesterol-dependent cytolysins and is able to kill endothelial cells by forming pores in their cell membranes (Tilley et al. 2005).

## 8.3 Role of Neutrophils, Monocytes and Thrombocytes in Pulmonary Endothelial Barrier Disruption

Upon acute inflammation, neutrophils are the first cells to be recruited into the lungs (Grommes and Soehnlein 2011). In contrast to other vascular beds, in the lungs neutrophils transmigrate across the capillary endothelium. Stimulation of neutrophils with various inflammatory agents causes cytoskeletal rearrangements, thereby forming peripheral actin rims, leading to neutrophil stiffening and trapping in the capillary bed (Yoshida et al. 2006). Although the initial trapping is independent from cell surface expression of integrins and selectins, further neutrophil recruitment may depend on these cell adhesion molecules in distinct scenarios (reviewed in Grommes and Soehnlein 2011). Interestingly, adhesion of neutrophils to the endothelium and alveolar recruitment of neutrophils do not necessarily cause a significant change in vascular permeability (Martin et al. 1989; Rosengren et al. 1991). In human umbilical vein endothelial cells (HUVECs) or cremaster vessel preparations, it was shown that during the process of neutrophil transmigration the endothelium forms “transmigratory cups/endothelial domes” that completely encapsulate the emigrating neutrophils, thereby retaining barrier function (Carman and Springer 2004; Phillipson et al. 2008). Furthermore, ring-like structures of neutrophil leukocyte integrin lymphocyte function-associated antigen 1 (LFA-1) and endothelial intercellular adhesion molecule 1 (ICAM-1) were shown to be associated with neutrophil transmigration (Shaw et al. 2004).

However, under pathologic circumstances neutrophils contribute to vascular barrier dysfunction by secretion of soluble mediators causing endothelial contraction, neutrophil–endothelial adhesion-mediated mechanisms, generation of reactive oxygen species (ROS) and liberation of neutrophil extracellular traps (NETs).

One important soluble mediator secreted by neutrophils is tumour necrosis factor (TNF)α, which is known to induce vascular permeability. TNFα leads to MLCK and Rho kinase (ROCK)-dependent actin stress fibre generation in endothelial cells and induces p38 mitogen-activated protein kinase (MAPK)-dependent disarrangement of the microtubule system and thereby loss of intercellular VE-cadherin. However, only blocking microtubule breakdown strongly protected against barrier failure induced by TNFα, whereas inhibiting ROCK or MLCK did not increase transcellular resistance (Petrache et al. 2001). Other soluble mediators of neutrophils involved in endothelial barrier disruption include: (1) thromboxane A2 (TXA2), which is

processed from neutrophil-derived arachidonic acid by endothelial cyclooxygenase-2 (COX2) and binds to the TXR (Kim et al. 2010); (2) leukotriene A4 (LTA4), which is metabolized into LTC4 by endothelial LTC4 synthetase and binds to the endothelial cysteinyl LT receptor subtype 2 (CysLT2R); and (3) CXC chemokine ligands CXCL1, -2, -3 and -8 which bind to CXC chemokine receptor CXCR2 (reviewed in DiStasi and Ley 2009).

Endothelial contraction resulting in hyperpermeability is also caused by the interaction of neutrophils with the endothelium via LFA-1/macrophage receptor 1 (Mac-1) and ICAM-1. This neutrophil–endothelial interaction leads to rapid increase of endothelial $[Ca^{2+}]_i$, which mediates actin polymerization and cytoskeletal reorganization as well as phosphorylation of VE-cadherin causing junctional disruption. Further, neutrophil–endothelial contact and neutrophil activation by leukotriene B4 (LTB4) release lead to secretion of heparin-binding protein (HBP) which in turn increases endothelial permeability (for detailed review see DiStasi and Ley 2009).

Neutrophil-derived ROS may also induce barrier failure. ROS generation upon TNFα stimulation was shown to be mediated by class IA phosphoinositide 3 (PI3) kinase regulating CD11b/CD18 integrin-dependent neutrophil adhesion and NADPH oxidase activation and finally generation of ROS, causing vascular leakage (Gao et al. 2007).

Another defence mechanism of neutrophils is the formation of NETs, which constitute an extracellular fibrous web of DNA–histone complexes to which antimicrobial peptides and proteases like neutrophil elastase (NE) or myeloperoxidase (MPO) are attached in high concentrations (Brinkmann et al. 2004). NETs can trap and kill bacteria but on the other hand may also cause harm. NETs and particularly NET-bound histones possess high cellular cytotoxicity, leading to destabilization of endothelial and potentially epithelial barrier function (Saffarzadeh et al. 2012). In the lungs, this may result in high permeability lung edema. NET formation has been observed in lung injury induced by lipopolysaccharide (LPS), transfusion, influenza virus or *Klebsiella pneumoniae* (Papayannopoulos et al. 2010; Narasaraju et al. 2011; Caudrillier et al. 2012; Saffarzadeh et al. 2012). The induction of NET formation by neutrophils is highly accelerated by binding of activated thrombocytes to neutrophils and is involved in organ failure in septic mice (Clark et al. 2007). Accordingly, NET formation was ameliorated by antiplatelet therapy in transfusion-related lung injury (TRALI) (Caudrillier et al. 2012). To date, the significance of pulmonary NET formation in acute lung injury (ALI) has not been determined, but remains a field of interest as degradation of NETs by DNAse, neutralization of histone-mediated cytotoxicity by for example, polysialic acids, or reduction of netosis by targeting thrombocytes represent potential therapeutic approaches in humans. However, further preclinical evidence is needed to assess the significance and rationale of therapeutic NET targeting in ARDS.

Platelets directly and indirectly mediate vascular permeability. Upon activation, they secrete various factors, including TXA2, which was shown to increase endothelial permeability in vitro and in vivo through upregulation of interleukin (IL)-8 (Kim et al. 2010). Furthermore, in infection and inflammation they activate neutrophils, thereby indirectly contributing to barrier dysfunction (He et al. 2006; Zarbock

et al. 2006; Looney et al. 2009). The formation of permeability-mediating platelet–neutrophil complexes was shown to be associated with TXA2 formation (Zarbock et al. 2006). In contrast, vascular permeability was not increased by neutrophils solely attached to the endothelium after activation by TNFα (He et al. 2006). In a murine model of TRALI, pulmonary neutrophil sequestration was platelet-dependent, and platelet inhibition or depletion protected animals from development of lung injury (Looney et al. 2009). As outlined above, in TRALI activated platelets induce the formation of NETs (Caudrillier et al. 2012) that can trap and kill bacteria (Brinkmann et al. 2004), but may also contribute to lung endothelial permeability (Clark et al. 2007; Caudrillier et al. 2012; Saffarzadeh et al. 2012).

Among the heterogenous population of peripheral blood monocytes, the murine Gr-1$^{high}$/CCR2$^{+}$/CX$_3$CR1$^{low}$ monocyte subset is actively recruited to sites of inflammation (Geissmann et al. 2003). These inflammatory subset monocytes rapidly home in the pulmonary microcirculation upon LPS infusion or the onset of high-stretch mechanical ventilation and prime the lung for the development of pulmonary edema towards further stimuli like LPS, zymosan or ventilator-induced lung injury (VILI; O'Dea et al. 2009; Wilson et al. 2009). However, the mechanism by which marginated monocytes contribute to endothelial barrier dysfunction is not fully understood. O'Dea et al. demonstrated that lung-marginated monocytes express TNFα and directly activate pulmonary endothelial cells via TNF- and contact-dependent mechanisms (O'Dea et al. 2005). In addition, blood monocytes were shown to be involved in the regulation of neutrophil recruitment in ALI (Dhaliwal et al. 2012).

A lot of research effort is being made to unravel the mechanisms underlying leukocyte-mediated barrier disruption. However, therapeutic strategies based on depletion or blocking of cell recruitment to attenuate ALI should raise concerns as neutrophils and monocytes are central in the pulmonary and systemic innate immune responses, and therapeutic intervention at this level might induce functional immunosuppression.

## 8.4 Complement and Coagulation Systems and Vascular Permeability

The complement system consists of plasma and membrane-bound proteins and plays an important role in host defence and inflammation (Mastellos et al. 2003). There are three different complement activation pathways, that all converge at the central molecule C3 (Markiewski and Lambris 2007). The classical pathway is activated by antigen–antibody complexes binding to C1q, thereby activating C1s which then cleaves C4 and C2 to form the C3 convertase enzyme complex C4bC2a. In the lectin pathway, mannose binding lectins (MBL) associated with mannose-binding lectin proteases (MBLP) 1 and 2 bind to PAMPs on bacteria, thereby leading to the generation of the C3 convertase C4bC2a. The alternative pathway is triggered after contact with, for example, bacterial surfaces by spontaneous hydrolysis of C3 leading to generation of a conformationally altered C3 capable of binding factor B,

thereby forming the CbBb complex, the alternative C3 convertase. Both C3 convertases lead to cleavage of C3 to generate C3a and C3b. C3a is an anaphylatoxic peptide and C3b contributes to the assembly of the C5 convertase that processes C5 to the anaphylatoxin C5a and to C5b which is part of the membrane attack complex C5b-9. While C5b-9 causes cell lysis, C3a and C5a induce inflammatory responses and vascular permeability. In endothelial cells, both anaphylatoxins evoked stress fibre generation and thereby cell contraction, although with a different response kinetic. C3a stimulation led to a transient increase in stress fibre generation, while the response after exposure to C5a was delayed and prolonged (Schraufstatter et al. 2002). Notably, C3a and C5a activate different signal transduction cascades in endothelial cells. While C5a-induced permeability was dependent on activation of phosphatidylinositol-3 kinase, Src kinase and epidermal growth factor (EGF) receptor, C3a triggered signal transduction pathways controlled by ROCK (Schraufstatter et al. 2002).

In murine models of ALI and systemic inflammatory responses, silencing of C5a resulted in reduced permeability in multiple organs including the lungs (Liu et al. 2010). Interestingly, C3 deficiency in mice was not associated with attenuated immune complex-mediated lung injury and vascular permeability, while blocking of C5a was shown to be protective. These findings suggest a different complement activation pathway in the absence of C3 with thrombin acting as C5 convertase (Huber-Lang et al. 2006). This compensatory adaptive pathway was also demonstrated to be active in C3 knockout mice suffering from acute tracheal allograft rejection that showed aggravated microvascular injury, while C5a inhibition was protective (Khan et al. 2013).

Another system organized into proteolytic cascades and involved in tissue injury and inflammation is the coagulation system. Intrapulmonary fibrin deposition resulting from abnormal fibrin turnover is a characteristic feature of ALI and some components of the coagulation system may correlate with disease severity (Prabhakaran et al. 2003; Glas et al. 2013). Elevated fibrin turnover is caused by activation of the tissue factor VII pathway, increased plasminogen activator inhibitor 1 (PAI-1) levels and therefore decreased fibrinolytic activity and reduced antithrombin III levels (Prabhakaran et al. 2003; Hofstra et al. 2011). Further, decreased activity of the anticoagulant protein C contributes to intrapulmonary fibrin deposition. This decreased protein C activity is based on reduced protein C production as well as shedding of the cell surface protein thrombomodulin which is an important cofactor for the activation of protein C (Ware et al. 2003). Pulmonary coagulopathy is observed after severe pulmonary permeability edema with alveolar flooding, but it may also promote inflammation and vascular permeability and worsen ALI. The serine protease thrombin is the key enzyme in the coagulation cascade converting fibrinogen into fibrin. Protease activated receptor (PAR) ligation mediates proinflammatory effects of thrombin including release of cytokines and vascular endothelial growth factor (VEGF), which increases vascular permeability (Hippenstiel et al. 1998). Moreover, thrombin induces activation of endothelial MLCK and thereby cell contraction, and acts as C5 convertase generating the anaphylatoxic peptide C5a, which induces inflammatory responses and vascular permeability (Cirino et al. 1996; Huber-Lang et al. 2006; Liu et al. 2010; Glas et al. 2013; Khan et al. 2013).

## 8.5 Role of Toll-like Receptor 4 in the Regulation of Pulmonary Vascular Permeability

As outlined above, pattern recognition receptor signalling is involved in the development of barrier dysfunction. More specifically, and as an example, TLR4 signalling has been intensively studied regarding its impact on endo–epithelial barrier dysfunction. TLR4 is activated by both exogenous (e.g. LPS; Chow et al. 1999) and endogenous (e.g. high mobility group box-1 (HMGB1) protein, oxidized phospholipid) pro-inflammatory stimuli (Park et al. 2004; Imai et al. 2008). Several in vitro and in vivo studies demonstrated the permeability-enhancing effect of LPS (Mehta and Malik 2006). Further, elevated systemic LPS levels were associated with the severity of sepsis and related organ failure (Marshall et al. 2004). The critical role of TLR4 in regulating vascular permeability was convincingly demonstrated by the observation that mice lacking TLR4 were protected against lung injury due to various stimuli including LPS, oleic acid, cecal ligation and puncture and gut or lung ischemia/reperfusion injury (Imai et al. 2008; Zanotti et al. 2009; Hilberath et al. 2011; Ben et al. 2012; Tauseef et al. 2012).

TLR4-mediated signalling predominantly activates the nuclear factor-kappa B (NF-κB) pathway which induces inflammatory gene transcription (Chow et al. 1999). LPS binds to the TLR4/MD2 receptor complex and NF-κB activation is induced via myeloid differentiation factor 88 (MyD88), interleukin-1 receptor-associated kinase 1 (IRAK1), IRAK2 and IRAK4 (Medvedev et al. 2002; Kawagoe et al. 2008). Furthermore, intracellular diacylglycerol (DAG) levels were increased after recognition of LPS by TLR4, leading to direct activation of transient receptor potential canonical 6 (TRPC6) channels. The resultant TRPC6-mediated calcium influx into endothelial cells activated MLCK and thereby phosphorylation of MLC leading to cell contraction. Further, MLCK also promoted LPS-induced NF-κB-related inflammatory responses that contribute to lung vascular barrier dysfunction (Tauseef et al. 2012). Binding of LPS to TLR4 was also shown to activate the Src family kinases leading to phosphorylation of zonula adherens proteins and consequently disruption of endothelial barrier integrity (Gong et al. 2008).

Whereas the receptor for advanced glycation end products (RAGE) was suggested to be the main endothelial HMGB1 receptor for induction of endothelial permeability (Wolfson et al. 2011), signalling through TLR4 was also shown to play a role in HMGB1-induced inflammatory responses in monocytes which again were found to be MyD88-, IRAK1,2,4- and NF-κB-dependent (Park et al. 2004). Further, HMGB1 was suggested to contribute to the development of VILI (Ogawa et al. 2006).

Oxidized phospholipids as further endogenous stimuli contributed to pulmonary edema by inducing TLR4-mediated activation of TRIF (TIR domain-containing adapter-inducing interferon-β) and TNF receptor-associated factor 6 (TRAF6) leading to NF-κB-mediated IL-6 secretion (Imai et al. 2008).

Since TLR4 was shown to play a crucial role in regulating pulmonary endothelial permeability, targeting TLR4-mediated signalling seemed to be a promising therapeutic approach. In this context, the synthetic TLR4 antagonist eritoran was

developed that inhibits binding of LPS to MD2 and therefore suppresses TLR4/MD2-mediated signalling. Indeed, eritoran was shown to reduce pulmonary inflammation in different animal models (Mullarkey et al. 2003) as well as in healthy humans exposed to a bolus infusion of LPS (Lynn et al. 2003). In a phase II, placebo-controlled trial, patients with severe sepsis and high predicted risk of death that were treated with eritoran showed a trend towards lower mortality (Tidswell et al. 2010). However, in a recent phase III trial of patients with severe sepsis, administration of eritoran had no significant impact on mortality or relevant secondary outcome parameters (Opal et al. 2013), questioning the rationale for the therapeutic use of TLR4 antagonists in sepsis and related organ failure including ARDS. Since various DAMPs and PAMPs are recognized by many PRRs leading to NF-κB-mediated transcription of inflammatory genes, targeting downstream effectors in the inflammatory cascade may be more reasonable (Opal et al. 2013).

## 8.6 The Angiopoietin/Tie2 System

The angiopoietins (Ang-1 to Ang-4) are ligands for the receptor tyrosine kinase Tie2 which is abundantly expressed by endothelial cells, but also present in polymorphonuclear leukocytes (PMNs) and a subpopulation of monocytes (Wong et al. 2000; Lemieux et al. 2005). Ang-1 and Ang-2 are currently the best described angiopoietins and well-known regulators of angiogenesis, inflammation and vascular leakage (reviewed in David et al. 2013; Eklund and Saharinen 2013). Constitutive Ang-1 expression is found in different cell types including pericytes, vascular smooth muscle cells, fibroblasts, thrombocytes and megakaryocytes (Eklund and Saharinen 2013). Activation of Tie2 by Ang-1 leads to endothelial quiescence and stabilization of barrier function. In contrast, Ang-2 is primarily expressed by endothelial cells and stored in Weibel–Palade bodies (Fiedler et al. 2004), from where it can be rapidly released upon endothelial activation by inflammatory stimuli including TNFα and thrombin (Fiedler et al. 2004; Fiedler et al. 2006). Ang-2 acts as a functionally antagonistic ligand at the Tie2 receptor, thereby destabilizing the quiescent endothelium and promoting inflammation and vascular permeability (Scharpfenecker et al. 2005; Fiedler et al. 2006).

The expression of Ang-2 is transcriptionally upregulated by different factors including thrombin, hypoxia and VEGF (Oh et al. 1999; Huang et al. 2002). In a murine model of endotoxemia induced by LPS injection, functional inhibition of the Ang-1/Tie-2 pathway was observed with increased pulmonary expression and synthesis of Ang-2 (Mofarrahi et al. 2008). In patients with sepsis, Ang-2 serum levels were higher than in healthy volunteers and even more increased in patients with sepsis-associated ARDS (Parikh et al. 2006). Further, plasma Ang-2 levels were shown to have prognostic value for mortality in non-infection-related, but not in infection-related ALI (Calfee et al. 2012). In two different experimental models of sepsis, Ang-2 heterozygous mice with reduced Ang-2 levels were protected against lung injury suggesting that Ang-2 contributes to the pathogenesis of sepsis

besides predicting disease severity (David et al. 2012). This conclusion was further supported by a recent study in which Ang-2 inhibition by antibody treatment reduced microvascular alterations, hypotension and mortality in a murine model of LPS-induced systemic inflammation (Ziegler et al. 2013). In vitro studies showed that expression of endothelial adhesion molecules as well as PMN adhesion were increased by Ang-2 and inhibited by Ang-1 (Gamble et al. 2000; Fiedler et al. 2006). Ang-2 was also shown to induce recruitment of monocytes expressing Tie2 to sites of inflammation (Murdoch et al. 2007). Moreover, in experimental models of ALI, transgenic Ang-1 overexpression or treatment was associated with reduced pulmonary cytokine and adhesion molecule expression, PMN recruitment and endothelial permeability (Witzenbichler et al. 2005; Mammoto et al. 2007; McCarter et al. 2007; Xu et al. 2008). The protective anti-inflammatory Ang-1 effect seems to involve the direct interaction of Tie2 with the NF-κB inhibitor A20 binding inhibitor (ABIN)-2 (Hughes et al. 2003).

Ang-1 was also shown to directly improve endothelial integrity. Tie2 phosphorylation by Ang-1 reduces F-actin stress fibre formation and enhances endothelial barrier function via PI3 kinase leading to the activation of Rac1 and inhibition of RhoA, both linked by the p190 Rho GTPase-activating protein (p190 RhoGAP; Mammoto et al. 2007). The importance of this pathway was further demonstrated by the observation that downregulation of pulmonary p190 RhoGAP expression abolished the protective anti-permeability effect of Ang-1 (Mammoto et al. 2007). In addition, IQ domain GTPase-activating protein 1 (IQGAP1) was suggested to be required for Ang-1-mediated Rac1 activation, thereby contributing to the regulation of endothelial permeability (David et al. 2011b).

Further molecular mechanisms underlying the barrier-protective effect of Ang-1 include (i) impeding the interaction of the inositol triphosphate (IP3) receptor with TRPC1, thereby inhibiting the VEGF-induced, TRPC1-dependent $Ca^{2+}$ influx and reducing endothelial permeability (Jho et al. 2005); (ii) counteracting VEGF-induced Src activation and signalling thereby preventing phosphorylation and internalization of VE-cadherin and disassembly of interendothelial adherens junctions (Gavard et al. 2008); and (iii) activating sphingosine kinase 1 (SphK1) through the extracellular signal-regulated kinase (ERK) 1/2-dependent pathway thereby tightening endothelial cell junctions (Li et al. 2008).

Several studies confirmed the hypothesis that excess Ang-1 would effectively protect against vascular leakage in experimental sepsis and ALI (Witzenbichler et al. 2005; Mammoto et al. 2007; McCarter et al. 2007; Mei et al. 2007; Huang et al. 2008; David et al. 2011c). However, the methods of Ang-1 application such as gene therapy or cell-based delivery were far from proof of clinical efficacy. Recently, a short synthetic peptide (later termed vasculotide) was discovered that activates the Tie2 receptor, thereby completely inhibiting binding of both ligands Ang-1 and Ang-2 (Tournaire et al. 2004). Vasculotide was then proven to have therapeutic potential by preventing or counteracting vascular barrier disruption and reducing mortality in endotoxemia and established abdominal sepsis in mice (David et al. 2011a; Kumpers et al. 2011).

## 8.7 Sphingosine-1-Phosphate and other Biologically Active Sphingolipids

Sphingolipids form one class of membrane lipids, but are more than just structural components of biological membranes. Some sphingolipids including sphingomyelin (SM), ceramide, sphingosine (Sph) and sphingosine-1-phosphate (S1P) are biologically active and have been implicated in the regulation of diverse signalling pathways. The multiple roles of the four mentioned and other sphingoid bases in the pathophysiology of lung injury have been recently summarized in detail (Natarajan et al. 2013; Uhlig and Yang 2013).

Ceramide is synthesized from serine and palmitoyl coenzyme A (CoA) by multiple enzymatic reactions or derived from SM by sphingomyelinase (SMase). Through the action of ceramidases, ceramide is deacylated to Sph (Canals et al. 2011), which in turn may be phosphorylated to S1P by SphK-1 and -2. S1P is either dephosphorylated to Sph by S1P phosphatases 1 and 2 (S1PPase) or by lipid phosphate phosphatases (LPP), or irreversibly cleaved by S1P lyase (S1PL) to ethanol–amine phosphate and trans-2-hexadecenal.

The effects of ceramide and S1P are often contradictory. While S1P improves barrier integrity, ceramide increases paracellular permeability. Interestingly, the Gram-negative endotoxin LPS and the pneumococcal exotoxin pneumolysin induce microvascular leakage by a PAF-dependent mechanism (Witzenrath et al. 2007; Uhlig and Yang 2013), with PAF increasing endothelial permeability via acid SMase (aSMase)-dependent generation of ceramide (Goggel et al. 2004). Briefly, ceramide generated by aSMase leads to recruitment of caveolin-1, endothelial nitric oxide synthase (eNOS) and TRPC6 channels into caveolae. TRPC6 channels are usually blocked by nitric oxide (NO), but caveolin-1 inhibits NO synthesis by eNOS, leading to TRPC6 activation followed by increase of $[Ca^{2+}]_i$, MLCK activation, MLC phosphorylation, endothelial cell contraction and finally increase in vascular permeability (Uhlig and Yang 2013).

Various cell types are able to generate S1P including platelets, erythrocytes, hematopoietic and vascular endothelial cells (Yatomi et al. 1995; Tani et al. 2005; Hanel et al. 2007; Venkataraman et al. 2008). Coordinated activities of the biosynthetic and biodegradative enzymes maintain S1P concentrations in the ranges required for optimal physiological activities including regulation of cell proliferation, migration, differentiation, survival, morphogenesis and barrier function (Le Stunff et al. 2004; Natarajan et al. 2013). Camerer et al. suggested that basal plasma S1P levels maintain vascular integrity. Mutant mice engineered to selectively lack S1P in the plasma displayed increased vascular leak and enhanced susceptibility to PAF stimulation, which could be reversed by S1P transfusion (Camerer et al. 2009).

S1P acts as both an intracellular messenger (Le Stunff et al. 2004) and an extracellular ligand of five cell surface receptors ($S1P_{1-5}$) that are differentially expressed and coupled to various G proteins (Uhlig and Yang 2013). Vascular endothelial cells primarily express $S1P_1$, $S1P_2$ and $S1P_3$ (Hla et al. 2001). Physiologic plasma S1P concentrations (0.5–1 μM) maintain microvascular integrity via ligation of the $G_i$-coupled $S1P_1$ (Wang and Dudek 2009), and exogenously added

S1P to pulmonary endothelial cells increased monolayer integrity rapidly and dose-dependently through $S1P_1$ (Garcia et al. 2001). Ligation of endothelial $S1P_1$ induces activation of Rac GTPase, phosphorylation of MLC and cytoskeletal alterations, thereby mediating the barrier-protective effect of S1P (Garcia et al. 2001). In influenza pneumonia, endothelial $S1P_1$ was identified to be critically involved in the regulation of immune responses. $S1P_1$ receptor activation attenuated cytokine storm, suppressed immune cell recruitment and reduced mortality during murine infection with a human pathogenic strain of influenza virus (Teijaro et al. 2011) suggesting that under these circumstances endothelial cells are controlling the innate immune response (Iwasaki and Medzhitov 2011).

In addition to receptor-dependent extracellular S1P signalling, intracellular S1P protected endothelial barrier function, and mice deficient of SphK1 are much more susceptible to LPS-induced lung injury compared to wildtype (WT) controls (Wadgaonkar et al. 2009). Likewise, LPS increased expression of the S1P cleaving enzyme S1PL, thereby decreasing S1P levels in lung tissue. Inhibiting S1PL expression or activity reduced LPS-induced lung injury and inflammation in vitro and in vivo (Zhao et al. 2011). Moreover, in different murine and canine in vivo models of lung injury, including ischemia/reperfusion, pancreatitis and endotoxin challenge, S1P infusion was shown to reduce pulmonary vascular leakage and inflammation (McVerry et al. 2004; Peng et al. 2004; Okazaki et al. 2007; Liu et al. 2008). However, at supraphysiologic concentrations (>5 μM) S1P induces RhoA-dependent barrier disruption through binding to $S1P_2$ and $S1P_3$, which couple to $G_i$, $G_q$ and $G_{12/13}$ (Siehler and Manning 2002; Wang and Dudek 2009; Sammani et al. 2010). Further, S1P stimulates human airway smooth muscle cell contractility (Rosenfeldt et al. 2003), triggers murine airway hyperresponsiveness (Roviezzo et al. 2007), and induces bradycardia through $S1P_3$ (Forrest et al. 2004). The latter findings implicate a rather narrow therapeutic window for S1P, which may limit the therapeutic potential of S1P and drugs designed to increase S1P production or reduce S1P catabolism.

For this reason, S1P receptor agonists have aroused considerable interest. For example, intratracheal or intravenous application of the selective $S1P_1$ agonist SEW-2871 reduced lung permeability upon endotoxin injection (Sammani et al. 2010). Further, in a murine influenza infection model lung permeability and mortality were shown to be improved after intratracheal treatment with the S1P receptor 1 and 3–5 agonist AAL-R (Walsh et al. 2011). More widely used in clinical application is the S1P receptor modulator fingolimod (FTY720), a derivative of the fungal metabolite myriocin, which shows close structural homology to Sph and has been approved as an immunomodulatory drug for the treatment of multiple sclerosis (Brinkmann et al. 2010). FTY720 besides being immunosuppressive, exerts endothelial barrier-protective effects in vitro (Sanchez et al. 2003) and in vivo (Dudek et al. 2007) and attenuated lung injury in mice following LPS stimulation (Peng et al. 2004; Natarajan et al. 2013). However, similar to S1P, FTY720 does affect endothelial integrity dose-dependently. We recently observed that FTY720 at lower concentrations improved barrier integrity in endothelial cell monolayers (0.01–1 μM FTY720) and in mechanically ventilated mice (0.1 mg/kg FTY720). However, higher concentrations of FTY720 induced apoptosis and barrier disruption in vitro (10–100 μM FTY720)

and in mechanically ventilated mice (2 mg/kg FTY720), but not in spontaneously breathing mice (Müller et al. 2011). Trying to translate these experimental findings into the clinical setting, it cannot be ruled out that in FTY720-treated, ventilated patients with multiple organ dysfunction syndrome and disturbed hepatic metabolism of FTY720, increased FTY720 plasma concentrations might harm lungs that are sensitized by mechanical ventilation towards barrier-disruptive effects of the drug.

It is well-known that FTY720 phosphate is the active metabolite mediating the barrier-protective effect in vivo; however, the underlying mechanisms are not well understood. SphK2 was identified to be the predominant enzyme in generating FTY720 phosphate, thereby increasing its affinity to S1P receptors (Billich et al. 2003; Sanchez et al. 2003). But inhibition of VEGF-induced vascular permeability by FTY720 was independent from $S1P_1$ expression (Sanchez et al. 2003), and $S1P_1$ internalization and degradation by FTY720 has been suggested (Cyster 2005). Further concepts that may explain the barrier-protective effect of FTY720 have recently been reviewed (Natarajan et al. 2013). However, similar to S1P, FTY720 induces bradycardia and dyspnea along with decreases in forced expiratory volume in 1 s ($FEV_1$) (Kappos et al. 2006), thereby limiting its therapeutic use as a barrier-protective agent in critically ill patients.

## 8.8 Role of Reactive Oxygen and Nitrogen Species in the Pathogenesis of Lung Injury

ROS and reactive nitrogen species (RNS) are critically involved in the regulation of cellular function. ROS include superoxide anions, hydroxyl radical, hydrogen peroxide, hypochloric acid and other partly reduced derivatives of molecular oxygen, while metabolites of the NO metabolism like nitrite or peroxynitirite with oxidative power are summarized as RNS. Levels of ROS and RNS are tightly controlled by the protective actions of antioxidants such as superoxide dismutase or glutathione. However, an imbalance of both systems due to either excessive ROS/RNS production or critical reduction of antioxidants leads to oxidative stress which contributes to the pathogenesis of lung injury and particularly vascular permeability.

ROS generated during mitochondrial oxidative phosphorylation can modulate cellular processes by reacting with redox-reactive cystein residues on proteins, thereby altering enzyme activities and controlling cell regulatory pathways (Ray et al. 2012). Upon inflammation, endothelial cells produce ROS/RNS involving various enzymatic systems such as NADPH oxidases, xanthine oxidase, COX and eNOS. Neutrophils generate even higher amounts of ROS due to NADPH oxydase activity, which are partly converted to the potent oxidant HOCl by myeloperoxidase. Under inflammatory conditions, neutrophils also generate RNS by inducible NO synthase (iNOS; Boueiz and Hassoun 2009). Increased levels of ROS and RNS contribute to the pathogenesis of ALI upon different insults. Perfusion of isolated rabbit lungs with $H_2O_2$ induces barrier dysfunction resulting in pulmonary edema formation (Seeger et al. 1995; Hippenstiel et al. 2002). Exposure of endothelial

cells to $H_2O_2$ led to a rapid and dramatic decrease in cAMP content, and adenylate cyclase activation inhibited $H_2O_2$-induced permeability increase in endothelial cells (Suttorp et al. 1993b). Mechanical ventilation was shown to induce enzymatic activity of xanthine oxidoreductase (XOR), and inhibiting XOR protected mice from development of pulmonary hyperpermeability (Abdulnour et al. 2006). Thereby, the MAPK-dependent pathway is involved in permeability induction in rodents subjected to VILI (Abdulnour et al. 2006; Dolinay et al. 2008; Park et al. 2012). The underlying mechanisms are pro-inflammatory functions of this pathway as well as heat shock protein 25 (HSP25) phosphorylation leading to stress fibre formation and endothelial contraction (Abdulnour et al. 2006; Dolinay et al. 2008; Damarla et al. 2009). Furthermore, aggravated permeability and lung injury in VILI were demonstrated in mice lacking the transcription factor Nrf2 that regulates expression of several antioxidant enzymes, and antioxidant supplementation was able to rescue from exacerbation of lung injury (Papaiahgari et al. 2007).

NO is a reactive free radical and also a highly diffusible gas that is produced in the lungs from L-arginin in endothelial cells by constitutively expressed eNOS and in macrophages by iNOS. Activity of eNOS can be enhanced while its expression generally stays constant. In contrast, expression of iNOS is inducible, while its activity is more or less constant. Upon inflammation, different stimuli induce NO production and release, such as pore-forming bacterial exotoxins (Suttorp et al. 1993a). NO has multiple biological activities including control of vascular tone and permeability, regulation of mitochondrial respiration and adhesion of platelets and leukocytes. NO protects cells against oxidant injury and microbial threats, but it can also have detrimental effects, for example activation of inflammatory processes, enzyme inhibition and DNA damage. It is suggested that these varying cellular responses are highly dependent on the relative NO concentrations (Thomas et al. 2008).

The molecular mechanisms underlying NO activities are (i) reaction with transition metals like iron, copper and zinc, (ii) nitrolysation of cystein residues, and (iii) reaction with superoxide anion and formation of the oxidant peroxynitrite which leads to nitration of proteins involved in the regulation of cellular function (Korhonen et al. 2005).

Inhalation of NO is applied as rescue therapy in individual cases of hypoxic respiratory failure in adults, children and newborns along with respiratory support and other therapeutic measures. By inhalation, the potent vasodilator selectively decreases pulmonary arterial pressure without causing systemic vasodilation and redistributes pulmonary blood flow towards ventilated lung regions, thereby reducing intrapulmonary shunting and improving arterial oxygenation (Raoof et al. 2010). Nonetheless, although inhaled NO results in a transient improvement of oxygenation during the first 24 h of treatment, it does not increase ventilator-free days or survival of ARDS patients (Afshari et al. 2011).

Besides being a vasodilator, NO exerts endothelial barrier-regulating effects in the lungs; however, contradictory results have been reported. Inhaled NO was shown to maintain endothelial integrity in isolated perfused and ventilated murine lungs upon oxidative stress or ischemia/reperfusion (Kavanagh et al. 1994; Poss

et al. 1995; Schutte et al. 2001b). Further, inhaled NO decreased pulmonary transvascular albumin flux in patients with ALI (Benzing et al. 1995). How exactly NO exerts this barrier-stabilizing effect is largely unknown, but it is suggested that an increase in cyclic guanosine monophosphate (cGMP) through activation of guanylate cyclase (GC) may play a role. In rabbit lung ischemia/reperfusion, NO-induced barrier protection was associated with enhanced cGMP production and could be further increased by inhibition of the cGMP-specific phosphodiesterase (PDE) 5 (Schutte et al. 2001b). cGMP-dependent mechanisms mediating barrier protection could also be demonstrated in lung endothelial cells upon $H_2O_2$ treatment (Seeger et al. 1995; Suttorp et al. 1996), in endothelial cells and perfused mouse lungs stimulated with thrombin (Seybold et al. 2005), and in mice with severe pneumococcal pneumonia (Witzenrath et al. 2009). The barrier-protective effect of NO and cGMP can be partly explained by a negative feedback loop that regulates specific endothelial TRP channels (Yin et al. 2008), some of which are crucial for $[Ca^{2+}]_i$ increase, EC contraction and pulmonary hyperpermeability in response to different stimuli (Tiruppathi et al. 2002; Alvarez et al. 2006; Hamanaka et al. 2007; Jian et al. 2008; Yin et al. 2008; Boueiz and Hassoun 2009; Kuebler et al. 2010).

In contrast to its barrier-protective effect, endogenous NO was also shown to contribute to lung injury in isolated rabbit lungs upon hypoxic ischemia/reperfusion (Schutte et al. 2001a). Further, iNOS expression was upregulated in mice subjected to mechanical ventilation, and ventilated iNOS-deficient mice as well as mice treated with an iNOS inhibitor showed reduced permeability and lung inflammation compared to control WT mice (Peng et al. 2005). Similarly, development of pulmonary hyperpermeability in response to mechanical ventilation in rats was prevented by pharmacologic inhibition of NOS (Choi et al. 2003). Murine gain and loss of function studies verified a contribution of soluble GC to VILI (Schmidt et al. 2008). Moreover, inhaled NO increased endothelial permeability in a rat model of *Pseudomonas aeruginosa* pneumonia and this effect was not related to an enhanced inflammatory response (Ader et al. 2007). Consequently, the individual effects of NO on pulmonary endothelial barrier function might be determined by local NO concentrations and the prevalent pathologic circumstances.

## 8.9 Adrenomedullin (AM) and Endothelial Barrier Function

Adrenomedullin (AM) is a multifunctional, endogenous peptide that was shown to have endothelial barrier-stabilizing properties. It is expressed by different cell types including endothelial and epithelial cells, vascular smooth muscle cells, cardiomyocytes and leukocytes. AM is derived from a larger precursor peptide (prepro-AM) by posttranslational processing including amidation by peptidoglycine alpha-amidating monooxygenase (PAM; Temmesfeld-Wollbruck et al. 2007b). AM is a ligand for the calcitonin receptor like receptor (CRLR), which associates with receptor activity modifying proteins (RAMP)-2 and RAMP-3. AM receptor

binding in endothelial cells leads to accumulation of the second messenger cAMP and activation of different kinases including protein kinase A (PKA), PKC, MAP kinases (Hippenstiel et al. 2002; Temmesfeld-Wollbruck et al. 2007b).

The importance of AM for vascular barrier integrity was highlighted by the demonstration that mice deficient for AM, CRLR, PAM or RAMP2 die prematurely of hydrops fetalis (Caron and Smithies 2001; Czyzyk et al. 2005; Dackor et al. 2006; Ichikawa-Shindo et al. 2008). Further, expression of AM is increased under inflammatory conditions like sepsis or ALI (Matheson et al. 2003; Cheung et al. 2004; Agorreta et al. 2005) and mice heterozygous for the AM gene exhibit an aggravated inflammatory response upon LPS challenge (Dackor and Caron 2007).

In different in vitro, ex vivo and in vivo models, AM reduced pulmonary endothelial hyperpermeability induced by various stimuli such as hydrogen peroxide, LPS or *Staphylococcus aureus* alpha-toxin and protected against VILI in mice with and without pneumonia (Hippenstiel et al. 2002; Itoh et al. 2007; Temmesfeld-Wollbruck et al. 2007a; Müller et al. 2010; Muller-Redetzky et al. 2014b). In a two-hit model of relatively high clinical relevance, mice were subjected to pneumococcal pneumonia before being mechanically ventilated. Further, treatment with exogenous AM protected against gut barrier disruption after *Staphylococcus aureus* alpha-toxin stimulation and in ischemia/reperfusion injury, and improved blood–brain barrier function (Kis et al. 2003; Brell et al. 2005a; Brell et al. 2005b; Honda et al. 2006; Higuchi et al. 2008; Temmesfeld-Wollbruck et al. 2009).

There are at least two central mechanisms by which AM mediates endothelial barrier stabilization. The first is based on AM capability to block generation of actin stress fibres and actin myosin interaction thereby leading to endothelial cell relaxation (Temmesfeld-Wollbruck et al. 2007b). Briefly, AM was shown to increase intracellular cAMP levels in endothelial cells, thereby inhibiting MLC phosphorylation and actin myosin interaction and finally cell contraction induced by thrombin or hydrogen peroxide in vitro, or caused by mechanical ventilation in vivo (Hippenstiel et al. 2002; Brell et al. 2005b; Hocke et al. 2006; Müller et al. 2010; Muller-Redetzky et al. 2014b). However, in gut epithelial cells AM was shown to exert barrier-stabilizing effects independently of cAMP (Temmesfeld-Wollbruck et al. 2009). The second mechanism underlying AM-mediated barrier stabilization is through an increase of intercellular adherence. In a rat model of isolated perfused ileum, *Staphylococcus aureus* alpha-toxin-induced loss of the junctional protein VE-cadherin was prevented by treatment with AM (Hocke et al. 2006). In vitro, AM protected against *Staphylococcus aureus* alpha-toxin- or thrombin-mediated loss of VE-cadherin and occludin, and increased expression of claudin-5 in brain microvascular endothelial cells (Hocke et al. 2006; Honda et al. 2006). AM was also shown to exert immunomodulatory effects (Gonzalez-Rey et al. 2006), however we observed that the AM-mediated improvement of barrier function was not associated with a downregulated inflammatory response (Müller et al. 2010; Muller-Redetzky et al. 2014b). Although the obviously cell specific mechanisms underlying AM-mediated barrier protection are only partly understood, the impressive effects observed in complex experimental models regardless of the stimulus and uncoupled to immunosuppressive properties suggest a high translational potential for AM.

## 8.10 Stem Cells in Lung Injury

In lung injury, inflammatory signalling cascades are activated and chemoattractant factors released, including granulocyte-macrophage stimulating factor (GM-CSF), granulocyte colony stimulating factor (G-CSF), and stromal cell-derived factor 1α (SDF-1α) and its receptor CXCR4, which results in mobilization of stem cells from bone marrow to the injured lung (Maron-Gutierrez et al. 2014). Stem cells are able to renew themselves and to differentiate into multiple cell types, which may contribute to regeneration of damaged organs (Cribbs et al. 2010). In lung injury, stem cells engraft into tissue and interact with neighbouring cells, thereby directly contributing to epithelial and endothelial repair. However, the levels of engraftment seem to be too low to account for all the observed positive effects. Indeed, stem cells may additionally alter the immune response in a beneficial manner to diminish destructive inflammation while preserving the host's ability to combat pathogens (Cribbs et al. 2010). Alterations of immune responses and improvement of cellular functions seem to result in particular from of delivery of paracrine mediators and mitochondrion-containing microvesicles by stem cells (Bhattacharya and Matthay 2013). Allogeneic human mesenchymal stem cells were also shown to restore compromised alveolar fluid clearance ex vivo in human lungs rejected for transplantation due to lung injury and dysfunction after prolonged ischemia (McAuley et al. 2014).

Endothelial progenitor cells (EPCs) are a subtype of hematopoietic stem cells, which exclusively differentiate into endothelial cells and can be derived from mononuclear cells from bone marrow, cord blood and circulating blood. Patients with ARDS had increased numbers of circulating EPCs, and higher EPC counts correlated with improved survival (Burnham et al. 2005). Notably, EPCs engrafted into endothelial tissue of injured, but not of healthy lungs, again implying that injured lung tissue produces chemoattractants that mobilize EPCs specifically to damaged tissue areas.

However, although EPC recruitment was enhanced in patients with sepsis, proliferation, adhesion and migration of endogenous EPCs were reduced (Luo et al. 2009; Patschan et al. 2011). Two different experimental strategies were pursued to enhance beneficial functions of EPCs. First, autologous transplantation of EPCs from healthy donors was performed in rabbit and rat models of ALI, and exogenous EPCs reduced lung edema and hyaline membrane formation most likely due to reendothelialization of damaged lung vasculature (Lam et al. 2008; Mao et al. 2010). Second, autologous EPC transplantation was recently combined with SDF-1α treatment, which enhanced functional properties of EPCs (Fan et al. 2014). Exogenous EPCs and SDF-1α synergistically improved survival in mice with polymicrobial sepsis (Fan et al. 2014).

In summary, stem cells probably have prognostic value and provide a therapeutic perspective in ALI. Currently, bone marrow-derived human mesenchymal stem cells are tested as adjuvant therapy for the treatment of ARDS in a clinical phase I (NCT01775774), and in a multicenter phase II trial (NCT02097641).

## 8.11 Conclusions and Future Perspectives

ARDS may result from acute inflammatory diseases such as pneumonia or sepsis and still carries an unacceptably high mortality rate. In various studies, basic pathomechanisms involved in the development of ARDS were unraveled leading to improvements in therapy including ventilation and resuscitation strategies. Pulmonary endothelial cells have long been identified as key players in the pathogenesis of ARDS and researchers have discovered numerous central mechanisms underlying increased vascular permeability (Muller-Redetzky et al. 2014a). However, most therapeutic approaches based on the understanding of pathomechanisms underlying pulmonary endothelial barrier dysfunction have been frustrating so far. Nevertheless, these drawbacks should not discourage scientists from further research, quite the contrary they should be understood as important sources of perception. In this context, it is worth considering some general aspects when moving forward in this field.

First, to reverse a barrier dysfunction of an already injured endothelium may be a hardly achievable goal. Notably, the only therapeutic approaches reducing ARDS mortality so far, reduction of tidal volume and probably early prone positioning, short term use of neuromuscular blockers, and esophageal pressure-guided PEEP adjustment (Network ARDS 2000; Talmor et al. 2008; Papazian et al. 2010; Guerin et al. 2013), are aiming at prevention of further inflammatory stress by mechanical ventilation, thus being rather preventive. To focus on therapeutic approaches that slow down the development of pneumonia or sepsis to ARDS seems to be more promising than trying to reverse severe tissue inflammation and injury. Therefore, clinical and biological predictors of development towards ARDS are required, and future therapeutic strategies should be introduced before full-blown ARDS has developed. However, this notion should not tempt researchers to perform experimental studies that focus on preventive strategies with the start of the specific treatment before onset of the preceding disease (pneumonia or sepsis in this case), because they are far from translation into clinics.

Second, the real-life scenario should always be considered. Due to numerous simultaneous incidents, ICU patients are often susceptible to the development of ARDS. This is in contrast to experimental studies using, for example, LPS-treated mice, implicating that many redundant pathways may be differentially involved and should probably be targeted therapeutically at once. Furthermore, important interindividual differences need to be reflected.

Third, complexity is an aspect that should not be underestimated. The greater our understanding of the pathomechanisms contributing to lung injury is, the more aware we become of the differential pathomechanistic roles one and the same signalling system may have. For example, S1P was shown to differentially affect endothelial barrier function, depending on S1P concentration, receptor expression and the specific local cellular environment, which adds a further dimension to the big picture of mechanisms involved in endothelial barrier disruption. Presumably, systems biology combined with mathematical multi-scale models that integrate knowledge from experimental studies (in vitro, in vivo and in silico), clinical trials and clinical and biological predictors of individual patients will facilitate development of successful novel therapies and improvement of ARDS prevention.

## References

Abdulnour RE, Peng X, Finigan JH, Han EJ, Hasan EJ, Birukov KG, et al. Mechanical stress activates xanthine oxidoreductase through MAP kinase-dependent pathways. Am J Physiol Lung Cell Mol Physiol. 2006;291(3):L345–53.

Ader F, Berre R L, Lancel S, Faure K, Viget NB, Nowak E, et al. Inhaled nitric oxide increases endothelial permeability in Pseudomonas aeruginosa pneumonia. Intensive Care Med. 2007;33(3):503–10.

Afshari A, Brok J, Moller AM, Wetterslev J. Inhaled nitric oxide for acute respiratory distress syndrome and acute lung injury in adults and children: a systematic review with meta-analysis and trial sequential analysis. Anesth Analg. 2011;112(6):1411–21.

Agorreta J, Zulueta JJ, Montuenga LM, Garayoa M. Adrenomedullin expression in a rat model of acute lung injury induced by hypoxia and LPS. Am J Physiol Lung Cell Mol Physiol. 2005;288(3):L536–45.

Alvarez DF, King JA, Weber D, Addison E, Liedtke W, Townsley MI. Transient receptor potential vanilloid 4-mediated disruption of the alveolar septal barrier: a novel mechanism of acute lung injury. Circ Res. 2006;99(9):988–95.

Ben DF, Yu XY, Ji GY, Zheng DY, Lv KY, Ma B, et al. TLR4 mediates lung injury and inflammation in intestinal ischemia-reperfusion. J Surg Res. 2012;174(2):326–33.

Benzing A, Brautigam P, Geiger K, Loop T, Beyer U, Moser E. Inhaled nitric oxide reduces pulmonary transvascular albumin flux in patients with acute lung injury. Anesthesiology. 1995;83(6):1153–61.

Bhattacharya J, Matthay MA. Regulation and repair of the alveolar-capillary barrier in acute lung injury. Annu Rev Physiol. 2013;75:593–615.

Billich A, Bornancin F, Devay P, Mechtcheriakova D, Urtz N, Baumruker T. Phosphorylation of the immunomodulatory drug FTY720 by sphingosine kinases. J Biol Chem. 2003;278(48): 47408–15.

Boueiz A, Hassoun PM. Regulation of endothelial barrier function by reactive oxygen and nitrogen species. Microvasc Res. 2009;77(1):26–34.

Brell B, Hippenstiel S, David I, Pries AR, Habazettl H, Schmeck B, et al. Adrenomedullin treatment abolishes ileal mucosal hypoperfusion induced by Staphylococcus aureus alpha-toxin–an intravital microscopic study on an isolated rat ileum. Crit Care Med. 2005a;33(12):2810–016.

Brell B, Temmesfeld-Wollbruck B, Altzschner I, Frisch E, Schmeck B, Hocke AC, et al. Adrenomedullin reduces Staphylococcus aureus alpha-toxin-induced rat ileum microcirculatory damage. Crit Care Med. 2005b;33(4):819–26.

Brinkmann V, Reichard U, Goosmann C, Fauler B, Uhlemann Y, Weiss DS, et al. Neutrophil extracellular traps kill bacteria. Science. 2004;303(5663):1532–5.

Brinkmann V, Billich A, Baumruker T, Heining P, Schmouder R, Francis G, et al. Fingolimod (FTY720): discovery and development of an oral drug to treat multiple sclerosis. Nat Rev Drug Discov. 2010;9(11):883–97.

Burnham EL, Taylor WR, Quyyumi AA, Rojas M, Brigham KL, Moss M. Increased circulating endothelial progenitor cells are associated with survival in acute lung injury. Am J Respir Crit Care Med. 2005;172(7):854–60.

Calfee CS, Gallagher D, Abbott J, Thompson BT, Matthay MA. Plasma angiopoietin-2 in clinical acute lung injury: prognostic and pathogenetic significance. Crit Care Med. 2012;40(6): 1731–7.

Camerer E, Regard JB, Cornelissen I, Srinivasan Y, Duong DN, Palmer D, et al. Sphingosine-1-phosphate in the plasma compartment regulates basal and inflammation-induced vascular leak in mice. J Clin Invest. 2009;119(7):1871–9.

Canals D, Perry DM, Jenkins RW, Hannun YA. Drug targeting of sphingolipid metabolism: sphingomyelinases and ceramidases. Br J Pharmacol. 2011;163(4):694–712.

Carman CV, Springer TA. A transmigratory cup in leukocyte diapedesis both through individual vascular endothelial cells and between them. J Cell Biol. 2004;167(2):377–88.

Caron KM, Smithies O. Extreme hydrops fetalis and cardiovascular abnormalities in mice lacking a functional Adrenomedullin gene. Proc Natl Acad Sci U S A. 2001;98(2):615–9.
Caudrillier A, Kessenbrock K, Gilliss BM, Nguyen JX, Marques MB, Monestier M, et al. Platelets induce neutrophil extracellular traps in transfusion-related acute lung injury. J Clin Invest. 2012;122(7):2661–71.
Cheung BM, Hwang IS, Li CY, O WS, Tsang KW, Leung RY, et al. Increased adrenomedullin expression in lungs in endotoxaemia. J Endocrinol. 2004;181(2):339–45.
Choi WI, Quinn DA, Park KM, Moufarrej RK, Jafari B, Syrkina O, et al. Systemic microvascular leak in an in vivo rat model of ventilator-induced lung injury. Am J Respir Crit Care Med. 2003;167(12):1627–32.
Chow JC, Young DW, Golenbock DT, Christ WJ, Gusovsky F. Toll-like receptor-4 mediates lipopolysaccharide-induced signal transduction. J Biol Chem. 1999;274(16):10689–92.
Cirino G, Cicala C, Bucci MR, Sorrentino L, Maraganore JM, Stone SR. Thrombin functions as an inflammatory mediator through activation of its receptor. J Exp Med. 1996;183(3):821–7.
Clark SR, Ma AC, Tavener SA, McDonald B, Goodarzi Z, Kelly MM, et al. Platelet TLR4 activates neutrophil extracellular traps to ensnare bacteria in septic blood. Nat Med. 2007;13(4):463–9.
Cribbs SK, Matthay MA, Martin GS. Stem cells in sepsis and acute lung injury. Crit Care Med. 2010;38(12):2379–85.
Cyster JG. Chemokines, sphingosine-1-phosphate, and cell migration in secondary lymphoid organs. Annu Rev Immunol. 2005;23:127–59.
Czyzyk TA, Ning Y, Hsu MS, Peng B, Mains RE, Eipper BA, et al. Deletion of peptide amidation enzymatic activity leads to edema and embryonic lethality in the mouse. Dev Biol. 2005;287(2):301–13.
Dackor R, Caron K. Mice heterozygous for adrenomedullin exhibit a more extreme inflammatory response to endotoxin-induced septic shock. Peptides. 2007;28(11):2164–70.
Dackor RT, Fritz-Six K, Dunworth WP, Gibbons CL, Smithies O, Caron KM. Hydrops fetalis, cardiovascular defects, and embryonic lethality in mice lacking the calcitonin receptor-like receptor gene. Mol Cell Biol. 2006;26(7):2511–8.
Damarla M, Hasan E, Boueiz A, Le A, Pae HH, Montouchet C, et al. Mitogen activated protein kinase activated protein kinase 2 regulates actin polymerization and vascular leak in ventilator associated lung injury. PLoS One. 2009;4(2):e4600.
David S, Ghosh CC, Kumpers P, Shushakova N, van Slyke P, Khankin EV, et al. Effects of a synthetic PEG-ylated Tie-2 agonist peptide on endotoxemic lung injury and mortality. Am J Physiol Lung Cell Mol Physiol. 2011a;300(6):L851–62.
David S, Ghosh CC, Mukherjee A, Parikh SM. Angiopoietin-1 requires IQ domain GTPase-activating protein 1 to activate Rac1 and promote endothelial barrier defense. Arterioscler Thromb Vasc Biol. 2011b;31(11):2643–52.
David S, Park JK, Meurs M, Zijlstra JG, Koenecke C, Schrimpf C, et al. Acute administration of recombinant Angiopoietin-1 ameliorates multiple-organ dysfunction syndrome and improves survival in murine sepsis. Cytokine. 2011c;55(2):251–9.
David S, Mukherjee A, Ghosh CC, Yano M, Khankin EV, Wenger JB, et al. Angiopoietin-2 may contribute to multiple organ dysfunction and death in sepsis*. Crit Care Med. 2012;40(11):3034–41.
David S, Kumpers P, van Slyke P, Parikh SM. Mending leaky blood vessels: the angiopoietin-Tie2 pathway in sepsis. J Pharmacol Exp Ther. 2013;345(1):2–6.
Dhaliwal K, Scholefield E, Ferenbach D, Gibbons M, Duffin R, Dorward DA, et al. Monocytes control second-phase neutrophil emigration in established lipopolysaccharide-induced murine lung injury. Am J Respir Crit Care Med. 2012;186(6):514–24.
DiStasi MR, Ley K. Opening the flood-gates: how neutrophil-endothelial interactions regulate permeability. Trends Immunol. 2009;30(11):547–56.
Dolinay T, Wu W, Kaminski N, Ifedigbo E, Kaynar AM, Szilasi M, et al. Mitogen-activated protein kinases regulate susceptibility to ventilator-induced lung injury. PLoS One. 2008;3(2):e1601.
Dudek SM, Camp SM, Chiang ET, Singleton PA, Usatyuk PV, Zhao Y, et al. Pulmonary endothelial cell barrier enhancement by FTY720 does not require the S1P1 receptor. Cell Signal. 2007;19(8):1754–64.

Eklund L, Saharinen P. Angiopoietin signaling in the vasculature. Exp Cell Res. 2013;319(9): 1271–80.
Fan H, Goodwin AJ, Chang E, Zingarelli B, Borg K, Guan S, et al. Endothelial progenitor cells and a SDF-1alpha analogue synergistically improve survival in sepsis. Am J Respir Crit Care Med. 2014. doi:10.1164/rccm.201312-2163OC.
Fiedler U, Scharpfenecker M, Koidl S, Hegen A, Grunow V, Schmidt JM, et al. The Tie-2 ligand angiopoietin-2 is stored in and rapidly released upon stimulation from endothelial cell Weibel-Palade bodies. Blood. 2004;103(11):4150–6.
Fiedler U, Reiss Y, Scharpfenecker M, Grunow V, Koidl S, Thurston G, et al. Angiopoietin-2 sensitizes endothelial cells to TNF-alpha and has a crucial role in the induction of inflammation. Nat Med. 2006;12(2):235–9.
Forrest M, Sun SY, Hajdu R, Bergstrom J, Card D, Doherty G, et al. Immune cell regulation and cardiovascular effects of sphingosine 1-phosphate receptor agonists in rodents are mediated via distinct receptor subtypes. J Pharmacol Exp Ther. 2004;309(2):758–68.
Gamble JR, Drew J, Trezise L, Underwood A, Parsons M, Kasminkas L, et al. Angiopoietin-1 is an antipermeability and anti-inflammatory agent in vitro and targets cell junctions. Circ Res. 2000;87(7):603–7.
Gao XP, Zhu X, Fu J, Liu Q, Frey RS, Malik AB. Blockade of class IA phosphoinositide 3-kinase in neutrophils prevents NADPH oxidase activation- and adhesion-dependent inflammation. J Biol Chem. 2007;282(9):6116–25.
Garcia JG, Liu F, Verin AD, Birukova A, Dechert MA, Gerthoffer WT, et al. Sphingosine 1-phosphate promotes endothelial cell barrier integrity by Edg-dependent cytoskeletal rearrangement. J Clin Invest. 2001;108(5):689–701.
Gavard J, Patel V, Gutkind JS. Angiopoietin-1 prevents VEGF-induced endothelial permeability by sequestering Src through mDia. Dev Cell. 2008;14(1):25–36.
Geissmann F, Jung S, Littman DR. Blood monocytes consist of two principal subsets with distinct migratory properties. Immunity. 2003;19(1):71–82.
Glas GJ, Van Der Sluijs KF, Schultz MJ, Hofstra JJ, Van Der Poll T, Levi M. Bronchoalveolar hemostasis in lung injury and acute respiratory distress syndrome. J Thromb Haemost. 2013;11(1):17–25.
Goggel R, Winoto-Morbach S, Vielhaber G, Imai Y, Lindner K, Brade L, et al. PAF-mediated pulmonary edema: a new role for acid sphingomyelinase and ceramide. Nat Med. 2004;10(2): 155–60.
Gong P, Angelini DJ, Yang S, Xia G, Cross AS, Mann D, et al. TLR4 signaling is coupled to SRC family kinase activation, tyrosine phosphorylation of zonula adherens proteins, and opening of the paracellular pathway in human lung microvascular endothelia. J Biol Chem. 2008;283(19):13437–49.
Gonzalez-Rey E, Chorny A, Varela N, Robledo G, Delgado M. Urocortin and adrenomedullin prevent lethal endotoxemia by down-regulating the inflammatory response. Am J Pathol. 2006;168(6):1921–30.
Grommes J, Soehnlein O. Contribution of neutrophils to acute lung injury. Mol Med. 2011;17(3–4):293–307.
Guerin C, Reignier J, Richard JC, Beuret P, Gacouin A, Boulain T, et al. Prone positioning in severe acute respiratory distress syndrome. N Engl J Med. 2013;368(23):2159–68.
Hamanaka K, Jian MY, Weber DS, Alvarez DF, Townsley MI, Al-Mehdi AB, et al. TRPV4 initiates the acute calcium-dependent permeability increase during ventilator-induced lung injury in isolated mouse lungs. Am J Physiol Lung Cell Mol Physiol. 2007;293(4):L923–32.
Hanel P, Andreani P, Graler MH. Erythrocytes store and release sphingosine 1-phosphate in blood. FASEB J. 2007;21(4):1202–9.
He P, Zhang H, Zhu L, Jiang Y, Zhou X. Leukocyte-platelet aggregate adhesion and vascular permeability in intact microvessels: role of activated endothelial cells. Am J Physiol Heart Circ Physiol. 2006;291(2):H591–9.
Higuchi S, Wu R, Zhou M, Marini CP, Ravikumar TS, Wang P. Gut hyperpermiability after ischemia and reperfusion: attenuation with adrenomedullin and its binding protein treatment. Int J Clin Exp Pathol. 2008;1(5):409–18.

Hilberath JN, Carlo T, Pfeffer MA, Croze RH, Hastrup F, Levy BD. Resolution of Toll-like receptor 4-mediated acute lung injury is linked to eicosanoids and suppressor of cytokine signaling 3. FASEB J. 2011;25(6):1827–35.

Hippenstiel S, Tannert-Otto S, Vollrath N, Krull M, Just I, Aktories K, et al. Glucosylation of small GTP-binding Rho proteins disrupts endothelial barrier function. Am J Physiol. 1997;272(1 Pt 1):L38–L43.

Hippenstiel S, Krull M, Ikemann A, Risau W, Clauss M, Suttorp N. VEGF induces hyperpermeability by a direct action on endothelial cells. Am J Physiol. 1998;274(5 Pt 1):L678–84.

Hippenstiel S, Witzenrath M, Schmeck B, Hocke A, Krisp M, Krull M, et al. Adrenomedullin reduces endothelial hyperpermeability. Circ Res. 2002;91(7):618–25.

Hla T, Lee MJ, Ancellin N, Paik JH, Kluk MJ. Lysophospholipids–receptor revelations. Science. 2001;294(5548):1875–8.

Hocke AC, Temmesfeld-Wollbrueck B, Schmeck B, Berger K, Frisch EM, Witzenrath M, et al. Perturbation of endothelial junction proteins by Staphylococcus aureus alpha-toxin: inhibition of endothelial gap formation by adrenomedullin. Histochem Cell Biol. 2006;126(3):305–16.

Hofstra JJ, Vlaar AP, Knape P, Mackie DP, Determann RM, Choi G, et al. Pulmonary activation of coagulation and inhibition of fibrinolysis after burn injuries and inhalation trauma. J Trauma. 2011;70(6):1389–97.

Honda M, Nakagawa S, Hayashi K, Kitagawa N, Tsutsumi K, Nagata I, et al. Adrenomedullin improves the blood-brain barrier function through the expression of claudin-5. Cell Mol Neurobiol. 2006;26(2):109–18.

Huang YQ, Li JJ, Hu L, Lee M, Karpatkin S. Thrombin induces increased expression and secretion of angiopoietin-2 from human umbilical vein endothelial cells. Blood. 2002;99(5):1646–50.

Huang YQ, Sauthoff H, Herscovici P, Pipiya T, Cheng J, Heitner S, et al. Angiopoietin-1 increases survival and reduces the development of lung edema induced by endotoxin administration in a murine model of acute lung injury. Crit Care Med. 2008;36(1):262–7.

Huber-Lang M, Sarma JV, Zetoune FS, Rittirsch D, Neff TA, McGuire SR, et al. Generation of C5a in the absence of C3: a new complement activation pathway. Nat Med. 2006;12(6):682–7.

Hughes DP, Marron MB, Brindle NP. The antiinflammatory endothelial tyrosine kinase Tie2 interacts with a novel nuclear factor-kappaB inhibitor ABIN-2. Circ Res. 2003;92(6):630–6.

Ichikawa-Shindo Y, Sakurai T, Kamiyoshi A, Kawate H, Iinuma N, Yoshizawa T, et al. The GPCR modulator protein RAMP2 is essential for angiogenesis and vascular integrity. J Clin Invest. 2008;118(1):29–39.

Imai Y, Kuba K, Neely GG, Yaghubian-Malhami R, Perkmann T, van Loo G, et al. Identification of oxidative stress and Toll-like receptor 4 signaling as a key pathway of acute lung injury. Cell. 2008;133(2):235–49.

Itoh T, Obata H, Murakami S, Hamada K, Kangawa K, Kimura H, et al. Adrenomedullin ameliorates lipopolysaccharide-induced acute lung injury in rats. Am J Physiol Lung Cell Mol Physiol. 2007;293(2):L446–52.

Iwasaki A, Medzhitov R. A new shield for a cytokine storm. Cell. 2011;146(6):861–2.

Jho D, Mehta D, Ahmmed G, Gao XP, Tiruppathi C, Broman M, et al. Angiopoietin-1 opposes VEGF-induced increase in endothelial permeability by inhibiting TRPC1-dependent Ca2 influx. Circ Res. 2005;96(12):1282–90.

Jian MY, King JA, Al-Mehdi AB, Liedtke W, Townsley MI. High vascular pressure-induced lung injury requires P450 epoxygenase-dependent activation of TRPV4. Am J Respir Cell Mol Biol. 2008;38(4):386–92.

Kappos L, Antel J, Comi G, Montalban X, O'Connor P, Polman CH, et al. Oral fingolimod (FTY720) for relapsing multiple sclerosis. N Engl J Med. 2006;355(11):1124–40.

Kavanagh BP, Mouchawar A, Goldsmith J, Pearl RG. Effects of inhaled NO and inhibition of endogenous NO synthesis in oxidant-induced acute lung injury. J Appl Physiol. 1994;76(3):1324–9.

Kawagoe T, Sato S, Matsushita K, Kato H, Matsui K, Kumagai Y, et al. Sequential control of Toll-like receptor-dependent responses by IRAK1 and IRAK2. Nat Immunol. 2008;9(6):684–91.

Khan MA, Maasch C, Vater A, Klussmann S, Morser J, Leung LL, et al. Targeting complement component 5a promotes vascular integrity and limits airway remodeling. Proc Natl Acad Sci U S A. 2013;110(15):6061–6.

Kim SR, Bae SK, Park HJ, Kim MK, Kim K, Park SY, et al. Thromboxane A(2) increases endothelial permeability through upregulation of interleukin-8. Biochem Biophys Res Commun. 2010;397(3):413–9.

Kis B, Snipes JA, Deli MA, Abraham CS, Yamashita H, Ueta Y, et al. Chronic adrenomedullin treatment improves blood-brain barrier function but has no effects on expression of tight junction proteins. Acta Neurochir Suppl. 2003;86:565–8.

Korhonen R, Lahti A, Kankaanranta H, Moilanen E. Nitric oxide production and signaling in inflammation. Curr Drug Targets Inflamm Allergy. 2005;4(4):471–9.

Kuebler WM, Yang Y, Samapati R, Uhlig S. Vascular barrier regulation by PAF, ceramide, caveolae, and NO—an intricate signaling network with discrepant effects in the pulmonary and systemic vasculature. Cell Physiol Biochem. 2010;26(1):29–40.

Kumpers P, Gueler F, David S, Slyke PV, Dumont DJ, Park JK, et al. The synthetic tie2 agonist peptide vasculotide protects against vascular leakage and reduces mortality in murine abdominal sepsis. Crit Care. 2011;15(5):R261.

Lam CF, Liu YC, Hsu JK, Yeh PA, Su TY, Huang CC, et al. Autologous transplantation of endothelial progenitor cells attenuates acute lung injury in rabbits. Anesthesiology. 2008;108(3):392–401.

Lemieux C, Maliba R, Favier J, Theoret JF, Merhi Y, Sirois MG. Angiopoietins can directly activate endothelial cells and neutrophils to promote proinflammatory responses. Blood. 2005;105(4):1523–30.

Li X, Stankovic M, Bonder CS, Hahn CN, Parsons M, Pitson SM, et al. Basal and angiopoietin-1-mediated endothelial permeability is regulated by sphingosine kinase-1. Blood. 2008;111(7):3489–97.

Liu HB, Cui NQ, Wang Q, Li DH, Xue XP. Sphingosine-1-phosphate and its analogue FTY720 diminish acute pulmonary injury in rats with acute necrotizing pancreatitis. Pancreas. 2008;36(3):e10–5.

Liu ZM, Zhu SM, Qin XJ, Cheng ZD, Liu MY, Zhang HM, et al. Silencing of C5a receptor gene with siRNA for protection from Gram-negative bacterial lipopolysaccharide-induced vascular permeability. Mol Immunol. 2010;47(6):1325–33.

Looney MR, Nguyen JX, Hu Y, Van Ziffle JA, Lowell CA, Matthay MA. Platelet depletion and aspirin treatment protect mice in a two-event model of transfusion-related acute lung injury. J Clin Invest. 2009;119(11):3450–61.

Lucas R, Yang G, Gorshkov BA, Zemskov EA, Sridhar S, Umapathy NS, et al. Protein kinase C-alpha and arginase I mediate pneumolysin-induced pulmonary endothelial hyperpermeability. Am J Respir Cell Mol Biol. 2012;47(4):445–53.

Luo TH, Wang Y, Lu ZM, Zhou H, Xue XC, Bi JW, et al. The change and effect of endothelial progenitor cells in pig with multiple organ dysfunction syndromes. Critical care. 2009;13(4):R118.

Lynn M, Rossignol DP, Wheeler JL, Kao RJ, Perdomo CA, Noveck R, et al. Blocking of responses to endotoxin by E5564 in healthy volunteers with experimental endotoxemia. J Infect Dis. 2003;187(4):631–9.

Mammoto T, Parikh SM, Mammoto A, Gallagher D, Chan B, Mostoslavsky G, et al. Angiopoietin-1 requires p190 RhoGAP to protect against vascular leakage in vivo. J Biol Chem. 2007;282(33):23910–8.

Mao M, Wang SN, Lv XJ, Wang Y, Xu JC. Intravenous delivery of bone marrow-derived endothelial progenitor cells improves survival and attenuates lipopolysaccharide-induced lung injury in rats. Shock. 2010;34(2):196–204.

Markiewski MM, Lambris JD. The role of complement in inflammatory diseases from behind the scenes into the spotlight. Am J Pathol. 2007;171(3):715–27.

Maron-Gutierrez T, Laffey JG, Pelosi P, Rocco PR. Cell-based therapies for the acute respiratory distress syndrome. Curr Opin Crit Care. 2014;20(1):122–31.

Marshall JC, Foster D, Vincent JL, Cook DJ, Cohen J, Dellinger RP, et al. Diagnostic and prognostic implications of endotoxemia in critical illness: results of the MEDIC study. J Infect Dis. 2004;190(3):527–34.

Martin TR, Pistorese BP, Chi EY, Goodman RB, Matthay MA. Effects of leukotriene B4 in the human lung. Recruitment of neutrophils into the alveolar spaces without a change in protein permeability. J Clin Invest. 1989;84(5):1609–19.

Mastellos D, Morikis D, Isaacs SN, Holland MC, Strey CW, Lambris JD. Complement: structure, functions, evolution, and viral molecular mimicry. Immunol Res. 2003;27(2–3):367–86.

Matheson PJ, Mays MP, Hurt RT, Harris PD, Garrison RN. Adrenomedullin is increased in the portal circulation during chronic sepsis in rats. Am J Surg. 2003;186(5):519–25.

Matthay MA, Ware LB, Zimmerman GA. The acute respiratory distress syndrome. J Clin Invest. 2012;122(8):2731–40.

McAuley DF, Curley GF, Hamid UI, Laffey JG, Abbott J, McKenna DH, et al. Clinical grade allogeneic human mesenchymal stem cells restore alveolar fluid clearance in human lungs rejected for transplantation. Am J Physiol Lung Cell Mol Physiol. 2014;306(9):L809–15.

McCarter SD, Mei SH, Lai PF, Zhang QW, Parker CH, Suen RS, et al. Cell-based angiopoietin-1 gene therapy for acute lung injury. Am J Respir Crit Care Med. 2007;175(10):1014–26.

McVerry BJ, Peng X, Hassoun PM, Sammani S, Simon BA, Garcia JG. Sphingosine 1-phosphate reduces vascular leak in murine and canine models of acute lung injury. Am J Respir Crit Care Med. 2004;170(9):987–93.

Medvedev AE, Lentschat A, Wahl LM, Golenbock DT, Vogel SN. Dysregulation of LPS-induced Toll-like receptor 4-MyD88 complex formation and IL-1 receptor-associated kinase 1 activation in endotoxin-tolerant cells. J Immunol. 2002;169(9):5209–16.

Mehta D, Malik AB. Signaling mechanisms regulating endothelial permeability. Physiol Rev. 2006;86(1):279–367.

Mei SH, McCarter SD, Deng Y, Parker CH, Liles WC, Stewart DJ. Prevention of LPS-induced acute lung injury in mice by mesenchymal stem cells overexpressing angiopoietin 1. PLoS Med. 2007;4(9):e269.

Mofarrahi M, Nouh T, Qureshi S, Guillot L, Mayaki D, Hussain SN. Regulation of angiopoietin expression by bacterial lipopolysaccharide. Am J Physiol Lung Cell Mol Physiol. 2008;294(5):L955–63.

Mullarkey M, Rose JR, Bristol J, Kawata T, Kimura A, Kobayashi S, et al. Inhibition of endotoxin response by e5564, a novel Toll-like receptor 4-directed endotoxin antagonist. J Pharmacol Exp Ther. 2003;304(3):1093–102.

Müller HC, Witzenrath M, Tschernig T, Gutbier B, Hippenstiel S, Santel A, et al. Adrenomedullin attenuates ventilator-induced lung injury in mice. Thorax. 2010;65(12):1077–84.

Müller HC, Hocke AC, Hellwig K, Gutbier B, Peters H, Schonrock SM, et al. The Sphingosine-1 Phosphate receptor agonist FTY720 dose dependently affected endothelial integrity in vitro and aggravated ventilator-induced lung injury in mice. Pulm Pharmacol Ther. 2011;24(4):377–85.

Muller-Redetzky HC, Suttorp N, Witzenrath M. Dynamics of pulmonary endothelial barrier function in acute inflammation: mechanisms and therapeutic perspectives. Cell Tissue Res. 2014a;355(3):657–73.

Muller-Redetzky HC, Will D, Hellwig K, Kummer W, Tschernig T, Pfeil U, et al. Mechanical ventilation drives pneumococcal pneumonia into lung injury and sepsis in mice: protection by adrenomedullin. Critical Care. 2014b;18(2):R73.

Murdoch C, Tazzyman S, Webster S, Lewis CE. Expression of Tie-2 by human monocytes and their responses to angiopoietin-2. J Immunol. 2007;178(11):7405–11.

Narasaraju T, Yang E, Samy RP, Ng HH, Poh WP, Liew AA, et al. Excessive neutrophils and neutrophil extracellular traps contribute to acute lung injury of influenza pneumonitis. Am J Pathol. 2011;179(1):199–210.

Natarajan V, Dudek SM, Jacobson JR, Moreno-Vinasco L, Huang LS, Abassi T, et al. Sphingosine-1-phosphate, FTY720, and sphingosine-1-phosphate receptors in the pathobiology of acute lung injury. Am J Respir Cell Mol Biol. 2013;49(1):6–17.

Network ARDS. Ventilation with lower tidal volumes as compared with traditional tidal volumes for acute lung injury and the acute respiratory distress syndrome. The Acute Respiratory Distress Syndrome Network. N Engl J Med. 2000;342(18):1301–8.

O'Dea KP, Young AJ, Yamamoto H, Robotham JL, Brennan FM, Takata M. Lung-marginated monocytes modulate pulmonary microvascular injury during early endotoxemia. Am J Respir Crit Care Med. 2005;172(9):1119–27.

O'Dea KP, Wilson MR, Dokpesi JO, Wakabayashi K, Tatton L, van Rooijen N, et al. Mobilization and margination of bone marrow Gr-1high monocytes during subclinical endotoxemia predisposes the lungs toward acute injury. J Immunol. 2009;182(2):1155–66.

Ogawa EN, Ishizaka A, Tasaka S, Koh H, Ueno H, Amaya F, et al. Contribution of high-mobility group box-1 to the development of ventilator-induced lung injury. Am J Respir Crit Care Med. 2006;174(4):400–7.

Oh H, Takagi H, Suzuma K, Otani A, Matsumura M, Honda Y. Hypoxia and vascular endothelial growth factor selectively up-regulate angiopoietin-2 in bovine microvascular endothelial cells. J Biol Chem. 1999;274(22):15732–9.

Okazaki M, Kreisel F, Richardson SB, Kreisel D, Krupnick AS, Patterson GA, et al. Sphingosine 1-phosphate inhibits ischemia reperfusion injury following experimental lung transplantation. Am J Transplant. 2007;7(4):751–8.

Opal SM, Laterre PF, Francois B, LaRosa SP, Angus DC, Mira JP, et al. Effect of eritoran, an antagonist of MD2-TLR4, on mortality in patients with severe sepsis: the ACCESS randomized trial. JAMA. 2013;309(11):1154–62.

Opitz B, van Laak V, Eitel J, Suttorp N. Innate immune recognition in infectious and noninfectious diseases of the lung. Am J Respir Crit Care Med. 2010;181(12):1294–309.

Papaiahgari S, Yerrapureddy A, Reddy SR, Reddy NM, Dodd OJ, Crow MT, et al. Genetic and pharmacologic evidence links oxidative stress to ventilator-induced lung injury in mice. Am J Respir Crit Care Med. 2007;176(12):1222–35.

Papayannopoulos V, Metzler KD, Hakkim A, Zychlinsky A. Neutrophil elastase and myeloperoxidase regulate the formation of neutrophil extracellular traps. J Cell Biol. 2010;191(3):677–91.

Papazian L, Forel JM, Gacouin A, Penot-Ragon C, Perrin G, Loundou A, et al. Neuromuscular blockers in early acute respiratory distress syndrome. N Engl J Med. 2010;363(12):1107–16.

Parikh SM, Mammoto T, Schultz A, Yuan HT, Christiani D, Karumanchi SA, et al. Excess circulating angiopoietin-2 may contribute to pulmonary vascular leak in sepsis in humans. PLoS Med. 2006;3(3):e46.

Park JS, Svetkauskaite D, He Q, Kim JY, Strassheim D, Ishizaka A, et al. Involvement of toll-like receptors 2 and 4 in cellular activation by high mobility group box 1 protein. J Biol Chem. 2004;279(9):7370–7.

Park MS, He Q, Edwards MG, Sergew A, Riches DW, Albert RK, et al. Mitogen-activated protein kinase phosphatase-1 modulates regional effects of injurious mechanical ventilation in rodent lungs. Am J Respir Crit Care Med. 2012;186(1):72–81.

Patschan SA, Patschan D, Temme J, Korsten P, Wessels JT, Koziolek M, et al. Endothelial progenitor cells (EPC) in sepsis with acute renal dysfunction (ARD). Critical care. 2011;15(2):R94.

Peng X, Hassoun PM, Sammani S, McVerry BJ, Burne MJ, Rabb H, et al. Protective effects of sphingosine 1-phosphate in murine endotoxin-induced inflammatory lung injury. Am J Respir Crit Care Med. 2004;169(11):1245–51.

Peng X, Abdulnour RE, Sammani S, Ma SF, Han EJ, Hasan EJ, et al. Inducible nitric oxide synthase contributes to ventilator-induced lung injury. Am J Respir Crit Care Med. 2005;172(4):470–9.

Petrache I, Verin AD, Crow MT, Birukova A, Liu F, Garcia JG. Differential effect of MLC kinase in TNF-alpha-induced endothelial cell apoptosis and barrier dysfunction. Am J Physiol Lung Cell Mol Physiol. 2001;280(6):L1168–78.

Phillipson M, Kaur J, Colarusso P, Ballantyne CM, Kubes P. Endothelial domes encapsulate adherent neutrophils and minimize increases in vascular permeability in paracellular and transcellular emigration. PLoS One. 2008;3(2):e1649.

Poss WB, Timmons OD, Farrukh IS, Hoidal JR, Michael JR. Inhaled nitric oxide prevents the increase in pulmonary vascular permeability caused by hydrogen peroxide. J Appl Physiol. 1995;79(3):886–91.

Prabhakaran P, Ware LB, White KE, Cross MT, Matthay MA, Olman MA. Elevated levels of plasminogen activator inhibitor-1 in pulmonary edema fluid are associated with mortality in acute lung injury. Am J Physiol Lung Cell Mol Physiol. 2003;285(1):L20–8.

Predescu SA, Predescu DN, Malik AB. Molecular determinants of endothelial transcytosis and their role in endothelial permeability. Am J Physiol Lung Cell Mol Physiol. 2007;293(4):L823–42.

Ranieri VM, Rubenfeld GD, Thompson BT, Ferguson ND, Caldwell E, Fan E, et al. Acute respiratory distress syndrome: the Berlin Definition. JAMA. 2012;307(23):2526–33.

Raoof S, Goulet K, Esan A, Hess DR, Sessler CN. Severe hypoxemic respiratory failure: part 2–nonventilatory strategies. Chest. 2010;137(6):1437–48.

Ray PD, Huang BW, Tsuji Y. Reactive oxygen species (ROS) homeostasis and redox regulation in cellular signaling. Cell Signal. 2012;24(5):981–90.

Rosenfeldt HM, Amrani Y, Watterson KR, Murthy KS, Panettieri RA Jr, Spiegel S. Sphingosine-1-phosphate stimulates contraction of human airway smooth muscle cells. FASEB J. 2003;17(13):1789–99.

Rosengren S, Olofsson AM, von Andrian UH, Lundgren-Akerlund E, Arfors KE. Leukotriene B4-induced neutrophil-mediated endothelial leakage in vitro and in vivo. J Appl Physiol. 1991;71(4):1322–30.

Roviezzo F, Lorenzo A D, Bucci M, Brancaleone V, Vellecco V, De Nardo M, et al. Sphingosine-1-phosphate/sphingosine kinase pathway is involved in mouse airway hyperresponsiveness. Am J Respir Cell Mol Biol. 2007;36(6):757–62.

Saffarzadeh M, Juenemann C, Queisser MA, Lochnit G, Barreto G, Galuska SP, et al. Neutrophil extracellular traps directly induce epithelial and endothelial cell death: a predominant role of histones. PLoS One. 2012;7(2):e32366.

Sammani S, Moreno-Vinasco L, Mirzapoiazova T, Singleton PA, Chiang ET, Evenoski CL, et al. Differential effects of sphingosine 1-phosphate receptors on airway and vascular barrier function in the murine lung. Am J Respir Cell Mol Biol. 2010;43(4):394–402.

Sanchez T, Estrada-Hernandez T, Paik JH, Wu MT, Venkataraman K, Brinkmann V, et al. Phosphorylation and action of the immunomodulator FTY720 inhibits vascular endothelial cell growth factor-induced vascular permeability. J Biol Chem. 2003;278(47):47281–90.

Scharpfenecker M, Fiedler U, Reiss Y, Augustin HG. The Tie-2 ligand angiopoietin-2 destabilizes quiescent endothelium through an internal autocrine loop mechanism. J Cell Sci. 2005;118(Pt 4):771–80.

Schmidt EP, Damarla M, Rentsendorj O, Servinsky LE, Zhu B, Moldobaeva A, et al. Soluble guanylyl cyclase contributes to ventilator-induced lung injury in mice. Am J Physiol Lung Cell Mol Physiol. 2008;295(6):L1056–65.

Schraufstatter IU, Trieu K, Sikora L, Sriramarao P, DiScipio R. Complement c3a and c5a induce different signal transduction cascades in endothelial cells. J Immunol. 2002;169(4):2102–10.

Schutte H, Mayer K, Burger H, Witzenrath M, Gessler T, Seeger W, et al. Endogenous nitric oxide synthesis and vascular leakage in ischemic-reperfused rabbit lungs. Am J Respir Crit Care Med. 2001a;164(3):412–8.

Schutte H, Witzenrath M, Mayer K, Rosseau S, Seeger W, Grimminger F. Short-term "preconditioning" with inhaled nitric oxide protects rabbit lungs against ischemia-reperfusion injury. Transplantation. 2001b;72(8):1363–70.

Seeger W, Hansen T, Rossig R, Schmehl T, Schutte H, Kramer HJ, et al. Hydrogen peroxide-induced increase in lung endothelial and epithelial permeability–effect of adenylate cyclase stimulation and phosphodiesterase inhibition. Microvasc Res. 1995;50(1):1–17.

Seybold J, Thomas D, Witzenrath M, Boral S, Hocke AC, Burger A, et al. Tumor necrosis factor-alpha-dependent expression of phosphodiesterase 2: role in endothelial hyperpermeability. Blood. 2005;105(9):3569–76.

Shaw SK, Ma S, Kim MB, Rao RM, Hartman CU, Froio RM, et al. Coordinated redistribution of leukocyte LFA-1 and endothelial cell ICAM-1 accompany neutrophil transmigration. J Exp Med. 2004;200(12):1571–80.

Shen Q, Rigor RR, Pivetti CD, Wu MH, Yuan SY. Myosin light chain kinase in microvascular endothelial barrier function. Cardiovasc Res. 2010;87(2):272–80.

Siehler S, Manning DR. Pathways of transduction engaged by sphingosine 1-phosphate through G protein-coupled receptors. Biochim Biophys Acta. 2002;1582(1–3):94–9.

Le Stunff H, Milstien S, Spiegel S. Generation and metabolism of bioactive sphingosine-1-phosphate. J Cell Biochem. 2004;92(5):882–99.

Suttorp N, Fuhrmann M, Tannert-Otto S, Grimminger F, Bhadki S. Pore-forming bacterial toxins potently induce release of nitric oxide in porcine endothelial cells. J Exp Med. 1993a;178(1):337–41.

Suttorp N, Weber U, Welsch T, Schudt C. Role of phosphodiesterases in the regulation of endothelial permeability in vitro. J Clin Invest. 1993b;91(4):1421–8.

Suttorp N, Hippenstiel S, Fuhrmann M, Krull M, Podzuweit T. Role of nitric oxide and phosphodiesterase isoenzyme II for reduction of endothelial hyperpermeability. Am J Physiol. 1996;270(3 Pt 1):C778–85.

Talmor D, Sarge T, Malhotra A, O'Donnell CR, Ritz R, Lisbon A, et al. Mechanical ventilation guided by esophageal pressure in acute lung injury. N Engl J Med. 2008;359(20):2095–104.

Tani M, Sano T, Ito M, Igarashi Y. Mechanisms of sphingosine and sphingosine 1-phosphate generation in human platelets. J Lipid Res. 2005;46(11):2458–67.

Tauseef M, Knezevic N, Chava KR, Smith M, Sukriti S, Gianaris N, et al. TLR4 activation of TRPC6-dependent calcium signaling mediates endotoxin-induced lung vascular permeability and inflammation. J Exp Med. 2012;209(11):1953–68.

Teijaro JR, Walsh KB, Cahalan S, Fremgen DM, Roberts E, Scott F, et al. Endothelial cells are central orchestrators of cytokine amplification during influenza virus infection. Cell. 2011;146(6):980–91.

Temmesfeld-Wollbruck B, Brell B, David I, Dorenberg M, Adolphs J, Schmeck B, et al. Adrenomedullin reduces vascular hyperpermeability and improves survival in rat septic shock. Intensive Care Med. 2007a;33(4):703–10.

Temmesfeld-Wollbruck B, Hocke AC, Suttorp N, Hippenstiel S. Adrenomedullin and endothelial barrier function. Thromb Haemost. 2007b;98(5):944–51.

Temmesfeld-Wollbruck B, Brell B, zu Dohna C, Dorenberg M, Hocke AC, Martens H, et al. Adrenomedullin reduces intestinal epithelial permeability in vivo and in vitro. Am J Physiol Gastrointest Liver Physiol. 2009;297(1):G43–G51.

Thomas DD, Ridnour LA, Isenberg JS, Flores-Santana W, Switzer CH, Donzelli S, et al. The chemical biology of nitric oxide: implications in cellular signaling. Free Radic Biol Med. 2008;45(1):18–31.

Tidswell M, Tillis W, Larosa SP, Lynn M, Wittek AE, Kao R, et al. Phase 2 trial of eritoran tetrasodium (E5564), a toll-like receptor 4 antagonist, in patients with severe sepsis. Crit Care Med. 2010;38(1):72–83.

Tilley SJ, Orlova EV, Gilbert RJ, Andrew PW, Saibil HR. Structural basis of pore formation by the bacterial toxin pneumolysin. Cell. 2005;121(2):247–56.

Tiruppathi C, Freichel M, Vogel SM, Paria BC, Mehta D, Flockerzi V, et al. Impairment of store-operated Ca2 + entry in TRPC4(-/-) mice interferes with increase in lung microvascular permeability. Circ Res. 2002;91(1):70–6.

Tournaire R, Simon MP, le Noble F, Eichmann A, England P, Pouyssegur J. A short synthetic peptide inhibits signal transduction, migration and angiogenesis mediated by Tie2 receptor. EMBO Rep. 2004;5(3):262–7.

Uhlig S, Yang Y. Sphingolipids in acute lung injury. Handb Exp Pharmacol. 2013;(216):227–46.

Venkataraman K, Lee YM, Michaud J, Thangada S, Ai Y, Bonkovsky HL, et al. Vascular endothelium as a contributor of plasma sphingosine 1-phosphate. Circ Res. 2008;102(6): 669–76.

Verbrugge SJ, Lachmann B, Kesecioglu J. Lung protective ventilatory strategies in acute lung injury and acute respiratory distress syndrome: from experimental findings to clinical application. Clin Physiol Funct Imaging. 2007;27(2):67–90.

Wadgaonkar R, Patel V, Grinkina N, Romano C, Liu J, Zhao Y, et al. Differential regulation of sphingosine kinases 1 and 2 in lung injury. Am J Physiol Lung Cell Mol Physiol. 2009;296(4):L603–13.

Walsh KB, Teijaro JR, Wilker PR, Jatzek A, Fremgen DM, Das SC, et al. Suppression of cytokine storm with a sphingosine analog provides protection against pathogenic influenza virus. Proc Natl Acad Sci U S A. 2011;108(29):12018–23.

Wang L, Dudek SM. Regulation of vascular permeability by sphingosine 1-phosphate. Microvasc Res. 2009;77(1):39–45.

Ware LB, Fang X, Matthay MA. Protein C and thrombomodulin in human acute lung injury. Am J Physiol Lung Cell Mol Physiol. 2003;285(3):L514–21.

Wilson MR, O'Dea KP, Zhang D, Shearman AD, van Rooijen N, Takata M. Role of lung-marginated monocytes in an in vivo mouse model of ventilator-induced lung injury. Am J Respir Crit Care Med. 2009;179(10):914–22.

Witzenbichler B, Westermann D, Knueppel S, Schultheiss HP, Tschope C. Protective role of angiopoietin-1 in endotoxic shock. Circulation. 2005;111(1):97–105.

Witzenrath M, Gutbier B, Owen JS, Schmeck B, Mitchell TJ, Mayer K, et al. Role of platelet-activating factor in pneumolysin-induced acute lung injury. Crit Care Med. 2007;35(7):1756–62.

Witzenrath M, Gutbier B, Schmeck B, Tenor H, Seybold J, Kuelzer R, et al. Phosphodiesterase 2 inhibition diminished acute lung injury in murine pneumococcal pneumonia. Crit Care Med. 2009;37(2):584–90.

Wolfson RK, Chiang ET, Garcia JG. HMGB1 induces human lung endothelial cell cytoskeletal rearrangement and barrier disruption. Microvasc Res. 2011;81(2):189–97.

Wong MP, Chan SY, Fu KH, Leung SY, Cheung N, Yuen ST, et al. The angiopoietins, tie2 and vascular endothelial growth factor are differentially expressed in the transformation of normal lung to non-small cell lung carcinomas. Lung Cancer. 2000;29(1):11–22.

World-Health-Organisation. (2013) The 10 leading causes of death in the world, 2000 and 2011. www.who.int/mediacentre/factsheets/fs310/en. Accessed -16. Aug. 2013.

Xu J, Qu J, Cao L, Sai Y, Chen C, He L, et al. Mesenchymal stem cell-based angiopoietin-1 gene therapy for acute lung injury induced by lipopolysaccharide in mice. J Pathol. 2008;214(4):472–81.

Yatomi Y, Ruan F, Hakomori S, Igarashi Y. Sphingosine-1-phosphate: a platelet-activating sphingolipid released from agonist-stimulated human platelets. Blood. 1995;86(1):193–202.

Yin J, Hoffmann J, Kaestle SM, Neye N, Wang L, Baeurle J, et al. Negative-feedback loop attenuates hydrostatic lung edema via a cGMP-dependent regulation of transient receptor potential vanilloid 4. Circ Res. 2008;102(8):966–74.

Yoshida K, Kondo R, Wang Q, Doerschuk CM. Neutrophil cytoskeletal rearrangements during capillary sequestration in bacterial pneumonia in rats. Am J Respir Crit Care Med. 2006;174(6):689–98.

Zanotti G, Casiraghi M, Abano JB, Tatreau JR, Sevala M, Berlin H, et al. Novel critical role of Toll-like receptor 4 in lung ischemia-reperfusion injury and edema. Am J Physiol Lung Cell Mol Physiol. 2009;297(1):L52–L63.

Zarbock A, Singbartl K, Ley K. Complete reversal of acid-induced acute lung injury by blocking of platelet-neutrophil aggregation. J Clin Invest. 2006;116(12):3211–9.

Zhao Y, Gorshkova IA, Berdyshev E, He D, Fu P, Ma W, et al. Protection of LPS-induced murine acute lung injury by sphingosine-1-phosphate lyase suppression. Am J Respir Cell Mol Biol. 2011;45(2):426–35.

Ziegler T, Horstkotte J, Schwab C, Pfetsch V, Weinmann K, Dietzel S, et al. Angiopoietin 2 mediates microvascular and hemodynamic alterations in sepsis. J Clin Invest. 2013;123(8):3436–45.

# Chapter 9
# Lung Transplantation and the Blood-Gas Barrier

**Anke Schnapper and Matthias Ochs**

**List of Abbreviations**

| | |
|---|---|
| ALI | Acute lung injury |
| AMR | Acute antibody-mediated rejection |
| ARDS | Acute respiratory distress syndrome |
| BAL | Bronchoalveolar lavage |
| BGB | Blood-gas barrier |
| BOS | Bronchiolitis obliterans syndrome |
| C4d | Complement 4d |
| CICD | Caspase-independent cell death |
| CLAD | Chronic lung allograft dysfunction |
| DBD | Donated after brain death |
| DCD | Donated after cardiac death |
| DSA | Donor-specific antibodies |
| ECMO | Extracorporal membrane oxygenation |
| EVLP | Ex vivo lung perfusion |
| $FEV_1$ | Forced expiratory volume in 1 s |
| IR | Ischemia-reperfusion |
| ISHLT | International Society for Heart and Lung Transplantation |
| LPD | Low-potassium dextran |
| NHBD | Non-heart-beating donors |
| NK | Natural killer cells |
| NO | Nitric oxide |

A. Schnapper (✉) · M. Ochs
Institute of Functional and Applied Anatomy, Hannover Medical School, Carl-Neuberg-Str. 1, 30625 Hannover, Germany
e-mail: Schnapper.Anke@mh-hannover.de

M. Ochs
e-mail: Ochs.Matthias@mh-hannover.de



A. N. Makanya (ed.), *The Vertebrate Blood-Gas Barrier in Health and Disease,*
DOI 10.1007/978-3-319-18392-3_9

| | |
|---|---|
| OB | Obliterative bronchiolitis |
| PEEP | Positive end-expiratory pressure |
| PGD | Primary graft dysfunction |
| PVR | Pulmonary vascular resistance |
| RAS | Restrictive allograft syndrome |
| ROS | Reactive oxygen species |
| SA/LA ratio | Small aggregate to large aggregate ratio |
| SP | Surfactant protein |
| TLC | Total lung capacity |

## 9.1 Introduction

Today, lung transplantation is a well-established treatment for patients with end-stage lung disease. In 2011, 3640 lung transplantations had been performed in more than 150 centers worldwide (Yusen et al. 2013). The integrity of the blood-gas barrier (BGB) is the center of concern during and after lung transplantation. It is subjected to a multitude of stressors during the transplantation process and thus is in great danger of injury in particular in the immediate transplantation and posttransplantation period.

## 9.2 Evaluation of BGB Function After Transplantation

### *9.2.1 Physiological and Biochemical Parameters*

Evaluation of the functional integrity of the BGB is indispensable in clinical lung transplantation to monitor the outcome and optimize postoperative patient care. Comparable fundamental evaluation parameters are used in experimental lung transplantation, usually complemented by valuable aim-specific parameters. The most commonly used evaluation parameters are discussed below.

The most important and straightforward physiological parameter regarding BGB function in both experimental and clinical lung transplantation is pulmonary oxygenation capacity, expressed as arterial partial pressure of oxygen in relation to the fraction of inspired oxygen ($PaO_2/FiO_2$; Christie et al. 2005a; Cypel et al. 2012; Knudsen et al. 2012; Yeung and Keshavjee 2014). This parameter summarizes the functional capability of the total organ and represents the most relevant pulmonary output for the organism. However, as $PaO_2$ is dependent on alveolar ventilation, diffusion, and perfusion (Ochs and O'Brodovich 2012), it is a parameter not exclusively correlated to direct BGB function. Impairment of alveolar ventilation or a ventilation–perfusion mismatch rather affects the BGB in an indirect way: They render non-ventilated or non-perfused parts of the barrier nonfunctional.

Biomechanical properties of the lung are associated with BGB integrity. Pulmonary edema negatively correlates with lung compliance and thus alters the ventilation parameters particularly recorded during mechanical ventilation (peak airway pressure, plateau airway pressure, mean airway pressure, necessary positive end-expiratory pressure; Dreyer et al. 2008; Cypel et al. 2009b; Meers et al. 2011; Knudsen et al. 2012; Wallinder et al. 2012; George et al. 2013). In return, elevated airway pressures can lead to barotrauma at the BGB (Oczenski 2008).

Lung perfusion and the condition of the pulmonary vasculature are mutually interdependent of BGB functionality. Pulmonary artery pressure and pulmonary vascular resistance (PVR) are commonly assessed in transplantation studies (Dreyer et al. 2008; Mühlfeld et al. 2009; Meers et al. 2011; Wallinder et al. 2012; George et al. 2013).

As a surrogate marker for lung edema formation, the wet weight of the total lung or a tissue sample is compared to the weight after drying (wet/dry ratio; Okada et al. 2000; Warnecke et al. 2001; Yang et al. 2009; Meers et al. 2011).

Bronchoalveolar lavage (BAL) material is used for biochemical and biophysical surfactant analysis. Surfactant composition, that is, small aggregate to large aggregate ratio (SA/LA ratio), phospholipid and surfactant protein content as well as surface tension give information about the surfactant function which is essential for BGB integrity (Veldhuizen et al. 1996; Warnecke et al. 2001; Strüber et al. 2002, 2007; Ochs 2006, 2010). Additionally, protein content, cellular composition (leukocyte infiltration), and cytokine expression in BAL fluid can give valuable information (Yang et al. 2009).

### *9.2.2 Structural Parameters*

To obtain direct information about the condition of the BGB, various imaging methods are available and indispensable for a more detailed analysis.

Light microscopy gives valuable information on the integrity of lung parenchyma, including atelectasis, microatelectasis, intra-alveolar edema, peribronchovascular edema, and evaluation of alveolar septa (Mühlfeld et al. 2007, 2009; Dreyer et al. 2008; Aoyama et al. 2009; Cypel et al. 2009b; Meers et al. 2011; Knudsen et al. 2012). However, structural details of the BGB are beyond the resolution of light microscopy. Electron microscopical evaluation can discriminate between alterations of alveolar epithelium, septal interstitium, and capillary endothelium. Additionally, surfactant subtypes can be distinguished (Ochs et al. 1999; Mühlfeld et al. 2007, 2009, 2010; Dreyer et al. 2008, Knudsen et al. 2012).

A quantitative assessment of lung structure is often essential as the quantity of structural alterations correlates with the quantity of functional impairment. The gold standard for quantitative lung structure analysis is represented by stereology (Hsia et al. 2010). Stereology allows for a quantitative characterization of 3D objects based on measurements in 2D sections. It gives unbiased estimations using geometric probes (Weibel et al. 2007). Stereology can be applied to the analysis of

histological and ultrastructural samples, as well as to in vivo imaging methods, for example, computed tomography, magnetic resonance imaging, and positron emission tomography (Hsia et al. 2010). The requirements for stereological evaluation include adequate fixation (preferably vascular perfusion or instillation) and tissue processing. To ensure results representative for the whole organ, samples are generated by the method of systematic uniform random sampling. The availability of the total lung as a reference space and for unbiased sampling is of importance (Ochs 2006, 2010; Weibel et al. 2007). Thus, a complete stereological analysis on histological and ultrastructural level is only possible in experimental transplantation, but selected parameters can also be analyzed in clinical biopsy material. Informative stereological parameters regarding the integrity of the BGB are: cell volumes and cell numbers of different cell types in the alveolar septum, volumes of intra-alveolar, septal and peribronchovascular edema, volumes of intra-alveolar and intracellular surfactant forms, surface fractions of normal, swollen, and fragmented BGB components as well as arithmetic mean thickness and/or harmonic mean thickness of the BGB and its components (Weibel and Knight 1964; Fehrenbach et al. 2001; Ochs 2006, 2010; Weibel et al. 2007).

## 9.3 Blood-Gas Barrier Stress During Transplantation

During all phases of lung transplantation, the BGB is subjected to a considerable amount of stress which may lead to its injury or even failure.

Depending on inherent donor criteria, lungs are differentially susceptible to transplantation stress. Criteria associated with a higher risk of graft dysfunction include donor age >45 years, female gender, and a smoking history >10 pack years (Lee and Christie 2010). Terminally acquired risk factors are direct lung/chest trauma and aspiration. In the potential donor, the BGB may be damaged during intensive care due to prolonged mechanical ventilation with subsequent ventilator-induced lung injury and oxygen toxicity. Fluid therapy, in particular volume overload, can induce lung edema already at this time point (Yeung and Keshavjee 2014).

The classic organ donor is the brain-dead patient, though attempts are made to use the lungs donated after cardiac death, and living donor lobar lung transplantation is rarely performed. (The International Society for Heart & Lung Transplantation 2014). The brain death process itself represents a major stressor for the BGB. Brain death evokes a systemic inflammatory response, a “cytokine storm,” which alone can cause lung injury up to acute respiratory distress syndrome (ARDS; Yeung and Keshavjee 2014). In a rat brain death model, a massive rise of macrophage-related (IL-1, IL-6, TNF-α) and Th1-related (IL-2, INF-γ) cytokine mRNA expression was noted in various organs including lungs (Takada et al. 1998). In brain-dead patients, plasma IL-6, soluble TNF receptor II, and soluble IL2-receptor were elevated (Lopau et al. 2000). Gene expression profiles differed between lungs donated after brain death (DBD) and after cardiac death (DCD). Upregulated gene sets in DBD lungs mapped to innate immunity, intracellular signalling, cytokine interaction, cell

communication, and apoptosis pathways, and the transcripts were correlated with IL-6, IL-8, and IL-1 levels. In contrast, gene sets in DCD lungs did not map to functional pathways (Kang et al. 2011). A functional association of elevated serum and BAL cytokine levels (IL-1β, CINC-1, CINC-3, TNF-α) with impaired oxygenation, higher peak airway pressure, PVR, and graft water index in lungs from brain-dead donors was demonstrated in a rat lung transplantation model (Avlonitis et al. 2007). Likewise, a "catecholamine storm" is described during brain death. Serum epinephrine and norepinephrine concentrations increased, accompanied by a rise of angiotensin II and plasma renin activities (Lopau et al. 2000). This resulted in systemic hypertension and was correlated to interstitial edema and alveolar hemorrhage (Yeung and Keshavjee 2014) as well as poor oxygenation and elevated airway pressures and PVR (Avlonitis et al. 2007).

The time period after brain death until explantation surgery is at the crossroads between further organ damage and optimal organ preservation and even offers the opportunity to attenuate preceding injury (see Sect. 9.4.3.1 "Donor Selection and Management"). Optimal organ conservation focuses on lung-protective ventilation and a balanced hemodynamic management. The latter is challenging in a prospective multiorgan donor since lung preservation requires a rather restrictive fluid management to prevent edema formation, while the other organs, for example, kidneys, require sufficient volume to ensure adequate organ perfusion (Munshi et al. 2013).

Lung procurement surgery is critical to lung preservation as it stands at the starting point and sets its conditions. Immanent stressors comprise flush conditions (solution composition, volume, pressure) and lung inflation upon explantation (pressure/volume, gas composition). Much effort has been put into minimizing organ damage and optimizing preservation at this point, and work in this field is still ongoing (Munshi et al. 2013).

Being eponymous for ischemia-reperfusion (IR) injury, ischemia imposes well-recognized stress on the allograft. Today's standard in clinical lung transplantation is cold static preservation, that is, the explanted, inflated lung is transported and stored in a cold preservation solution until implantation. In contrast to other organs, the hypothermic ischemic state allows for a reduced aerobic metabolism due to the alveolar oxygen reservoir for a limited time period (Date et al. 1993). Ischemic times greater than 6–8 h are associated with the occurrence of early graft dysfunction and reduced short- and long-term survival in clinical lung transplantation (Thabut et al. 2005). In the case of using lungs from non-heart-beating donors (NHBD), a period of warm ischemia is added before organ retrieval. Around 1 h is often considered as a landmark before major cellular damage occurs; however, evidence is limited regarding tolerable periods of warm ischemia (Steen et al. 2001; Van de Wauwer et al. 2009; Aoyama et al. 2009).

In the recipient, reperfusion of the allograft is the cardinal event. It is the single most important stressor during the transplantation process (Ng et al. 2006). Earlier cell injury manifests at this time point and/or renders transplants more susceptible to reperfusion stress (Stammberger et al. 2000; Yeung and Keshavjee 2014). During reperfusion, metabolic activity of resident lung cells is resumed, which at the

beginning can be unbalanced and is influenced by previous damage, resulting in the generation of reactive oxygen species (ROS), lipid peroxidation, and activation of inflammatory signaling pathways (den Hengst et al. 2010). Moreover, recipient inflammatory cell infiltration occurs and perpetuates the inflammatory cascade (Eppinger et al. 1997). Finally, postoperative intensive care management and possible complications (mechanical ventilation, aspiration, and infection) influence the allograft BGB integrity (Yeung and Keshavjee 2014).

## 9.4 IR Injury and the BGB

### *9.4.1 Definition, Incidence, and Clinical Relevance*

Most or even all lungs will have some degree of injury after transplantation due to the sum of stressors during the transplantation procedure. Focusing on the sequence of events and pathogenesis, it is usually referred to as IR injury in the preclinical setting (Christie et al. 2005a; Ochs 2006). Severe forms of injury manifest clinically as an acute organ dysfunction. On the consensus of the International Society for Heart and Lung Transplantation (ISHLT) Working Group, the syndrome has been termed primary graft dysfunction (PGD) in the clinical context and graded according to clinical parameters (Table 9.1; Christie et al. 2005a).

As PGD represents a special form of acute lung injury (ALI), oxygenation thresholds for PGD grading have been set analogous to those of ALI/ARDS. PGD is the major cause of early morbidity and mortality after lung transplantation (Yusen et al. 2013). Grade 3 PGD occurs after 10–30 % of lung transplantations with a 30-day mortality rate up to 60 % in these patients (Christie et al. 2005c; Diamond et al. 2013).

### *9.4.2 Morphology and Physiology of IR Injury*

Apart from the two defining criteria for PGD, impaired oxygenation ($PaO_2/FiO_2$), and radiographically visible pulmonary edema, several other global physiological lung function parameters are altered due to IR injury such as elevation of airway

**Table 9.1** ISHLT grading score for PGD (primary graft dysfunction). (Christie et al. 2005a)

| PGD grade | $PaO_2/FiO_2$ | Pulmonary edema, radiographic |
|---|---|---|
| 0 | >300 | − |
| 1 | >300 | + |
| 2 | 200–300 | + |
| 3 | <200 | + |

*$PaO_2/FiO_2$* pressure of oxygen in relation to fraction of inspired oxygen

pressures, reduction in lung compliance, and increase in PVR and pulmonary artery pressure (Fiser et al. 2001; Warnecke et al. 2001; Strüber et al. 2002; Zhao et al. 2006, 2011; Mühlfeld et al. 2009; Yang et al. 2009; Knudsen et al. 2012).

The BGB is the structural and functional entity of the lung, which is directly and mainly affected by IR injury. Additionally, pre- and post-barrier blood vessels are involved. Subsequently, interstitial and intra-alveolar alterations develop.

IR injury is characterized by cellular and structural damage as well as functional impairment of the BGB. It affects all components of the BGB but with differential distribution regarding cause, effects, time scale, and localization.

#### 9.4.2.1 Alveolar Epithelium

A common finding in IR injury was swelling and necrosis of type I alveolar epithelial cells (Fehrenbach et al. 2000; Ochs 2006; Mühlfeld et al. 2009). Due to swelling, the thickness of the alveolar epithelium increased in a rat IR model by 27% (Mühlfeld et al. 2009). IR injury could also induce severe epithelial damage with epithelial fragmentation (Fig. 9.1a) and thus denudation of underlying parts of the basal lamina (Fehrenbach et al. 2000; Ochs 2006; Mühlfeld et al. 2009). Functional perturbation of alveolar epithelial cells was shown in a rat transplantation model to correlate with the level of IR injury. $Na^+/K^+$-ATPase, which is located on the basolateral surface of alveolar epithelial cells, is involved in the regulation of pulmonary edema formation and particularly in edema resolution. In moderate IR injury, $Na^+/K^+$-ATPase mRNA was upregulated and protein expression unchanged, while in severe IR injury both $Na^+/K^+$-ATPase mRNA and protein significantly decreased (Kim et al. 2000).

Ultrastructural changes in type II alveolar epithelial cells following IR injury in rat models include cell swelling (larger total volume and number-weighted mean volume), volume increase of nucleus and mitochondria, which also present with electron translucent matrix, and dilatation of endoplasmatic reticulum (Fehrenbach et al. 1998a, 2000; Dreyer et al. 2008).

Lamellar bodies as the surfactant-synthesizing cell organelles became smaller after IR injury with a high variability in size (Fehrenbach et al. 1998a; Dreyer et al. 2008). This was in contrast to ALI due to lipopolysaccharide (LPS) stimulation, also in a rat model, which resulted in larger lamellar bodies (Fehrenbach et al. 1998a). The effect of IR injury on the number of lamellar bodies per type II cell gave conflicting results. They were found to either increase or decrease, and the latter was attributed to exocytosis into the alveolar lumen (Dreyer et al. 2008, Knudsen et al. 2011).

In canine type II cells, lipid body formation was noted already early in the phase of cold ischemia. Lipid bodies are regarded as organelles for eicosanoid synthesis, and in vitro studies have demonstrated eicosanoid generation in type II cells (Grimminger et al. 1992; Ochs et al. 2004). Specifically in type II cells, lipid bodies could provide fatty acid substrates for surfactant synthesis (Ochs et al. 2004). Surfactant proteins (SP) A and D play a role in innate immunity and immunomodulation. Low levels of SP-A mRNA measured in human donor lung biopsies before transplantation

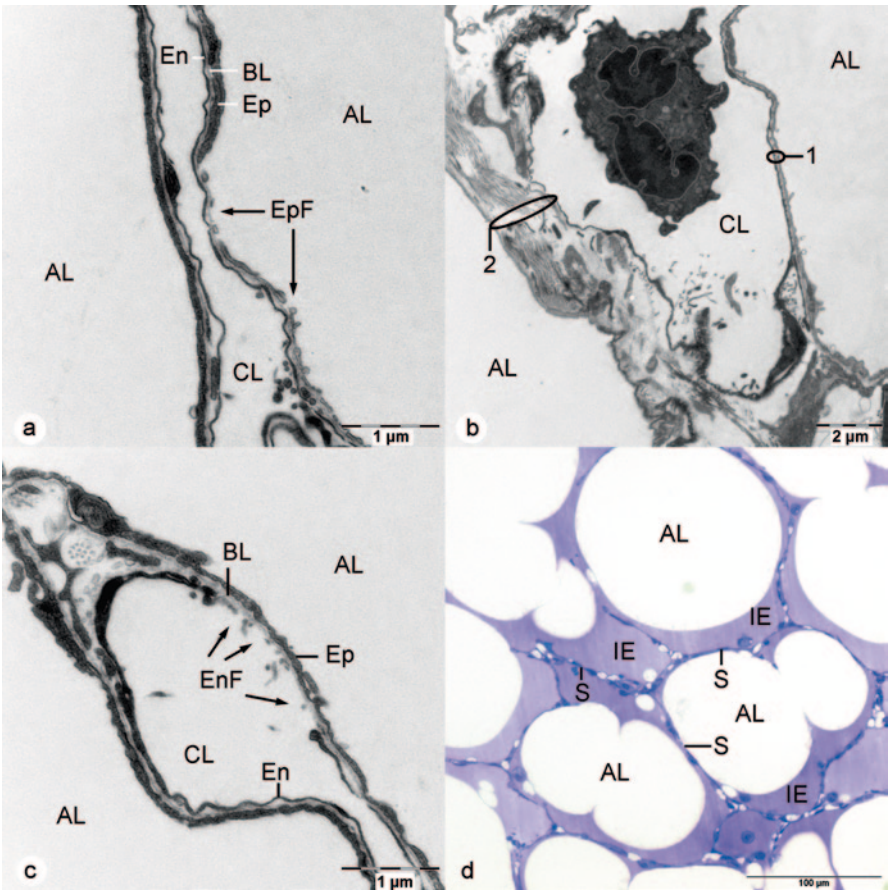


**Fig. 9.1** IR injury, **a-c** rat, **d** pig. **a** An alveolar septum separates two alveoli and encloses a capillary. The alveolar epithelium is fragmented and indicates BGB damage. **b** Alveolar septum with thin *(1)* and thick *(2)* side of the BGB. The thin side consisting of alveolar epithelium, basal lamina, and capillary endothelium is unaltered. The thick side contains interstitium, which is interposed between alveolar epithelium and capillary endothelium, and shows edematous swelling. **c** Within an alveolar septum, the BGB presents with fragmentation of the capillary endothelium. **d** Intra-alveolar edema: Alveolar lumina are partially filled with edema fluid which lines the alveolar septa and thus increases the width of the BGB. *AL* alveolar lumen, *CL* capillary lumen, *Ep* alveolar epithelium, *BL* basal lamina, *En* capillary endothelium, *EpF* epithelial fragmentation, *EnF* endothelial fragmentation, *IE* intra-alveolar edema, *S* alveolar septum

were related with a trend towards lower SP-A protein expression in BAL post transplantation and were associated with reduced survival of recipients and a greater incidence of acute allograft rejection. The level of SP-A expression in the donor lung correlated with the genotype $1A1A^0$ in SP-A2 polymorphism (D'Ovidio et al. 2013). Following lung injury, type II cells synthesize proinflammatory cytokines and chemokines (Sato et al. 2002; Vanderbilt et al. 2003). Thus, type II cells are involved in several ways in the inflammatory response of IR injury, and the formation

of lipid bodies is regarded as a morphological sign of activation of proinflammatory pathways (Ochs et al. 2004).

Fehrenbach et al. (Fehrenbach et al. 1998b) studied the non-transplanted contralateral lungs in 12 cases of clinical single-lung transplantation. These lungs had been exposed to all the potential donor-, explantation-, preservation-, and ischemia-related noxae, but not to reperfusion. The duration of donor intubation was correlated with swelling of total cells, nuclei, cytoplasm, and mitochondria of type II cells. Interestingly, in cases where the transplanted lung developed PGD, type II cells in the contralateral lung were characterized by larger lamellar bodies and also contained lipid bodies.

Finally, IR injury can result in apoptosis of alveolar epithelial type II cells in both experimental models and clinical lung transplantation, where type II cells were the main lung cell type affected (Fischer et al. 2000a; Knudsen et al. 2011).

#### 9.4.2.2 Surfactant

The functional pool of surfactant is represented by intra-alveolar surfactant after exocytosis of lamellar bodies from alveolar epithelial type II cells. Inactivation of intra-alveolar surfactant is both the cause and the effect of IR injury and intra-alveolar edema formation (Ochs et al. 1999).

IR injury reduced the amount of active forms of intra-alveolar surfactant, in particular tubular myelin, and increased the amount of inactive forms (unilamellar vesicles; Ochs et al. 2000; Mühlfeld et al. 2010). Tubular myelin in injured lungs was organized into larger and wider lattices than in control lungs. In noninjured lungs, 93% of tubular myelin was found in direct proximity of the alveolar epithelium, while IR injured lungs had only 14% in this location, and the major part was found displaced into the alveolar lumen. The integrity of tubular myelin after ischemia and reperfusion was associated with a higher parenchymal air space and improved oxygenation (Fehrenbach et al. 2000).

The quantitative finding of a lower parenchymal air space was accompanied by the qualitative finding of microatelectases and is an indicator of less efficient stabilization of alveoli at end-expiration and less effective surfactant function (Knudsen et al. 2012). Atelectases/microatelectases render the BGB nonfunctional in these areas due to a lack of alveolar ventilation. Additionally, the BGB may be damaged directly in atelectatic areas. Rhythmic collapse and reopening of alveoli during the ventilation cycle impose high shear stress upon the alveolar wall. During alveolar collapse, surfactant is compressed and squeezed out of the alveoli, an event that promotes further atelectasis formation (Verbrugge et al. 2007). Since not only functional but also nutritive oxygen supply of alveolar septa is by direct diffusion from the alveolar space (Ochs and O'Brodovich 2012), the BGB will be affected by hypooxygenation in permanently collapsed alveoli.

#### 9.4.2.3 Septal Interstitium

The thick side of the BGB contains a small amount of connective tissue between epithelial and endothelial cell layers. Septal interstitium comprises several subpopulations of fibroblasts/fibrocytes, elastic fibers, few collagen fibers, and amorphous ground substance; thus, it conveys mechanical stability to the alveolar septa, as well as being a site of fluid exchange (Ochs and O'Brodovich 2012). In rat models, the alveolar septal interstitium was swollen after IR injury (see Fig. 9.1b), leading to an increased thickness of this BGB component (Fehrenbach et al. 1999; Mühlfeld et al. 2009). The interstitial width more than doubled in a model of severe IR injury (oxygenation comparable to grade 3 PGD), which was the largest relative increase in thickness of all three BGB layers (Mühlfeld et al. 2009).

#### 9.4.2.4 Endothelium

On the endothelial side of the BGB, cell swelling was also noted after IR injury, resulting in an increase of mean arithmetic endothelial thickness by 42 % (Ochs 2006; Mühlfeld et al. 2009). Additionally, necrosis of capillary endothelial cells and denudation of the basal lamina was seen (Ochs 2006), cf. Figure 9.1c. In a rat lung transplantation model, apoptosis of endothelial cells was identified. A rise in caspases 3, 8, and 9 revealed that the intrinsic and extrinsic pathways were involved. Caspase activity increased already after lung flush during explantation (7 ×), and 17-fold after 6 h of cold ischemia, which suggested that apoptosis was initiated at a very early stage of the IR process (Quadri et al. 2005).

Pulmonary diffusion capacity is determined by Fick's law of diffusion; thus, it is inversely proportional to the thickness and directly proportional to the functional surface area of the BGB (Ochs 2006, Weibel et al. 2007). In this context, quantitative values of morphological BGB alterations must be interpreted.

For the BGB in total, intracellular and extracellular edema formation was a common finding in all three functional layers (Mühlfeld et al. 2009, Knudsen et al. 2012). A quantitative measure for the formation of septal edema is represented by an increase in BGB thickness (Ochs 2006). In a rat IR model, the mean thickness of the total BGB increased by 46 %. The fraction of swollen parts of the BGB amounted to 63 % of the alveolar surface area; additional 27 % were even fragmented. Such severe BGB damage was accompanied by extravasation of erythrocytes into alveolar air spaces (Mühlfeld et al. 2009). Since these quantitative values were obtained in a way representative for the whole lung, they become functionally relevant. Consequently, these morphological changes were associated with oxygenation values comparable to PGD grade 3 lungs (Mühlfeld et al. 2009).

#### 9.4.2.5 Pulmonary Edema

Pulmonary edema is a defining symptom for IR injury (Mühlfeld et al. 2007; Knudsen et al. 2012) and is both the result and the cause of BGB damage. In IR-injured

lung, peribronchovascular, septal, and intra-alveolar edema (Fig. 9.1b and d) can be differentiated and quantified (Ochs et al. 1999, 2000; Fehrenbach et al. 2000; Mühlfeld et al. 2009).

After IR injury, microvascular permeability increased up to tenfold. Most permeability (52 %) was found in postalveolar venules. In contrast to noninjured lungs where prealveolar and alveolar vessels exhibited almost no permeability, in injured lungs these segments of microvasculature contributed 26 and 22 %, respectively, to total permeability (Khimenko and Taylor 1999; Ng et al. 2006). Regarding leakage from septal capillaries, also functional impairment of type I alveolar epithelial cells (Kim et al. 2000) must be taken into account. Permeability increase was shown to be biphasic in a model with peaks at 30 min and 4 h of reperfusion. The initial phase was governed by mediators originating from activated alveolar macrophages (TNF-α, IFN-γ, MCP-1), whereas the second phase depended on neutrophil recruitment and activation (Eppinger et al. 1997). Edema formation in IR-injured lung is further promoted by an increase in PVR, which rises mainly due to vasoconstriction in precapillary vessels and leads to higher blood pressures in the pulmonary circulation (Löckinger et al. 2001; Ng et al. 2006; Mühlfeld et al. 2009; Aoyama et al. 2009).

Pulmonary edema reduces the oxygenation capacity of the lung in several ways. Septal edema increases BGB thickness (see above). In addition, intra-alveolar edema fluid lining the alveolar wall contributes to barrier thickness. Completely flooded alveoli are excluded from gas exchange, and their alveolar wall is cut off from its nutritive oxygen supply. Extravasated plasma proteins and, in particular, fibrin monomers interfere with surfactant function, which further aggravates the primary surfactant dysfunction present in IR injury (Seeger et al. 1985; Ochs et al. 1999). Edema also alters the biomechanical ventilation characteristics of the lung. Lung compliance decreases, and thus airway pressures increase which, in return, may lead to pressure-induced damage or even rupture of alveolar septa (Verbrugge et al. 2007; Knudsen et al. 2012).

#### 9.4.2.6 Cell Death

Cell death within the allograft plays an important role in IR injury. Of the different forms of cell death, apoptosis has been studied most intensively with respect to IR injury. Lung biopsies taken in standard clinical lung transplantation revealed high numbers of apoptotic cells as determined by terminal deoxynucleotidyl transferase-mediated dUTP nick-end labeling (TUNEL) reaction. Almost no apoptosis was detected after ischemia alone; after implantation, the amount of apoptotic cells increased with reperfusion time from 16 (30 min) to 35 % after 120 min. In particular, type II alveolar epithelial cells were affected. However, the amount of TUNEL-positive cells was not significantly correlated with short-term clinical outcome, and the patients showed a normal recovery process as expected in standard clinical lung transplantation (Fischer et al. 2000a).

In contrast to human lung transplantation, apoptosis was detected predominantly in endothelial cells and intravascular lymphocytes in the rat (Quadri et al. 2005). In

two rat lung transplantation models, the extent and mode of cell death was related to cold ischemic time (Fischer et al. 2000b; Quadri et al. 2005). Minimal cell death was noted after 6 and 12 h of cold ischemia; significant numbers of mostly necrotic cells were found after 18 and 24 h of cold preservation (Fischer et al. 2000b). Caspase activities representing both the extrinsic and intrinsic apoptosis pathway (caspases 3, 8, and 9) increased after pulmonary flush and more intensively after 6 h of cold ischemia, but the activity was reduced to post-flush levels after 18 h of cold ischemia (Quadri et al. 2005). After 2 h of transplant reperfusion, about 30% dead cells were detected, independently of the duration of previous ischemic time. However, almost all dead cells were apoptotic in the 6- and 12-h ischemia groups, while most were necrotic in the 18- and 24-h ischemia groups. Only the percentage of necrotic cells, but not apoptotic cells or total amount of dead cells, was correlated with organ function ($PaO_2$; Fischer et al. 2000b). All three caspases exhibited very low levels of activity after reperfusion, but only at this time point and only in the 6-h ischemia group were TUNEL-positive cells visible. In contrast, lung function was severely impaired after 18 h cold ischemia and 2 h reperfusion (Quadri et al. 2005). This suggested that long periods of cold ischemia induced severe cell damage, which prohibited apoptosis but promoted necrosis or other cell death modes (Fischer et al. 2000b; Quadri et al. 2005). Interestingly, caspase inhibitors improved lung function in the 18-h ischemia group despite lower caspase activities after ischemia and a lack of TUNEL-positive cells after reperfusion, implying a role for apoptosis pathways in initiating cell death sequences even though the cells were forced into other cell death pathways later on (Quadri et al. 2005). Regarding the differentiation between apoptosis and other cell death modes, it has to be taken into account that the TUNEL reaction detects any type of DNA fragmentation and thus is not entirely specific for apoptosis (Van Cruchten and Van den Broeck 2002).

Cell death modes apart from apoptosis include nonapoptotic cell death, caspase-independent cell death (CICD), oncosis, autophagy, and necrosis (Van Cruchten and Van den Broeck 2002; Fink and Cookson 2005; Kroemer and Jäättelä 2005; Kroemer and Martin 2005; Tang et al. 2008; Mizushima et al. 2008). Their role in IR injury has not been studied intensively so far. Evidence is accumulating that they coexist with apoptosis during ALI/ARDS but each form may be of different importance according to the etiology of ALI/ARDS. Possibly, the distinction of death pathways could influence diagnosis and treatment (Tang et al. 2008). The relationship between the different death pathways is not entirely clear yet. The traditional concept of necrosis versus apoptosis has been challenged by two new models. The first model sees a continuous spectrum of cell death forms ranging from apoptosis to necrosis with the other dying processes in between (Leist and Jaattela 2001; Kroemer and Jäättelä 2005; Kroemer and Martin 2005). The second model proposes that necrosis represents the irreversible end point of cell death or even postmortem changes, independently of cell death mode (Majno and Joris 1995; Van Cruchten and Van den Broeck 2002; Fink and Cookson 2005).

#### 9.4.2.7 Inflammatory Cell Infiltration and Activation

An inflammatory response of the lung is central to the development of IR injury. Leukocyte involvement follows a biphasic pattern, first proposed by Eppinger et al. (1997). The first phase was found to occur within 30 min after reperfusion started and depended on the activation of graft pulmonary macrophages in rat and rabbit models. It was characterized by macrophage-associated cytokines (TNF-α, IFN-γ, MCP-1; Eppinger et al. 1997; Zhao et al. 2006) and attenuated by macrophage inhibition (Fiser et al. 2001; Naidu et al. 2003; Zhao et al. 2006). ROS and cytokines released from activated pulmonary macrophages were thought to be responsible for early vascular permeability increase. Furthermore, macrophage cytokines initiated neutrophil recruitment to the transplant (Eppinger et al. 1997).

The second phase of IR injury was detected within 4 h after reperfusion. It depended on the infiltration of the allograft with recipient neutrophils and their activation. Neutrophils accumulated in lung parenchyma and infiltrated the alveolar lumen with comparable findings in mouse, rat, rabbit, and dog (Adoumie et al. 1992; Eppinger et al. 1997; Fiser et al. 2001; Yang et al. 2009). Neutrophils are considered as end effectors of IR-induced tissue destruction by secretion of ROS, and proteases and neutrophil depletion significantly attenuated IR injury (Yang et al. 2009).

Parallel to or even preceding neutrophil accumulation, a moderate lymphocyte influx into lung parenchyma was recorded (Adoumie et al. 1992; Van Putte et al. 2005; Yang et al. 2009). The majority was identified as CD4+ T cells, and their activation correlated with the intensity of IR injury. The expression of TNF-α, IL-17, CCL3, and CXCL1 was attributed to this lymphocyte subset which is consistent with the antigen-independent mechanism of T cell activation (Yang et al. 2009). Further contributions to IR injury may come from natural killer cells. Natural killer cell (NK) cytotoxicity of BAL fluid peaked at 4 h of reperfusion (Adoumie et al. 1992).

#### 9.4.2.8 Mediators of IR Injury

The above cellular reactions described in IR injured lung are governed by a complex interplay of a large number of mediators that have been studied extensively. Table 9.2 summarizes the main groups of mediators, their cellular origin in IR-injured lungs if known, and their function within the signaling cascades leading to IR injury.

### *9.4.3 Prevention, Management, and Therapy of IR Injury*

Strategies for prevention or attenuation of IR injury have been oriented at the stressors in lung transplantation and identified mechanisms in IR injury development described above. Measures are undertaken at every step of lung transplantation

**Table 9.2** Mediators of IR injury

| Product | Cellular origin/cells involved in secretion | Functional significance | Reference |
|---|---|---|---|
| *Cytokines* | | | |
| IL-1β | | Neutrophil infiltration, vascular permeability ↑, edema, early stages of IR injury | Krishnadasan et al. 2003; Ng et al. 2006 |
| IL-8 | Alveolar macrophages | Increase after reperfusion, neutrophil migration and activation, IR injury | De Perrot et al. 2001a; de Perrot et al. 2002 |
| IL-10 | Endothelial cells | Elevated during ischemia, anti-inflammatory, apoptosis ↑, necrosis ↓, endogenous fibrinolysis | Okada et al. 2000; McRae et al. 2001; de Perrot et al. 2002; Fischer et al. 2003 |
| IL-12 | | Elevated during ischemia | De Perrot et al. 2002 |
| IL-17 | CD4+ T cells | Activation of alveolar macrophages and type II alveolar epithelial cells | Yang et al. 2009 |
| TNF-α | Alveolar macrophages, CD4+ T cells | Macrophage respiratory burst, neutrophil infiltration and activation, vascular permeability ↑ | Eppinger et al. 1997; Liu et al. 2000; Krishnadasan et al. 2003; Naidu et al. 2003; Zhao et al. 2006; Yang et al. 2009 |
| INF-γ | Alveolar macrophages | IR injury | Eppinger et al. 1997 |
| CCL2 (MCP-1) | Alveolar macrophages | IR injury | Eppinger et al. 1997; Zhao et al. 2006 |
| CCL3 (MIP-1α) | Alveolar macrophages, CD4+ T cells | IR injury | Naidu et al. 2003; Yang et al. 2009 |
| CXCL1 (GRO) | CD4+ T cells; type II alveolar epithelial cells | Neutrophil infiltration | Vanderbilt et al. 2003; Yang et al. 2009 |
| CXCL2 (MIP-2, CINC-2α) | Alveolar macrophages, type II alveolar epithelial cells | IR injury, neutrophil chemoattractant | Naidu et al. 2003; Vanderbilt et al. 2003; Zhao et al. 2006 |
| *NO-NOS* | | | |
| iNOS | Type II alveolar epithelial cells | NO release, platelet adhesion to endothelial cells, vasoconstriction, alveolar perfusion ↓ | Liu et al. 2000; Ovechkin et al. 2005 |
| eNOS | Endothelial cells | Prevention of platelet and neutrophil adhesion, vasodilatation | Liu et al. 2000; Weiss et al. 2009 |
| NO | | Controversial role in IR injury | Ovechkin et al. 2005; Botha et al. 2007 |

**Table 9.2** (continued)

| Product | Cellular origin/cells involved in secretion | Functional significance | Reference |
|---|---|---|---|
| *PAF* | Neutrophils, pulmonary macrophages, endothelial cells | PVR↑, edema, apoptosis induction | Iwazaki et al. 2001; Wittwer et al. 2001 |
| *Endothelin-1* | Endothelial cells, smooth muscle cells | Edema formation, PVR ↑, vasoconstriction | Mizutani et al. 1998 |
| *Plasminogen activator system* | | | |
| Tissue plasminogen activator t-PA | Endothelial cells | Microvascular thrombosis ↓, endogenous fibrinolysis ↑, microvascular permeability ↑, neutrophil extravasation | Okada et al. 2000; Zhao et al. 2011 |
| PAI | | Microvascular thrombosis ↑, endogenous fibrinolysis ↓ | Okada et al. 2000 |
| *Arachnoidonic acid derivatives* | | | |
| Leukotrienes $B_4$,$C_4$, $D_4$ | | IR injury | Shimizu et al. 1991; Palace et al. 1992; Su et al. 1993 |
| PGE1 | | Reduces IR injury, TNF-α, INF-γ, IL12 ↓, IL-10 ↑ | De Perrot et al. 2001b |
| PGE2, PGF1-α | | IR injury | Palace et al. 1992 |
| Thromboxane $B_2$ | | IR injury | Su et al. 1993; Sunose et al. 2001 |
| HETE, HPETE, HHT | | IR injury | Palace et al. 1992 |
| *Cell adhesion molecules* | | | |
| CD18 | Neutrophils | Neutrophil adhesion, neutrophil infiltration, capillary permeability ↑ | Moore et al. 1995 |
| I-CAM-1 | Endothelial cells | Neutrophil adhesion, neutrophil infiltration, capillary permeability ↑ | Moore et al. 1995 |
| P-selectin | Endothelial cells | Neutrophil adhesion, neutrophil infiltration, capillary permeability ↑, PVR ↑ | Moore et al. 1995; Naka et al. 1997 |

**Table 9.2** (continued)

| Product | Cellular origin/cells involved in secretion | Functional significance | Reference |
|---|---|---|---|
| *Transcription factors* | | | |
| NF-κB | | Expression of inflammatory cytokines and cell adhesion molecules, apoptosis, edema | Naidu et al. 2003 |
| *ROS* | Neutrophils, pulmonary macrophages | Tissue destruction, vascular permeability increase, lipid peroxidation, DNA damage | Eppinger et al. 1997; Akao et al. 2006; Weiss et al. 2009; den Hengst et al. 2010 |
| *Degrading enzymes* | | | |
| MMPs | Neutrophils | Degradation of endothelial basal lamina, capillary permeability ↑ | Soccal et al. 2000 |
| Myeloperoxidase | Neutrophils | ROS generation | Eppinger et al. 1997; Fiser et al. 2001; Naidu et al. 2003; Krishnadasan et al. 2003; Yang et al. 2009 |
| Phospholipase A2 | Alveolar macrophages | Surfactant degradation | Abe et al. 2004 |

*IR* ischemia-reperfusion, *NO* nitric oxide, *PVR* pulmonary vascular resistance, *PAI* plasminogen activator inhibitor, *ROS* reactive oxygen species, *MMP* matrix metalloproteinase

from donor through organ preservation to recipient. Recently, ex vivo techniques of lung preservation and reconditioning have emerged.

#### 9.4.3.1 Donor Selection and Management

To obviate donor-associated risk factors, a catalogue of quite restrictive standard criteria was developed for acceptance of donor lungs. Though generally helpful, they are a cause for the low utilization rate of donor lungs, which is only around 20–30 % and further aggravates the problem of serious donor shortage in lung transplantation (Yeung and Keshavjee 2014). Due to the need for a larger donor pool, attempts have been made to apply extended donor criteria, and studies have shown that carefully selected marginal lungs can be used without negative impact on transplantation outcome for the patient (Bhorade et al. 2000; Orens et al. 2003). A second strategy to expand the donor pool is the utilization of lungs from NHBD/donation after cardiac death. In contrast to other organs, the use of lungs from DCD donors is still limited to few transplant centers (Cypel and Keshavjee 2013). In particular, concerns regarding the risk of microvascular thrombosis in DCD lungs precluded a more widespread use so far. Promising results come from two large single-center studies which showed that lung function, the incidence of PGD, and both short- and long-term survival rates were equivalent in patients receiving DBD and DCD lungs (De Oliveira et al. 2010; Erasmus et al. 2010). The absence of brain-death-mediated lung injury could be an advantage of DCD over DBD donors (Kang et al. 2011; Cypel and Keshavjee 2013).

After declaration of brain death, a donor management aimed at the preservation of potential donor organs can be initiated. Treatment should be in the best interest of all organs (Rostron and Dark 2010; Munshi et al. 2013). For lung preservation, lung-protective ventilation with low tidal volumes, sufficient positive end-expiratory pressure (PEEP), and recruitment maneuvers is of particular importance (Paries et al. 2012; Parto et al. 2013; Minambres et al. 2014). Hemodynamic management with fluid restriction is recommended (Minambres et al. 2014). Intensive lung donor management increased the rate of lung donors from 20 to 50 % of DBD, without constraints in PGD or recipient survival (Minambres et al. 2014).

In Fig. 9.2, pharmacological substances are specified which are administered to the (brain-dead) donor prior to flushing to counteract the effects of brain death and/or prevent the initiation of injury cascades at this early time point during the transplantation process. Glucocorticoids and PGE1 are commonly used in clinical lung transplantation while the other agents have shown a protective effect mainly in experimental transplantation studies or extracorporal IR injury models (Moore et al. 1995; Eppinger et al. 1997; Stammberger et al. 1999; Itano et al. 2000; Iwazaki et al. 2001; Quadri et al. 2005; Gohrbandt et al. 2006; Weiss et al. 2009; Cypel et al. 2010; Lapar et al. 2011).

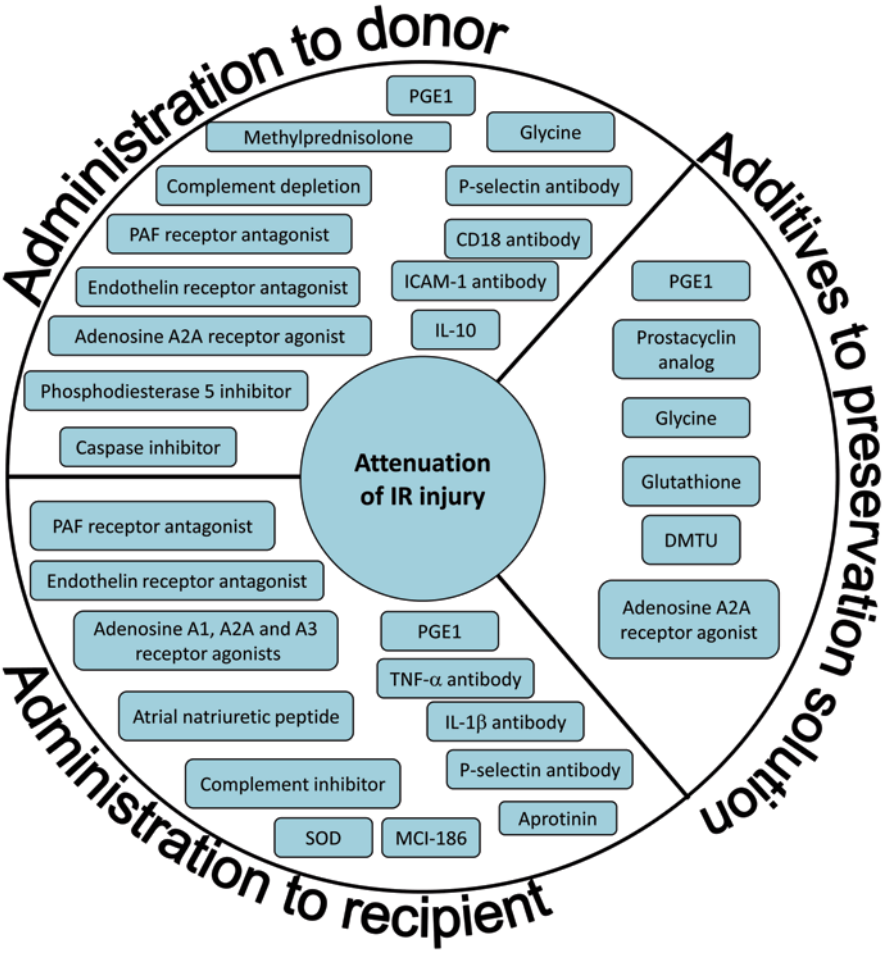


**Fig. 9.2** Additives to preservation solution and pharmacological agents administered to donor or recipient/reperfusion solution. The substances depicted here have been found to be effective in attenuating IR injury

### 9.4.3.2 Lung Preservation

**Preservation Solution** Lung preservation solutions play a prominent role in the prevention of IR injury in lung transplantation. The introduction of low-potassium dextran (LPD) solutions greatly improved the outcome of lung transplantation and was essential for its widespread successful clinical application. Several experimental and clinical studies have demonstrated a superior outcome of transplantation with regard to physiological and morphological parameters as well as a lower rate of PGD and better short- and long-term survival when using LPD solutions compared to Celsior, Euro-Collins, or other intracellular-type solutions

(Maccherini et al. 1991; Steen et al. 1994; Ingemansson et al. 1995; Strüber et al. 2001; Fischer et al. 2001; Mühlfeld et al. 2007).

**Preservation Technique** Retrograde flush perfusion at the time of lung procurement has been shown to convey an advantage over antegrade flush with respect to graft function after transplantation. This was attributed to additional perfusion of the bronchial arterial system and an improved clearance of thrombi from the pulmonary vascular bed (Strüber et al. 2002; Van de Wauwer et al. 2009). Today, antegrade flush perfusion and additional retrograde flush of the explanted organ are commonly used in clinical and experimental lung transplantation (Munshi et al. 2013).

**Additives to Preservation Solution** Pharmacological additives to preservation solution are administered at the time of flush perfusion during organ procurement and persist within the vascular bed during ischemia. Beneficial effects in prevention or reduction of IR injury were found for a variety of substances (Fig. 9.2; De Perrot et al. 2001c; Sommer et al. 2005; Gohrbandt et al. 2006; Chen et al. 2010).

**Additives to Ventilation Gas** Lung biology offers a second route for efficiently distributing drugs, which has been used successfully at pre-ischemic/donor or post-ischemic/recipient time points.

Instillation of exogenous surfactant preparations reduced IR injury as demonstrated by functional and structural parameters (Warnecke et al. 2001; Strüber et al. 2007; Dreyer et al. 2008; Mühlfeld et al. 2009,2010; Knudsen et al. 2012; Ohsumi et al. 2013). Surfactant preparations derived from modified natural porcine (Curosurf) or bovine (Survanta) surfactant and synthetic preparations revealed differential protective potential, with best results using Curosurf (Knudsen et al. 2012). Pre-ischemic application was more effective than post-ischemic instillation (Mühlfeld et al. 2009).

Recipient prophylactic inhalation of nitric oxide (NO) was studied in animal models and clinical trials with controversial results (Warnecke et al. 2001; Mulligan 2006; Botha et al. 2007). However, a positive effect on manifestation of PGD in clinical lung transplantation could not be demonstrated (Botha et al. 2007).

In further animal studies, attenuation of IR injury was achieved by ventilation with carbon monoxide (Kohmoto et al. 2007; Dong et al. 2013), aerolized PGE1 or prostaglandin analog (Löckinger et al. 2001), phosphodieesterase III inhibitor (Zhang et al. 2009), and IL-10 gene transfection (Fischer et al. 2003).

#### 9.4.3.3 Recipient Management

To ameliorate the manifestation of IR injury and prevent PGD, elaborate intensive-care management of the transplant recipient is necessary. Central concepts are lung-protective ventilation and restrictive fluid management (Mulligan 2006; Yeung and Keshavjee 2014). In the experimental setting, several approaches of prophylactic drug application to the recipient during reperfusion

or pharmacological additives to reperfusion solution in extracorporal models reduced the severity of IR injury (Fig. 9.2; Eppinger et al. 1997; Naka et al. 1997; Pierre et al. 1998; Stammberger et al. 1999; Iwazaki et al. 2001; de Perrot et al. 2001d; Krishnadasan et al. 2003; Keshavjee et al. 2005; Akao et al. 2006; Bittner et al. 2006; Sharma et al. 2009; Aoyama et al. 2009; Gazoni et al. 2010; Sharma et al. 2010; Lapar et al. 2011). However, none of them is routinely used in clinical lung transplantation to date due to a lack of clinical validation or severe side effects (Lee and Christie 2010).

Treatment of patients with manifest PGD is mainly supportive (Shargall et al. 2005; Mulligan 2006; Lee and Christie 2010; Suzuki et al. 2013). Specific interventions that have been found beneficial in clinical trials include NO inhalation (Date et al. 1996), complement inhibitor (Keshavjee et al. 2005), and C1-esterase inhibitor (Sommer et al. 2014). In severe cases, extracorporal membrane oxygenation (ECMO) can bridge a period of life-threatening hypoxia (Shargall et al. 2005; Yeung and Keshavjee 2014). Retransplantation has been performed in severe PGD, but the outcome is generally considered poor (Shargall et al. 2005; Lee and Christie 2010).

#### 9.4.3.4 Ex Vivo Lung Perfusion (EVLP)

One major constraint in lung transplantation is a serious shortage of donor lungs, largely due to the low utilization rate of 20–30 % of potential allografts (Yeung and Keshavjee 2014; Van Raemdonck et al. 2014). To increase the percentage of transplantable donor lungs, the new technique of EVLP has shown promising results in experimental and clinical application (Steen et al. 2003; Wierup et al. 2006; Cypel et al. 2009b, 2012; Cypel and Keshavjee 2011; Meers et al. 2011; Wallinder et al. 2012).

For EVLP, the lung is connected to a perfusion circuit that allows normothermic, antegrade perfusion via the pulmonary artery with a hyperoncotic, extracellular-type perfusion solution. The venous outflow from the left atrium is collected and recirculated. Additionally, lung-protective ventilation is executed (Steen et al. 2001; Wierup et al. 2006; Cypel and Keshavjee 2011; Van Raemdonck et al. 2014). For the procedure, either center-specific self-assembled circuits or one of the commercially available devices (Vivoline, XPS, Lung Assist, OCS) is in use. Depending on the device and transplantation center, protocols differ to some extent regarding perfusate, perfusion, and ventilation parameters (Steen et al. 2001; Wierup et al. 2006; Cypel and Keshavjee 2011; Wallinder et al. 2012; Van Raemdonck et al. 2014).

The EVLP period offers possibilities for evaluation, reconditioning, and injury-specific therapies of potential donor lungs. Functional assessment of oxygenation capacity, PVR and compliance, for example, enables transplant teams to identify acceptable lungs from the pool of marginal organs from DBD and to test lungs from uncontrolled DCD (Steen et al. 2001, 2003; Wallinder

et al. 2012; Cypel et al. 2012). Reconditioning, that is, ameliorating precedent lung injury can render lungs acceptable through edema reduction, wash-out of toxic substances, and alveolar recruitment (Wallinder et al. 2012; Van Raemdonck et al. 2014). First clinical experiences after the transplantation of originally unacceptable lungs, reconditioned and assessed by EVLP, demonstrated similar short-term outcomes compared to conventional transplantation (Ingemansson et al. 2009; Lindstedt et al. 2011; Cypel et al. 2012; Wallinder et al. 2012; Aigner et al. 2012; Dark et al. 2014).

Injury-specific treatment of donor lungs during EVLP is emerging. A case report described a successful transplantation after thrombolytic intervention during EVLP in an organ with confirmed pulmonary embolism (Machuca et al. 2013). Experimental studies further elucidate the potential of EVLP in preconditioning allografts against the manifestation of IR injury during the reperfusion period by additives to perfusate (plasmin (Motoyama et al. 2013), adenosine A2A receptor agonist (Emaminia et al. 2011)) or ventilation (IL-10 (Cypel et al. 2009a), and CO (Dong et al. 2013)).

### *9.4.4 Long-Term Effects of IR Injury*

PGD grade 3 patients not only have a high short-term mortality rate (40–60 % at 30 days) (Christie et al. 2005b; Christie et al. 2005c) but also significantly reduced long-term survival. Conditional on 90-day survival and 1-year survival, former PGD patients showed a higher mortality risk in subsequent years compared to the non-PGD group (Christie et al. 2005b; Huang et al. 2008). Physical performance, assessed as 6-min walk test distance, within 12 months after transplantation was significantly lower in the PGD group (Christie et al. 2005c). PGD was associated with a higher risk for the development of bronchiolitis obliterans syndrome (BOS), a major late complication in lung transplantation. The increase in relative risk of BOS was even demonstrable in lower-grade PGD and amounted to 1.9 (PGD grade 1), 2.3 (PGD grade 2), and 3.3 (PGD grade 3) compared to no PGD (Huang et al. 2008).

## 9.5 Acute Allograft Rejection and the BGB

To prevent lung transplant rejection, usually a three-drug regimen of immunosuppression is used postoperatively. It comprises corticosteroids, calcineurin inhibitors, and nucleotide blocking agents. About half of the lung transplant centers additionally use T cell depletion agents as initial induction therapy (Christie et al. 2012; Yeung and Keshavjee 2014).

Despite elaborate immunosuppression regimens, 33 % of the patients experience at least one episode of acute rejection within the first year after lung transplantation (Yusen et al. 2013). It is generally considered reversible (Sato 2013).

**Acute Cellular Rejection** It is classified as "Acute rejection Grade A" according to histopathologic criteria in the ISHLT working formulation (Stewart et al. 2007) and represents the most common form of acute rejection. Grade A rejection is mainly encountered between 2 and 9 months after transplantation but can occur any time from days to >10 years (Gordon and Husain 2010; Yusen et al. 2013). Per definition, grade A rejection is characterized by mononuclear cell infiltrates in perivascular tissues (Stewart et al. 2007). The BGB is affected only in moderate to severe cases (grades A3 and A4) when inflammatory cell infiltration extends into alveolar septa. Additionally, accumulations of intra-alveolar macrophages and type II cell hyperplasia can be found in grade A3. In grade A4, extensive damage of the alveolar epithelium as well as endothelialitis occurs. In the air spaces, necrotic epithelial cells, macrophages, neutrophils, hyaline membranes, and hemorrhage can be seen (Stewart et al. 2007).

"Airway inflammation Grade B" can occur alone or in combination with grade A rejection. It is characterized by mononuclear cell infiltrates around bronchioli (Stewart et al. 2007). The BGB is not involved.

**Acute Antibody-Mediated Rejection (AMR)** After lung transplantation, this form of rejection is rare. However, recent studies have demonstrated a growing interest in the pathologic processes involved in this entity (DeNicola et al. 2013; Berry et al. 2013; Witt et al. 2013; Lobo et al. 2013).

Today, pulmonary AMR is diagnosed on the basis of clinical allograft dysfunction, histopathology, capillary complement 4d (C4d) deposition, and circulating donor-specific antibodies (DSA). The BGB is a primary target of AMR. Histopathologic findings include diffuse alveolar damage, septal capillaritis, capillary neutrophilia, and hyaline membrane formation but are rather unspecific (Witt et al. 2013; DeNicola et al. 2013; Berry et al. 2013). When present, immunohistochemical staining with C4d antibodies as well as performing serology for DSA is recommended (Berry et al. 2013).

## 9.6 Chronic Lung Allograft Dysfunction (CLAD) and the BGB

The median survival time after lung transplantation is 5.6 years (Yusen et al. 2013). Long-term survival is limited by CLAD, an irreversible condition that affects approximately 50 % of the lung transplant recipients within 5 years posttransplantation (Sato 2013; Yeung and Keshavjee 2014). BOS has long been considered synonymous with chronic rejection and chronic allograft dysfunction. Only recently was the heterogeneous nature of CLAD recognized with BOS being

only one form of CLAD (Pakhale et al. 2005; Woodrow et al. 2010; Sato et al. 2011; Sato 2013). Since alloimmune-independent mechanisms contribute significantly to pathogenesis, the more restrictive term "chronic rejection" does not seem appropriate anymore, and CLAD is preferred (Sato 2013).

*BOS* comprises around 65–75 % of the cases with CLAD (Sato et al. 2011). BOS is characterized by irreversible obstructive changes in pulmonary function tests. The basis for a diagnosis of BOS is an irreversible decline in the forced expiratory volume in 1 s ($FEV_1$) ≤80 % of baseline values and a total lung capacity (TLC) >90 % of the baseline. The latter parameter is suitable to distinguish BOS from restrictive allograft syndrome (RAS; Sato et al. 2011). BOS represents the clinical surrogate diagnosis of the histological diagnosis of obliterative bronchiolitis (OB; Stewart et al. 2007; Sato 2013). Histological findings in OB include fibrous remodeling of the submucosa of bronchioli with various degrees of inflammation. Alterations can extend into peribronchiolar interstitium. The BGB is not affected (Stewart et al. 2007).

*RAS,* on the other hand, is a condition of peripheral lung structures and the BGB (Pakhale et al. 2005; Woodrow et al. 2010; Sato et al. 2011). It accounts for approximately 25–35 % of CLAD cases. Prognosis of RAS is much poorer than in BOS with a median survival time of 18 vs. 47 months after onset of graft dysfunction (Sato et al. 2011). Characteristic of RAS are restrictive alterations of lung physiology; thus, the clinical diagnosis of RAS is defined by an irreversible decrease in $FEV_1$ ≤80 % and a TLC <90 % of baseline values (Sato et al. 2011). Typical histologic findings in RAS comprise diffuse alveolar damage (new onset, later than 3 months after transplantation); fibrosis in the alveolar septal interstitium, interlobular septa, and pulmonary pleura; and high numbers of activated fibroblasts in peripheral lung tissues (Sato et al. 2011; Sato 2013). Both RAS and BOS are chronic inflammatory processes with alloimmune-dependent and alloimmune-independent factors (e.g., PGD, infections, gastroesophageal reflux, aspiration) contributing to their development (Sato 2013).

## 9.7 Final Remarks

The structural and functional integrity of the BGB is essential for the success of lung transplantation. Despite great efforts and progress in the immediate peritransplantation period, the development of IR injury remains a major challenge. Further research is needed in particular to elucidate pathogenetic mechanisms and to link structural and biochemical studies on a cellular and subcellular level. Regarding CLAD, forms affecting primarily the BGB are just coming into the focus of research.

## References

Abe A, Hiraoka M, Wild S, Wilcoxen SE, Paine R III, Shayman JA. Lysosomal phospholipase A2 is selectively expressed in alveolar macrophages. J Biol Chem. 2004;279:42605–11.

Adoumie R, Serrick C, Giaid A, Shennib H. Early cellular events in the lung allograft. Ann Thorac Surg. 1992;54:1071–6.

Aigner C, Slama A, Hotzenecker K, Scheed A, Urbanek B, Schmid W, et al. Clinical ex vivo lung perfusion–pushing the limits. Am J Transplant. 2012;12:1839–47.

Akao T, Takeyoshi I, Totsuka O, Arakawa K, Muraoka M, Kobayashi K, et al. Effect of the free radical scavenger MCI-186 on pulmonary ischemia-reperfusion injury in dogs. J Heart Lung Transplant. 2006;25:965–71.

Aoyama A, Chen F, Fujinaga T, Sato A, Tsuruyama T, Zhang J, et al. Post-ischemic infusion of atrial natriuretic peptide attenuates warm ischemia-reperfusion injury in rat lung. J Heart Lung Transplant. 2009;28:628–34.

Avlonitis VS, Wigfield CH, Golledge HD, Kirby JA, Dark JH. Early hemodynamic injury during donor brain death determines the severity of primary graft dysfunction after lung transplantation. Am J Transplant. 2007;7:83–90.

Berry G, Burke M, Andersen C, Angelini A, Bruneval P, Calabrese F, et al. Pathology of pulmonary antibody-mediated rejection: 2012 update from the Pathology Council of the ISHLT. J Heart Lung Transplant. 2013;32:14–21.

Bhorade SM, Vigneswaran W, McCabe MA, Garrity ER. Liberalization of donor criteria may expand the donor pool without adverse consequence in lung transplantation. J Heart Lung Transplant. 2000;19:1199–204.

Bittner HB, Richter M, Kuntze T, Rahmel A, Dahlberg P, Hertz M, et al. Aprotinin decreases reperfusion injury and allograft dysfunction in clinical lung transplantation. Eur J Cardiothorac Surg. 2006;29:210–5.

Botha P, Jeyakanthan M, Rao JN, Fisher AJ, Prabhu M, Dark JH, et al. Inhaled nitric oxide for modulation of ischemia-reperfusion injury in lung transplantation. J Heart Lung Transplant. 2007;26:1199–205.

Chen KH, Chao D, Liu CF, Chen CF, Wang D. Ischemia and reperfusion of the lung tissues induced increase of lung permeability and lung edema is attenuated by dimethylthiourea (PP69). Transplant Proc. 2010;42:748–50.

Christie JD, Carby M, Bag R, Corris P, Hertz M, Weill D. Report of the ISHLT Working Group on Primary Lung Graft Dysfunction part II: definition. A consensus statement of the International Society for Heart and Lung Transplantation. J Heart Lung Transplant. 2005a;24:1454–9.

Christie JD, Kotloff RM, Ahya VN, Tino G, Pochettino A, Gaughan C, et al. The effect of primary graft dysfunction on survival after lung transplantation. Am J Respir Crit Care Med. 2005b;171:1312–6.

Christie JD, Sager JS, Kimmel SE, Ahya VN, Gaughan C, Blumenthal NP, et al. Impact of primary graft failure on outcomes following lung transplantation. Chest. 2005c;127:161–5.

Christie JD, Edwards LB, Kucheryavaya AY, Benden C, Dipchand AI, Dobbels F, et al. The Registry of the International Society for Heart and Lung Transplantation: 29th adult lung and heart-lung transplant report-2012. J Heart Lung Transplant. 2012;31:1073–86.

Cypel M, Keshavjee S. Extracorporeal lung perfusion. Curr Opin Organ Transplant. 2011;16:469–75.

Cypel M, Keshavjee S. Strategies for safe donor expansion: donor management, donations after cardiac death, ex-vivo lung perfusion. Curr Opin Organ Transplant. 2013;18:513–7.

Cypel M, Liu M, Rubacha M, Yeung JC, Hirayama S, Anraku M, et al. Functional repair of human donor lungs by IL-10 gene therapy. Sci Transl Med. 2009a;1:4ra9.

Cypel M, Rubacha M, Yeung J, Hirayama S, Torbicki K, Madonik M, et al. Normothermic ex vivo perfusion prevents lung injury compared to extended cold preservation for transplantation. Am J Transplant. 2009b;9:2262–9.

Cypel M, Yeung JC, Keshavjee S. Preservation of the donor lung. In: Vigneswaran WT, Garrity ER, editors Lung transplantation. London: Informa healthcare; 2010. p. 115–24.
Cypel M, Yeung JC, Machuca T, Chen M, Singer LG, Yasufuku K, et al. Experience with the first 50 ex vivo lung perfusions in clinical transplantation. J Thorac Cardiovasc Surg. 2012;144:1200–6.
Dark JH, Karamanou D, Clark S, et al. Successful transplantation of unusable donor lungs using ex-vivo lung perfusion: The Newcastle experience. J Heart Lung Transplant. 2014;31:S115.
Date H, Matsumura A, Manchester JK, Cooper JM, Lowry OH, Cooper JD. Changes in alveolar oxygen and carbon dioxide concentration and oxygen consumption during lung preservation. The maintenance of aerobic metabolism during lung preservation. J Thorac Cardiovasc Surg. 1993;105:492–501.
Date H, Triantafillou AN, Trulock EP, Pohl MS, Cooper JD, Patterson GA. Inhaled nitric oxide reduces human lung allograft dysfunction. J Thorac Cardiovasc Surg. 1996;111:913–9.
De Oliveira NC, Osaki S, Maloney JD, Meyer KC, Kohmoto T, D'Alessandro AM, et al. Lung transplantation with donation after cardiac death donors: long-term follow-up in a single center. J Thorac Cardiovasc Surg. 2010;139:1306–15.
De Perrot M, Sekine Y, Fischer S, Waddell TK, McRae K, Liu M, et al. Interleukin-8 release during ischemia-reperfusion correlates with early graft function in human lung transplantation. J Heart Lung Transplant. 2001a;20:175–6.
De Perrot M, Fischer S, Liu M, Jin R, Bai XH, Waddell TK, et al. Prostaglandin E1 protects lung transplants from ischemia-reperfusion injury: a shift from pro- to anti-inflammatory cytokines. Transplantation. 2001b;72:1505–12.
De Perrot M, Fischer S, Liu M, Jin R, Bai XH, Waddell TK, et al. Prostaglandin E1 protects lung transplants from ischemia-reperfusion injury: a shift from pro- to anti-inflammatory cytokines. Transplantation. 2001c;72:1505–12.
De Perrot M, Fischer S, Liu M, Jin R, Bai XH, Waddell TK, et al. Prostaglandin E1 protects lung transplants from ischemia-reperfusion injury: a shift from pro- to anti-inflammatory cytokines. Transplantation. 2001d;72:1505–12.
De Perrot M, Sekine Y, Fischer S, Waddell TK, McRae K, Liu M, et al. Interleukin-8 release during early reperfusion predicts graft function in human lung transplantation. Am J Respir Crit Care Med. 2002;165:211–5.
Den Hengst WA, Gielis JF, Lin JY, Van Schil PE, De Windt LJ, Moens AL. Lung ischemia-reperfusion injury: a molecular and clinical view on a complex pathophysiological process. Am J Physiol Heart Circ Physiol. 2010;299:H1283–99.
DeNicola MM, Weigt SS, Belperio JA, Reed EF, Ross DJ, Wallace WD. Pathologic findings in lung allografts with anti-HLA antibodies. J Heart Lung Transplant. 2013;32:326–32.
Diamond JM, Lee JC, Kawut SM, Shah RJ, Localio AR, Bellamy SL, et al. Clinical risk factors for primary graft dysfunction after lung transplantation. Am J Respir Crit Care Med. 2013;187:527–34.
Dong B, Stewart PW, Egan TM. Postmortem and ex vivo carbon monoxide ventilation reduces injury in rat lungs transplanted from non-heart-beating donors. J Thorac Cardiovasc Surg. 2013;146:429–36.
D'Ovidio F, Kaneda H, Chaparro C, Mura M, Lederer D, Di AS, et al. Pilot study exploring lung allograft surfactant protein A (SP-A) expression in association with lung transplant outcome. Am J Transplant. 2013;13:2722–9.
Dreyer N, Mühlfeld C, Fehrenbach A, Pech T, von BS, Nagib R, et al. Exogenous surfactant application in a rat lung ischemia reperfusion injury model: effects on edema formation and alveolar type II cells. Respir Res. 2008;9:5.
Emaminia A, Lapar DJ, Zhao Y, Steidle JF, Harris DA, Laubach VE, et al. Adenosine A(2) A agonist improves lung function during ex vivo lung perfusion. Ann Thorac Surg. 2011;92:1840–6.
Eppinger MJ, Deeb GM, Bolling SF, Ward PA. Mediators of ischemia-reperfusion injury of rat lung. Am J Pathol. 1997;150:1773–84.

Erasmus ME, Verschuuren EA, Nijkamp DM, Vermeyden JW, van der Bij W. Lung transplantation from nonheparinized category III non-heart-beating donors. A single-centre report. Transplantation. 2010;89:452–7.

Fehrenbach H, Brasch F, Uhlig S, Weisser M, Stamme C, Wendel A, et al. Early alterations in intracellular and alveolar surfactant of the rat lung in response to endotoxin. Am J Respir Crit Care Med. 1998a;157:1630–9.

Fehrenbach H, Wahlers T, Ochs M, Brasch F, Schmiedl A, Hirt SW, et al. Ultrastructural pathology of the alveolar type II pneumocytes of human donor lungs. Electron microscopy, stereology, and microanalysis. Virchows Arch. 1998b;432:229–39.

Fehrenbach H, Schepelmann D, Albes JM, Bando T, Fischer F, Fehrenbach A, et al. Pulmonary ischemia/reperfusion injury: a quantitative study of structure and function in isolated heart-lungs of the rat. Anat Rec. 1999;255:84–9.

Fehrenbach A, Ochs M, Warnecke T, Wahlers T, Wittwer T, Schmiedl A, et al. Beneficial effect of lung preservation is related to ultrastructural integrity of tubular myelin after experimental ischemia and reperfusion. Am J Respir Crit Care Med. 2000;161:2058–65.

Fehrenbach A, Fehrenbach H, Wittwer T, Ochs M, Wahlers T, Richter J. Evaluation of pulmonary edema: stereological versus gravimetrical analysis. Eur Surg Res. 2001;33:270–8.

Fink SL, Cookson BT. Apoptosis, pyroptosis, and necrosis: mechanistic description of dead and dying eukaryotic cells. Infect Immun. 2005;73:1907–16.

Fischer S, Cassivi SD, Xavier AM, Cardella JA, Cutz E, Edwards V, et al. Cell death in human lung transplantation: apoptosis induction in human lungs during ischemia and after transplantation. Ann Surg. 2000a;231:424–31.

Fischer S, Maclean AA, Liu M, Cardella JA, Slutsky AS, Suga M, et al. Dynamic changes in apoptotic and necrotic cell death correlate with severity of ischemia-reperfusion injury in lung transplantation. Am J Respir Crit Care Med. 2000b;162:1932–9.

Fischer S, Matte-Martyn A, de PM, Waddell TK, Sekine Y, Hutcheon M, et al. Low-potassium dextran preservation solution improves lung function after human lung transplantation. J Thorac Cardiovasc Surg. 2001;121:594–6.

Fischer S, de Perrot M, Liu M, Maclean AA, Cardella JA, Imai Y, et al. Interleukin 10 gene transfection of donor lungs ameliorates posttransplant cell death by a switch from cellular necrosis to apoptosis. J Thorac Cardiovasc Surg. 2003;126:1174–80.

Fiser SM, Tribble CG, Long SM, Kaza AK, Cope JT, Laubach VE, et al. Lung transplant reperfusion injury involves pulmonary macrophages and circulating leukocytes in a biphasic response. J Thorac Cardiovasc Surg. 2001;121:1069–75.

Gazoni LM, Walters DM, Unger EB, Linden J, Kron IL, Laubach VE. Activation of A1, A2A, or A3 adenosine receptors attenuates lung ischemia-reperfusion injury. J Thorac Cardiovasc Surg. 2010;140:440–6.

George TJ, Arnaoutakis GJ, Beaty CA, Jandu SK, Santhanam L, Berkowitz DE, et al. A physiologic and biochemical profile of clinically rejected lungs on a normothermic ex vivo lung perfusion platform. J Surg Res. 2013;183:75–83.

Gohrbandt B, Fischer S, Warnecke G, Avsar M, Sommer SP, Haverich A, et al. Glycine intravenous donor preconditioning is superior to glycine supplementation to low-potassium dextran flush preservation and improves graft function in a large animal lung transplantation model after 24 h of cold ischemia. J Thorac Cardiovasc Surg. 2006;131:724–9.

Gordon IO, Husain AN. Post-transplant lung pathology. In: Vigneswaran WT, Garrity ER, editors Lung Transplantation. London: Informa healthcare; 2010. p. 320–7.

Grimminger F, von Kurten I, Walmrath D, Seeger W. Type II alveolar epithelial eicosanoid metabolism: predominance of cyclooxygenase pathways and transcellular lipoxygenase metabolism in co-culture with neutrophils. Am J Respir Cell Mol Biol. 1992;6:9–16.

Hsia CC, Hyde DM, Ochs M, Weibel ER. An official research policy statement of the American Thoracic Society/European Respiratory Society: standards for quantitative assessment of lung structure. Am J Respir Crit Care Med. 2010;181:394–418.

Huang HJ, Yusen RD, Meyers BF, Walter MJ, Mohanakumar T, Patterson GA, et al. Late primary graft dysfunction after lung transplantation and bronchiolitis obliterans syndrome. Am J Transplant. 2008;8:2454–62.

Ingemansson R, Massa G, Pandita RK, Sjoberg T, Steen S. Perfadex is superior to Euro-Collins solution regarding 24-hour preservation of vascular function. Ann Thorac Surg. 1995;60:1210–4.

Ingemansson R, Eyjolfsson A, Mared L, Pierre L, Algotsson L, Ekmehag B, et al. Clinical transplantation of initially rejected donor lungs after reconditioning ex vivo. Ann Thorac Surg. 2009;87:255–60.

Itano H, Zhang W, Ritter JH, McCarthy TJ, Mohanakumar T, Patterson GA. Adenovirus-mediated gene transfer of human interleukin 10 ameliorates reperfusion injury of rat lung isografts. J Thorac Cardiovasc Surg. 2000;120:947–56.

Iwazaki S, Takeyoshi I, Ohwada S, Sunose Y, Aiba M, Tsutsumi H, et al. FR128998 (a PAF receptor antagonist) counters the increased pulmonary vascular resistance associated with ischemia-reperfusion injury in the canine lung. Int J Angiol. 2001;10:10–4.

Kang CH, Anraku M, Cypel M, Sato M, Yeung J, Gharib SA, et al. Transcriptional signatures in donor lungs from donation after cardiac death vs after brain death: a functional pathway analysis. J Heart Lung Transplant. 2011;30:289–98.

Keshavjee S, Davis RD, Zamora MR, de PM, Patterson GA. A randomized, placebo-controlled trial of complement inhibition in ischemia-reperfusion injury after lung transplantation in human beings. J Thorac Cardiovasc Surg. 2005;129:423–8.

Khimenko PL, Taylor AE. Segmental microvascular permeability in ischemia-reperfusion injury in rat lung. Am J Physiol. 1999;276:L958–L60.

Kim JD, Baker CJ, Danto SI, Starnes VA, Barr ML. Modulation of pulmonary NA+ pump gene expression during cold storage and reperfusion. Transplantation. 2000;70:1016–20.

Knudsen L, Waizy H, Fehrenbach H, Richter J, Wahlers T, Wittwer T, et al. Ultrastructural changes of the intracellular surfactant pool in a rat model of lung transplantation-related events. Respir Res. 2011;12:79.

Knudsen L, Boxler L, Mühlfeld C, Schaefer IM, Becker L, Bussinger C, et al. Lung preservation in experimental ischemia/reperfusion injury and lung transplantation: a comparison of natural and synthetic surfactants. J Heart Lung Transplant. 2012;31:85–93.

Kohmoto J, Nakao A, Stolz DB, Kaizu T, Tsung A, Ikeda A, et al. Carbon monoxide protects rat lung transplants from ischemia-reperfusion injury via a mechanism involving p38 MAPK pathway. Am J Transplant. 2007;7:2279–90.

Krishnadasan B, Naidu BV, Byrne K, Fraga C, Verrier ED, Mulligan MS. The role of proinflammatory cytokines in lung ischemia-reperfusion injury. J Thorac Cardiovasc Surg. 2003;125:261–72.

Kroemer G, Jäättelä M. Lysosomes and autophagy in cell death control. Nat Rev Cancer. 2005;5:886–97.

Kroemer G, Martin SJ. Caspase-independent cell death. Nat Med. 2005;11:725–30.

Lapar DJ, Laubach VE, Emaminia A, Crosby IK, Hajzus VA, Sharma AK, et al. Pretreatment strategy with adenosine A2A receptor agonist attenuates reperfusion injury in a preclinical porcine lung transplantation model. J Thorac Cardiovasc Surg. 2011;142:887–94.

Lee JC, Christie JD. Primary graft dysfunction. In: Vigneswaran W, Garrity ER, editors Lung transplantation. London: Informa healthcare; 2010. p. 237–48.

Leist M, Jaattela M. Four deaths and a funeral: from caspases to alternative mechanisms. Nat Rev Mol Cell Biol. 2001;2:589–98.

Lindstedt S, Hlebowicz J, Koul B, Wierup P, Sjogren J, Gustafsson R, et al. Comparative outcome of double lung transplantation using conventional donor lungs and non-acceptable donor lungs reconditioned ex vivo. Interact Cardiovasc Thorac Surg. 2011;12:162–5.

Liu M, Tremblay L, Cassivi SD, Bai XH, Mourgeon E, Pierre AF, et al. Alterations of nitric oxide synthase expression and activity during rat lung transplantation. Am J Physiol Lung Cell Mol Physiol. 2000;278:L1071–81.

Lobo LJ, Aris RM, Schmitz J, Neuringer IP. Donor-specific antibodies are associated with antibody-mediated rejection, acute cellular rejection, bronchiolitis obliterans syndrome, and cystic fibrosis after lung transplantation. J Heart Lung Transplant. 2013;32:70–7.

Löckinger A, Schütte H, Walmrath D, Seeger W, Grimminger F. Protection against gas exchange abnormalities by pre-aerosolized PGE1, iloprost and nitroprusside in lung ischemia-reperfusion. Transplantation. 2001;71:185–93.

Lopau K, Mark J, Schramm L, Heidbreder E, Wanner C. Hormonal changes in brain death and immune activation in the donor. Transpl Int. 2000;13 Suppl 1:S282–5.

Maccherini M, Keshavjee SH, Slutsky AS, Patterson GA, Edelson JD. The effect of low-potassium-dextran versus Euro-Collins solution for preservation of isolated type II pneumocytes. Transplantation. 1991;52:621–6.

Machuca TN, Hsin MK, Ott HC, Chen M, Hwang DM, Cypel M, et al. Injury-specific ex vivo treatment of the donor lung: pulmonary thrombolysis followed by successful lung transplantation. Am J Respir Crit Care Med. 2013;188:878–80.

Majno G, Joris I. Apoptosis, oncosis, and necrosis. An overview of cell death. Am J Pathol. 1995;146:3–15.

McRae K, de Perrot M, Fischer S, Waddell TK, Liu M, Keshavjee S. Detection of IL-10 in the exhaled breath condensate, plasma and tissue during ischemia-reperfusion injury in experimental lung transplantation. J Heart Lung Transplant. 2001;20:184.

Meers CM, Tsagkaropoulos S, Wauters S, Verbeken E, Vanaudenaerde B, Scheers H, et al. A model of ex vivo perfusion of porcine donor lungs injured by gastric aspiration: a step towards pretransplant reconditioning. J Surg Res. 2011;170:e159–67.

Minambres E, Coll E, Duerto J, Suberviola B, Mons R, Cifrian JM, et al. Effect of an intensive lung donor-management protocol on lung transplantation outcomes. J Heart Lung Transplant. 2014;33:178–84.

Mizushima N, Levine B, Cuervo AM, Klionsky DJ. Autophagy fights disease through cellular self-digestion. Nature. 2008;451:1069–75.

Mizutani H, Minamoto K, Aoe M, Yamashita M, Date H, Andou A, et al. Expression of endothelin-1 and effects of an endothelin receptor antagonist, TAK-044, at reperfusion after cold preservation in a canine lung transplantation model. J Heart Lung Transplant. 1998;17:835–45.

Moore TM, Khimenko P, Adkins WK, Miyasaka M, Taylor AE. Adhesion molecules contribute to ischemia and reperfusion-induced injury in the isolated rat lung. J Appl Physiol. 1995;78:2245–52.

Motoyama H, Chen F, Ohsumi A, Hijiya K, Okita K, Nakajima D, et al. Protective effect of plasmin in marginal donor lungs in an ex vivo lung perfusion model. J Heart Lung Transplant. 2013;32:505–10.

Mühlfeld C, Müller K, Pallesen LP, Sandhaus T, Madershahian N, Richter J, et al. Impact of preservation solution on the extent of blood-air barrier damage and edema formation in experimental lung transplantation. Anat Rec. 2007;290:491–500.

Mühlfeld C, Schaefer IM, Becker L, Bussinger C, Vollroth M, Bosch A, et al. Pre-ischaemic exogenous surfactant reduces pulmonary injury in rat ischaemia/reperfusion. Eur Respir J. 2009;33:625–33.

Mühlfeld C, Becker L, Bussinger C, Vollroth M, Nagib R, Schaefer IM, et al. Exogenous surfactant in ischemia/reperfusion: Effects on endogenous surfactant pools. J Heart Lung Transplant. 2010;29:327–34.

Mulligan MS. Primary graft dysfunction following lung transplantation: Pathogenesis and impact on early and late outcome. In: Lynch JP, Ross DJ, editors Lung and heart-lung transplantation. Taylor & Francis; 2006. p. 437–63.

Munshi L, Keshavjee S, Cypel M. Donor management and lung preservation for lung transplantation. Lancet Respir Med. 2013;1:318–28.

Naidu BV, Krishnadasan B, Farivar AS, Woolley SM, Thomas R, Van Rooijen N, et al. Early activation of the alveolar macrophage is critical to the development of lung ischemia-reperfusion injury. J Thorac Cardiovasc Surg. 2003;126:200–7.

Naka Y, Toda K, Kayano K, Oz MC, Pinsky DJ. Failure to express the P-selectin gene or P-selectin blockade confers early pulmonary protection after lung ischemia or transplantation. Proc Natl Acad Sci U S A. 1997;94:757–61.

Ng CS, Wan S, Arifi AA, Yim AP. Inflammatory response to pulmonary ischemia-reperfusion injury. Surg Today. 2006;36:205–14.

Ochs M. Stereological analysis of acute lung injury. Eur Respir Rev. 2006;15:115–21.

Ochs M. The closer we look the more we see? Quantitative microscopic analysis of the pulmonary surfactant system. Cell Physiol Biochem. 2010;25:27–40.

Ochs M, O'Brodovich H. The structural and physiologic basis of respiratory disease. In: Wilmott RW, Boat TF, Bush A, Chernick V, Deterding RR, Ratjen F, editors. Kendig and Chernick's disorders of the respiratory tact in children. 8th ed. Philadelphia: Elsevier; 2012. p. 35–74.

Ochs M, Nenadic I, Fehrenbach A, Albes JM, Wahlers T, Richter J, et al. Ultrastructural alterations in intraalveolar surfactant subtypes after experimental ischemia and reperfusion. Am J Respir Crit Care Med. 1999;160:718–24.

Ochs M, Fehrenbach H, Nenadic I, Bando T, Fehrenbach A, Schepelmann D, et al. Preservation of intraalveolar surfactant in a rat lung ischaemia/reperfusion injury model. Eur Respir J. 2000;15:526–31.

Ochs M, Fehrenbach H, Richter J. Occurence of lipid bodies in canine type II pneumocytes during hypothermic lung ischemia. Anat Rec A Discov Mol Cell Evol Biol. 2004;277:287–97.

Oczenski W. Atmen—Atemhilfen. 8th ed. Stuttgart: Thieme; 2008.

Ohsumi A, Chen F, Sakamoto J, Nakajima D, Kobayashi M, Bando T, et al. Protective effect of surfactant inhalation against warm ischemic injury in an isolated rat lung ventilation model. PLoS One. 2013;8:e72574.

Okada K, Fujita T, Minamoto K, Liao H, Naka Y, Pinsky DJ. Potentiation of endogenous fibrinolysis and rescue from lung ischemia/reperfusion injury in interleukin (IL)-10-reconstituted IL-10 null mice. J Biol Chem. 2000;275:21468–76.

Orens JB, Boehler A, de PM, Estenne M, Glanville AR, Keshavjee S, et al. A review of lung transplant donor acceptability criteria. J Heart Lung Transplant. 2003;22:1183–200.

Ovechkin AV, Lominadze D, Sedoris KC, Gozal E, Robinson TW, Roberts AM. Inhibition of inducible nitric oxide synthase attenuates platelet adhesion in subpleural arterioles caused by lung ischemia-reperfusion in rabbits. J Appl Physiol. 2005;99:2423–32.

Pakhale SS, Hadjiliadis D, Howell DN, Palmer SM, Gutierrez C, Waddell TK, et al. Upper lobe fibrosis: a novel manifestation of chronic allograft dysfunction in lung transplantation. J Heart Lung Transplant. 2005;24:1260–8.

Palace GP, Horgan MJ, Malik AB. Generation of 5-lipoxygenase metabolites following pulmonary reperfusion in isolated rabbit lungs. Prostaglandins. 1992;43:339–49.

Paries M, Boccheciampe N, Raux M, Riou B, Langeron O, Nicolas-Robin A. Benefit of a single recruitment maneuver after an apnea test for the diagnosis of brain death. Crit Care. 2012;16:R116.

Parto S, Shafaghi S, Khoddami-Vishteh HR, Makki SM, Abbasidezfuli A, Daneshvar A, et al. Efficacy of recruitment maneuver for improving the brain dead marginal lungs to ideal. Transplant Proc. 2013;45:3531–3.

Pierre AF, Xavier AM, Liu M, Cassivi SD, Lindsay TF, Marsh HC, et al. Effect of complement inhibition with soluble complement receptor 1 on pig allotransplant lung function. Transplantation. 1998;66:723–32.

Quadri SM, Segall L, de PM, Han B, Edwards V, Jones N, et al. Caspase inhibition improves ischemia-reperfusion injury after lung transplantation. Am J Transplant. 2005;5:292–9.

Rostron A, Dark JH. Donor management. In: Vigneswaran WT, Garrity ER, editors Lung transplantation. London: Informa healthcare; 2010. p. 115–24.

Sato M. Chronic lung allograft dysfunction after lung transplantation: the moving target. Gen Thorac Cardiovasc Surg. 2013;61:67–78.

Sato K, Tomioka H, Shimizu T, Gonda T, Ota F, Sano C. Type II alveolar cells play roles in macrophage-mediated host innate resistance to pulmonary mycobacterial infections by producing proinflammatory cytokines. J Infect Dis. 2002;185:1139–47.

Sato M, Waddell TK, Wagnetz U, Roberts HC, Hwang DM, Haroon A, et al. Restrictive allograft syndrome (RAS): a novel form of chronic lung allograft dysfunction. J Heart Lung Transplant. 2011;30:735–42.

Seeger W, Stöhr G, Wolf HR, Neuhof H. Alteration of surfactant function due to protein leakage: special interaction with fibrin monomer. J Appl Physiol. 1985;58:326–38.

Shargall Y, Guenther G, Ahya VN, Ardehali A, Singhal A, Keshavjee S. Report of the ISHLT Working Group on Primary Lung Graft Dysfunction part VI: treatment. J Heart Lung Transplant. 2005;24:1489–500.

Sharma AK, Linden J, Kron IL, Laubach VE. Protection from pulmonary ischemia-reperfusion injury by adenosine A2A receptor activation. Respir Res. 2009;10:58.

Sharma AK, Laubach VE, Ramos SI, Zhao Y, Stukenborg G, Linden J, et al. Adenosine A2A receptor activation on CD4 + T lymphocytes and neutrophils attenuates lung ischemia-reperfusion injury. J Thorac Cardiovasc Surg. 2010;139:474–82.

Shimizu N, Kita T, Aoe M, Nakata M, Miyai Y, Teramoto S. Changes in levels of arachidonic acid metabolites in blood and bronchoalveolar lavage fluid after warm ischemia-reperfusion of lung. Acta Med Okayama. 1991;45:417–22.

Soccal PM, Gasche Y, Pache JC, Schneuwly O, Slosman DO, Morel DR, et al. Matrix metalloproteinases correlate with alveolar-capillary permeability alteration in lung ischemia-reperfusion injury. Transplantation. 2000;70:998–1005.

Sommer SP, Gohrbandt B, Fischer S, Hohlfeld JM, Warnecke G, Avsar M, et al. Glutathione improves the function of porcine pulmonary grafts stored for twenty-four hours in low-potassium dextran solution. J Thorac Cardiovasc Surg. 2005;130:864–9.

Sommer W, Tudorache I, Kuhn C, Avsar M, Salman J, Ius F, et al. C1-Esterase-Inhibitor for Primary Graft Dysfunction in Lung Transplantation. Transplantation. 2014;97:1185–91.

Stammberger U, Carboni GL, Hillinger S, Schneiter D, Weder W, Schmid RA. Combined treatment with endothelin- and PAF-antagonists reduces posttransplant lung ischemia/reperfusion injury. J Heart Lung Transplant. 1999;18:862–8.

Stammberger U, Gaspert A, Hillinger S, Vogt P, Odermatt B, Weder W, et al. Apoptosis induced by ischemia and reperfusion in experimental lung transplantation. Ann Thorac Surg. 2000;69:1532–6.

Steen S, Kimblad PO, Sjoberg T, Lindberg L, Ingemansson R, Massa G. Safe lung preservation for twenty-four hours with Perfadex. Ann Thorac Surg. 1994;57:450–7.

Steen S, Sjoberg T, Pierre L, Liao Q, Eriksson L, Algotsson L. Transplantation of lungs from a non-heart-beating donor. The Lancet. 2001;357:825–9.

Steen S, Liao Q, Wierup PN, Bolys R, Pierre L, Sjoberg T. Transplantation of lungs from non-heart-beating donors after functional assessment ex vivo. Ann Thorac Surg. 2003;76:244–52.

Stewart S, Fishbein MC, Snell GI, Berry GJ, Boehler A, Burke MM, et al. Revision of the 1996 working formulation for the standardization of nomenclature in the diagnosis of lung rejection. J Heart Lung Transplant. 2007;26:1229–42.

Strüber M, Wilhelmi M, Harringer W, Niedermeyer J, Anssar M, Kunsebeck A, et al. Flush perfusion with low potassium dextran solution improves early graft function in clinical lung transplantation. Eur J Cardiothorac Surg. 2001;19:190–4.

Strüber M, Hohlfeld JM, Kofidis T, Warnecke G, Niedermeyer J, Sommer SP, et al. Surfactant function in lung transplantation after 24 h of ischemia: advantage of retrograde flush perfusion for preservation. J Thorac Cardiovasc Surg. 2002;123:98–103.

Strüber M, Fischer S, Niedermeyer J, Warnecke G, Gohrbandt B, Gorler A, et al. Effects of exogenous surfactant instillation in clinical lung transplantation: a prospective, randomized trial. J Thorac Cardiovasc Surg. 2007;133:1620–5.

Su M, Chi EY, Bishop MJ, Henderson WR Jr. Lung mast cells increase in number and degranulate during pulmonary artery occlusion/reperfusion injury in dogs. Am Rev Respir Dis. 1993;147:448–56.

Sunose Y, Takeyoshi I, Tsutsumi H, Kawata K, Tokumine M, Iwazaki S, et al. Effects of FK3311 on pulmonary ischemia-reperfusion injury in a canine model. J Surg Res. 2001;95:167–73.

Suzuki Y, Cantu E, Christie JD. Primary graft dysfunction. Semin Respir Crit Care Med. 2013;34:305–19.

Takada M, Nadeau KC, Hancock WW, Mackenzie HS, Shaw GD, Waaga AM, et al. Effects of explosive brain death on cytokine activation of peripheral organs in the rat. Transplantation. 1998;65:1533–42.

Tang PS, Mura M, Seth R, Liu M. Acute lung injury and cell death: how many ways can cells die? Am J Physiol Lung Cell Mol Physiol. 2008;294:L632–41.

Thabut G, Mal H, Cerrina J, Dartevelle P, Dromer C, Velly JF, et al. Graft ischemic time and outcome of lung transplantation: a multicenter analysis. Am J Respir Crit Care Med. 2005;171:786–91.

The International Society for Heart & Lung Transplantation. In: ISHLT transplant registry quarterly reports for lung. 2014. http://www.ishlt.org/registries/quarterlyDataReportResults.asp?organ=LU&rptType=all&continent=3. Accessed 14 May 2014.

Van Cruchten S, Van den Broeck W. Morphological and biochemical aspects of apoptosis, oncosis and necrosis. Anat Histol Embryol. 2002;31:214–23.

Van de Wauwer C, Neyrinck AP, Geudens N, Rega FR, Verleden GM, Verbeken E, et al. Retrograde flush following warm ischemia in the non-heart-beating donor results in superior graft performance at reperfusion. J Surg Res. 2009;154:118–25.

Van Putte BP, Kesecioglu J, Hendriks JM, Persy VP, van Marck E, van Schil PE, et al. Cellular infiltrates and injury evaluation in a rat model of warm pulmonary ischemia-reperfusion. Crit Care. 2005;9:R1–R8.

Van Raemdonck D, Neyrinck A, Cypel M, Keshavjee S. Ex-vivo Lung Perfusion. Transpl Int. 2015;28:643–56.

Vanderbilt JN, Mager EM, Allen L, Sawa T, Wiener-Kronish J, Gonzalez R, et al. CXC chemokines and their receptors are expressed in type II cells and upregulated following lung injury. Am J Respir Cell Mol Biol. 2003;29:661–8.

Veldhuizen RA, Marcou J, Yao LJ, McCaig L, Ito Y, Lewis JF. Alveolar surfactant aggregate conversion in ventilated normal and injured rabbits. Am J Physiol. 1996;270:L152–8.

Verbrugge SJ, Lachmann B, Kesecioglu J. Lung protective ventilatory strategies in acute lung injury and acute respiratory distress syndrome: from experimental findings to clinical application. Clin Physiol Funct Imaging. 2007;27:67–90.

Wallinder A, Ricksten SE, Hansson C, Riise GC, Silverborn M, Liden H, et al. Transplantation of initially rejected donor lungs after ex vivo lung perfusion. J Thorac Cardiovasc Surg. 2012;144:1222–8.

Warnecke G, Strüber M, Fraud S, Hohlfeld JM, Haverich A. Combined exogenous surfactant and inhaled nitric oxide therapy for lung ischemia-reperfusion injury in minipigs. Transplantation. 2001;71:1238–44.

Weibel ER, Knight BW. A morphometric study on the thickness of the pulmonary air-blood barrier. J Cell Biol. 1964;21:367–96.

Weibel ER, Hsia CC, Ochs M. How much is there really? Why stereology is essential in lung morphometry. J Appl Physiol. 2007;102:459–67.

Weiss ES, Champion HC, Williams JA, Baumgartner WA, Shah AS. Long-acting oral phosphodiesterase inhibition preconditions against reperfusion injury in an experimental lung transplantation model. J Thorac Cardiovasc Surg. 2009;137:1249–57.

Wierup P, Haraldsson A, Nilsson F, Pierre L, Schersten H, Silverborn M, et al. Ex vivo evaluation of nonacceptable donor lungs. Ann Thorac Surg. 2006;81:460–6.

Witt CA, Gaut JP, Yusen RD, Byers DE, Iuppa JA, Bennett BK, et al. Acute antibody-mediated rejection after lung transplantation. J Heart Lung Transplant. 2013;32:1034–40.

Wittwer T, Grote M, Oppelt P, Franke U, Schaefers HJ, Wahlers T. Impact of PAF antagonist BN 52021 (Ginkolide B) on post-ischemic graft function in clinical lung transplantation. J Heart Lung Transplant. 2001;20:358–63.

Woodrow JP, Shlobin OA, Barnett SD, Burton N, Nathan SD. Comparison of bronchiolitis obliterans syndrome to other forms of chronic lung allograft dysfunction after lung transplantation. J Heart Lung Transplant. 2010;29:1159–64.

Yang Z, Sharma AK, Linden J, Kron IL, Laubach VE. CD4+ T lymphocytes mediate acute pulmonary ischemia-reperfusion injury. J Thorac Cardiovasc Surg. 2009;137:695–702.

Yeung JC, Keshavjee S. Overview of clinical lung transplantation. Cold Spring Harb Perspect Med. 2014;4:a015628.

Yusen RD, Christie JD, Edwards LB, Kucheryavaya AY, Benden C, Dipchand AI, et al. The Registry of the International Society for Heart and Lung Transplantation: thirtieth adult lung and heart-lung transplant report—2013; focus theme: age. J Heart Lung Transplant. 2013;32:965–78.

Zhang J, Chen F, Zhao X, Aoyama A, Okamoto T, Fujinaga T, et al. Nebulized phosphodiesterase III inhibitor during warm ischemia attenuates pulmonary ischemia-reperfusion injury. J Heart Lung Transplant. 2009;28:79–84.

Zhao M, Fernandez LG, Doctor A, Sharma AK, Zarbock A, Tribble CG, et al. Alveolar macrophage activation is a key initiation signal for acute lung ischemia-reperfusion injury. Am J Physiol Lung Cell Mol Physiol. 2006;291:L1018–26.

Zhao Y, Sharma AK, Lapar DJ, Kron IL, Ailawadi G, Liu Y, et al. Depletion of tissue plasminogen activator attenuates lung ischemia-reperfusion injury via inhibition of neutrophil extravasation. Am J Physiol Lung Cell Mol Physiol. 2011;300:L718–29.

# Chapter 10
# Stereological Studies on Transient Gas Exchangers with Emphasis on the Structure and Function of the Human Placenta in Normal and Compromised Pregnancies

**Terry M. Mayhew**

## 10.1 Introduction

To leave the aquatic environment and survive on land, the early amniotes (forerunners of reptiles, birds and mammals) had to develop new strategies for ensuring that their reproductive outcomes were successful. The first eggs may have been laid in moist or shaded areas to reduce the risk of embryonic dessication but, subsequently, eggs became porous, leathery or protected by a tough shell. As evolution progressed, amniotes laid larger eggs in drier habitats and these developed into larger offspring and adults. All these changes had to be accompanied by improved ways of supplying the embryo with nutrients and respiratory oxygen ($O_2$).

In birds, the egg usually displays a rounded larger end and a more pointed smaller end. Its mass varies from about 1 g to 1.5 kg and is related to the size of the adult. The eggshell is pierced by numerous pores which allow the embryo to access ambient $O_2$, and pore density is greater at the rounded end beneath the shell of which lies an air sac (Wangensteen and Weibel 1982; Rahn et al. 1987; Reizis et al. 2005). The natural disposition of the egg (larger end uppermost) and its embryo (head at the larger end) facilitates $O_2$ flow to the embryonic head.

Monotremes (such as the platypus and echidna) are mammals that lay small eggs which possess a soft, porous, leathery shell and these mostly derive nutrients from the maternal circulation via the oviduct. Most mammals do not lay eggs but do nurture the embryo within the body of the female. However, they too were forced to develop new ways of supplying the growing embryo/fetus with nutrients and $O_2$. Gradients for doing so extend from the maternal uteroplacental circulation (the supplier), via the villous trophoblast (a significant consumer) and the developing fetoplacental circulation (the transporter) which delivers $O_2$ and nutrients to the

T. M. Mayhew (✉)
School of Life Sciences, Queen's Medical Centre, University of Nottingham, Nottingham, NG7 2UH, UK
e-mail: terry.mayhew@nottingham.ac.uk



A. N. Makanya (ed.), *The Vertebrate Blood-Gas Barrier in Health and Disease,*
DOI 10.1007/978-3-319-18392-3_10

developing fetus (the principal consumer). The mass of newborn terrestrial mammals can vary from 0.2 g to 100 kg and there is evidence from certain species that the functional capacity of the placenta is proportional to fetal size (Mayhew et al. 1993a; Mayhew 2006b).

Both the egg and placenta (whether a retained choriovitelline or yolk-sac placenta as in marsupials or a secondary chorioallantoic placenta as in eutherians) are transient structures which are usually discarded after hatching and parturition. Their capacity for passive diffusion of $O_2$ is expressed as a diffusive conductance ($DO_2$, in $cm^3\ min^{-1}\ kPa^{-1}$) which is determined partly by extensive surface areas and small diffusion distances. This article briefly summarises the common amniote structural features of the egg and placenta before focussing on the development of the human placenta and those tissue constituents which are pertinent to passive diffusion. It then reviews procedures for deriving morphometric estimates of $DO_2$ by combining stereological sampling and estimation tools with physiological data on the properties of $O_2$ and placental tissues. It emphasises that structural changes are integrated so that $O_2$ diffusion matches growth in fetal mass. Although the emphasis is on adaptations during normal gestation, changes in complicated pregnancies are also discussed. Whilst these include maternal diabetes mellitus, residence at high altitude and cigarette smoking, special attention is given to intrauterine growth restriction (IUGR) and pre-eclampsia (PE).

## 10.2 The Amniote Plan—Structural Overview of Egg and Placenta

Whether laid as eggs on land or nurtured within the female via the placenta, the embryos of amniotes are associated with a set of extensive membranes known as the allantois, amnion and chorion. In avian eggs, the chorioallantoic membrane (CAM) is found beneath the eggshell membranes and comprises mesenchyme together with chorionic and allantoic epithelia. The CAM is highly vascularised with capillaries and sinuses lying between the cells of the chorionic epithelium. This arrangement (Fig. 10.1) allows close contact with air in the pores of the eggshell and provides the embryo with access to $O_2$ (Wangensteen and Weibel 1982; Rahn et al. 1987; Reizis et al. 2005). In the chicken egg (Bissonnette and Metcalfe 1978), the conductance of the eggshell for gas diffusion does not alter during incubation but that of the CAM and capillary endothelium increase dramatically between 10 and 14 days and, thereafter, remain relatively constant. Attendant increases in conductance occur in the blood.

In mammals, the chorion is formed by extraembryonic mesoderm in contact with the amnion and two layers of trophoblast which surround the embryo. In different mammals, the chorion invades the uterine wall to varying degrees to form the definitive placenta and reduce diffusion distances (Enders and Carter 2004; Benirschke et al. 2012). In epitheliochorial and synepitheliochorial placentas (found, for example, in ruminants and horses), there is no invasion of the maternal tissues. In endotheliochorial placentas (e.g. in cats and dogs), uterine epithelium is eroded

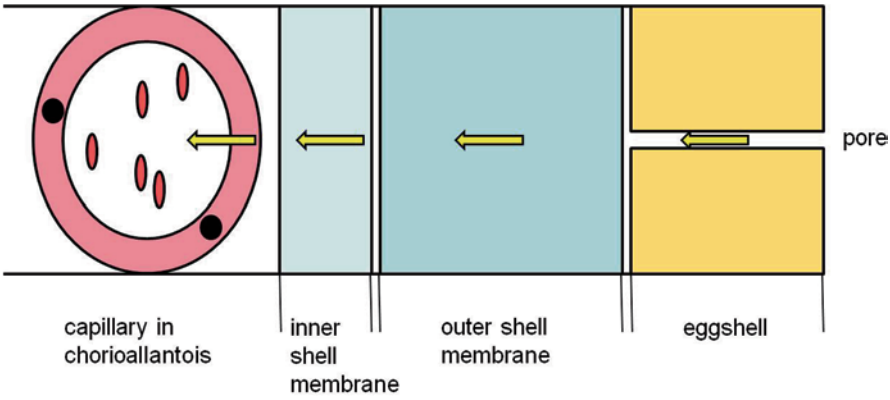


**Fig. 10.1** Graphical representation of the $O_2$ diffusion pathway across the avian egg. The *arrows* indicate the direction of $O_2$ travel from ambient air to the embryonic circulation. Upstream, environmental $O_2$ enters via pores in the shell and passes across the outer shell membrane, air sac (at the larger rounded end of the egg) and fibres of the inner shell membrane before reaching the dense capillary network of the chorioallantois where it binds to haemoglobin in erythrocytes. Not drawn to scale

and, in haemochorial placentas (e.g. in mice, rabbits and higher primates), even the endothelium of uterine blood vessels is eroded. In the human haemochorial placenta, the earliest chorionic villi are small and nonvascular but they soon acquire a mesenchymal core and become well vascularised. Thereafter, they proliferate, differentiate and ramify to produce an extensive surface area of trophoblast (roughly 12 $m^2$ at term) which separates the capillaries and sinusoids of the fetoplacental vasculature from the maternal intervillous part of the uteroplacental circulation (Jackson et al. 1992; Benirschke et al. 2012). During gestation, gas diffusive conductances within and between species decrease in a manner inversely related to fetal mass, at least in some species (Bissonnette et al. 1979; Smith et al. 1983; Mayhew et al. 1993a).

## 10.3 The Human Placenta and Its $O_2$ Environment

In the first trimester of normal pregnancy, extravillous trophoblast invades the decidua of the uterine wall and its spiral arteries. This invasive trophoblast blocks the terminal portions of arteries and, consequently, there is little maternal blood in the intervillous space and nutrition of the embryo is histiotrophic (derived from uterine secretions). The mean intervillous partial pressure of oxygen ($PO_2$) is about 2–3 kPa and this favours organogenesis and helps to protect the embryo from oxidative stress.

At roughly 12 week of gestation, the human embryo/fetus and its placenta experience a dramatic transition from low to high $O_2$ levels (Soothill et al. 1986; Rodesch et al. 1992; Jauniaux et al. 2003; Burton 2009; Schneider 2011; Tuuli et al. 2011). Fetal growth accelerates along with its metabolic and nutritional demands. To deal

with this, spiral arteries become dilated, low-resistance vessels which slow the flow of maternal blood into the intervillous space. At 10–12 week, the spiral arteries are unplugged, blood enters the intervillous space and $PO_2$ rises gradually to about 8 kPa by 16 week. An advantage of the slower flow into the intervillous space is an increase in transit time which facilitates gas exchange between the two placental circulations. It is precisely because maternal blood is in direct contact with the trophoblast of chorionic villi by the end of the first trimester that the human placenta is classified as haemochorial. The onset of maternal perfusion of the intervillous space is also accompanied by increases in the activities of antioxidant enzymes (Jauniaux et al. 2003). Nutrition now switches to haemotrophic (derived from the intervillous circulation) and, from this point onward, the placenta is the main vehicle for fetal nutrition and maternal–fetal exchange. Intervillous $PO_2$ slowly declines to 6–7 kPa at term.

## 10.4 The Human Placenta and Its Structural Variation Across Normal Gestation

The following account of villous development and differentiation is based on Castellucci et al. (2000) and Benirschke et al. (2012). Villi begin to form 12–18 days post conception (dpc) by proliferation of cytotrophoblast (CTB) cells and growth of CTB columns towards the decidua. These primary villi have a central core of CTB covered by a layer of syncytiotrophoblast (STB). About 2 days later, extraembryonic mesenchyme enters the central core of primary villi converting them into secondary villi. At 18–20 dpc, the first signs of fetoplacental microvessels are detected within the mesenchymal stroma and this initiates the conversion of secondary into tertiary villi. These tertiary villi constitute the first set of mesenchymal villi (MV) from which all other topological types of villi subsequently derive.

After week 5, increasing numbers of MV differentiate into immature intermediate villi (IIV) which are of larger diameter and themselves transform into stem villi (SV) by acquiring a more fibrous stroma. This does not result in the loss of MV and IIV because these topological types continue to be created by the process of trophoblastic sprouting followed by stromalisation and vascularisation. Villous sprouting begins at local sites of increased proliferative activity within the trophoblast and stroma. It leads to increases in exchange surface areas and continues until about mid-gestation. At this transition stage, MV begin to differentiate into mature intermediate villi (MIV) rather than IIV.

MIV are better vascularised and do not convert into SV, instead, produce substantial numbers of highly-vascularised, smaller diameter terminal villi (TV). This leads to an accelerated and remarkable amplification of the villous surface area available for maternal–fetal exchange and continues until term.

Villous morphogenesis is intimately associated with vascular morphogenesis (Kaufmann et al. 2004; Lisman et al. 2007). Fetoplacental capillarisation of the first villi occurs by de novo formation (vasculogenesis). Haemangioblastic cell cords, precursors of vascular endothelium, are found in the villous stroma at 15–21 dpc

and start to form endothelial tubes at about 21 dpc. The appearance of these unconnected capillary tubes signifies the transition from secondary to tertiary villi. By 28 dpc, the haemangioblastic cords of most villi have developed a lumen surrounded by flattened endothelial cells. Haematopoietic stem cells appear in the capillary lumen but do not circulate until anatomical connection is established between the umbilical cord and embryonic circulation (32–35 dpc) by fusion of villous capillaries with each other and with larger allantoic vessels. This process of vasculogenesis may continue until at least week 9.

From 32 dpc to the end of the first trimester, endothelial tube segments form primitive capillary networks by the dual process of non-branching and branching angiogenesis (Charnock-Jones et al. 2004). The former involves tube elongation and the latter involves sprouting angiogenesis possibly supplemented by intussusceptive microvascular growth. In the earliest MV, branching angiogenesis is less frequent than non-branching angiogenesis and capillary networks are poorly developed. With advancing gestation, branching angiogenesis assumes greater significance and capillary loops transform into a dense network which is especially prominent in IIV.

Towards the end of the first trimester, some endothelial tubes of IIV differentiate into centrally-situated primitive arteries and veins. In larger, proximal IIV, the adventitia of these precursors forms a fibrosed stromal core as part of the IIV–SV conversion. After mid-gestation, the fibrotic process extends radially outwards. The subtrophoblastic capillaries transform into a paravascular network but, by term, few paravascular capillaries remain in the larger SV.

In contrast to these events in more proximal parts of villous trees, outgrowths (MV and IIV) with new capillary networks are created in peripheral regions by branching and non-branching angiogenesis. From 25 weeks to term, vascular growth is associated with the development of long, slender (80–120 μm diameter) MIV containing one or two poorly branched capillary loops. The loops elongate at a rate which exceeds that of their parent villi, resulting in coiling of the capillaries. These may eventually obtrude into the overlying trophoblast and contribute to formation of TV (< 80 μm diameter) each of which harbours one or two capillary loops. With advancing gestation, capillaries in TV also dilate locally to form sinusoids (40–50 μm diameter). At certain sites, the capillaries and sinusoids are intimately associated with an attenuated region of trophoblast. These sites (vasculosyncytial membranes) are important for diffusional exchange.

Together, the changes identified above produce the morphological features seen typically in routine histological sections of term placenta (see Fig. 10.2).

## 10.5 Relative Growth Rates of Placental Compartments

Values of structural quantities characterising villi between 10 weeks of gestation and term are summarised in Table 10.1. Allometric studies on placentas from the end of the first trimester to term (Mayhew 2006b) have shown that growth of villi matches that of the intervillous space and of the placenta as a whole, but lags behind

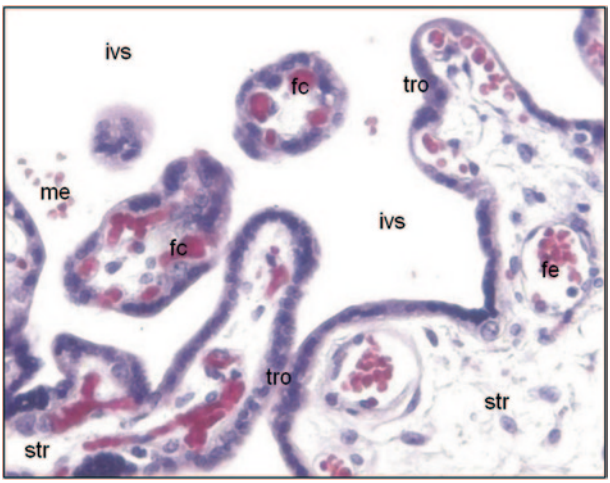


**Fig. 10.2** Paraffin wax section of formalin-fixed term human placenta stained by a connective tissue procedure. Maternal intervillous space (ivs) containing maternal erythrocytes (me) surrounds two topological types of villi (terminal and mature intermediate). Villi are covered by an epithelium, the trophoblast (tro), which invests the mesenchymal stroma (str). Stroma varies in amount and content according to villous type and contains fetoplacental capillaries (fc) and fetal erythrocytes (fe). To give an idea of scale, the mean diameter of an erythrocyte in such preparations is about 5–6 μm

that of the fetus. The increase in total volume of villi is exceeded by the expansion of villous surface area and the increase in total length. Within villi, capillary volume expands faster than trophoblast and this, in turn, grows faster than stroma. This is consistent with the production, after mid-gestation, of large numbers of mature TV and MIV characterised by smaller diameters and relatively less trophoblast and stroma.

**Table 10.1** Stereological estimates of some structural quantities of placental villi which are pertinent to passive diffusion. Values at different periods of gestation are based on data in Mayhew et al. (1993a)

| Variable | 10–22 week | 23–31 week | 32–36 week | 37–41 week |
|---|---|---|---|---|
| $V_{ivs}$ ($cm^3$) | 32.3 | 110 | 155 | 184 |
| $V_{fc}$ ($cm^3$) | 3.8 | 18.8 | 38.1 | 48.5 |
| $S_{utro}$ ($cm^2$) | 1.1 | 4.9 | 8.2 | 10.7 |
| $S_{dtro}$ ($cm^2$) | 1.2 | 5.2 | 8.7 | 11.1 |
| $S_{fc}$ ($cm^2$) | 0.7 | 8.0 | 8.2 | 11.0 |
| $T_{htro}$ (μm) | 5.7 | 3.3 | 2.5 | 2.0 |
| $T_{hstr}$ (μm) | 3.2 | 2.1 | 1.3 | 1.2 |

$V_{ivs}$ volume of the intervillous space, $V_{fc}$ volume of fetoplacental capillaries, $S_{utro}$ upstream (maternal-facing) surface area of trophoblast, $S_{dtro}$ downstream (fetal-facing) surface area of trophoblast, $S_{fc}$ luminal surface area of the fetoplacental vascular endothelium, $T_{htro}$ harmonic mean thickness of trophoblast, $T_{hstr}$ harmonic mean thickness of the villous stroma (between the downstream surface of trophoblast and the luminal surface of vascular endothelium)

Growth in total capillary volume is roughly commensurate with that of surface area and length, emphasising that growth favours length over calibre, despite the local distension that occurs in sinusoids. Although linear growth is driven by vascular endothelial proliferation, the mean area of endothelial squamous increases towards term. In contrast, the volume of trophoblast per nucleus is maintained whereas the volume of stroma per cell declines. Finally, peripheralisation of capillaries and reductions in stromal content affect both the arithmetic and harmonic mean distances across trophoblast and stroma. Across the villous membrane, thicknesses decline disproportionately, the decrease in harmonic mean being faster that in arithmetic mean. This is consistent with the villous membrane becoming more irregular in thickness. Trophoblast and stroma contribute equally to these villous membrane thickness changes.

## 10.6 The Significance of these Gestational Changes for Transplacental Exchange

The structural variables having the greatest impact on placental diffusion conductance for $O_2$ ($DpO_2$) are the harmonic mean thickness of the villous membrane and the surface areas of villi and their capillaries (Mayhew et al. 1986). From about 20 week of gestation, there are substantial increases in the total volume, surface area and length of the TV and the capillaries which they contain. Between the end of the first trimester and term, the total surface area of TV and IIV/MIV expands about 12-fold and total capillary surface area expands about 15-fold (Jackson et al. 1992).

Variation in thickness of the villous membrane influences its harmonic mean and is brought about by redistributing trophoblast volume. This occurs in response to obtrusion by fetoplacental vessels or by active protoplasmic flow within STB (Jackson et al. 1988; Burton and Feneley 1992). Obtrusion is influenced by the gradual peripheralisation of capillaries and formation of sinusoids. The walls of sinusoids are sensitive to perfusion pressure and local membrane thickness decreases as pressure rises (Karimu and Burton 1994a), suggesting that the placenta has the ability to act as an autoregulating gas exchanger with the harmonic thickness of the villous membrane changing to accommodate fetal demands.

Although vascular growth by non-branching angiogenesis has the potential to increase fetoplacental vascular impedance, branching angiogenesis may still take place towards term (Jirkovska et al. 2002, 2008). In fact, blood flows increase because fetal blood pressure rises and, presumably, because of the greater incidence of sinusoids. A rise in perfusion pressure can stimulate vascular endothelial cell proliferation and alter cell shape. There is evidence that the numbers of endothelial nuclei and the mean area of squamous endothelial cells increase as gestation progresses (Karimu and Burton 1994b; Mayhew et al. 1994; Mayhew 2002).

## 10.7 The Human Placenta and Morphometric Estimators of $DO_2$

The diffusive conductance of the human placenta has been estimated for the organ as a whole ($DpO_2$) and for the villous membrane alone ($DvmO_2$). The villous membrane is part of the diffusion pathway and includes villous trophoblast, fetoplacental vascular endothelium and varying amounts of villous stroma (Laga et al. 1973; Mayhew et al. 1984, 2007; Yin et al. 2009; Samson et al. 2011). The rationale for estimating $DvmO_2$ relies on the fact that the villous membrane in term placenta accounts for 80–90 % of total resistance to diffusion (Laga et al. 1973; Mayhew et al. 1986, 1990, 1993a). Therefore, $DvmO_2$ has been employed repeatedly as quicker way of obtaining a reasonable approximation of $DpO_2$.

Whichever conductance is chosen for estimation, Fick's law of diffusion provides a starting point for quantifying relevant aspects of placental structure (Mayhew 2014). For a tissue layer separating a delivery medium (here, maternal blood) from an uptake medium (fetal blood), the volume flow of $O_2$ depends on (i) the physical dimensions (surface area, S and thickness, T) of the layer, (ii) the partial pressure gradient across the layer and (iii) the physicochemical properties of $O_2$ and the layer, namely, Bunsen's solubility coefficient for $O_2$ and tissue diffusivity, the product of which is Krogh's diffusion constant (K). Given that conductance, $DO_2$, is equal to volume flow divided by partial pressure gradient, Fick's law provides the following basic equation:

$$DO_2 = (S/T) \cdot K.$$

This simplistic model must be modified to deal with biological reality. In fact, the complete intervascular diffusion pathway comprises six different tissue components arranged in series (see Fig. 10.3):

I. Maternal erythrocytes (me) containing $O_2$ bound to haemoglobin are found in the intervillous space, an open porous network surrounding the stems and branches of chorionic villi.
II. Maternal blood plasma (mp): once released from haemoglobin, $O_2$ passes through the erythrocyte membrane and crosses the blood plasma to reach the apical (or outer) surface of the villous trophoblast.
III. Villous trophoblast (tro): metabolically active epithelium where up to 40 % of the $O_2$ is consumed before passing across the basal (or inner) surface of the trophoblast and the epithelial basal lamina on which it lies.
IV. Villous stroma (str): the stroma proper is fibrocellular and lies deep to the trophoblastic epithelium. Here, the term villous stroma is used to describe what lies between the trophoblast and capillary lumen. It includes variable proportions of stroma proper together with vascular endothelium and endothelial basal lamina.
V. Fetal blood plasma (fp): lies between the inner endothelial membrane and the membrane surface of fetal erythrocytes.

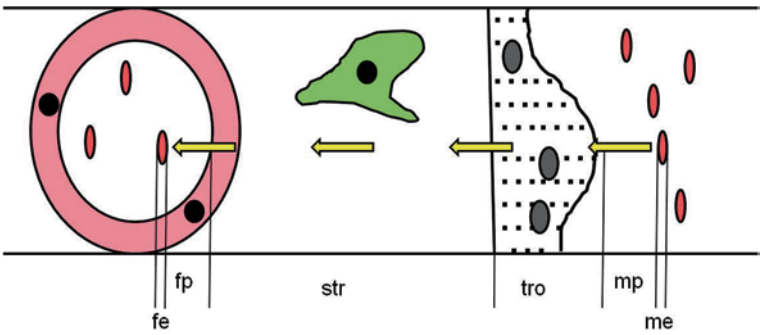


**Fig. 10.3** Graphical representation of the $O_2$ diffusion pathway across the human haemochorial placenta. $O_2$ travels in a maternal–fetal direction (*arrows*). Upstream, $O_2$ is released from haemoglobin in maternal erythrocytes (*me*) in the intervillous space and traverses maternal blood plasma (*mp*), villous trophoblast (*tro*), villous stroma (*str*) and fetal plasma (*fp*) before binding to haemoglobin in fetal erythrocytes *(fe)*. The amount of stromal tissue varies. Here, stroma proper and vascular endothelium separate trophoblast from fetal plasma but, in reality, both endothelium and trophoblast have a basal lamina. Trophoblast itself varies in local thickness. Not drawn to scale

VI. Fetal erythrocytes (fe): take up the $O_2$ from the blood plasma and it binds to haemoglobin.

Modifications of the Fick equation are required to cater for the fact that components of the diffusion pathway have both upstream (or maternal) and downstream (or fetal) surfaces which can differ in area. Moreover, these component layers are not uniformly thick but display thinner and thicker regions. Consequently, $O_2$ diffusion varies regionally across the villous surface. Villous trophoblast varies in local thickness for two main reasons. First, it possesses thin regions (vasculosyncytial membranes) which overlie fetoplacental capillaries showing varying degrees of distension, peripheralisation and obtrusion into trophoblast. In these regions, the diffusion distance may be only 1–2 μm. Second, there are thicker regions of STB (syncytial knots) which represent sites of local clustering of nuclei. At syncytial knots, the diffusion distance may be 10 μm or more.

Since tissue components are arranged in series, resistances can be summed to obtain a total resistance and this is the reciprocal of total placental conductance, $DpO_2$. The partial conductances can be summarised as follows (Mayhew et al. 1990, 1993a; Mayhew 2014):

I. $D_{me}$, involving dissociation of $O_2$ from maternal erythrocytes
II. $D_{mp}$, involving diffusion across maternal plasma
III. $D_{tro}$, involving diffusion across villous trophoblast
IV. $D_{str}$, involving diffusion across basal lamina, endothelium and villous stroma
V. $D_{fp}$, involving diffusion across fetal plasma
VI. $D_{fe}$, involving $O_2$ binding to haemoglobin in fetal erythrocytes

The total resistance to $O_2$ flow is estimated as:

$$1/DpO_2 = 1/D_{me} + 1/D_{mp} + 1/D_{tro} + 1/D_{str} + 1/D_{fp} + 1/D_{fe}.$$

As stated already, sometimes, the trophoblast + endothelium + stroma is treated as a single component, the villous membrane, with conductance $DvmO_2$ (Laga et al. 1973; Mayhew et al. 1984, 2007; Yin et al. 2009; Samson et al. 2011).

### *10.7.1 Estimating Partial Conductances*

$D_{me}$ and $D_{fe}$ depend on vascular space volumes and $O_2$–haemoglobin chemical reaction rates (Roughton and Forster 1957; Staub et al. 1962; Holland et al. 1977) calculated as the product of blood volume (V) and the diffusing capacity of 1 $cm^3$ of whole blood (θ):

$$D_{me} = V_{ivs} \cdot \theta \text{ and}$$

$$D_{fe} = V_{fc} \cdot \theta$$

where $V_{ivs}$ is the volume of blood in the intervillous space and $V_{fc}$ that of blood in fetoplacental capillaries. For adult and fetal blood, θ differs only at low saturations and so a value of 12.8 $cm^3\ cm^{-3}\ min^{-1}\ kPa^{-1}$ (Mayhew et al. 1990) can be used for present purposes.

To deal with local differences in diffusion distances, $D_{mp}$, $D_{tro}$, $D_{str}$ and $D_{fp}$ are calculated using estimates of harmonic rather than arithmetic mean thicknesses (Jackson et al. 1985). Being based on reciprocals of local thicknesses, harmonic means accord greater weighting to thinner regions.

Another factor to be taken into account is that the downstream side of the villous membrane is not of a simple sheet but is made up of the luminal endothelium of separate capillary loops. So, given that villous and capillary surface areas may not be equal, it is preferable to estimate them separately. Therefore, a more realistic version of the Fick equation for each tissue component is:

$$D = K.(S_u + S_d)/2T_h$$

where $T_h$ is the harmonic mean thickness and $S_u$ and $S_d$ are the upstream and downstream surface areas. Values of K, Krogh's diffusion constant, are available in the literature (see Power 1968; Weibel 1970; Laga et al. 1973). The median of published values for K in blood plasma is $24.4 \times 10^{-8}\ cm^2\ min^{-1}\ kPa^{-1}$ and, in placental tissue, $17.3 \times 10^{-8}\ cm^2\ min^{-1}\ kPa^{-1}$ (Mayhew et al. 1984, 1990). For $D_{mp}$, $S_u$ is the membrane surface area of maternal erythrocytes and $S_d$ the surface area of villi. For $D_{tro}$, $S_u$ and $S_d$ are the apical and basal surfaces respectively of villous trophoblast. For $D_{str}$, they are the basal surface of villous trophoblast and luminal surface of

vascular endothelium respectively and, for $D_{fp}$, they are the luminal surface of endothelium and membrane surface of fetal erythrocytes respectively.

The presentation of equations for each partial conductance reveals a practical benefit of substituting stereological data into diffusion equations. That is, structural changes involving every component of the pathway are integrated in a single quantity and, as a result, potential misinterpretations drawn from studies based on only one quantity (e.g. villous surface area) can be avoided.

Having obtained a value of $DpO_2$ for the whole placenta, a mass-specific conductance (in $cm^3\ min^{-1}\ kPa^{-1}\ kg^{-1}$) can be calculated by relating it to fetal weight.

For estimates based on $DvmO_2$ instead of $DpO_2$, the pertinent equation is:

$$DvmO_2 = K \cdot (S_u + S_d)/2T_h$$

where $S_u$ is the apical surface of villous trophoblast, $S_d$ is the luminal surface of vascular endothelium and $T_h$ refers to the harmonic mean thickness of the villous membrane.

### *10.7.2 Stereological Variables*

Placental microstructure is revealed usually by physical sectioning and 3D structural information is obtained using the sampling and estimation tools of design-based stereology (Gundersen and Jensen 1987; Howard and Reed 2005; Mayhew 2008; Veras et al. 2014). Stereological analysis delivers estimates which are unbiased (or minimally biased) and efficient provided that random sampling is applied at all stages of a multistage sampling scheme. At the highest stage is the intact organ which, at successive stages, is sampled randomly to provide microscopical fields of view which are analysed by means randomly oriented and/or randomly positioned test probes (lattices of test points and test lines).

Placental volume may be estimated by liquid displacement, from placental weight and tissue density or, in the case of small organs, by cutting parallel slices and applying the Cavalieri principle (Mayhew et al. 1984; Coan et al. 2004; Veras et al. 2014). Random sampling gives each position and direction within the placenta an equal chance of being selected and is, by definition, unbiased sampling (Mayhew 2008). Randomness of location and direction are necessary to estimate volumes, surface areas and harmonic mean thicknesses. Methods for achieving these sampling objectives in placentas from humans, baboons and mice are available (Jackson et al. 1985; Mayhew et al. 1993a; Coan et al. 2004; Mayhew 2006a, 2008; Veras et al. 2008, 2014; Samson et al. 2011).

Once sections have been sampled and stained for examination by light microscopy, volume densities of identified compartments can be estimated by test point counting and surface densities by counting chance intersections between surface traces and test lines (Howard and Reed 2005; Mayhew 2008). Placental volume is often required because it is used to convert relative quantities (volume and surface densities) into absolute quantities (volumes of the intervillous space and

fetoplacental capillaries and surface areas of erythrocytes, trophoblast and capillary endothelium).

As they deal more appropriately with tissue layers of varying local thickness, it is preferable to estimate harmonic rather than arithmetic means (Gundersen et al. 1978; Jackson et al. 1985). Variability in local thickness is beneficial because, for a given arithmetic mean, it allows diffusion to proceed more efficiently than would be the case for a layer of uniform thickness. In fact, the villous membrane in term placentas of humans and baboons is roughly 30% more efficient because of thickness variation (Jackson et al. 1985; Samson et al. 2011).

Harmonic mean thickness can be estimated on randomly positioned and randomly oriented sections by superimposing a lattice of parallel and equidistant test lines (Gundersen et al. 1978; Jackson et al. 1985). Where these lines intersect the traces of relevant surfaces, the lengths of intercepts across a tissue layer (e.g. trophoblast) can be measured or classified. The mean of the reciprocals of intercept lengths, corrected for magnification and tissue processing, provide an estimate of which the reciprocal is a harmonic mean intercept length, $L_h$. The harmonic mean thickness, $T_h$, is estimated as $2L_h/3$. Estimates of $T_h$ can be obtained also by measuring orthogonal intercept instead of random intercept lengths (Jensen et al. 1979; Veras et al. 2014)

## 10.8 Variation of $DpO_2$ of the Human Placenta During Normal Pregnancy

From at least the end of the first trimester to term, morphometric $DpO_2$ increases in a manner commensurate with changes in fetal mass (see Table 10.2 and Mayhew et al. 1993a). Allometric studies have indicated that this is largely due to alterations involving the villous membrane and the same seems to hold for the intervascular membrane of the mouse placenta (Mayhew 2006b). These findings are consistent with those from studies on placentas of guinea pigs and sheep where

**Table 10.2** Morphometric estimates of partial conductances, total $DpO_2$ (in $cm^3\ min^{-1}\ kPa^{-1}$) and mass-specific $DpO_2$ (in $cm^3\ min^{-1}\ kPa^{-1}\ kg^{-1}$) for human placentas at different periods of gestation. Values are based on data in Mayhew et al. (1993a)

| Conductance | 10–22 week | 23–31 week | 32–36 week | 37–41 week |
|---|---|---|---|---|
| $D_{me}$ | 373 | 1210 | 1600 | 2010 |
| $D_{mp}$ | 112 | 370 | 500 | 631 |
| $D_{tro}$ | 3.9 | 28 | 61 | 98 |
| $D_{str}$ | 6.5 | 44 | 117 | 179 |
| $D_{fp}$ | 65 | 328 | 671 | 864 |
| $D_{fe}$ | 48 | 239 | 486 | 620 |
| $DpO_2$ | 2.1 | 13.7 | 30.4 | 45.1 |
| Specific $DpO_2$ | 14.6 | 12.2 | 13.8 | 13.4 |

*D* conductance, *me* maternal erythrocyte, *mp* maternal plasma, *tro* trophoblast, *str* villous stroma, *fp* fetal plasma, *fe* fetal erythrocytes

indirect estimates of physiological $DpO_2$ are positively correlated with fetal mass (Bissonnette et al. 1979; Smith et al. 1983). These outcomes indicate that the placenta is capable of adapting incrementally over time and suggest that, regardless of type and fetal size, placentas from different species are, in some sense, equally successful at matching $O_2$ delivery to fetal size.

Values of physiological $DpO_2$ for term human placenta have been obtained either directly or indirectly, from DpCO values (Metcalfe et al. 1967; Bartels 1970; Forster 1973) and fall in the range 6.0–7.5 $cm^3\ min^{-1}\ kPa^{-1}$ (Mayhew et al. 1984). In contrast, morphometric estimates of total placental $DpO_2$ are in the range 15.7–45.1 $cm^3\ min^{-1}\ kPa^{-1}$ (Laga et al. 1973; Mayhew et al. 1984, 1986, 1990, 1993a, b, 2007; Reshetnikova et al. 1994, 1995; Bush et al. 2000; Ansari et al. 2003; Yin et al. 2009). How can we reconcile this discrepancy?

Morphometric $DpO_2$ is a theoretical maximum predicted by placental structure and this maximum may incorporate a reserve capacity which may not be attained all of the time. Indeed, the structure present may be seen as a compromise reflecting the fact that the placenta serves multiple functions and not just $O_2$ diffusion. On the other hand, physiological values of $DpO_2$ may be underestimated because of the difficulty in obtaining $O_2$ partial pressures at the actual sites of exchange (intervillous space and fetoplacental capillaries) rather than at more distant sites. When using major vessels to assess $O_2$ partial pressures, biases may arise because of (i) shunting of blood away from exchange regions, (ii) consumption of $O_2$ by villous trophoblast itself and (iii) placental heterogeneity in regional rates of vascular perfusion and $O_2$ diffusion (Mayhew et al. 1984; Mayhew 2014).

### *10.8.1 Does the Placenta have a Functional Reserve Capacity?*

It is informative to compare the diffusive performances of the avian egg, human placenta and human lung (Table 10.3). If the placenta has a reserve capacity, it is unlikely that this would match that of the mammalian pulmonary lung which must deal with extremes of respiratory demand between the resting state and maximal exercise. It is more likely that any placental reserve resides somewhere between the large reserve shown by the lung and the apparent lack of reserve displayed by the avian chorioallantois.

### *10.8.2 Predictions Based on Morphometric $DpO_2$ Changes*

Allometric findings concerning the relationship between $DvmO_2$ and fetal mass have allowed for testable predictions about transplacental and intervillous $O_2$ tensions and gradients (Mayhew 2006b). Using equations for predicting neonatal $O_2$ intakes from birthweights, a 3.5 kg newborn is expected to consume $O_2$ at about 27 $cm^3\ min^{-1}$. The high metabolic activity of the trophoblast would increase the initial flux to 40 $cm^3\ min^{-1}$. These consumption rates would require an $O_2$ partial

**Table 10.3** Comparison of physiological and morphometric $O_2$ diffusive conductances for three gas exchangers differing in reserve capacity. Physiological $DO_2$ values were estimated directly or calculated from DCO estimates. Morphometric values of $DpO_2$ were estimated directly or calculated from $DvmO_2$ values assuming that the villous membrane accounts for 90% of total resistance (see Mayhew 1990, 1993a)

| Estimation method | Chicken egg and CAM | Human term placenta | Human adult lung |
|---|---|---|---|
| *Physiological estimate* | 0.04–0.05 $cm^3\ min^{-1}\ kPa^{-1}$ | 6–15 $cm^3\ min^{-1}\ kPa^{-1}$ | 150–225 $cm^3\ min^{-1}\ kPa^{-1}$ (resting) 750 $cm^3\ min^{-1}\ kPa^{-1}$ (exercising) |
| Reference(s) | Tazawa and Mochizuki 1976; Piiper et al. 1980; Wangensteen and Weibel 1982 | Metcalfe et al. 1967; Bartels 1970; Forster 1973 | Gehr et al. 1978; Weibel 1984 |
| *Morphometric estimate* | 0.05 $cm^3\ min^{-1}\ kPa^{-1}$ | 16–42 $cm^3\ min^{-1}\ kPa^{-1}$ | 1030–1540 $cm^3\ min^{-1}\ kPa^{-1}$ |
| Reference(s) | Wangensteen and Weibel 1982 | Laga et al. 1973; Mayhew et al. 1984, 1986, 1990, 1993a, b; Reshetnikova et al. 1994, 1995; Bush et al. 2000; Ansari et al. 2003; Yin et al. 2009 | Gehr et al. 1978; Weibel 1984 |

pressure gradient across the villous membrane of less than 1 kPa. To avoid the dangers of vasoconstriction of the umbilical arteries and ductus arteriosus, umbilical venous $O_2$ tension near term should not exceed about 6–7 kPa and so $O_2$ flux probably proceeds from an intervillous partial pressure of no more than 8–9 kPa. As stated above, published values for $O_2$ tensions in the intervillous space at term are in the range 6–7 kPa.

Another prediction based on the discrepancy between exponents for fetal $O_2$ consumption and placental $DvmO_2$ is that transplacental $O_2$ partial pressure gradients decline during gestation. Again, observed changes in intervillous $O_2$ tensions indicate a peak of about 8 kPa at 16 weeks of gestation and a gradual decline to roughly 6–7 kPa at terms.

## 10.9 Morphometric $DpO_2$ and $DvmO_2$ in Complicated Human Pregnancies

Changes in placental structural composition and diffusive conductances occur in various pregnancy complications (including IUGR, PE, pregnancy at high altitude, maternal diabetes mellitus and cigarette smoking). Findings from some stereological studies undertaken by my research groups are summarised in Tables 10.4 and 10.5. Whilst many of these changes have been linked to fetal hypoxia, diabetes

**Table 10.4** Morphometric estimates of partial, total and mass-specific conductances in different pregnancy types and their departures from equivalent control values. Results are based on data in Mayhew et al. (1990, 1993b) and Bush et al. (2000)

| Conductance | Smoking | High altitude (3.6 km) | Diabetes mellitus |
|---|---|---|---|
| Birthweight | NSD | 9 % decrease | NSD |
| $D_{me}$ | 11 % increase | 62 % increase | NSD |
| $D_{mp}$ | 25 % increase | 92 % increase | 31 % increase |
| $D_{tro}$ | NSD | NSD | NSD |
| $D_{str}$ | NSD | 42 % increase | 20 % increase |
| $D_{fp}$ | NSD | NSD | 92 % increase |
| $D_{fe}$ | NSD | 18 % decrease | 47 % increase |
| $DpO_2$ | NSD | NSD | 16 % increase |
| Specific $DpO_2$ | NSD | 23 % increase | 12 % increase |

*D* conductance, *me* maternal erythrocyte, *mp* maternal plasma, *tro* trophoblast, *str* villous stroma, *fp* fetal plasma, *fe* fetal erythrocytes, *p* placenta

**Table 10.5** Surface areas ($m^2$), harmonic mean thicknesses (μm), morphometric $DvmO_2$ ($cm^3\ min^{-1}\ kPa^{-1}$) and mass-specific $DvmO_2$ ($cm^3\ min^{-1}\ kPa^{-1}\ kg^{-1}$) for the villous membrane in control and complicated pregnancies. Values are taken from Mayhew et al. (2007)

| Variable | Controls | PE alone | IUGR alone | PE + IUGR |
|---|---|---|---|---|
| $S_u$ [a] | 11.1 | 9.8 | 6.6 | 5.1 |
| $S_d$ [a] | 8.9 | 7.0 | 4.6 | 3.5 |
| $T_h$ | 3.81 | 3.98 | 4.36 | 4.29 |
| $DvmO_2$ [a] | 46.6 | 37.1 | 21.3 | 18.7 |
| Specific $DvmO_2$ | 13.5 | 14.4 | 9.0 | 18.0 |

$S_u$ upstream (maternal-facing) surface area of the villous membrane, $S_d$ downstream (fetal-facing) surface area of the villous membrane, $T_h$ harmonic mean thickness of the villous membrane

[a] Significant main effect of IUGR. Other apparent differences were not significant. Birthweights (not shown) were significantly reduced in PE and IUGR

mellitus and smoking are associated with other complications not associated with hypoxia per se. In addition, some pregnancy complications are linked to oxidative stress caused by fluctuating levels of $O_2$ (Burton 2009).

In pregnancy at high altitude, the most persistent stressor is chronic hypobaric hypoxia. At altitudes up to 2800 m, mean birthweight is maintained at lowland levels but morphometric $DvmO_2$ increases (Reshetnikova et al. 1994) as does its mass-specific $DvmO_2$. At the higher altitude of 3600 m, birthweights are reduced but total $DpO_2$ is maintained so mass-specific $DpO_2$ is greater (Mayhew et al. 1990). Together with the changes reported during gestation (see above), the altitudinal adaptations seem to indicate that the human placenta normally operates near its diffusion limit. Unlike the pulmonary lung, it has little or no immediately-accessible reserve capacity but can adapt in a gradual way over time. This is consistent with results from a study on the placenta of the Rhesus monkey in which loss of almost half of the fetoplacental vascular bed by vessel ligation led to compensatory growth of the placenta (Roberts et al. 2012).

IUGR and PE are of unresolved aetiologies, complicate a significant proportion of all pregnancies and contribute to adverse perinatal outcomes. In both PE and normotensive IUGR, placental trophoblast is less invasive and produces relatively shallow invasion of uterine spiral arteries and increased uteroplacental vascular resistance. The sequelae of these early events are long term and lead to compromised uteroplacental perfusion and reduced maternal–fetal transport of $O_2$ and nutrients (see Benirschke et al. 2012).

Stereological analysis has shown that placentas from cases of pure PE (not accompanied by IUGR) have similar tissue volumes and surface areas to controls (Teasdale 1985; Mayhew et al. 2003, 2004; Egbor et al. 2006). In contrast, compromised growth occurs in cases of pure IUGR and cases of IUGR associated with PE (Teasdale 1984, 1987; Mayhew et al. 2003, 2004; Egbor et al. 2006). Placentas in pure IUGR and PE + IUGR had smaller exchange surfaces of peripheral villi and fetal capillaries. Whilst there were no differences in the harmonic mean thickness of the villous membrane, estimates of the arithmetic mean thickness of the trophoblast were greater in IUGR placentas.

In placentas from small-for-gestational-age (SGA) pregnancies, morphometric $DvmO_2$ was found to be smaller than in controls primarily due to a reduction in villous surface areas of the villous membrane (Ansari et al. 2003). Using an efficient design based on four groups of placentas (control, IUGR, PE and PE + IUGR), it was found that PE had no significant effects on placental structure and there were no significant effects of PE or IUGR on villous membrane thickness (Mayhew et al. 2007). However, IUGR (with or without PE) was associated with reduced surface areas and this was the principal factor leading to a smaller morphometric $DvmO_2$ in these placentas, 18–21 $cm^3\ min^{-1}\ kPa^{-1}$ versus 47 $cm^3\ min^{-1}\ kPa^{-1}$ (see Table 10.5). When account was taken of fetal mass, there were no effects of PE or IUGR despite the mass-specific conductance in pure IUGR placentas appearing to be smaller than that in controls. The decline in conductances was associated with perturbations affecting the villous trophoblast and vasculature but the functional capacity of the placenta remained proportional to the mass of the fetus (Table 10.5). Such findings emphasise the clinical importance of distinguishing pure cases of PE and IUGR.

## 10.10 Concluding Remarks

Unlike the mammalian lung which has a reserve capacity capable of dealing with extremes of respiratory demand between resting and maximally active states, the avian chorioallantois and eutherian placenta are more limited in their adaptability. Whilst both of these transient exchangers successfully serve the needs of the developing embryo/fetus, their structural and functional remodelling is gradual and occurs over a more protracted period of time. Egg size across avian species is related to the size of the adult bird and the total morphometric diffusive conductance of the placenta is related directly to fetal size. In various types of pregnancy complication, the placenta exhibits changes in morphology and physiology which can

affect partial conductances at maternal, fetal and intermediate sites along the oxygen pathway. In some instances, these changes are associated with compromised fetal growth.

**Acknowledgements** Over the past three decades, I have been grateful for research awards from various funding agencies and for collaborations with, and contributions from, many colleagues and students who have shared an interest in the placenta.

## References

Ansari T, Fenlon S, Pasha S, O'Neill B, Gillan JE, Green CJ, Sibbons PD. Morphometric assessment of the oxygen diffusion conductance in placentae from pregnancies complicated by intrauterine growth restriction. Placenta. 2003;24:618–26.

Bartels H. The diffusion capacity of the placenta. In: Neuberger A, Tatum EL, editors. Frontiers of biology, Vol 17, Prenatal respiration. London: North-Holland; 1970. pp. 61–7.

Benirschke K, Burton GJ, Baergen RN. Pathology of the human placenta. 6th ed. Heidelberg: Springer; 2012.

Bissonnette JM, Metcalfe J. Gas exchange of the fertile hen's egg: components of resistance. Respir Physiol. 1978;1:209–18.

Bissonnette JM, Longo LD, Novy MJ, Murata Y, Martin CB. Placental diffusing capacity and its relation to fetal growth. J Dev Physiol. 1979;1:351–9.

Burton GJ. Oxygen, the Janus gas; its effects on human placental development and function. J Anat. 2009;215:27–35.

Burton GJ, Feneley MR. Capillary volume fraction is the principal determinant of villous membrane thickness in the human placenta at term. J Dev Physiol. 1992;17:39–45.

Bush PG, Mayhew TM, Abramovich DR, Aggett PJ, Burke MD, Page KR. Maternal cigarette smoking and oxygen diffusion across the placenta. Placenta. 2000;21:824–33.

Castellucci M, Kosanke G, Verdenelli F, Huppertz B, Kaufmann P. Villous sprouting: fundamental mechanisms of human placental development. Human Reprod. 2000;6:485–94.

Charnock-Jones DB, Kaufmann P, Mayhew TM. Aspects of human fetoplacental vasculogenesis and angiogenesis. I. Molecular regulation. Placenta. 2004;25:103–13.

Coan PM, Ferguson-Smith AC, Burton GJ. Developmental dynamics of the definitive mouse placenta assessed by stereology. Biol Reprod. 2004;70:1806–13.

Egbor M, Ansari T, Morris N, Green CJ, Sibbons PD. Pre-eclampsia and fetal growth restriction: How morphometrically different is the placenta? Placenta. 2006;27:727–34.

Enders AC, Carter AM. What can comparative studies of placental structure tell us?—a review. Placenta 25, suppl. A. Troph Res. 2004;18:S3–S9.

Forster RE. Some principles governing maternal-foetal transfer in the placenta. In: Comline KS, Cross KW, Dawes GS, Nathanielsz PW, editors. Foetal and neonatal physiology, proceedings of the Sir Joseph Barcroft Centenary Symposium. Cambridge: Cambridge University Press; 1973. pp. 223–37.

Gehr P, Bachofen M, Weibel ER. The normal human lung: ultrastructure and morphometric estimation of diffusion capacity. Respir Physiol. 1978;32:121–40.

Gundersen HJG, Jensen EB. The efficiency of systematic sampling in stereology and its prediction. J Microsc. 1987;147:229–63.

Gundersen HJG, Jensen EB, Østerby R. Distribution of membrane thickness determined by lineal analysis. J Microsc. 1978;113:27–43.

Holland RAB, van Hezewijk W, Zubzanda J. Velocity of oxygen uptake by partly saturated adult and fetal human red cells. Respir Physiol. 1977;29:303–14.

Howard CV, Reed MG. Unbiased stereology. Three-dimensional measurement in microscopy. 2nd ed. Abingdon: Garland Science/Bios Scientific; 2005.
Jackson MR, Joy CF, Mayhew TM, Haas JD. Stereological studies on the true thickness of the villous membrane in human term placentae: a study of placentae from high-altitude pregnancies. Placenta. 1985;6:249–58.
Jackson MR, Mayhew TM, Haas JD. On the factors which contribute to thinning of the villous membrane in human placentae at high altitude. II. An increase in the degree of peripheralization of fetal capillaries. Placenta. 1988;9:9–18.
Jackson MR, Joy CF, Mayhew TM, Boyd PA. Quantitative description of the elaboration and maturation of villi from 10 weeks of gestation to term. Placenta. 1992;13:357–70.
Jauniaux E, Hempstock J, Greenwold N, Burton GJ. Trophoblastic oxidative stress in relation to temporal and regional differences in maternal placental blood flow in normal and abnormal early pregnancies. Am J Pathol. 2003;162:115–25.
Jensen EB, Gundersen HJG, Østerby R. Determination of membrane thickness distribution from orthogonal intercepts. J Microsc. 1979;115:19–33.
Jirkovska M, Kubinova L, Janacek J, Moracova M, Krejci V, Karen P. Topological properties and spatial organization of villous capillaries in normal and diabetic placentas. J Vasc Res. 2002;39:268–78.
Jirkovska M, Janacek J, Kalab J, Kubinova L. Three-dimensional arrangement of the capillary bed and its relationship to microrheology in the terminal villi of normal term placenta. Placenta. 2008;29:892–7.
Karimu AL, Burton GJ. Compliance of the human placental villous membrane at term; the concept of the feto-placental unit as an autoregulating gas exchange system. Troph Res. 1994a;8:541–58.
Karimu AL, Burton GJ. The significance of changes in fetal perfusion pressure to factors controlling angiogenesis in the human term placenta. J Reprod Fertil. 1994b;102:447–50.
Kaufmann P, Mayhew TM, Charnock-Jones DS. Aspects of human fetoplacental vasculogenesis and angiogenesis. II. Changes during normal pregnancy. Placenta. 2004;25:114–26.
Laga EM, Driscoll SG, Munro HN. Quantitative studies of human placenta. I. Morphometry. Biol Neonate. 1973;23:231–59.
Lisman BAM, van den Hoff MJB, Boer K, Bleker OP, van Groningen K, Exalto N. The architecture of first trimester chorionic villous vascularisation: a confocal scanning microscopical study. Human Reprod. 2007;8:2254–60.
Mayhew TM. Fetoplacental angiogenesis during gestation is biphasic, longitudinal and occurs by proliferation and remodelling of vascular endothelial cells. Placenta. 2002;23:742–50.
Mayhew TM. Stereology and the placenta: where's the point?—a review. Placenta. 2006a; 27 (suppl. A):S17–S25. (Troph Res)
Mayhew TM. Allometric studies on growth and development of the human placenta: growth of tissue compartments and diffusive conductances in relation to placental volume and fetal mass. J Anat. 2006b;208:785–94.
Mayhew TM. Taking tissue samples from the placenta: an illustration of principles and strategies. Placenta. 2008;29:1–14.
Mayhew TM. Estimating oxygen diffusive conductances of gas-exchange systems: a stereological approach illustrated with the human placenta. Ann Anat. 2014;196:34–40.
Mayhew TM, Joy CF, Haas JD. Structure-function correlation in the human placenta: the morphometric diffusing capacity for oxygen at full term. J Anat. 1984;139:691–708.
Mayhew TM, Jackson MR, Haas JD. Microscopical morphology of the human placenta and its effects on oxygen diffusion: a morphometric model. Placenta. 1986;7:121–31.
Mayhew TM, Jackson MR, Haas JD. Oxygen diffusive conductances of human placentae from term pregnancies at low and high altitudes. Placenta. 1990;11:493–503.
Mayhew TM, Jackson MR, Boyd PA. Changes in oxygen diffusive conductances of human placentae during gestation (10–41 weeks) are commensurate with the gain in fetal weight. Placenta. 1993a;14:51–61.
Mayhew TM, Sørensen FB, Klebe JG, Jackson MR. Oxygen diffusive conductance in placentae from control and diabetic women. Diabetologia. 1993b;36:955–60.

Mayhew TM, Wadrop E, Simpson RA. Proliferative versus hypertrophic growth in tissue subcompartments of human placental villi during gestation. J Anat. 1994;184:535–43.
Mayhew TM, Ohadike C, Baker PN, Crocker IP, Mitchell C, Ong SS. Stereological investigation of placental morphology in pregnancies complicated by pre-eclampsia with and without intrauterine growth restriction. Placenta. 2003;24:219–26.
Mayhew TM, Wijesekara J, Baker PN, Ong SS. Morphometric evidence that villous development and fetoplacental angiogenesis are compromised by intrauterine growth restriction but not by pre-eclampsia. Placenta. 2004;25:829–33.
Mayhew TM, Manwani R, Ohadike C, Wijesekara J, Baker PN. The placenta in pre-eclampsia and intrauterine growth restriction: studies on exchange surface areas, diffusion distances and villous membrane diffusive conductances. Placenta. 2007;28:233–8.
Metcalfe J, Bartels H, Moll W. Gas exchange in the pregnant uterus. Physiol Rev. 1967;47:782–838.
Piiper J, Tazawa H, Ar A, Rahn H. Analysis of chorioallantoic gas exchange in the chick embryo. Respir Physiol. 1980;39:273–84.
Power GG. Solubility of $O_2$ and CO in blood and pulmonary and placental tissue. J Appl Physiol. 1968;24:468–74.
Rahn H, Paganelli CV, Ar A. Pores and gas exchange of avian eggs: a review. J Exp Zool. 1987;1:165–72.
Reizis A, Hammel I, Ar A. Regional and developmental variations of blood vessel morphometry in the chick embryo chorioallantoic membrane. J Exp Biol. 2005;208:2483–8.
Reshetnikova OS, Burton GJ, Milovanov AP. Effects of hypobaric hypoxia on the fetoplacental unit; the morphometric diffusing capacity of the villous membrane at high altitude. Am J Obstet Gynecol. 1994;171:1560–5.
Reshetnikova OS, Burton GJ, Teleshova OV. Placental histomorphometry and morphometric diffusing capacity of the villous membrane in pregnancies complicated by maternal iron-deficiency anemia. Am J Obstet Gynecol. 1995;173:724–7.
Roberts VHJ, Räsänen JP, Novy MJ, Frias A, Louey S, Morgan TK, Thornburg KL, Spindel ER, Grigsby PL. Restriction of placental vasculature in a non-human primate: a unique model to study placental plasticity. Placenta. 2012;33:736.
Rodesch F, Simon P, Donner C, Jauniaux E. Oxygen measurements in endometrial and trophoblastic tissues during early pregnancy. Obstet Gynecol. 1992;80:283–5.
Roughton FJW, Forster RE. Relative importance of diffusion and chemical reaction rates in determining rate of exchange of gases in the human lung, with special reference to true diffusing capacity of pulmonary membrane and volume of blood in the lung capillaries. J Appl Physiol. 1957;11:290–302.
Samson JE, Mari G, Dick EJ, Hubbard GB, Ferry RJ, Schlabritz-Loutsevitch NE. The morphometry of materno-fetal oxygen exchange barrier in a baboon model of obesity. Placenta. 2011;32:845–51.
Schneider H. Oxygenation of the placental-fetal unit in humans. Respir Physiol Neurobiol. 2011;178:51–8.
Smith AD, Gilbert RD, Lammers RJ, Longo LD. Placental exchange area in guinea pigs following long-term maternal exercise: a stereological analysis. J Dev Physiol. 1983;5:11–21.
Soothill PW, Nicolaides KH, Rodeck CH, Campbell S. Effects of gestational age on fetal and intervillous blood gas and acid-base values in human pregnancy. Fetal Ther. 1986;1:168–75.
Staub NC, Bishop JM, Forster RE. Importance of diffusion and chemical reaction rates in $O_2$ uptake in the lung. J Appl Physiol. 1962;17:21–7.
Tazawa H, Mochizuki M. Estimation of contact time and diffusing capacity for oxygen in the chorioallantoic vascular plexus. Respir Physiol. 1976;28:119–28.
Teasdale F. Idiopathic intrauterine growth retardation: histomorphometry of the human placenta. Placenta. 1984;5:83–92.
Teasdale F. Histomorphometry of the human placenta in maternal preeclampsia. Am J Obstet Gynecol. 1985;152:25–31.
Teasdale F. Histomorphometry of the human placenta in pre-eclampsia associated with severe intrauterine growth retardation. Placenta. 1987;8:119–28.

Tuuli MG, Longtine MS, Nelson DM. Review: oxygen and trophoblast biology—a source of controversy. Placenta suppl A. 2011;32:S109–S118.
Veras MM, Damaceno-Rodrigues NR, Caldini EG, Ribeiro AACM, Mayhew TM, Saldiva PHN, Dolhnikoff M. Particulate urban air pollution affects the functional morphology of mouse placenta. Biol Reprod. 2008;79:578–84.
Veras MM, Costa NSX, Mayhew TM. Best practice for quantifying the microscopic structure of mouse placenta: the stereological approach. In: Croy A, Yamada AT, DeMayo FJ, Adamson SL, editors. The guide to investigation of mouse pregnancy. London: Academic Press; Elsevier Inc; 2014. pp. 545–56.
Wangensteen D, Weibel ER. Morphometric evaluation of chorioallantoic oxygen transport in the chick embryo. Respir Physiol. 1982;47:1–20.
Weibel ER. Morphometric estimation of pulmonary diffusion capacity. I. Model and method. Respir Physiol. 1970;11:54–75.
Weibel ER. The pathway for oxygen. Structure and function in the mammalian respiratory system. Cambridge: Harvard University Press; 1984.
Yin TT, Loughna P, Ong SS, Padfield J, Mayhew TM. No correlation between ultrasound placental grading at 31–34 weeks of gestation and a surrogate estimate of organ function at term obtained by stereological analysis. Placenta. 2009;30:726–30.

# Index





A. N. Makanya (ed.), *The Vertebrate Blood-Gas Barrier in Health and Disease,*
DOI 10.1007/978-3-319-18392-3